University of Alberta

The Application of Wall Jets in Stirred Tanks with Solids Distribution

by

Kevin J. Bittorf ©

A thesis submitted to the Faculty of Graduate Studies and Research in partial
fulfillment of the requirements of the degree of Doctor of Philosophy
in Chemical Engineering

Department of Chemical and Materials Engineering

Edmonton, Alberta

Fall 2000

National Library
of Canada

Acquisitions and
Bibliographic Services

395 Wellington Street
Ottawa ON K1A 0N4
Canada

Bibliothèque nationale
du Canada

Acquisitions et
services bibliographiques

395, rue Wellington
Ottawa ON K1A 0N4
Canada

Your file Votre référence

Our file Notre référence

The author has granted a non-exclusive licence allowing the National Library of Canada to reproduce, loan, distribute or sell copies of this thesis in microform, paper or electronic formats.

The author retains ownership of the copyright in this thesis. Neither the thesis nor substantial extracts from it may be printed or otherwise reproduced without the author's permission.

L'auteur a accordé une licence non exclusive permettant à la Bibliothèque nationale du Canada de reproduire, prêter, distribuer ou vendre des copies de cette thèse sous la forme de microfiche/film, de reproduction sur papier ou sur format électronique.

L'auteur conserve la propriété du droit d'auteur qui protège cette thèse. Ni la thèse ni des extraits substantiels de celle-ci ne doivent être imprimés ou autrement reproduits sans son autorisation.

0-612-59565-X

Canadä

University of Alberta

Library Release Form

Name of Author: Kevin J. Bittorf

Title of Thesis: The Application of Wall Jets in Stirred Tanks with Solids Distribution

Degree: Doctor of Philosophy

Year this Degree Granted: 2000

Permission is hereby granted to the University of Alberta Library to reproduce single copies of this thesis and to lend or sell such copies for private, scholarly or scientific research purposes only.

The author reserves all other publication and other rights in association with the copyright in the thesis, and except as herein before provided, neither the thesis nor any substantial portion thereof may be printed or otherwise reproduced in any material form whatever without the author's prior permission.

Kevin J. Bittorf
60 Marion Cr.
Red Deer, AB
T4R 1N2

Date: Aug/29/00

University of Alberta

Faculty of Graduate Studies and Research

This undersigned certify that they have read, and recommend to the Faculty of Graduate Studies and Research for acceptance, a thesis entitled *Wall Jets in Stirred Tanks with Application to Turbulent Limits and Solids Distribution* submitted by KEVIN J. BITTORF in partial fulfillment of the requirements for the degree of DOCTOR of PHILOSOPHY in CHEMICAL ENGINEERING.

S.M. Kresta (Supervisor)

R.E. Hayes

J.H Masliyah

D. Wilson

D.J. Wilson

A.W. Nienow

Date: August 23, 2000

Abstract

In this work the bulk flow field in the stirred tank was examined to clarify our the understanding of the bulk flow in a stirred tank. Laser Doppler velocimetry was used to measure axial velocities in order to examine two phenomena: the nature of the flow along the wall and the active volume of circulation.

The axial impellers studied all created a three-dimensional wall jet along the wall and baffle of the tank. The expansion of the jet is linear and the maximum velocity decays with 1/x (x= dimensionless axial distance). For radial impellers, the flow impinges directly on the wall of the tank, and forms an axi-symmetric internal annular wall jet. The wall jet expands linearly and decays with $1/x^{0.5}$. The similarity model developed for this type of jet accounts for the recirculating flow in the system.

The objective of the thesis was to determine the influence of the impeller on the flow field in the bulk of the tank. It is shown in this thesis that for stirred tanks agitated with axial impellers the active volume of mean circulation is not the whole tank, but a height equivalent to 2/3 of the tank diameter. The upward flow is dominated by the upward flow at the wall of the tank, which is successfully reduced using turbulent wall jet theory.

The principle of the wall jet was applied to determine two limits: the point where the jet is no longer turbulent and the cloud height in a suspension of solids. It was found that the turbulent height of the wall jet is proportional to the impeller Reynolds number (Re). For the whole tank (H=T) to be fully turbulent, $Re \geq 1.5 \times 10^5$, which requires much more energy than the Re_I required to induce fully turbulent flow in the impeller region ($Re = 2 \times 10^4$). Finally, a model for predicting the solids liquid interface, or cloud height, was developed based on the properties of the three dimensional wall jet. The local maximum velocity in the jet was used to determine the height to which solids can be suspended.

"Now I believe there comes a time
where everything just falls in line
we live an' learn from our mistakes
the deepest cuts are healed by faith"

P. Benatar

Preface

The majority of the thesis is a compilation of chapters that have either been accepted for publication, submitted for publication or presented at conferences.

- Chapter 3: "Internal Annular Wall Jets: application to stirred tanks agitated with Rushton turbines" submitted, AIChE Journal, 2000
- Chapter 4: " Three Dimensional Wall Jets Driven by Axial Impellers," submitted, AIChE Journal, 2000.
- Chapter 5: "Active Volume of Mean Circulation for Stirred Tanks Agitated with Axial Impellers," *Chem. Eng. Sci.*, **55**, 1325-1335 (2000).
- Chapter 6: "Limits of Fully Developed Turbulence in a Stirred Tank," *Proceedings of the 10th European Conference on Mixing*, pp. 17-24 (2000)
- Chapter 7: "Prediction of Cloud Height for Slow Settling Solids in Stirred Tanks" presented at Mixing XVII, Banff, 1999, and the Canadian Chemical Engineering Conference, Saskatoon, 1999.

All other chapters are specific only to this thesis.

Acknowledgements

I have been at the University of Alberta for 9 years while completing three degrees (B.Sc. Chem. Eng., MBA and Ph.D. Chem. Eng.); because of this I have many people to thank. Of course there are always the primary acknowledgements: my parents (Mom and Dad) my thesis supervisor, Dr. Suzanne M. Kresta, and my committee members (Dr. Masliyah, Dr. Hayes, Dr. Wilson and Dr. Nienow). I am grateful to all of these people, especially my parents. However, as we go through life many other people have had a great influence in molding my life.

Many graduate students have provided me with fond memories. Every Friday afternoon at RATT hinged around many discussions about sports, women, music, WWF, our hockey pool and plenty of outright bizarre topics. These long hours at RATT which kept me sane were spent productively with Roach (who believes concrete stairs are comfortable to sleep on and 'we don't need no breaks'), J.M. (who believes Red Deer is the best place to meet a woman), Shawn "Garth Brooks" Taylor, Jonny "the mountain man", Jason "Mr. Boat Race", Peppin ('guess we weren't meant to stop….'), T-bone, Steve in France, Pfaff (whose girlfriend knows the real meaning of 'Red Neck Girl') and many other individuals. Thanks to Mark the Bartender and the entire waitress staff at RATT for knowing exactly what we wanted every time we arrived and making it the happiest place on earth or at least a place to forget/complain about our school work.

I would like to thank the boys from Red Deer: Davis, Lannon, Thull (a.k.a. Skully) and Carfantan. We spent many pleasurable hours at the Place and driving up and down Gaetz Avenue. Who could ever forget the events that occurred at Pizza 73 and Billy Bob's? Whether they knew it or not, these boys help push me to do better.

As in any university career, there are always many unforgettable women to thank for helping keep me semi-sane. As Willie Nelson and Julio Iglesias put it, this goes out "To All of the Girls I've Loved Before": Diane "Plivalittlelick", Sandra "Schweitzenegger" and Vera "you're my green eyed girl". Without them, the last nine years would have been boring, to say the least.

A few more people I need to be recognized. Teddi, for helping me write and edit my thesis, without your help it would not have been nearly as good. I am appreciative of the Simpson family who made me laugh at life's misgivings, which put this thesis into perspective. I would like to thank my sister Alicya, nieces or nephews-to-be, Cluster the cat, and all of my aunts, uncles, grandparents and cousins because they all had an influence.

It is difficult to write acknowledgments because it is like a Grammy awards speech-you do end up forgetting people, which is purely unintentional. So if I inadvertently missed your name please add it here ______________. I would like to thank my parents one more time because without them my university career would not have been possible. Thanks to all of you and I know I will have more names to add to the acknowledgement list over my life.

Table of Contents

CHAPTER 1: Introduction 1
1.1 Turbulent Length Scales 4
1.2 Dimensionless Numbers and Scale-Up 10
1.3 Jets 15
1.4 Solid Suspension 25
1.5 Conclusion 31
1.6 Nomenclature 33
1.7 References 35

CHAPTER 2: Experimental Setup and Procedures 53
2.1 Introduction 54
2.2 Experimental Equipment 54
2.2.1 Tank 54
2.2.2 Impellers 55
2.2.3 Motors 55
2.2.4 Traverse System 55
2.2.5 Fluids Examined 56
2.3 Laser Doppler Velocimetry (LDV) 57
2.4 Experimental Repeatability 59
2.5 Trouble Shooting with Experiments and Data Analysis 61
2.6 Conclusion 62
2.7 Nomenclature 63
2.8 References 64

CHAPTER 3: Internal Annular Wall Jets: application to stirred tanks agitated with Rushton turbines 73
3.1 Introduction 74
3.2 Theory 76
3.2.1 Wall Jet Decay and Expansion 76
3.2.2 Self-similar Velocity Profiles 79
3.2.3 Determination of B Through Application of Continuity Constraint 81
3.2.4 Momentum Balance 86
3.2.5 Summary of Similarity Profile Results 87
3.3 Experimental 87
3.4 Results 88
3.4.1 Axisymmetry 88
3.4.2 Similarity Profile 89
3.4.3 Jet Decay and Expansion Rate 90
3.4.4 Turbulent Intensities 91
3.5 Conclusions 91
3.6 Nomenclature 93
3.7 References 95

CHAPTER 4: Three Dimensional Wall Jets Driven by Axial Impellers 115
4.1 Introduction 116
4.2 Theory 118
4.3 Experimental Conditions 121
4.4 Results 121
4.4.1 Similarity Profile 122
4.4.2 Jet Decay 123
4.4.3 Three Dimensional Characteristics 124
4.4.4 Jet Expansion and its Originating Position 124
4.4.5. Turbulent Intensities 125
4.5 Conclusions 125
4.6 Nomenclature 127
4.7 References 128

CHAPTER 5: Active Volume Of Mean Circulation For Stirred Tanks Agitated With Axial Impellers 146
5.1 Introduction 147
5.1.1 Mean Circulation Patterns 148
5.1.2 Active Volume or Penetration Height 150
5.1.3 Effect of Off-Bottom Clearance 152
5.2 Experimental Set-up 155
5.3 Results and Discussion 158
5.3.1 Experimental Data 158
5.3.2 Comparison to What Other Authors Have Shown 162
5.3.3 Possible Implications 163
5.4 Conclusions 164
5.5 Nomenclature 166
5.6 References 167

CHAPTER 6: Fully Turbulent Flow in a Stirred Tank with Axial Flow 185
6.1 Introduction 186
6.1.2 Scaling in the Bulk of the Tank 189
6.2 Experimental 190
6.3 Results 191
6.3.1 Criteria for Assessing Fully Developed Turbulence 192
6.3.2 Limits of Fully Developed Turbulence 192
6.4 Conclusion 195
6.5 Nomenclature 196
6.6 References 197

CHAPTER 7: Prediction Of Cloud Height For Slow Settling Solids In Stirred Tanks 219
7.1 Introduction 220
7.1.1 Cloud Height and Solids Distribution 221
7.1.2 Effect of Solids Loading 222
7.1.3 Just Suspended Speed (Njs) 224
7.2 Model Development 225
7.2.1 Validation of Steady Flow Assumption 226
7.2.2 Wall Jet Model: determining fluid velocity at the wall 228
7.2.3 Cloud Height Models 231
7.2.4 Scale-Up of Cloud Height 236
7.3 Conclusions and Recommendations 237
7.4 Nomenclature 239
7.5 References 240

CHAPTER 8: Conclusions 259
8.1 Conclusions 260

APPENDIX A: Additional Data Supporting Chapter 6 263

Table of Tables

Table 1-1: Boundary conditions for a jet in a stagnant fluid. 20

Table 2 - 1: PBT and RT Impeller Configuration 65
Table 2 - 2: Motor Specifications 65
Table 2 - 3: Traverse Specification 65
Table 2 - 4: Liquid Properties at Room Temperature 66
Table 2 - 5: Laser Specifications 66
Table 2 - 6: Fringe Spacing 66

Table 3-1: Boundary conditions for a jet in a stagnant fluid. 97
Table 3-2: Boundary Conditions for a Jet in recirculating flow 97
Table 3-3: Equipment Specifications 98
Table 3-4: Measured Values of B for Equation 3.28 to Fit the Similarity profiles in Figures 3-8B & 3-9B 99
Table 3-5: Expansion and Virtual Origin of a the Wall Jet in a Stirred Tank 99

Table 4-1: Equipment Specifications 130
Table 4-2: Experimental Conditions 131
Table 4-3: Decay Coefficients of the Wall Jet for Axial Impellers 132
Table 4-4: Expansion and Virtual Origin of a the Wall Jet in a Stirred Tank 132

Table 5-1: Equipment Specifications 170
Table 5-2: Experimental Runs 171
Table 5-3: Maximum Active Volume 172
Table 5-4: The Range of Clearances at which the Discharge Stream Reaches the Tank Wall Before the Bottom of the Tank 172

Table 6- 1: Experimental Variables 198
Table 6- 2: Equipment Specifications 199
Table 6- 3: Last Known Turbulent Height (z/T) Compared to Re (PBT D=T/3) 200
Table 6- 4: Last Known Turbulent Height (z/T) Compared to Re (A310 D=T/2) 200
Table 6- 5: Last Known Turbulent Height (z/T) Compared to Re (PBT D=T/2) 200
Table 6- 6: Last Known Turbulent Height (z/T) Compared to Re (A310 D=T/3) 201
Table 6- 7: Last Known Turbulent Height (z/T) Compared to Re (HE3 D=T/4) 201

Table 7-1: Description of Experimental Conditions 243
Table 7-2: Laser Doppler Velocimeter Specifications 244
Table 7-3: Reduction of RMS due to the addition of solids 245
Table 7-4: Measured Ucore Values 245
Table 7-5: K values calculated for Hicks et al. (1997) data. 246
Table 7-6:K values calculated for Bujalski et al. (1999) data. 247
Table 7-7: K on scale-up for Mak's (1992) data in Appendices A-E 247

Table of Figures

Figure 1 - 1: Tank configuration with geometric nomenclature four baffles are equally spaced around the perimeter of the tank 43
Figure 1 - 2: Flow pattern for an axial impeller 44
Figure 1 - 3: Flow patterns for the radial impeller 46
Figure 1 - 4: Length scales in a stirred tank (Kresta, 1998) showing the mean circulation loop (scale of macro instability), trailing vortex (integral length scale) and various sizes of turbulent eddies. 49
Figure 1 - 5: Instantaneous flow pattern taken from Myers et al. (1997). Note that now two patterns are similar and that the mean "single eight" circulation loop does not exist in any of the four images. 53
Figure 1 - 6: Effect of clearance and rotational speed on the frequency of the macro instabilities (data from Bruha et al. 1994) 58
Figure 1 - 7: Effect of different methods of scale-up on Re 64
Figure 1 - 8: Effect of different methods of scale-down on Re 70
Figure 1 - 9: Development of the inner and outer layers of a wall jet (Rajaratnam 1976) 77
Figure 1 - 10: Velocity profiles of a Wall jet (Rajaratnam 1976) 85
Figure 1 - 11: Similarity of the velocities in Figure 1-10 (Rajaratnam 1976) 94

Figure 2 - 1: Experimental Apparatus (Zhou, 1997): 67
Figure 2 - 2: Tank configuration showing geometric nomenclature. 68
Figure 2 - 3: The Four Impellers Used in this work: 69
Figure 2 - 4: Dependence of viscosity on temperature for triethylene glycol and water mixtures. This show the range of viscosities used in Chapter 5. Because of the strong dependence and variable composition, viscosities were measured independently for each run. 70
Figure 2 - 5: Schematic of the laser Doppler velocimeter (LDV) optical configuration 71

Figure 3 - 1A: Wall jet produced by an annular nozzle inside a cylinder with stagnant fluid. $d_{cylinder}$ is large relative to the nozzle opening and the end of the cylinder is open. 100
Figure 3 - 1B: Wall jet produced by an annular nozzle inside a cylinder with recirculating fluid. $d_{cylinder}$ is large relative to the nozzle opening (d_{nozzle}) . The top of the cylinder is closed and the bottom of the cylinder is open. 101
Figure 3 - 2: Wall jet profile produced by an annular nozzle inside a cylinder with recirculating fluid. This figure shows the area for the upward and downward flows and the nomenclature (b, P, R, and B) 102
Figure 3 - 3: Jet profiles for various values of B. As the minimum velocity becomes larger the value of B increase. 103
Figure 3 - 4: Solution to variables B, P/R and □ and experimental values obtained for B. The upward momentum and downward momentum are equal at b/R=0.19. For the experimental data b/R=0.19 occurs at a z/T=0.16. 104
Figure 3 - 5: Location of the jets in a Rushton Turbine stirred tank. 105
Figure 3 - 6A: Tank configuration (side view) showing geometric nomenclature. 106
Figure 3 - 6B: Position of measurements (top view) 107

Figure 3 - 7: Dimensionless velocity profile along the wall of the tank (Traverse B in Figure 3 - 6B) for the Rushton turbine showing that the jet can be treated as axisymmetric. 108
Figure 3 - 8A: Dimensionless velocity distribution for the Rushton turbine at C/D=0.75 and Re=5×10^4. The velocity distributions match Glauert's theory to η_y=1.2 after which recirculation affects the profiles. The recirculating annular jet matches the data well up to U/Um=-0.2 with little variation between the profiles 109
Figure 3 - 8B: Dimensionless velocity distribution for the Rushton Turbine at C/D=1.75 and Re=5×10^4. The velocity distributions match Glauert's theory to η_y =1.2 after which recirculation affects the profiles. The recirculating annular jet matches the data well up U/Um =0.2 with little variation between the profiles. 110
Figure 3 - 9A: Dimensionless velocity distribution for the Rushton turbine at C/D=0.75 and Re=5×10^4. Similarity is maintained beyond U/U_m =0 and the profiles match new similarity solution well. 111
Figure 3 - 9B: Dimensionless velocity profiles for the Rushton Turbine at C/D=1.75 and Re=5×10^4. Similarity is maintained beyond U/U_m =0 and the profiles match new similarity solution well. 112
Figure 3 - 10: Decay of maximum velocity for a wall jet produced by the Rushton turbine impeller. The decay of velocity closely matches the similarity scaling. 113
Figure 3 - 11: Turbulence in the internal annular wall jet produced by an RT impeller (D/T=0.33, C/D=0.75, N=500 rpm). After a z/T=0.41 the fluctuating velocities show similarity. 114

Figure 4 - 1: Three dimensional wall jet produced by a square nozzle. b is the half width of the jet in the y direction. In the tank the baffle is in the y-z plane and the tank wall is in the x-z plane. 133
Figure 4 - 2: Location of the virtual origins for a three dimensional wall jet driven by an axial impeller system. The virtual origins are located approximately one baffle width below the tank. 134
Figure 4 - 3A: Tank configuration (side view) showing geometric nomenclature. 135
Figure 4 - 3B: Position of measurements (top view) 136
Figure 4 - 4A: Dimensionless velocity distribution for the A310 impeller at C/D=0.68 and Re=1.96×10^5. Profile fits U/Um=0.5 and at 1.0 by definition. Similarity is maintained beyond the end of the jet model (U/Um =0) except for one traverse below the impeller (z/T=0.354) where additional momentum is injected into the flow. 137
Figure 4 - 4B: Dimensionless velocity distribution for the PBT impeller at C/D=0.4 and Re=5.33×10^4. Profile fits at U/Um =0.5 and 1.0 by definition. Similarity is maintained beyond U/Um =0 for all profiles. 138
Figure 4 - 4C: Dimensionless velocity distribution for the HE3 impeller at C/D=0.5 and Re=2.40×10^4. Profile fits at U/Um =0.5 and 1.0 by definition. Similarity is maintained beyond U/Um =0 for all profiles. 139
Figure 4 - 5: Comparison of velocity distributions for the three axial impellers with the theoretical wall jet model. The velocity distributions match Glauert's theory to η=1.2 after which recirculation affects the profiles. Similarity between all three impellers is maintained up to η=2.3. 140
Figure 4 - 6A: Decay of maximum velocity for the wall jet produced by the A310 impeller for various dimensionless clearances (C/D) and rotational speeds. 141
Figure 4 - 6B: Decay of maximum velocity for the wall jet produced by the 142

PBT impeller for various dimensionless clearances (C/D) and rotational speeds.
Figure 4 - 6C: Decay of maximum velocity for the wall jet produced by the HE3 impeller for various dimensionless clearances (C/D) and rotational speeds. 143
Figure 4 - 7: Velocity profile along the wall of the tank (Traverse B in Figure 4 - 3B) for the PBT impeller at C/D=1. The jet becomes the dominant flow in the theta direction only after a dimensionless height of z/T=0.67. 144
Figure 4 - 8: Turbulence in the three dimensional wall jet produced by an A310 impeller (D/T=0.58, C/D=0.68, N=600 rpm). It takes a distance of z/T=0.67 before fluctuating velocities show similarity. 145

Figure 5 - 1:Axial Velocity Measurements for an A310 D/T=058 C/D=0.68 173
Figure 5 - 2A: Discharge of a PBT in the Horizontal Plane 174
Figure 5 - 3A: Tank Set-Up (Side View) 176
Figure 5 - 3B: Position of Measurements (Top View) 176
Figure 5 - 4: Effect of Off-Bottom Clearance on Dimensionless Velocity Gradient for a D=0.19T PBT Impeller 177
Figure 5 - 5: Effect of Off-Bottom Clearance on Dimensionless Velocity Gradient for a D=0.33 PBT Impeller 178
Figure 5 - 6: Effect of Off-Bottom Clearance on Dimensionless Velocity Gradient for a D=0.50T PBT Impeller 179
Figure 5 - 7A: Effect of Off-Bottom Clearance on Dimensionless Velocity Gradient for a D=0.58T Lightnin A310 Impeller 180
Figure 3-7B: Effect of Off-Bottom Clearance on Dimensionless Velocity Gradient for a D=0.33T Chemineer HE3 Impeller 181
Figure 5 - 8: Effect of Off-Bottom Clearance on Dimensionless Velocity Gradient for a D=0.33 PBT Impeller in Bayol-35 182
Figure 5 - 9: Effect of Off-Bottom Clearance on Dimensionless Velocity Gradient with a Reduction of Scale(Tsmall/Tlarge=0.58) using PBT Impellers. 183
Figure 5 - 10: Comparison of Data from Different Experimental Configurations 184

Figure 6-1: Experimental configuration, traverse locations and location of the three dimensional wall jets in the stirred tank. 202
Figure 6-2: Three dimensional wall jet produced by a square nozzle. b is the half width of the jet in the y direction. In the tank the baffle is in the y-z plane and the tank wall is in the x-z plane. 203
Figure 6-3: Two types of three dimensional wall jet profiles. Glauert's profile is for a jet in a stagnant fluid. Bittorf's profile is for a jet with recirculating flow and is broken into two parts: the wall jet and the recirculating flow. 204
Figure 6-4 A: Dimensionless velocity profile taken below an A310 impeller, (C/T=0.33, D/T=0.5, z/T=0.29) showing that scaling of axial velocity with the tip speed produces a single profile. 205
Figure 6-4B: Dimensionless velocity profile taken above an A310 impeller (C/T=0.33, D/T=0.5, z/T=0.46) showing that the profiles no longer collapse. 205
Figure 6-5: Similarity profile for the three dimensional wall jet in based on data from Bittorf 2000. This profile is used to test local velocity profiles for scalability and thus for fully turbulent flow. Note that all data is forced to fit at U/Um=1.0 and U/Um =0.5 206
Figure 6-6A: Fully turbulent velocity profiles at z/T=0.46, C=D and D=T/3 207

for a PBT. All profiles collapse onto the jet profile
Figure 6-6B: Fully turbulent velocity profiles at z/T=0.58, C=D and D=T/3 for a PBT (see Figure 6-6A for legend). All profiles collapse. 208
Figure 6-7A: Velocity Profiles at z/T=0.71, C=D and D=T/3 for a PBT (see Figure 6-6A for legend) 209
Figure 6-7B: Fully turbulent velocity profiles at z/T=0.71, C=D and D=T/3 for a PBT with Profiles 6 & 7 eliminated (see Figure 6-6A for legend) 209
Figure 6-8A: Velocity Profiles at z/T=0.83, C=D and D=T/3 for a PBT (See Figure 6-6A for legend) 210
Figure 6-8B: Fully turbulent velocity profiles at z/T=0.83, C=D and D=T/3 for a PBT with profiles 6 & 7 eliminated. (see Figure 6-6A for legend) 210
Figure 6-9A: Velocity profiles at z/T=0.92, C=D and D=T/3 for a PBT (see Figure 6-6A for legend) 211
Figure 6-9B: Fully turbulent velocity profiles at z/T=0.92, C=D and D=T/3 for a PBT with profiles 4,5,6, &7 eliminated (See Figure 6-6A for legend) 211
Figure 6-10A: Velocity profiles at z/T=0.46, C=D/2 and D=T/2 for an A310 impeller. 212
Figure 6-10B: Fully turbulent velocity profiles at z/T=0.46, C=D/2 and D=T/2 for an A310 with profiles 7 & 8 eliminated (see Figure 6-10A for legend). 213
Figure 6- 11A: Velocity profiles at z/T=0.58, C=D/2 and D=T/2 for an A310 (see Figure 5-10A for legend). 214
Figure 6-11B: Fully turbulent velocity profiles at z/T=0.58, C=D/2 and D=T/2 for A310 with profiles 6,7& 8 eliminated (see Figure 5-10A for legend). 214
Figure 6- 12A: Velocity profiles at z/T=0.71, C=D/2 and D=T/2 for an A310 (See Figure 5-10A for legend). 215
Figure 6-12B: Fully turbulent velocity profiles at z/T=0.71, C=D/2 and D=T/2 for an A310 with profiles 5, 6, 7& 8 eliminated (see Figure 6-10A for legend). 215
Figure 6-13A: Velocity profiles at z/T=0.83, C=D/2 and D=T/2 for an A310 (see Figure 5-10A for legend). 216
Figure 6-13B: Fully turbulent velocity profiles at z/T=0.83, C=D/2 and D=T/2 for an A310 with profiles 5,6,7& 8 eliminated (see Figure 6-10A for legend) 216
Figure 6-14A: Velocity profiles at z/T=0.92, C=D/2 and D=T/2 for an A310 (see Figure 5-10A for legend). 217
Figure 6-14B: Fully turbulent velocity profiles at z/T=0.92, C=D/2 and D=T/2 for an A310 with profiles 2, 3, 4, 5, 6, 7& 8 eliminated (see Figure 5-10A for legend) 217
Figure 6-15: Impeller Reynolds number required to achieve fully turbulent conditions as z/T increases. Only at the impeller is Re=2□104 sufficient to attain fully turbulent flow. 218

Figure 7 - 1: Tank configuration and Location of Wall Jets 248
Figure 7 - 2:Tank cross section at z/T=0.9 showing measurement points for Figures 7-3 and 7-4 249
Figure 7 - 3A: Raw time series data for a A310 flow field in clear liquid (z/T=0.9, 2r/D=1.5, C/T=1/6, D/T=0.5, N=530 rpm) Note the intensity of the turbulence and the scale of the macro instability at 5 seconds. 250
Figure 7 – 3B: Smoothed time series data for a A310 flow field in clear 250

liquid (z/T=0.9, 2r/D=1.5, C/T=1/6, D/T=0.5, N=530rpm)

Figure 7 - 3C: Smoothed time series data for an A310 flow field with a solids concentration X=24wt.% and experimental conditions duplicated from Figure 7-3B. Notice the large reduction in turbulent intensity and the absence of macro instabilities. 251

Figure 7 - 4: RMS Velocity as a function of solids cloud height for an A310 impeller. There is no significant difference between the measured RMS velocities at different cloud heights and solids concentrations. (z/T=0.9, 2r/D=1.5, C/T=1/6, D/T=0.5) 252

Figure 7 - 5: Decay of maximum velocity for a wall jet produced by an A310 impeller, D/T=0.58, taken from Chapter 4. This decay of maximum velocity is used to predict cloud height 253

Figure 7 - 6: Direction of the impeller discharge stream assuming an angular discharge. The angle □ is the direction of the maximum velocity vector in the horizontal plane. 254

Figure 7 - 7: Prediction of Ucore using Model 2. Unless otherwise noted the data is for PBT impellers in water for the off-bottom clearances listed in Table 7-1. 255

Figure 7 - 8: Local maximum jet velocity at cloud height for nine cases examined by Hicks et al. (1997). The velocities remain constant between a CH=0.6 and CH=0.95. The velocities remain constant between a CH=0.6 and CH=0.95, assuming that the mean fluid velocity is unchanged by the addition of solids. 256

Figure 7 - 9: Velocity st the cloud height made dimensionless with Vtip at Njs (see legend in Figure 7-8). The data collapses and remains constant at 0.11 above a cloud height of 0.6. 257

Figure 7 - 10: Validation of the cloud height velocity models using data from Bujalski et al. (1999). (Experiments were completed using a Lightnin A310) 258

Figure A - 1: Fully Turbulent Profile at z/T=0.46 for a PBT C/D=0.5 D/T=0.33 265

Figure A - 2: Fully Turbulent Profile at z/T=0.58 for a PBT C/D=0.5 D/T=0.33 266

Figure A - 3: Velocity Profile at z/T=0.71 for a PBT C/D=0.5 D/T=0.33 267

Figure A - 4: Fully Turbulent Profile at z/T=0.71 for a PBT C/D=0.5 D/T=0.33 (Profiles 6 & 7 eliminated) 267

Figure A - 5: Velocity Profile at z/T=0.83 for a PBT C/D=0.5 D/T=0.33 268

Figure A - 6: Fully Turbulent Profile at z/T=0.83 for a PBT C/D=0.5 D/T=0.33 (Profiles 6 & 7 eliminated) 268

Figure A - 7: Velocity Profile at z/T=0.92 for a PBT C/D=1 D/T=0.33 269

Figure A - 8: Fully Turbulent Profile at z/T=0.92 for a PBT C/D=1 D/T=0.33 (Profiles 4, 5, 6 & 7 eliminated) 269

Figure A - 9: Fully Turbulent Profile at z/T=0.46 for a A310 C/D=0.67 D/T=0.5 271

Figure A - 10: Velocity Profile at z/T=0.58 for a A310 C/D=0.67 D/T=0.5 272

Figure A - 11: Fully Turbulent Profile at z/T=0.58 for a A310 C/D=0.67 D/T=0.5 (Profile 8 eliminated) 272

Figure A - 12: Velocity Profile at z/T=0.71 for a A310 C/D=0.67 D/T=0.5 273

Figure A - 13: Fully Turbulent Profile at z/T=0.71 for a A310 C/D=0.67 D/T=0.5 (Profiles 5, 6, 7 & 8 eliminated) 273

Figure A - 14: Velocity Profile at z/T=0.83 for a A310 C/D=0.67 D/T=0.5 274

Figure A - 15: Fully Turbulent Profile at z/T=0.83 for a A310 C/D=0.67 D/T=0.5 (Profiles 2, 3, 4, 5, 6, 7 & 8 eliminated) 274

Figure A - 16: Velocity Profile at z/T=0.92 for a A310 C/D=0.67 D/T=0.5 275

Figure A - 17: Fully Turbulent Profile at z/T=0.92 for a A310 C/D=0.67 D/T=0.5 (Profiles 1, 2, 3, 4, 5, 6, 7, 8 eliminated) 275
Figure A - 18: Fully Turbulent Profile at z/T=0.46 for a PBT C/D=0.5 D/T=0.5 277
Figure A - 19: Velocity Profile at z/T=0.58 for a PBT C/D=0.5 D/T=0.5 278
Figure A - 20: Fully Turbulent Profile at z/T=0.58 for a PBT C/D=0.5 D/T=0.5 (Profile 5 eliminated) 278
Figure A - 21: Velocity Profile at z/T=0.71 for a PBT C/D=0.5 D/T=0.5 279
Figure A - 22: Fully Turbulent Profile at z/T=0.71 for a PBT C/D=0.5 D/T=0.5 (Profile 5 eliminated) 279
Figure A - 23: Velocity Profile at z/T=0.83 for a PBT C/D=0.5 D/T=0.5 280
Figure A - 24: Fully Turbulent Profile at z/T=0.83 for a PBT C/D=0.5 D/T=0.5 (Profile 5 eliminated) 280
Figure A - 25: Velocity Profile at z/T=0.92 for a PBT C/D=0.5 D/T=0.5 281
Figure A - 26: Fully Turbulent Profile at z/T=0.92 for a PBT C/D=0.5 D/T=0.5 (Profiles 4 & 5 eliminated) 281
Figure A - 27: Fully Turbulent Profile at z/T=0.46 for a PBT C/D=0.67 D/T=0.5 283
Figure A - 28: Fully Turbulent Profile at z/T=0.58 for a PBT C/D=0.67 D/T=0.5 284
Figure A - 29: Velocity Profile at z/T=0.71 for a PBT C/D=0.67 D/T=0.5 285
Figure A - 30: Fully Turbulent Profile at z/T=0.71 for a PBT C/D=0.67 D/T=0.5 (Profile 5 eliminated) 285
Figure A - 31: Velocity Profile at z/T=0.83 for a PBT C/D=0.67 D/T=0.5 286
Figure A - 32: Fully Turbulent Profile at z/T=0.83 for a PBT C/D=0.67 D/T=0.5 (Profiles 3, 4 & 5 eliminated) 286
Figure A - 33: Velocity Profile at z/T=0.92 for a PBT C/D=0.67 D/T=0.5 287
Figure A - 34: Fully Turbulent Profile at z/T=0.92 for a PBT C/D=0.67 D/T=0.5 (Profiles 3, 4 & 5 eliminated) 287
Figure A - 35: Fully Turbulent Profile at z/T=0.58 for a A310 C/D=0.5 D/T=0.33 289
Figure A - 36: Fully Turbulent Profile at z/T=0.58 for a A310 C/D=0.5 D/T=0.33 290
Figure A - 37: Velocity Profile at z/T=0.71 for a A310 C/D=0.5 D/T=0.33 291
Figure A - 38: Fully Turbulent Profile at z/T=0.71 for a A310 C/D=0.5 D/T=0.33 (Profiles 6 & 7 eliminated) 291
Figure A - 39: Velocity Profile at z/T=0.83 for a A310 C/D=0.5 D/T=0.33 292
Figure A - 40: Fully Turbulent Profile at z/T=0.83 for a A310 C/D=0.5 D/T=0.33 (Profiles 4, 5, 6 & 7 eliminated) 292
Figure A - 41: Velocity Profile at z/T=0.92 for a A310 C/D=0.5 D/T=0.33 293
Figure A - 42: Fully Turbulent Profile at z/T=0.92 for a A310 C/D=0.5 D/T=0.33 (Profiles 3,4,5,6 & 7 eliminated) 293
Figure A - 43: Velocity Profile at z/T=0.46 for a A310 C/D=1 D/T=0.33 295
Figure A - 44: Fully Turbulent Profile at z/T=0.46 for a A310 C/D=1 D/T=0.33 (Profile 7 eliminated) 295
Figure A - 45: Velocity Profile at z/T=0.58 for a A310 C/D=1 D/T=0.33 296
Figure A - 46: Fully Turbulent Profile at z/T=0.58 for a A310 C/D=1 D/T=0.33 (Profiles 6 & 7 eliminated) 296
Figure A - 47: Velocity Profile at z/T=0.71 for a A310 C/D=1 D/T=0.33 297
Figure A - 48: Fully Turbulent Profile at z/T=0.71 for a A310 C/D=1 D/T=0.33 (Profiles 4, 5, 6 & 7 eliminated) 297
Figure A - 49: Velocity Profile at z/T=0.83 for a A310 C/D=0.5 D/T=0.33 298
Figure A - 50: Fully Turbulent Profile at z/T=0.83 for a A310 C/D=0.5 D/T=0.33 (Profiles 1, 2, 3, 4, 5, 6 & 7 eliminated) 298

Figure A - 51: Fully Turbulent Profile at z/T=0.46 for a HE3 C/D=0.5 D/T=0.25 300
Figure A - 52: Velocity Profile at z/T=0.58 for a HE3 C/D=0.5 D/T=0.25 301
Figure A - 53: Fully Turbulent Profile at z/T=0.58 for a HE3 C/D=0.5 D/T=0.25 (Profiles 6 & 7 eliminated) 301
Figure A - 54: Velocity Profile at z/T=0.71 for a HE3 C/D=0.5 D/T=0.25 302
Figure A - 55: Fully Turbulent Profile at z/T=0.71 for a HE3 C/D=0.5 D/T=0.25 (Profiles 5, 6 & 7 eliminated) 302
Figure A - 56: Velocity Profile at z/T=0.83 for a HE3 C/D=0.5 D/T=0.25 303
Figure A - 57: Fully Turbulent Profile at z/T=0.83 for a HE3 C/D=0.5 D/T=0.25 (Profiles 5, 6 & 7 eliminated) 303
Figure A - 58: Velocity Profile at z/T=0.92 for a HE3 C/D=0.5 D/T=0.25 304
Figure A - 59: Fully Turbulent Profile at z/T=0.92 for a HE3 C/D=0.5 D/T=0.25 (Profiles 5, 6 & 7 eliminated) 304
Figure A - 60: Velocity Profile at z/T=0.46 for a HE3 C/D=1.33 D/T=0.25 306
Figure A - 61: Fully Turbulent Profile at z/T=0.46 for a HE3 C/D=1.33 D/T=0.25 (Profile 7 eliminated) 306
Figure A - 62: Velocity Profile at z/T=0.58 for a HE3 C/D=1.33 D/T=0.25 307
Figure A - 63: Fully Turbulent Profile at z/T=0.58 for a HE3 C/D=1.33 D/T=0.25 (Profile 7 eliminated) 307
Figure A - 64: Velocity Profile at z/T=0.71 for a HE3 C/D=1.33 D/T=0.25 308
Figure A - 65: Fully Turbulent Profile at z/T=0.71 for a HE3 C/D=1.33 D/T=0.25 (Profile 7 eliminated) 308
Figure A - 66: Velocity Profile at z/T=0.83 for a HE3 C/D=1.33 D/T=0.25 309
Figure A - 67: Fully Turbulent Profile at z/T=0.83 for a HE3 C/D=1.33 D/T=0.25 (Profiles 4, 5, 6, & 7 eliminated) 309
Figure A - 68: Velocity Profile at z/T=0.92 for a HE3 C/D=1.33 D/T=0.25 310
Figure A - 69: Fully Turbulent Profile at z/T=0.92 for a HE3 C/D=1.33 D/T=0.25 (Profiles 4, 5, 6, & 7 eliminated) 310

Chapter 1

Introduction

Scientific investigation of stirred tanks started in the 1940s when Rushton first examined how the tank configuration affects power consumption for various impellers. From this beginning, investigations into various issues of mixing has led to a better understanding of all aspects of mixing. Despite the advances in the scientific knowledge of mixing technology, a better fundamental understanding is needed before mixing design can be based on well defined physical principles.

Numerous stirred tank designs are used in both industrial processes and laboratory experiments. The shape of the tank can vary from a flat bottom to a tank with a hemispherical bottom. Baffles, which reduce swirling and vortexing, come in a variety of sizes and shapes, they are generally evenly spaced along the wall, with the most common number of baffles (N_f) being three or four. Figure 1-1 shows a typical experimental configuration for a cylindrical flat bottomed tank. The baffles are of standard width (T/10), the bottom of the tank is at $z=0$, the tank height is equivalent to the tank diameter ($H=T$) and the off bottom clearance of the impeller, C, typically varies from $0.1<C/T<0.5$.

The selection of impeller determines the flow field in a stirred tank and the choice of impeller depends on the power requirements, fluid viscosity, and turbulence requirements of the process. Close clearance impellers such as the helical ribbon and the anchor impeller are commonly used in high viscosity systems, compared to axial or radial impellers that are employed in low viscosity systems. This work focuses on axial and radial impellers mixing low viscosity fluids.

Figure 1-2 shows the flow pattern for an axial impeller. The general flow pattern is downward in the center of the tank and upward along the tank wall. Flow fields for different axial impeller designs and configurations have been investigated by various authors: Ranade and Joshi (1989) Jaworski et al. (1991), Kresta and Wood (1993), Fort et al. (1993), Bakker et al. (1996), Hockey and Nouri (1996), Myers et al.

(1996), Mao et al. (1997), Sheng et al. (1998), Mishra et al. (1998), Schafer et al. (1998), and Fentiman et al. (1998). These recent investigations have shown that some impellers are good choices for gas dispersion and solid suspension while others produce low turbulence to prevent break up of microorganisms, crystals and other fragile products.

The flow pattern for a radial impeller is different from that for an axial impeller. The radial impeller produces a swirling radial jet that impinges on the wall producing upward and downward flow, with the impeller intake coming from both the top and bottom of the tank as shown in Figure 1-3. If the off bottom clearance is reduced, the flow pattern changes from a double eight to a single eight configuration (Schafer et al., 1997 Bakker and Van Den Akker 1994, and Harnby et al. 1992). For multiple RT's the clearance between the impellers dictates the flow pattern observed. The closer the impellers are, the more interactions they have with each other (Rutherford et al. 1996). In addition to the flow pattern, one of the largest differences between the radial and axial impellers is that the radial impeller requires significantly more power to operate (Harnby et al. 1992).

This chapter summarizes fundamental information for four topics that will be built upon in the remainder of the thesis: turbulent length scales in a stirred tank, dimensionless numbers and scale-up, jets, and solids suspension. The flow in a stirred tank is a semi-random cycle of turbulent structures that can be averaged over time to show the flow patterns discussed above. The various turbulent length scales allow definition of a range of dimensionless groups, which can be used to scale-up the bench scale model to a full size industrial reactor. Besides the various turbulent scales the mean flow field in the tank is important for determining the more active regions inside the stirred reactor. Fort (1986) first suggested, the mean flow pattern in a stirred tank can be considered as a series of jets. Given mean flow pattern and turbulence structures in the stirred tank, models can be developed for how solid particles are suspended in the tank and in particular for the solids distribution throughout the tank.

1.1 Turbulent Length Scales

In a stirred tank, turbulence is created by the rotation of the impeller and this energy goes into mixing the fluid. Whenever turbulence is present, characteristic length scales or eddy sizes characterize the flow in the system. Figure 1-4 shows representative eddy sizes in a stirred tank. In this figure, three important length scales are shown: the most energetic eddies are trailing vortices attached to the impeller blade; the smallest length scales or the Kolmogorov length scale are limited by the viscosity of the fluid; and the largest scales appear as macro-instabilities in the mean circulation pattern. The impeller region is important to examine because it is the location at which mixing in the tank starts and the turbulence is created. The turbulence inside the tank determines the best areas for micro mixing and governs mixing in the outer regions of the tank.

The turbulent length scale theory is applied in two chapters of this work. Chapter 5 examines the extent of which the mean flow pattern influences mixing in the stirred tanks and concludes that the large scale structures inside the tank contribute ot much of the mixing in the outer regions. While, Chapter 7 examines the turbulent structures in the top of the tank and influence solids have on the turbulent structures. While much of the work concentrates on the large scale structures inside the tanks it is important to examine the impeller region because this is the location at which the turbulence is created. Micromixing is closely associated with the smaller turbulent scales created by the impeller region. Micromixing is examined to show that the best feed location for competitive reactive systems is in the impeller region and not near the top of the tank were the mixing is dominated by the large scale structures. Finally the large scale structures or macro-instabilities (MI's) are examined.

Turbulence in the impeller region

The impeller region is important to examine because this is the location at which the mixing in a stirred tank begins also this is the location at which the most energetic eddies, integral length scale (L), are created. The eddies of length scale, L, are formed as vortices attached to the impeller blades. Van't Riet and Smith (1975) first examined these for the Rushton turbine, followed by Mahouast et al. (1989) Wu and Patterson (1989), Yianneskis and Whitelaw (1993), Stoots and Calabrese (1995), Rutherford et al. (1996), and Lee and Yianneskis (1998). Once the vortices behind the RT blades were discovered investigation into other impellers showed similar vortex structures attached to other impeller blades. Kresta and Wood (1993) examined the PBT and showed that the size of the integral length scale is a fraction of the impeller diameter, L=D/10. Schafer et al. (1998) and Zhou and Kresta (1996) also examined the vortex structures for the PBT and showed that the size of the vortex structure is comparable to that for the RT. Zhou and Kresta (1996) suggested that the vortices behind the A310 airfoil blades are also on the order of one-tenth the impeller diameter in size, based on flow visualization experiments.

The flow in the impeller discharge stream is highly turbulent and is treated as locally isotropic, based on the observation that the values of the fluctuating velocities in all three directions are equal in value (Zhou and Kresta, 1996, Hockey and Nouri, 1996). More recently, Lee and Yianneskis (1998) questioned the assumption of local isotropy in the impeller discharge stream. They show time averaged, angle resolved measurements in a RT discharge stream. Angle resolved measurements take a velocity measurement at the same point in the impeller rotation each time. For example, one angle resolved measurement would occur at 10° in front of the impeller blade while the next angle resolved velocity measurement might occur at 25° in front of the impeller blade. Lee and Yianneskis (1998) show small regions in the discharge that can not be considered locally isotropic. This can only be shown when angle resolved measurements are taken because as was previously stated, Zhou and Kresta (1996) and Hockey and Nouri (1996) showed that the fluctuating velocities are equal in all directions when time averaged measurements are used.

After the energy is transferred from the impeller to the fluid, the energy must be dissipated. The energy dissipation rate (ε) is frequently estimated using the impeller power input divided by the liquid mass inside the tank (Baldi et al. 1978). Zhou and Kresta (1996), and Mersmann et al. (1998) showed that the energy dissipation rate depends on the location in the tank and on the type of impeller. The impeller region generally has a higher dissipation rate than the rest of the tank, which indicates that most of the energy the impeller generates is dissipated in a small portion of the tank (Zhou and Kresta, 1996). One equation used for estimating the dissipation rate is:

$$\varepsilon = A\frac{v_l^3}{L} \tag{1.1}$$

The value of A is equal to 1 if the flow is isotropic, v_l is the characteristic fluctuating velocity and L is the integral length scale. Assuming mean and spatially averaged velocity fluctuations Equation 1.1 can be used to estimate the dissipation rate in the impeller region.

Micromixing

Micromixing is important because this is the last length scale that reactance see before they react and is governed by the smallest turbulent length scale that occurs inside the stirred reactor. The smallest scale is determined by the local dissipation rate which is dependent on location in side the stirred reactor (Zhou and Kresta, 1996). The dissipation rate is determined by turbulent eddy energy spectrum which is shown in Figure 1-4.

The turbulent energy is transferred through the energy spectrum until the smallest scale dissipates the remaining energy. The smallest possible turbulent scales are the Kolmogorov length scales:

$$\lambda_k = \left(\frac{\nu^3}{\varepsilon}\right)^{1/4} \tag{1.2}$$

The higher the rate of energy dissipation, the smaller the Kolmogorov length scale. This has been shown to be an important scale when examining reacting processes and was linked with micro-mixing process in a stirred tank by Bourne and Dell'ava (1987).

Although many papers have been published on micromixing, one of the key authors in the design of stirred tank reactors using the concept of micromixing is J.R. Bourne. Bourne and co-authors completed many semi-batch experiments based on competing reactions:

$$A+B \Rightarrow C$$

$$C+A \Rightarrow D$$

(Baldyga and Bourne, 1989, 1989, 1991, 1992, Bourne and Hibbler 1990, Gholap, et al. 1994 Baldyga et al. 1997). In these reactions, stoichometric amounts of A and B are fed into the stirred reactor. A and B react instantaneously and can not exist together. If the system is perfectly mixed, the only product produced is C. If the reaction goes to D, inhomogenity at the microscopic level is present and, therefore, the tank is not perfectly mixed. Micromixing (and therefore the reaction) does not occur in the inertial-convective range; it occurs in the viscous-diffusive subrange. Bourne and his associates have tested the degree to which systems are mixed for different sets of conditions. They varied the viscosities, feed pipe diameters, feed locations, tank diameters and impeller diameters. The results Bourne obtained, in short, are:

- The lower the viscosity the better the micromixing at a constant Reynolds number (Gohlop, et al. 1994).
- The conversion of product remains constant with tank scale up using a constant mixing modulus (M) $\left[M = k_2 c_B \frac{\lambda_k}{4 * Diffusivity}\right]$ where k_2 is a second order rate constant and c_B is the concentration of reactant B (Baldyga & Bourne 1988).
- The best placement for the inlet is in the suction zone of the impeller (Gohlop, Petrozzi & Bourne 1994).

Bourne and his associates developed the mixing modulus for scale up using theory and experimental evidence and a detailed review can be found in Baldyga and Pohorecki (1995).

Another model, the generalized mixing model, examines mixing fresh or new fluid into the system and is divided into four stages. The first three are meso-mixing stages that consist of erosion, dilution and incorporation of the fresh fluid. The fourth is a micromixing stage of interaction for reaction (Villermaux and Falk 1994). Meso-mixing becomes a factor when the mixing rate is less than the reacting rate (Baldyga and Bourne, 1991). Experimental evidence for the four-stage model was obtained using a semi-batch mixing system (Villermaux and Falk, 1994).

Large Scale Instabilities

The flow field in stirred tanks can be very unstable with many factors affecting the instantaneous flow pattern. One of the major phenomena relevant to the instantaneous flow pattern is large scale or macro-instabilities (MI). Macro-instabilities are important to examine because they are such large scales of motion that the mechanical integrity of the internals can be compromised. The larger and stronger the MI's, the stronger the vessel needs to be. Shown later is the ways in which MI's affect solids distribution and other mixing process results.

Although much is understood about the mean impeller discharge field and the mean flow throughout the stirred tank, understanding of the specifics of the instantaneous and macro instabilities of the flow is still developing. Bakker et al. (1996) and Myers et al. (1997) used digital particle image velocimetry (DIPV) to show that none of the instantaneous flow fields measured reproduces the mean flow field. The flow is chaotic and is dominated by various structures as seen in Figure 1-5 from Bakker et al. (1996). In this figure, large-scale structures can be identified and the only constraint upon maximum size of the macro instabilities is the tank size. The frequency of MI's varies depending upon the system being examined. Throughout the papers examined, the authors have all agreed that the frequency of the MI's is much lower then the blade passage frequency (Montes et al., 1997, Bruha et al., 1996, 1995, 1994 and 1993).

The occurrence of MIs along the tank baffles was examined by Bruha et al. in 1992. Frequencies were measured for three types of axial impellers (3, 4 & 6 bladed-pitched blade turbines with a blade angle of 45°). Bruha et al. (1993) found that the frequency of the large-scale phenomenon was dependent upon impeller size and type and baffle configuration. The larger impeller produced a more dominant frequency in the MI. The baffle configuration that increased the strength of the MI was a multiple of the number of impeller blades; hence, for a four bladed PBT 4 baffles gave the highest occurrence of MI's. The aligning of the impeller blades also appeared to affect the MI's, especially in a geometry with a large impeller.

The frequency of the macro-instabilities increases linearly with the impeller tip speed as seen in figures from Bruha et al. (1996 and 1993). Their data also shows that the impeller clearance affects the relationship between N and f_{MI}. For the three different clearances examined (C/T=0.2, 0.35 and 0.5), as the impeller speed increases at the lower clearance, the frequency of the MI's increases at a rate faster than at the higher clearance, as is shown in Figure 1-6 (data from Bruha et al. 1994). Bruha used a mean turbulent macro instability frequency to collapse his data. He chose a reference point and forced the other two clearances to scale with that reference point. Grgic (1998) showed that the frequencies are dependent on the impeller geometry, with the PBT producing the strongest and most coherent instabilities and fluid flow impellers having a more stable flow pattern.

Understanding the turbulent structures in any fluid system is important to determine the what the dominant mixing structures for micro, meso and macro mixing.

It is shown in Chapter 7 how the macro scale mixing structures are affected is a two phase solids-liquid system.

1.2 Dimensionless Numbers and Scale-Up

Dimensionless numbers are important for scaling of any system. For stirred tanks, a variety of dimensionless numbers are used to define its operation. Although some dimensionless variables are used for scale-up, not all scale up approaches are dimensionless. Various methods can be used to determine dimensionless variables.

Chapter 7 examines scale-up of solid suspension systems in which new dimensionless equations are created to scale the system. It is important to determine ways in which dimensionless variables are created and the review the important dimensionless variables that define flow in a stirred tank. Using the dimensionless variables scale-up techniques for stirred reactors are shown.

Dimensionless Numbers

One method to determine dimensionless numbers is the Buckingham Π-Theorem, which is a dimensional analysis method that relates the number of variables (density, diameter, velocity, etc.), to the number of dimensions (length, time, weight, etc.) (Bird et al., 1960). Subtracting the dimensions from the variables gives the number of independent dimensionless variables. After the number of independent variables has been determined, the next step is to form a combination of these variables. This is sometimes done by guessing or by the series method approach. Because of the lack of fundamental physics contained in this step, the Buckingham Π-Theorem is not the most reliable method of determining dimensionless variables.

Dimensional analysis is important in connection with scale-up and scale-down and is significant when converting lab results to the industrial setting. The process of scale-up assumes that there are observations independent of size that are consistent over some range (Dickey 1992). If the dimensionless variables are based on physical interpretations, like a ratio of forces, they may provide additional interpretation for the processes occurring in the system. Next we consider the important dimensionless groups for a stirred tank, and their application to scaling of experimental results.

Dimensionless Numbers for Stirred Tanks

The theory behind standard dimensionless variables in defining a stirred tank flow started to be developed in the 1940's and is still under development. The first numbers defined for a stirred tank are the Reynolds number and the power number (Rushton et al., 1946, 1950a and 1950b):

$$\mathrm{Re} = \frac{N D^2}{\nu} \tag{1.3}$$

$$\mathrm{Po} = \frac{P}{\rho N^3 D^5} \tag{1.4}$$

Here N, is the rotational speed, D is the impeller diameter, P is the power input, ρ is the density and ν is the kinimatic viscosity. These dimensionless variables are related to definine the point at which fully turbulent flow occurs in the impeller region. The limits of the Reynolds number were determined from the power number curve. When the power number becomes constant with increasing Reynolds numbers, the flow is considered fully turbulent. The laminar regime extends over the range for which the power number decreases linearly with increasing Reynolds numbers. The fully turbulent region starts at $\mathrm{Re}=2\times10^4$ and the laminar region ends at Re=10 (Rushton, 1946, 1950a and 1950b).

The Froude number, the ratio of inertial to gravitational forces, shows the way gravity affects the stirred vessel (Harnby et al. 1992):

$$\mathrm{Fr} = \frac{N^2 D}{g} \tag{1.5}$$

This dimensionless variable determines when surface vortexing occurs and is generally not considered for baffled tanks since baffles prevent the formation of the surface vortex.

The pumping capacity, or the volume of fluid that an impeller moves through its blades, is an important characteristic of the impeller. Flow through the impeller is sometimes used for scaling and is defined as (Harnby et al. 1992):

$$\mathrm{Fl} = \frac{Q}{ND^3} \qquad \textbf{(1.6)}$$

The flow number, Fl, is impeller specific. Another variable is the momentum number (Grenville and Musgrove, 1998):

$$\mathrm{Mo} = \frac{M}{N^2D^4} \qquad \textbf{(1.7)}$$

M is the momentum per unit mass produced and Mo is the momentum number. Variables like Fl, Mo, and Po are all dependent on the impeller type but can be approximately related to each other (Grenville and Musgrove, 1998):

- $\mathrm{Fl} \propto \mathrm{Po}^{1/3}$
- $\mathrm{Mo} \propto \mathrm{Po}^{2/3}$

Dimensionless groups are used as tools for scale-up but using the wrong dimensionless number in analysis and scale-up may lead to improper conclusions. Care should be taken in choosing the basis of scaling, since the flow regime may change, and since scaling-up also results in a larger range of turbulent eddies in, which may cause some problems. Scaling with dimensionless numbers and similarity are useful concepts, but only if used carefully with the key physical constraints well defined.

Scale Up

Maintenance of similarity upon scale-up is an important factor in the success of a design. Similarity defines the physical situation, whereas dimensional analysis justifies it mathematically (Dickey 1993). Tatterson (1993) and Dickey (1992) defined many types of similarity: process similarity, geometric similarity, mechanical similarity, and less common types of similarity. Examples and explanations of each type are given below:

1) Process Similarity- a tank mixed by a jet or an impeller is similar given the fact that energy is being used to mix the fluid (the general process is similar)
2) Geometric Similarity - a tank that is scaled up simply by the proportion of increased size on all dimensions.
3) Mechanical Similarity - consists of Static Similarity, Kinematic Similarity, and Dynamic Similarity.
    - Static Similarity applies to solid bodies where static conditions apply.
    - Kinematic Similarity applies to moving systems, with particles that flow along geometrically similar paths.
    - Dynamic Similarity applies to moving systems, where the ratio of corresponding forces is equal, e.g. the Reynolds number.
4) Less Common Types of Similarity- Thermal and Chemical Similarity.
    - Thermal Similarity has the same temperature gradients
    - Chemical Similarity has the same concentration gradients.

Similarity is a useful tool in scale-up, but it needs to be justified and experimentally proven to work well. Bench scale models or pilot plants are built so improvements can be made or to determine if the desired process will work. Zlokarnik (1998) outlined the applicability of dimensional analysis and the available knowledge of the problem based on a five-step procedure:

1. Is the physics of the phenomenon known? If not, dimensional analysis can not be applied.
2. If only enough is known about the physics to compile a list of variables for Buckingham Π, the Π list is unreliable.

3. If all relevant physical variables of the system are known and can be maintained, the application of dimensional analysis for scale-up is reliable.
4. If the problem can be expressed in terms of a mathematical equation there will be more insight into the Π relationship and a reduction of the dimensionless variables may be possible.
5. If a mathematical solution to the problem exists, dimensional analysis is not needed.

If geometric similarity is maintained on scale-up, only one factor can still be varied: how fast to rotate the impeller. This is dependent on what will be kept constant:

- Tip speed $N_2 = N_1\left(\frac{D_1}{D_2}\right)$
- Reynolds number or momentum number (Eq. 1.3 & 1.7) $N_2 = N_1\left(\frac{D_1}{D_2}\right)^2$
- Power per impeller sweep volume (Eq. 1.5) $N_2 = N_1\left(\frac{D_1}{D_2}\right)^{2/3}$
- Constant tank turnover time (Eq. 1.6) $N_2 = N_1$

Each one of these variables can be used for scale-up but each has a different effect on the turbulence in the tank. Figure 1-7 shows what happens to the Reynolds number on scale up for each of the scaling methods above. The figure shows scale-up for a bench scale model operated at a $Re=3\times10^4$ and a $D=0.1$m. Notice that in one of the cases, constant tank turn over time, the turbulence drops below the fully developed regime almost immediately. On the other hand, when power per unit volume and tip speed are kept constant the turbulence in the impeller sweep volume increases.

Scale-down is also important, and Figure 1-8 shows what happens to the turbulence when the process is scaled down. The model was scaled down from $Re=1\times10^6$ and $D=5$m. Figure 1-8 shows that for scale down based on constant power per unit volume and tip speed the flow becomes transitional for a scale down factor greater than 5. This is can be a problem when trying to model what is occurring in an industrial scale reactor. If Re is kept constant on a bench scale D=0.1m the rotational speed of the impeller would have to be 6000RPM. This is not a realistic speed for a bench scale model.

Scale up is an important part of mixing, it is dependent on what process requirements are needed, and there is not necessarily a best method. Each system must be individually examined to determine the best method for scale-up.

1.3 Jets

Jets are an important part of fluid dynamics. Jets have been well researched and analytical solutions for velocity decay, expansion and velocity profile have been mathematically defined. There are two main types of jets: free jets and wall jets. With the only physical difference is that the wall jet travels along a boundary with a no slip condition, despite this difference the outer layer of the wall jet is identical to that of a free jet. Figure 1-9 shows the path of a wall jet as it travels. This figure shows as the jet travels it expands and the velocity decays.

Regardless of this distinction between wall and free jets, all turbulent jets obey similarity of the velocity profile with decay of the maximum velocity and expansion predicted by the Reynolds Averaged Navier-Stokes (RANS) equations. Jets maintain a self-similar profile that is maintained throughout the jets path. Figure 1-10 shows the velocity profiles of a wall jet and Figure 1-11 shows the velocity profiles collapsed into a single similarity profile. The similarity profile consists of streamwise velocities in the jet made dimensionless with the local maximum velocity, and distances made dimensionless with the half width of the jet. A wall jet consists of two parts: the outer layer and the inner layer. The outer layer is modeled as a free jet and the free jet properties are covered in the next section. The inner layer of the wall jet is affected by the wall boundary; however, the inner layer does not affect the decay and the expansion, which follow the same results as free jet theory.

Wall jets are extensively used in this thesis and are referred to in Chapters 3, 4, 5, 6 and 7. Free jet theory is covered here mainly for is application to the outer layer of the wall jet, this section also provides the basic scaling theory which is applied to the wall jet. The wall jet section covers basic theory but concentrates on the innerlayer of the wall jet because the outer layer theory is covered in the free jet section. Finally shown are locations at which jets have already been shown in a stirred tank.

Free Jets

A jet's cross-stream expansion and its streamwise velocity decay can be derived from the Reynolds Averaged Navier-Stokes (RANS) equations . These can be derived from the RANS equations in Cartesian coordinates where position components are x, y, z and the corresponding velocity components are u, v, w. In cylindrical coordinates, the position components are z, r, θ and the corresponding velocities components are u, v, w. The derivation of the decay and expansion has been done for various types of free jets and can be found in Rajaratnam (1976). The derivation involves several assumptions:

- the flow is fully turbulent, hence the viscous shear stress can be neglected relative to the turbulent stresses
- body forces are balanced by static pressure
- the jet is axi-symmetric
  - in radial coordinates $\partial/\partial\theta=0$
  - in axial coordinates $(\partial/\partial y)_{0\rightarrow y}=(\partial/\partial y)_{0\rightarrow -y}$
    - this in not true for jets in cross flows
- tangential velocities within the jet are taken to be zero
  - this is not true for swirling jets
- the length scale in the cross-stream direction is much smaller then the length scale in the co-stream direction.
  - radial coordinates $\partial/\partial r >> \partial/\partial z$ or
  - axial coordinates $\partial/\partial y >> \partial/\partial z$

- the velocity in the streamwise direction is much larger then the velocity in the cross stream direction, hence,
    - axial and radial coordinates u>>v
- Momentum flux remains constant at any point along the jet

Using the assumptions above the reduced form of the RANS equations for a three dimensional free jet in Cartesian coordinates:

$$U\frac{\partial U}{\partial z}+V\frac{\partial U}{\partial y}+W\frac{\partial U}{\partial x}=-\left[\frac{\partial \overline{u'v'}}{\partial y}+\frac{\partial \overline{u'w'}}{\partial x}\right] \tag{1.8}$$

The V (or W) component of the equation reduces the dynamic pressure gradient is balanced by the Reynolds stress.

For a two dimensional free jet the equations reduce to:

$$U\frac{\partial U}{\partial z}+V\frac{\partial U}{\partial y}=-\left[\frac{\partial \overline{u'v'}}{\partial y}\right] \tag{1.9}$$

Here the V component shows that the dynamic pressure gradient is balanced by the Reynolds stress.

From this point a variety of dimensionless distance, velocity and shear stress variables are used to determine the similarity solution (See Rajaratnam and co-authors 1970, 1974 & 1976). The solution found from the dimensionless form of Equation 1.8 and 1.9 is:

$$U_m \propto z^p \quad b \propto z^q \tag{1.10}$$

The other equation required to attain the similarity solution for the exponents, p and q, is the integral momentum equation which must remain constant at any point in the jet:

$$\frac{d}{dz}\int_{-\infty}^{\infty}\int_{-\infty}^{\infty}U^2 dydx \qquad (1.11)$$

From this equation, the variables p and q are solved. Equation 1.11 for a two dimensional system does not have to be integrated with respect to x. Based on the derivation by Rajaratnam (1970, 1974 & 1976) the expansion rate for a two dimensional or three dimensional jet is:

$$b_{1/2} \propto x \qquad (1.12)$$

However the velocity decay depends on the type of jet and decays one of two ways:

$$u_m \propto \frac{1}{x} \qquad (1.13a)$$

This is the decay rate for most jets.

$$u_m \propto \frac{1}{\sqrt{x}} \qquad (1.13b)$$

This is the decay rate for a two dimensional plane jet. Besides expansion and decay of the jet, the similarity profile also defines the jet. Most of the common types of jets have been reviewed by Rajaratnam (1976).

Besides the velocity decay and expansion, the similarity profile can also be mathematically defined. The similarity profile for a two dimensional jet begins with the equations of motion in their reduced two-dimensional form:

$$U\frac{\partial U}{\partial z} + V\frac{\partial U}{\partial y} = \frac{1}{\rho}\frac{\partial \tau}{\partial y} \qquad (1.14)$$

One similarity solution the jet profile is derived using the Goertler approximation. Goertler (1942) used Prandtl's approximation for the turbulent shear stress:

$$\tau = \rho\varepsilon\frac{\partial U}{\partial y} \qquad (1.15)$$

Here, ε is the kinematic eddy viscosity and it is assumed that $\rho\varepsilon >> \mu$. Goertler further assumed that the eddy viscosity is proportional to the local maximum velocity and the half width of the jet:

$$\varepsilon \propto U_m b \qquad \varepsilon = kU_m b \tag{1.16}$$

Here, k is a proportionality constant. From this, Goertler assumed the dimensionless velocity was a function of the distance traveled as well as the transverse location in the jet:

$$\frac{U}{U_m} = F'\left(\sigma\frac{y}{z}\right) = F'(\xi) \tag{1.17}$$

Here, σ is a constant, y is the distance from the center of the jet and z is the distance the jet has traveled. Substituting this information into the equations of motion (Equation 16) the integrated form becomes:

$$F^2 + F' = \text{Constant}$$

Here, F' is the first derivative and F is the solved form. Using the boundary conditions in Table 1 for a jet in a stagnant fluid Goertler 's (1942) similarity solution in Rajaratnam (1976) is obtained:

$$F' = \frac{U}{U_m} = 1 - \tanh^2(\xi) \tag{1.18}$$

This solution works very well for jets in stagnant fluid (Rajarnatam, 1976). Other similarity solutions include the Tollmien(1926) Solution who approximates the shear stress using the Prandtl mixing length formula where ℓ is the mixing length:

$$\tau = -\rho\ell^2\left(\frac{\partial U}{\partial y}\right)^2 \tag{1.19}$$

His solutions is a non-linear second-order differential equation:

$$(F'')^2 + FF' = 0 \tag{1.20}$$

This equation was numerical solved to obtain the similarity solution. The numerical results can also be found in Rajarnatam, 1976. Many other types of assumptions can be made for the approximation can be made to determine a free jet profile. Weidman et al. (1997) analytically and numerically solved the Prandtl boundary layer equations for various types of systems including jets. Pozzi and Bassano (1995) applied the Pade approximations to solve for the free jet similarity solution. Newman et al. (1972) approximated the similarity solution to be an exponential.

Free jets are an important part of fluid mechanics and theory intruduced here is applied later in the thesis.

Table 1-1: Boundary conditions for a jet in a stagnant fluid.

I)	$y=0$	$\xi=0$	$U/U_m = F'(0) = 1$
II)	$y=0$	$\xi=0$	$\tau=0$
III)	$y=0$	$\xi=0$	$V=0$
IV)	$y=\infty$	$\xi=\infty$	$F'=0$
V)	$y=\infty$	$\xi=\infty$	$\tau=0$

Wall Jets

The difference between a free jet and a wall jet is that a wall jet has two asymmetric parts (Figure 1-9): the inner layer resembling a boundary layer and the outer layer acting like a free jet. The initial theoretical investigation into wall jets was reported by Glauert (1956). Bakke (1957) was the first to experimentally investigate a radial wall jet. Since this time wall jets in various experimental configurations have been investigated: in a moving stream (Kruka and Eskinazi, 1964), along a cylinder (Starr and Sparrow, 1967), buoyant vertical (Bains, 1985), two dimensional (Glauert 1956, Bakke, 1957 Chao & Sandborn, 1966, Launder & Rodi 1983, and Eriksson et al., 1998) and three-dimensional (Rajaratnam & Pani, 1970 & 1974, Newman et al., 1972, Swamy & Bandyopadhyay, 1975 and Padmanabham & Gowda, 1991). The properties of each these are slightly different.

The two-dimensional wall jet was first type of wall jet to be examined (Glauert 1956 and Bakke 1957). Typical experiments for two-dimensional wall jet analysis involve a circular jet impinging on a plate creating a two dimensional radial jet (Bakke, 1957, Chao & Sandborn, 1966 Launder and Rodi 1983). Alternately, a nozzle parallel to the plate can create a two-dimensional wall jet (Launder and Rodi 1981 & 1983, Eriksson et al., 1998). Through the work accumulated on two-dimensional wall jets, the jet width, expansion and velocity decay have been derived and confirmed. Launder and Rodi (1981 and 1983) review the expansion and decay rates for all experiments completed up to 1983. Since this time, the work on wall jets has mostly considered accurate measurement of near wall turbulence (Eriksson et al., 1998).

The three-dimensional wall jet has been examined by Newman et al. (1972), and reviewed by Rajaratnam & Pani (1970 & 1974) who compiled all available data and compared the similarity profiles for three-dimensional wall jets. Swamy and Bandyopadhyay (1975) showed that there are three stages to any three-dimensional wall jet:

- Potential Core
    - Region where the jet develops before it starts to decay
    - Velocities in this area are usually constant
- Characteristic Decay
    - Decay is dependent on the orifice configuration
    - $u_m \propto x^n$
- Radial Decay
    - Decays ideally according as derived by the Navier-Stokes equations
    - $u_m \propto x^{-1}$

The expansion rate for a wall jet is linear as it is for the free jet. Wall jets have been produced using different types of nozzles: circular, square, triangular, and oblong (Rajaratnam and Pani, 1974). For all of these configurations, the velocity in the radial decay region decays inversely with the distance traveled. Padmanabham and Gowda

(1991) reviewed the literature for experimental data completed on wall jets. They found that the decay exponent in the radial decay region, n, varied from –0.16 to –0.85 depending on the experimental configuration. Padmanabham and Gowda (1991) also show that literature values for the radial decay region have varied from the ideal of -1. The variation of the decay exponent in the radial decay region ranged from -1.0 to -1.27. This shows that depending on the experimental configuration the decay exponent may deviate from the ideal.

The expansion of the wall jet also depends on the configuration. Bains (1985) examined the expansion rate for a circular three-dimensional wall jet in three different wall configurations: in the corner of two walls perpendicular to each other, along a plane, and a jet flowing along a rod. Bains (1985) showed that the expansion of the jet depends on the wall configuration and each side of the jet may expand at different rates.

Recently a study of a three-dimensional wall jet on a convex cylindrical surface was done by Gowda and Durbha (1999). They created a circular wall jet using a 10mm orifice. The jet traveled 600 mm on a flat plate before traveling 1250mm on a curved surface of one of three different radii varying from a sight curvature to a large curvature (radius=3500, 1500 and 350mm). Gowda and Durbha (1999) found that the curvature affected both the decay of the jet and the expansion rate of the jet. At the highest curvature the jet decay has a decay exponent more then double the ideal decay exponent ($u_m \propto x^{-2.19}$), however the lower the curvature the smaller the deviation from ideal (medium curvature $u_m \propto x^{-1.63}$; lowest curvature $u_m \propto x^{-1.42}$). The jet not only decayed faster on the highest curvature, it also expanded faster.

The similarity solution of a wall jet consists of two part: the outer layer and the inner boundary layer (Glauert, 1956). The velocity profile of the outer layer of the wall can be defined as a free jet while the inner layer is defined by boundary layer solutions.

The inner layer or boundary layer of the wall jet is influenced by the shear stress along the wall. The shear stress along the boundary of the wall jet influences the velocity profile of the inner layer and the boundary layer thickness (δ) of the jet.

To determine the velocity profile of the inner layer the dimensionless variables need to be defined. The dimensionless distance is, y^+ and the dimensionless velocity is u^+ these dimensionless variables are defined differently for the inner layer:

$$y^+ = \frac{u^* y}{v} \qquad u^+ = \frac{u}{u^*} \qquad u^* = \sqrt{\frac{\tau_o}{\rho}} \tag{1.21}$$

The shear stress τ_o is required to calculate the velocity u^*, which in turn is required to determine the dimensionless distance, y^+, and dimensionless velocity u^+. Abrahamsson et al., 1994 showed that shear stress can be estimated from the skin friction coefficient, c_f, at the wall:

$$c_f = \frac{\tau_o}{\frac{1}{2}\rho U_{Nozzle}^2} \tag{1.22}$$

The skin friction coefficient is a function of nozzle Reynolds number (Abrahamsson et al., 1994):

$$c_f = 0.0315 \mathrm{Re}_{max}^{-0.182} \tag{1.23}$$

This correlation matches data from Eriksson et al. (1998). Equations 1.14-1.16 are used to help determine the velocity profile of the inner layer of the wall jet. Abrahamsson et al. (1994) measured the velocity profile and determined that it follows a logarithmic function:

$$u^+ = 2.44 \ln y^+ + 5.0 \tag{1.24}$$

This equation is valid from a range of $y^+=10$ to $y=\delta$ (or $y^+=u^*\delta/v$). Gerodimos and So (1997) showed that Equation 1.17 is valid in the boundary layer of a wall jet. To complete the profile in the inner layer, a linear relationship is used to determine the profile for values of $y^+<10$:

$$u^+ = y^+ \tag{1.25}$$

Here y^+ is the dimensional distance and u^+ is the dimensionless velocity: Equations 1.17 and 1.18 fully define the inner layer of the wall jet. This along with a

The inner layer along with the solutions for the outer layer of the wall jet as defined by the free jet similarity equations determine the completed similarity profile as shown in Figure 1-10. The similarly solution for the wall jet is later applied in this thesis.

Free Jets in Stirred Tanks

The first location at which jets were found in a stirred tank was the impeller region. The impeller discharge stream for both radial and axial impellers can be considered a type of swirling jet. Investigation into swirling jets began with Rose (1962), Chigier and Chervinsky (1965 and 1967), when they examined the swirling jet issuing from a round office. The reduced RANS equation for a swirling radial jet is different then that of a radial free jet:

$$U\frac{\partial U}{\partial z}+V\frac{\partial U}{\partial r}+W\frac{\partial U}{\partial \theta}=-\left[\frac{\partial \overline{u'v'}}{\partial y}+\frac{\partial \overline{u'w'}}{\partial \theta}\right] \qquad \textbf{(1.26)}$$

The major difference between this equation and the radial jet equation is the θ and W terms are no longer zero because of the swirl.

Chigier and Chervinsky, 1965 and 1967 classified there are three types of swirling jet with, weak, moderate and strong swirl. The strength of the swirl affects the shape of the free jet (Chigier and Chervinsky, 1965 and 1967):

- Weak swirl ($W_m/U_m<0.2$)
    - the shape of the jet is the same as a jet with no swirl
    - slight reduction in the magnitude of the jet (maximum velocity)

- Moderate swirl ($0.4 \leq W_m/U_m < 0.6$)
    - larger reduction in the magnitude of the velocity
    - the jet profile is more spread out in the radial direction
- Strong swirl ($W_m/U_m \geq 0.6$)
    - the maximum is no longer at the center
    - the jet profile is even more spread out in the radial direction

Here W_m is the local maximum swirl velocity and u_m is the local maximum velocity in the jet. The more swirl within the jet, the faster it expands (Rajaratnam, 1976). This analysis was done for a swirling jet issuing from a circular nozzle. This is similar to the discharge from an axial impeller. Per et al. (1996) examined the discharge from a marine impeller. They found that it took three impeller diameters before the mean axial velocity became self-similar and 12 impeller diameters for the other quantities to become self-similar. In a stirred tank, the impeller is clearance is less then three diameters; hence, there is not enough room for the impeller jet to become self-similar.

Another type of swirling jet is the radial swirling jet and this was first investigated by Kolar (1982). In this jet, the maximum is always at the center of the jet but the decay of the maximum depends on the swirl of the jet. Kolar et al. (1984) showed that the discharge stream from a RT has similarity, which has also been shown by Nouri et al. (1987), and Kresta and Wood (1991).

Throughout the thesis it is shown that jets are an integral part of explaining the flow in a stirred tank. It is shown that the flow along the walls of a stirred tank can be modeled as a wall jet.

1.4 Solid Suspension

Solids suspension is an important part of mixing that has been examined since Zwietering (1958), who examined the point when all of the solids are suspended off the bottom of the tank. There are three different phases of off bottom solid suspension:

1) bottom or corner fillets
2) just suspended speed (Njs), or complete off bottom suspension
3) complete uniformity or homogeneous suspension

Each of these has operational advantages and disadvantages. Just suspended speed is the point at which no solids are on the bottom of the tank for more than 1-2 seconds. At just suspended conditions, there is maximum contact between the liquid and the particles. The entire particle is surrounded by the liquid, ensuring maximum surface contact for reactions and mass transfer (Nienow, 1968, Harnby et al. 1992).

The advantage to having bottom / corner fillets is the considerable power savings. Bottom/corner fillet conditions occur at speeds up to 30% lower than Njs. Since power is proportional to rotational speed cubed, operating at a speed lower then Njs reduces the power requirements significantly (Harnby et al., 1992 and Brucato and Brucato, 1998). Complete uniformity is important for some industrial applications, as slurry catalyst reactors and some configurations of ore leaching vessels.

Chapter 7 uses the concepts of just suspended speed and solids distribution. Both of which are covered here in some detail.

Just suspended speed

The just suspended speed (Njs) is the most common value examined, because this is the point at which the fluid has maximum contact with the particle. However, many factors affect just suspended conditions: impeller diameter, clearance and type; particle size, density and loading; fluid density and viscosity. This topic was first examined by Zwietering (1968) where he formed the correlation for predicting the point at which solids rest on the bottom of the tank for less than 1 or 2 seconds:

$$\mathrm{Njs} = \mathrm{S}\cdot\left(\frac{g\cdot\Delta\rho}{\rho_L}\right)^{0.45}\frac{X^{0.13}\,d_p^{0.2}\,\nu^{0.1}}{D^{0.85}} \tag{1.27}$$

Here Z is a constant that is dependent on the system parameters: impeller type, impeller clearance, and solid shape. The Njs correlation was confirmed by Nienow (1968), Baldi et al. (1978) and many others. A review of Njs is covered in Rieger and Ditl (1994).

Baldi et al. (1978) used turbulent scaling to predict Njs:

$$\mathrm{Njs} = \left(\frac{g\cdot\Delta\rho}{\rho_L}\right)^{1/2}\frac{d_p^{1/6}}{\mathrm{Po}^{1/3}}\left(\frac{T}{D}\right)\frac{1}{D^{2/3}\cdot Z} \tag{1.28}$$

Here S is the constant that is dependent on system parameters that has not been taken into account in other variables. Baldi et al. (1978) assumed that a critical eddy size would lift the particles off the bottom of the tank. This actual eddy size was estimated using the local dissipation of turbulent kinetic energy per unit volume. Baldi et al.'s (1978) hypothesis is that dissipation near the bottom of the tank is proportional to total energy in the system. If the local dissipation near the bottom of the tank could be accurately calculated, S would not be needed as a fitting constant in Equation 1.11.

Mersmann et al. (1998) suggested that there are two mechanisms for suspending solids: off bottom lifting and the avoidance of settling. Molerus and Latzeel (1987a & b) showed that off bottom lifting of the particle depends on the effect of particle size on the boundary layer at the bottom of the tank. Mersmann et al.'s (1998) model is based on the local specific power input, similar to Baldi et al.'s (1978) method for determining Equation 1.11. Mersmann et al. (1998) showed that if the local specific power required for off bottom lifting was greater than the power to avoid settling then the criterion for off bottom lifting must be fulfilled in order to maintain suspension.

Comparison of Impeller Types

Currently research tends to compare the minimum energy dissipation of each type impeller at Njs to compare their respective efficiency for solids suspension. Ibrahim and Nienow (1996) compared the RT, 6-blade up and down pumping PBT impellers, A310, HE3 and Ekato Intermigs, single and dual impellers. They found that the two fluid foil impellers (A310 and HE3) needed the least amount of energy to suspend the particles; however, they also found that the RT requires less power than some of the other impellers depending on the configuration used. Other reviews comparing impeller types have been done by Corpstein et al. (1994) and Harnby et al. (1992).

Effect of Clearance and Impeller Diameter

Clearance has always been recognized as a factor in determining Njs. Many authors have shown that as the impeller clearance increases so does the Njs. This has been taken into account in the S or Z factors in Equations 1.10 and 1.11 (Zweitering 1958 Nienow 1968). Myers et al. (1996) explained that the effect of clearance is due to flow reversals at the bottom of the tank at high impeller clearances. Instead of the flow going radially outward at the bottom of the tank, the flow proceeds radially inward. Myers et al. (1996) showed a limiting point at which flow reversal becomes a factor; for a PBT, C/T became a factor at a lower clearance than for the HE3. When flow reversal occurs, there is a dramatic effect on the suspension speed required; however, before the flow reversal occurs, Njs only increases slightly with increasing C/T (Myers et al., 1996)

Non-Spherical Particles

Takahashi and Fujita (1995) compared various diameters (d_p) of non-spherical particles using the longest characteristic length (i.e. the length of a cylinder or the diameter of a disk), equivalent spherical diameter of equal volume, and the Stokes diameter. The Stokes diameter is determined by measuring the settling velocity of the particle in a still fluid to calculating the equivalent diameter based on the particles settling velocity (Takahashi and Fujita, 1995). Through this, they found that the Stokes diameter gave the best results and that the Njs value measured was almost identical to the calculated value. Myers et al. (1996) used a mass average to determine the particle diameter. They examined spheres, and rectangular cylinders. Their results did not vary from the spherical data. Tay et al. (1984) examined hollow cylinders and found the Njs to be independent of L/D ratio, indicating that there was no size effect; however, they did not determine the Stokes diameter, consequently their results can not be compared directly to those of Takahashi and Fujita (1995).

Power Consumption

As was shown in Equation 1.2, the power consumption is based on the power number. For the most part, this remains true for solid suspension; however, solids concentration needs to be considered to determine the correct power consumption. For low concentrations this correction may not be necessary because the particles will not affect the relative density of the mixture; however, at higher solids concentrations the particles affect the relative density. Bubbico et al. (1998) found that power was related to:

$$P = Po\left(1 + k\, c_S\right) N^3 D^5 \rho \qquad \textbf{(1.29)}$$

Here c_S is the volume concentration of solids and k is a measure of additional energy dissipation and varies depending on particle and impeller type.

Solids Distribution

Investigations into solids distribution have generally concentrated on low solids loadings X<5% (Shamlou and Koutsakos, 1989, Barresi and Baldi, 1987, Bohnet and Niesmak 1980). Solids distribution is a complex function of the velocity field, the distribution of turbulence, macro instabilities and fluid solid interaction (Barresi and Baldi, 1987). Generally, the concentration profiles are reported as a dimensionless quantity of concentration (Bohnet and Niesmak, 1980). From this, the suspension quality can be determined from the standard deviation:

$$\sigma = \sqrt{\frac{1}{i}\sum_{1}^{i}\left(\frac{c}{c_{av}}-1\right)^{2}} \qquad \textbf{(1.30)}$$

The average concentration is easily calculated; however, research into methods for determining accurate solids withdrawal methods has also been (Barresi and Baldi, 1987, MacTaggart, 1991 and Nasr El Din et al. 1996).

Barresi and Baldi (1987) showed that the concentration of the solids is the inverse of the Peclet number:

$$\frac{1}{Pe} = K = \frac{u_t L_C}{D_p} \qquad \textbf{(1.31)}$$

Here, D_p is the particle turbulent diffusivity, u_t is the particle terminal velocity and L is a characteristic dimension of the system. Baldi et al.'s (1978) Njs correlation used turbulent scaling, as did Barresi and Baldi (1987) to determine the terms in the Peclet number, but this time turbulent scaling was used to determine the turbulent diffusivity. Both Shamlou and Koutsakos (1989) and Barresi and Baldi (1987) found that:

$$K \propto \frac{ND}{u_t} \qquad \textbf{(1.32)}$$

This K value is related to the concentration profile with different values of K producing slightly different concentration profiles. Because K is related to concentration profiles, it is also related to the quality of the solids distribution and σ can be predicted for any given K and solids concentration (Barsi and Baldi, 1987). This relationship is linear in most cases but when concentrations get above 5% there is some deviation in the profile.

In scaling solid suspension concentration profiles, scaling by maintaining constant power per unit volume, P/V, is recommended by Mak et al. (1997). This method is used in order to keep the dissipation, ε, remains constant. Mak et al. (1997) showed that for any geometrically similar system with constant P/V the concentration profiles collapse for scales of 0.3 to 2.67m. Blend time was also shown to scale with constant power per unit volume (Grenville et al., 1995). They showed that this was valid for four different tank sizes ranging from 0.3 to 2.67m.

1.5 Conclusion

The concepts introduced in this chapter have gone beyond the area of mixing, into jet theory, dimensional analysis and turbulent scaling. These ideas will be used in the remainder of the thesis to characterize the flow in a stirred tank and to model solids distribution in the tank. First it will be shown that a wall jet exists close to the baffle in a stirred tank and that this jet can be used to determine the point where active circulation ends. This suggests limits on the liquid height in the tank (H/T) and on spacing between impellers. Secondly, the wall jet is combined with our knowledge of solid suspension to develop a model for predicting the average location of the solid-liquid interface, of cloud height, in a system with high solids concentration. Finally, the similarity profile of the wall jet is used to determine the onset of transitional flow in the stirred tank. This is defined as the point where the jet no longer exhibits similarity. To summarize, the thesis contains four contribution to the body of knowledge in the area of mixing:

- A similarity solution for an internal annular wall jet is developed and applied to the flow at the wall of a radial impeller stirred (Chapter 3).

- A three dimensional wall jet exists along the baffle of axial impeller stirred tank (Chapter 4).

- The active zone of mean circulation for an axial impeller is examined. On average, it fills only 2/3 of the tank volume (Chapter 5).

- Using the similarity profile for the wall jet, it is shown that the impeller Reynolds number is not sufficient to define fully turbulent flow throughout the tank (Chapter 6).

- The wall jet is also used to develop a model for the cloud height in suspensions with a high solids concentration (Chapter 7).

1.6 Nomenclature

A	constant
$b_{1/2}$	half width of the jet (m)
c	solids concentration (kg m^{-3})
c_{av}	average concentration (kg m^{-3})
c_B	concentration (mol m^{-3})
c_f	firction coeficient
c_s	volume concentration of solids
D	impeller diameter (m)
D_p	particle turbulent diffusivity (m^2 s^{-1})
d_p	particle diameter (m)
Fl	flow number (Eq. 1.6)
Fr	Froude number (Eq. 1.5)
g	acceleration due to gravity (9.81 m s^{-2})
H	liquid level in a stirred tank (m)
K	inverse Peclet number
k	constant
k_2	second order rate constant
L	integral length scale (m)
L_C	characteristic length (m)
M	momentum flux per unit mass (m^4 s^{-2})
Mo	momentum number (Eq. 1.7)
N	impeller rotational speed (rev s^{-1})
Njs	just suspended impeller rotational speed (s^{-1})
P	power (W)
Pe	Peclet number (Eq. 1.12)
Po	power number (Eq. 1.4)
r	cross-stream cylindrical coordinate
Re	Reynolds Number (Eq. 1.3)
S	constant (Eq. 1.27)
T	tank diameter (m)
U	velocity (m s^{-1})
U_m	local maximum jet velocity (m s^{-1})
U_{nozzle}	nozzle velocity (m s^{-1})
u_t	particle terminal velocity (m s^{-1})
u^+	dimensionless velicty
u^*	shear velocity (L t^{-1})
V	velocity (m s^{-1})
V_r	radial velocity component (m s^{-1})
V_z	axial velocity component (m s^{-1})
V_θ	tangential velocity component (m s^{-1})

v_l	fluctuating velocity (m/s)
W	velocity (m s^{-1})
W_m	swirling velocity (m/s)
X	solids loading
x	streamwise Cartesian coordinate
y	cross-stream Cartesian coordinate
y^+	dimensionless distance (Eq. 1.21)
Z	constant (Eq. 1.28)
z	cross-stream Cartesian and streamwise cylindrical coordinate

Greek

ε	dissipation rate(m^2s^{-3})
ϕ	impeller blade angle (°)
λ_k	Kolmogorov length scale (m)
ν	kinematic viscosity (m^2s^{-1})
θ	tangential coordinate
ρ	density (kg m^{-3})
σ	standard deviation

1.7 References

Abrahamsson H., B. Johansson, and L. Fofdahl, 1994, A turbulent plane two-dimensional wall-jet in a quiescent surrounding, *Eur. J. Mech., B/Fluids,* **13**, 533-556.

Baldi G., R. Conti and E. Alaria, 1978, Complete suspension of particles in mechanically agitated vessels, *Chem. Eng. Sci.* **33**, 21-25.

Bains D.W. ,1985, Entrainment by a buoyant jet flowing along vertical walls, *Journal of Hydraulic Research* **23**, 221-228.

Bakke P., 1957, An experimental investigation of wall jet, *J. Fluid. Mec.,* **2, 467-472.**

Bakker, A., K. J. Myers, R.W. Ward, and C.K. Lee, 1996, The laminar and turbulent flow pattern of a pitched blade turbine. *Trans. I. Chem. E. Part A* **74**, 485-491.

Bakker A. and H.E.A. Van Den Akker, 1994, Single-phase flow in stirred reactors, *Tans IChemE,* **72**, 583-593.

Baldyga J., & J.R. Bourne, 1991, Interactions between mixing on various scales in stirred tank reactors, *Chem. Eng. Sci.,* **47**, 1839-1848.

Baldyga J., & J.R. Bourne, Some consequence for turbulent mixing of fine-scale intermittency, Chem. Eng. Sci., 47(1992)p.3949-3948

Baldyga J., & J.R. Bourne., Simplification of micromixing calculations. I. Derivation and application of new model, Chem. Eng. J., 42(1989)p.83-92

Baldyga J., & J.R. Bourne, Calculation of micromixing in inhomogeneous stirred tank reactors, Chem. Eng. Res. Des., 66(1988)p.33-38

Baldyga J., J.R. Bourne, and S.J. Hearn, 1987, Interactions between chemical reactions and mixing on various scales, *Chem. Eng. Sci,* **52**, 457-466.

Baldyga J. and R. Pohorecki, 1995, Turbulent micro-mixing in chemical reactors – a review, *Chem. Eng. J.,* **58**, 183-195.

Barresi A. and G. Baldi, 1987, Solid dispersion in an agitated vessel, *Chem. Eng. Sci.* **42**, 2949-2956.

Bird R.B., W.E. Stewart, and E.N. Lightfoot, 1960, *Transport Phenomena,* John Eiley and Sons, Toronto.

Bourne J.R. and P. dell Ava, 1987, Micro and macro mixing in stirred tank reactors of different sizes, *Trans ICheme*, **65**, 180-186.

Bourne J.R. & C.P. Hibbler, 1990, The productivity of micromixing-controlled reactions: effect of feed distributions in stirred tanks, *Trans IChemE*, **68**, 51-56

Bohnet M. and G. Niesmak, 1980, Distribution of solids in Stirred Suspensions, *Ger. Chem. Eng.*, **3**, 57-65.

Brucato A., and V. Brucato ,1998, Unsuspended mass of solid particles in stirred tank, *Can. J. Chem. Eng.*, **76**, 420-427.

Bruha, O., I. Fort, and P. Smolka, 1993, Large scale unsteady phenomenon in a mixing vessel. *Acta Polytechnica, Czech Tech. Univ. Prague* **27**, 33.

Bruha, O., I. Fort, and P. Smolka, 1994, Flow transition phenomenon in an axially agitated system. *Proceedings of the Eighth European Conference on Mixing, IChEME Symposium series* **136**, 121-128.

Bruha, O., I. Fort, and P. Smolka, 1995, Phenomenon of turbulent macroinstabilities in agitated systems. *Collect. Czech. Chem. Commun.* **60**, 85-94.

Bruha, O., I. Fort, P. Smolka, and M. Jahoda (1996) Experimental study of turbulent macroinstabilities in an agitated system with axial high-speed impeller and with radial baffles. *Collect. Czech. Chem. Commun.* **61**, 856-867.

Bubbico R., S.D. Cave, and B. Mazzorotta, 1998, Agitation power for solid-liquid suspensions containing large particles, *Can. J. Chem. Eng.*, **76**, 428-432.

Chigier N.A. and A. Chervinsky, 1965, Experimental and theoretical study of turbulent swirling jets issuing from a round orifice, *Isreal J. Tech.*, **4**, 44-54.

Chigier N.A. and A. Chervinsky, 1967, Experimental investigations of swirling vortex motion jets, *J. of Applied. Mech.*, 443-451.

Corpstein R.R., J.B. Fasano and K.J. Myers, 1994, The high efficiency road to liquid solid agitation, *Chem. Eng.*, Oct 1994, 138-144

Dickey D.S., Dimensional analysis, similarity and Scale-up, AIChE Annual Meeting Tutorial, 1992

Dickey D.S., 1993,Dimensional analysis, similarity and Scale-up, Process Mixing Part 2, **89**, 143-150

Eriksson J.G., R.I. Karlsson, and J. Person, 1998, An experimental study of a two-dimensional plane turbulent wall jet, *Exp. in Fluids*, **25**, 50-60.

Fentiman N.J., N.ST. Hill, K.C. Lee, G.R. Paul and M. Yianneskis, 1998, A novel profiled blade impeller for homogenization of miscible liquids in stirred vessels, *Trans IChemE*, **76**, 835-842.

Fort I., 1986, Flow and turbulence in vessels with axial impellers, in the book: *Mixing: Theory and Practice*, Vol. III, V.W. Uhl and J.B. Gray ed., New York: Academic Press Inc., 133-197.

Fort I., M. Vozny, and T. Makovsky,1993, Flow and turbulence in a baffled system with impeller with inclined blades. *ACTA Polytechnica* **33**, 31-44.

Gerodimos G. and R.M.C. So, 1997, Near-wall modeling of plane turbulent wall jets, *J. Fluids Eng.*, **119**, 304-313

Gholap R.V., S. Petrozzi, & J.R. Bourne, 1994, Influence of viscosity on product distribution of fast competitive reactions chemical reactions, *Chem. Eng. Technol.*, **17**, 102-107

Glauert M.B. 1956 The wall jet, *J. Fluid Mech.* **1**, 625-643.

Goertler V.H., 1942, Berechnung von Aufgaben der frein Turbulenz auf Grund eines neuen Naherungsansatzes, *Z.A.M.M.*, **22**, 244-254

Gowda L.H.B. and V.S.B. Durbha, 1999, Mean and turbulence characteristics of three dimensional wall jet on convex cylindrical surfaces, *J. Fluids Eng.*, **121**, 596-604.

Grenville R.K. and M.E. Musgrove, Comparison of blend times in agitated and mixed vessels: the role of momentum, Fluid Mixing Processes Consortium Steering Committee Meetings, Sept. 1998.

Grenville R., S. Ruszkowski, E. Garred, Blending of miscible liquids in the turbulent and transitional regimes, Mixing XV, Banff, Alberta, June 20-25 1995.

Grgic B., 1998, *Influence of the impeller and tank geometry on low frequency phenomena and flow stability*. M.Sc. thesis, University of Alberta, Edmonton, Canada.

Harnby N., M.F. Edwards and A.W. Nienow (1993) *Mixing in the Process Industries, 2nd ed.*, Butterworth Heinemann, Toronto.

Hockey R.M. and J.M. Nouri (1996) Turbulent flow in a baffled vessel stirred by a 60° pitched blade impeller. *Chem. Eng. Sci.* **51,** 4405-4421.

Ibrahim S. and A.W. Nienow, 1996, Particle suspension in the turbulent regime: the effect of impeller type and impeller/vessel configuration, *Trans ICHemE*, **74**, 679-688.

Jaworski Z., A.W. Nienow, K.N. Dyster, and W. Bujalski, 1991, An LDA study of turbulent flow in a baffled vessel agitated by a pitched blade turbine. *Trans IchemE*, **60**, 313-320.

Kolar V., P. Filip & A.G Curev, 1982, The swirling radial jet, *Applied. Sci. Res.*, **39**, 329-335.

Kolar V., P. Filip & A.G. Curev, 1984, Hydrodynamics of a radially discharging impeller stream in agitated vessels, *Chem. Eng. Commun.*, **27**, 313-326.

Kresta S., 1998, Turbulence in stirred tanks: anisotropic, approximate and applied, *Can. J. Chem. Eng.*, **76**, 563-576.

Kresta S.M. & P.E. Wood, 1991, Prediction of the three dimensional turbulent flow in stirred tanks, *AIChE Journal*, **37**, 448-460.

Kresta S.M., and P.E.Wood, 1993, The mean flow field produced by a 45° pitch blade turbine: changes in the circulation pattern due to off bottom clearance, *Can. J. of Chem. Eng.*, **71**, 42-53.

Kruka V., and S. Eskinazi, 1964, The wall-jet in a moving stream, *J. Fluid Mech.*, **20**, 555-579..

Launder B.E. and W. Rodi, 1981, The turbulent wall jet, *Prog. Aerospace Sci.* **19**, 81-128.

Lee K.C. and M. Yianneskis, 1998, Turbulence properties of the impeller stream of a Rushton turbine, *AIChE J.*, **44**, 13-24.

Mak A. S., S.Yang, and N.G. Ozcan-Taskin, 1997, The effect of scale on the suspension and distribution of solids in stirred vessels, *Recents Progres en Gente des Procedes*, **11,** 97-104.

Mao D., L. Feng, K. Wang and Y. Li, 1997, The mean flow field generated by a pitched blade turbine: changes in the circulation pattern due to impeller geometry, *Can. J. Chem. Eng.*, **75**, 307-316.

MacTaggart S.R., 1991, *Local solids concentration in a mixing tank,* M.Sc. thesis, University of Alberta, Edmonton, Canada.

Mersmann A., F. Werner, S. Maurer and K. Bartosch, 1998, Theoretical prediction of the minimum stirrer speed in mechanically agitated suspensions, *Chem. Eng. Processing*, **37**, 503-510.

Mishra V.P., K.N. Dyster, Z. Jaworski, A.W. Nienow and J. McKemmie, A study of up and down pumping wide blade hydrofoil impeller: Part I. LDA measurements, *Can J. Chem. Eng.* **76**, 577-588

Molerus O. and W. Latzel, 1987a, Suspension of solid particles in agitated vessels-I. Archimedes number ≤ 40, *Chem. Eng. Sci.*, **42**, 1423-1430.

Molerus O. and W. Latzel, 1987a, Suspension of solid particles in agitated vessels-II. Archimedes number > 40, reliable prediction of minimum stirrer angular velocities, *Chem. Eng. Sci.*, **42**, 1431-1437.

Montes, J.L., H.C. Boisson, I. Fort, and M. Jahoda (1997) Velocity field macro-instabilities in an axial agitated mixing vessel. *Chem. Eng. J.* **67**, 139-145.

Myers K.J., A. Bakker and R.R. Corpstein, 1996, The effect of flow reversal on solid suspension in agitated vessels, *Can. J. Chem. Eng.*, **74**, 1028-1033.

Myers K.J., R.W. Ward, A. Bakker, 1997, A digital particle image velocimetry investigation of flow field instabilities of axial flow impellers, *J. Fluids Eng.*, **119**, 623-632.

Myers K.J., J.B. Fasano and R.R. Corpstein, 1994, The influence of solid properties on the just-suspended agitation requirements of pitched-blade and high-efficiency impellers, *Can. J. Chem. Eng.*, **72**, 745-748.

Nasr El Din H.A., R.S. MacTaggart and J.H. Masliyah, 1996, Local solids concentration measurements in a slurry mixing tank, *Chem. Eng. Sci.*, **51**, 1209-1220.

Nienow A.W., 1968, Suspension of solid particles in turbine agitated, baffled vessels, *Chem. Eng. Sci.*, **23**, 1453-1459.

Newman B.G., R.P. Patel, S.B. Savage & H.K. Tjio, 1972, Three-dimensional wall jet originating from a circular orifice, *Aero. Quarterly* **23**, 188-200.

Nouri J.M., J.H. Whitelaw, and M. Yianneskis, 1987, The scaling of the flow field with impeller size and rotational speed in a stirred reactor. *Second International*

Conference on Laser Anemometry – Advances and Applications, Strathclyde, UK, (Sept.)

Padmanabham G. and B.H. Gowda, 1991, Mean and turbulence characteristics as a class of three-dimensional wall jets – Part 1: Mean flow characteristics, *J. of Fluids Engineering* **113**, 620-628.

Per P., Magnus L., and J. Lennart, 1996, Measurements of the velocity field downstream of an impeller, *J. of Fluids Engineering* **118**, 602-610.

Pozzi A.and E. Bassano, 1995, Application of Pade approximats to the study of plane jets, *Computers Math. Applic.*, **30**, 107-123.

Rajaratnam N. & B.S. Pani, 1974, Three-dimensional turbulent wall jets, *Proc. ASCE J. Hydraulics Div.* ***100**, 69-83.*

Rajaratnam N., 1976, *Developments in water sciences, Turbulent Jets,* Elsevier Scientific Publishing Company, New York.

Ranade V.V. and J.B. Joshi, 1989, Flow generated by pitched blade turbines I: Measurements using laser Doppler anemometer, *Chem. Eng. Comm.*, **81**, 197-224.

Rieger F. P. Ditl, 1994, Suspension of solid particles, *Chem. Eng. Sci.*,**49**, 2219-2227.

Rose W.G., 1962, A swirling round turbulent jet, *J. Applied Mech.*, **29**, 615-625

Rushton J.H., 1946, Technology of Mixing, *Can. Chem. & Proc. Ind.*,

Rushton J.H., E.W. Costich, and H.J. Everett, 1950a, Power Characteristics of mixing impellers Part 1, *Chem. Eng. Progress*, **46**, 395-404

Rushton J.H., E.W. Costich, and H.J. Everett, 1950b, Power Characteristics of mixing impellers Part 2, *Chem. Eng. Progress*, **46**, 467-476

Rutherford K., Lee K.C., Mahmoudi S.M.S., Yianneskis M., 1996, Hydrodynamic characteristics of dual Rushton impeller stirred vessels, *AIChE J.*, **42**, 332-346

Schafer M., M. Yianneskis, P. Wachter, and F. Durst, 1998, Trailing vortices around a 45° pitched blade impeller, *AIChE J.*, **44**, 1233-1246.

Schwarz W.H. and W.P. Cosart, 1960, The two-dimensional wall-jet, *J. Fluid Mech.* **10**, 481-495.

Schafer M., M. Hofken and F. Durst, 1997, Detailed LDV measurements for visualization of the flow field within a stirred-tank reactor equipped with a Rushton turbine, *Trans. IChemE*, **75**, 729-736.

Shamlou P.A. and E. Koutsakos, 1987, Solids suspension and distribution in liquids under turbulent agitation, *Chem. Eng. Sci.* **44**, 529-542.

Sheng J., H. Meng, and R.O. Fox, 1998, Validation of CFD simulations of a stirred tank using particle image velocimetry data, *Can. J. Chem. Eng.*, **76**, 611-625.

Starr J.B. and E.M. Sparrow, 1967, Experiments on a turbulent cylindrical wall jet, *J. Fluid Mech.*, **29**, 495-512.

Swamy N.V. & P. Bandyopadhyay, 1975, Mean and turbulence characteristics of three-dimensional wall jets, *J. Fluid. Mech.* **71**, 541-562.

Takahashi K., and H. Fujita, 1995, A study of the agitation speed to just cause complete suspension for non-spherical particles, *J. Chem. Eng. Japan*, **28**, 237-240.

Tatterson G.B., 1993, Scaling based upon process similarity and scale matching concepts, Process Mixing Part 2, **89**, 164-168

Tay M., B. Deutshlander and G. Tatterson, 1984, Suspension characteristics of large cylinders in agitated tanks, *Chem. Eng. Commun.*, **29**, 89-99.

Stoots C.M., and R.V. Calabrese, 1995, Mean velocity field relative to a Rushton turbine blade, *AIChE J.*, **41**, 1-11

Takahashi K., A.W. and Nienow, 1992, Vortex cavity shape and the associated path-line of discharged bubbles in an aerated vessel agitated by a Rushton turbine *J. Chem. Eng. of Japan*, **25**, 539-543

Van't Riet K., W.Bruijn , and J.M. Smith, 1976, Real and Pseudo-Turbulence in the discharge stream from a Rushton turbine, *Chem. Eng. Sci.*, **31**, 407-412.

Van't Riet K., and J.M. Smith, 1975, The trailing vortex system produced by Rushton turbine agitators, *Chem. Eng. Sci.*, **30**, 1093-1105.

Villermaux J. and L. Falk, 1994, A generalized mixing model for initial contacting of reactive fluids, *Chem. Eng. Sci.*, **49**, 5127-5140.

Weidman P.D., G.D. Kubitschek and S.N. Brown, 1997, Boundary layer similarity flow driven by power-law shear, *Acta Mechanica*, **120**, 199-215

Wu H., G.K. and Patterson, 1989, Laser- Doppler Measurements of Turbulent-Flow Parameters in a stirred Mixer, *Chem. Eng. Sci.*, **44**, 2207-2221

Yianneskis M., Z. Popiolek, and J.H. Whitelaw, 1987, An experimental study of the steady and unsteady flow characteristics of stirred reactors, *J. Fluid Mech.*, **175**, 537-555

Yianneskis M., and J.H. Whitelaw, 1993, On the Structure of the Trailing Vortices Around Rushton Turbine Blades, *Trans IChemE*, **71**, 543-550

Zhou G. & S.M. Kresta, 1996, Distribution of energy between convective and turbulent flow for three frequently used impellers, *Trans IChemE* **74**, 379-389.

Zlokarnik M., 1998, Problems in the application of dimensional analysis and scale-up of mixing operations, *Chem. Eng. Sci.*, **53**, 3023-3030.

Zwietering Th. N., 1958, Suspending of solid particles in liquid by agitators. *Chem. Eng. Sci.* **8**, 244-253.

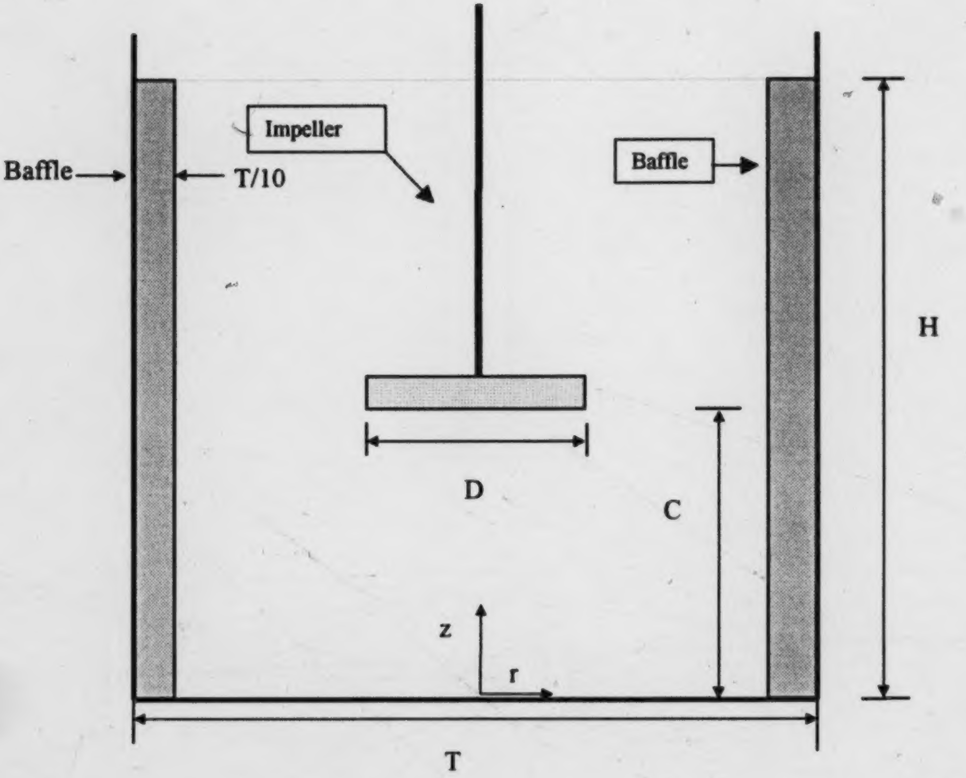
Impeller
Baffle
T/10
Baffle
H
D
C
z
r
T

Figure 1 - 1: Tank configuration with geometric nomenclature four baffles are equally spaced around the perimeter of the tank

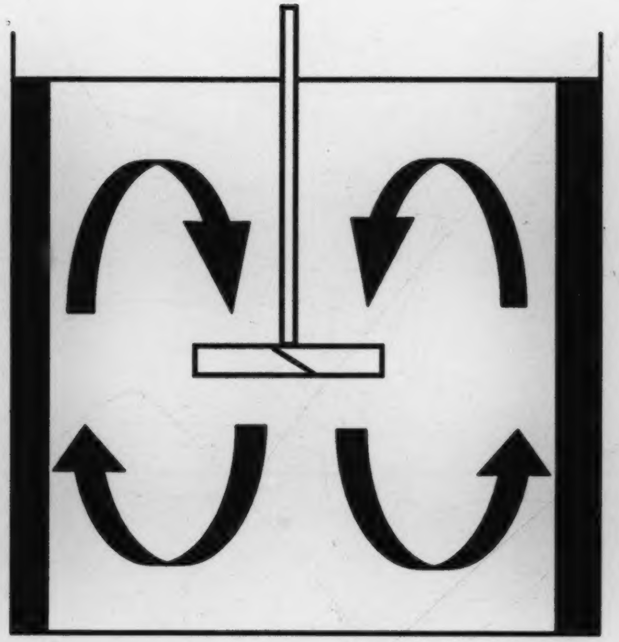

Figure 1 - 2: Flow pattern for an axial impeller

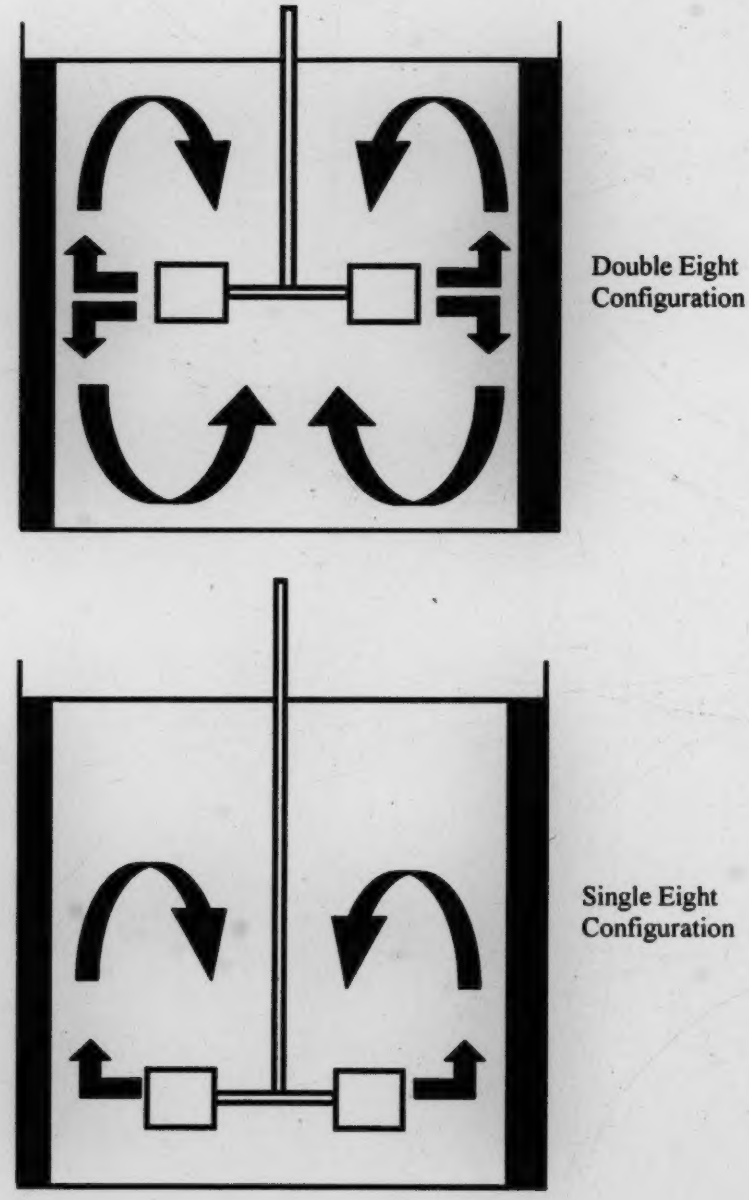
Double Eight
Configuration
Single Eight
Configuration

Figure 1 - 3: Flow patterns for the radial impeller

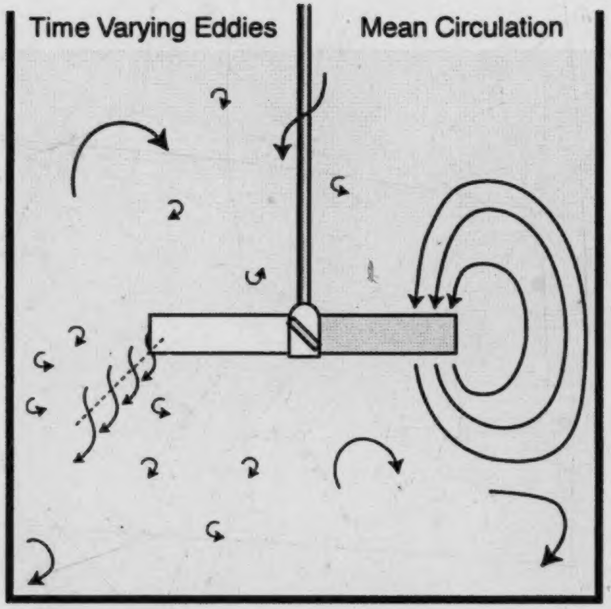
Time Varying Eddies
Mean Circulation

Figure 1 - 4: Length scales in a stirred tank (Kresta, 1998) showing the mean circulation loop (scale of macro instability), trailing vortex (integral length scale) and various sizes of turbulent eddies.

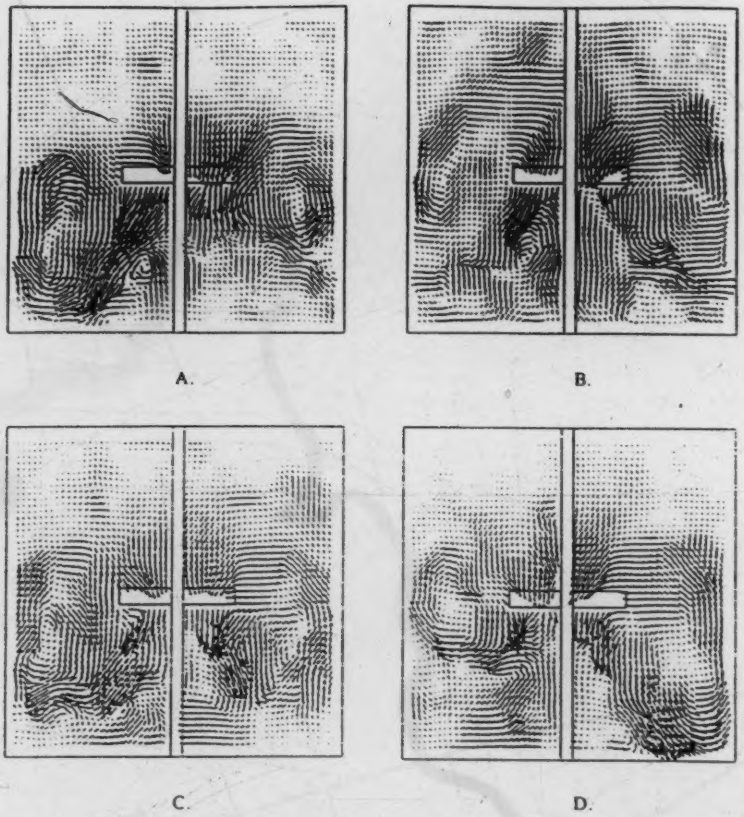

Figure 1 - 5: Instantaneous flow pattern for the PBT taken from Bakker et al. (1996). Note that no two patterns are similar and that the mean "single eight" circulation loop does not exist in any of the four images.

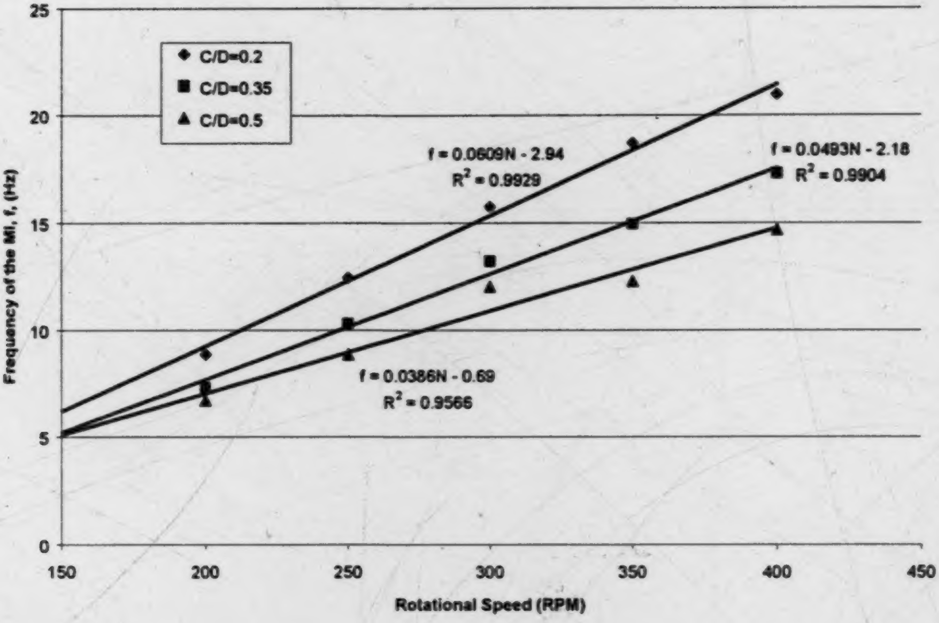

Figure 1 - 6: Effect of clearance and rotational speed on the frequency of the macro instabilities (data from Bruha et al. 1994)

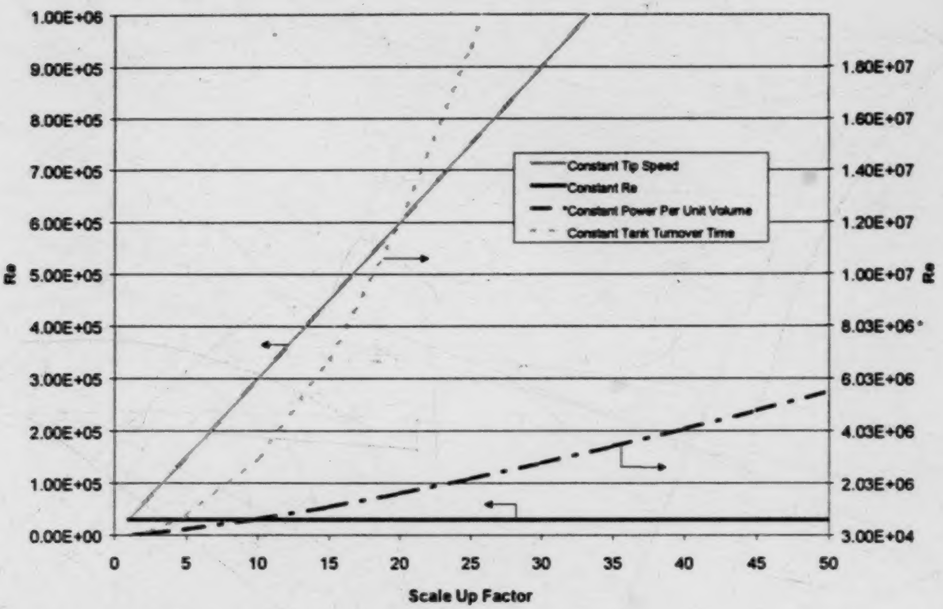

Figure 1 - 7: Effect of different methods of scale-up on Re

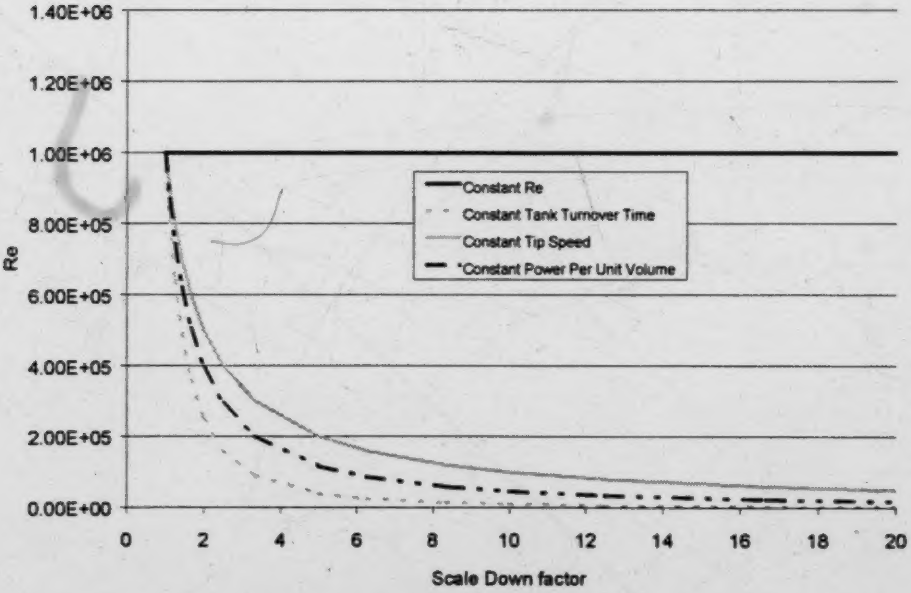

Figure 1 - 8: Effect of different methods of scale-down on Re.

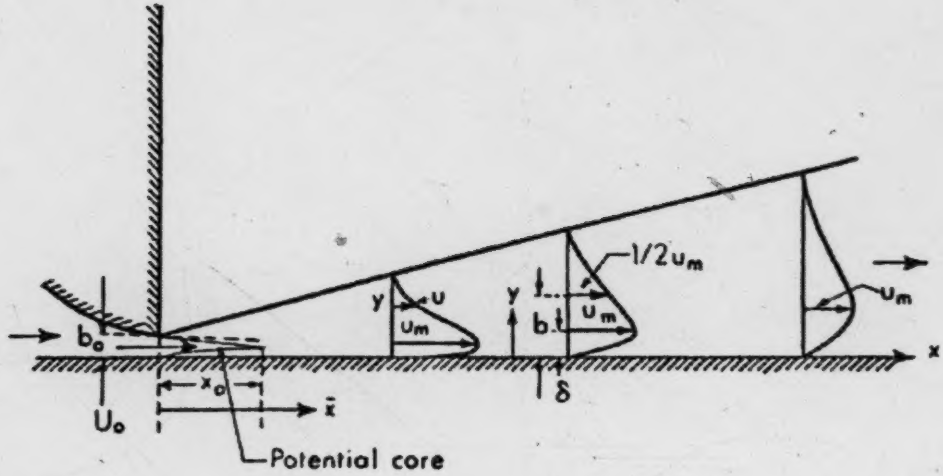
b₀
U₀
x₀
x̄
Potential core
y
u
um
y
b
um
1/2um
δ
um
x

Figure 1 - 9: Development of the inner and outer layers of a wall jet (Rajaratnam, 1976)

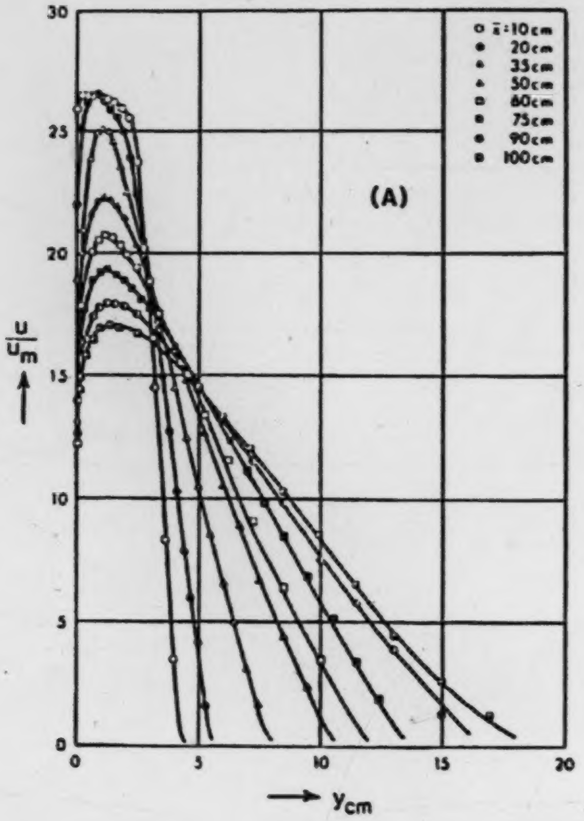

Figure 1 - 10: Velocity profiles in wall jet (Rajaratnam, 1976)

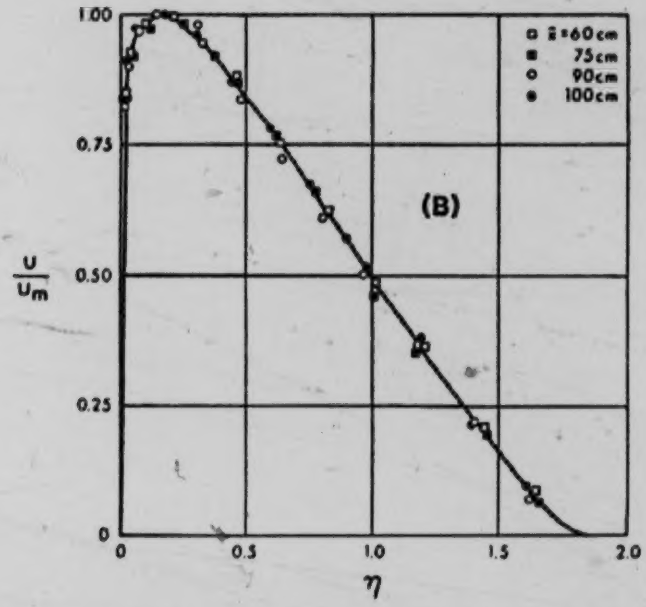

Figure 1 - 11: Similarity of the velocities in Figure 1-10 (Rajaratnam, 1976)

Chapter 2

Experimental Setup and Procedures

2.1 Introduction

This chapter reviews the experimental equipment and procedures used through the course of this study. All of the experiments shared a common theme; they were completed in an agitated cylindrical tank, using laser Doppler velocimetry (LDV) to measure the velocities at specific locations in the tank. Various types of radial and axial impellers were used and specific areas of the flow field were measured. Detailed measurement locations are given in the relevant chapters. This discussion will consist of these four areas:

1. Experimental equipment
2. Optical parameters of the LDV
3. Experimental procedure
4. Trouble shooting

2.2 Experimental Equipment

Figure 2-1, a schematic of the experimental apparatus, depicts the major pieces of equipment: tank, impeller, motor, traverse system, and laser. Axial velocities were measured using a laser Doppler velocimeter (LDV) and the tank was mounted on an automated traverse system. The details of the equipment and fluids properties are below.

2.2.1 Tank

Two fully baffled flat bottom tanks with diameters T=240mm and T=140mm, (Figure 2-2) were filled with liquid. The flow field was examined in both lidded and unlidded conditions. The lid was used to eliminate air entrainment at higher rotational speeds. The 240mm tank was filled to a liquid height equivalent to the tank diameter. The 140mm tank was filled to a height of 1.21T to minimize air entrainment.

Because an LDV was used, the optical effect due to the curvature of the tank needed to be minimized. To accomplish this, the cylindrical tank was placed inside a square tank filled with the same fluid that is used within the cylindrical tank.

2.2.2 Impellers

Three axial impellers were investigated and are shown in Figure 2-3: a 4 bladed, 45° pitched blade turbine (PBT), a Chemineer HE3 and a Lightnin A310. Also shown in Figure 2-3 is the Rushton Turbine (RT), which was the only radial impeller used. Each of the impellers was of standard configuration and ranged from 45mm to 170mm in diameter. The configuration of the PBT and RT impellers are shown in Table 2-1.

2.2.3 Motors

Four motors were used over the course of the investigation: Heller HST20, Lighnin L5U08F, Lighnin L1U08 and Caframo 3030. The Heller HST20 motor speed was manually controlled while the other three motors had digital displays. Details for each of the motors are given in Table 2-2.

2.2.4 Traverse System

Positioning of the tank was both automated and manual. The Unidex 11, an automated traverse system, controlled positioning in the x-y (horizontal) plane, while positioning in the z (vertical) direction and the off-bottom clearance adjustment for the impeller were done manually. Table 2-3 gives the accuracy of the traversing equipment.

Various methods were used to determine the zero position for the x, y, and z and the off bottom clearance of the impeller. The off bottom clearance was set by moving the impeller shaft to the bottom of the tank and marking this position as zero. The vertical motor traverse was then used to position the impeller. Once the clearance was set, the z position of the tank was adjusted until the cross point of the laser was at the same height as the lower edge of the impeller. This position was noted on the indicator for the z traverse and the adjustment was repeated at a different clearance to ensure accuracy.

The horizontal position of the x and y traverse system was determined using the distance from the tip of the impeller to the tank wall. A five step procedure was used done to zero the traverse system and set the step size for automated traverse:

1) Position the laser at the tip of the impeller (x=D/2)
2) Ensure the computer reading matches the location of the traverse
    - If the reading is not identical enter in the correct value
3) Move traverse to the wall of the tank (x=120mm)
4) Ensure the reading is correct
    - If the reading is not identical, the step size is incorrect. Change by: New step size = current step size*(120mm/current reading (mm))
5) Repeat for the y-traverse

After these steps have been successfully completed the error associated with the horizontal traverse system is ± 0.5mm.

2.2.5 Fluids Examined

Various fluids were investigated throughout the experiments. The primary fluid was water, although Bayol and solutions of triethylene glycol (TEG) in water were used as well. Table 2-4 shows the properties of each of the fluids. During one set of experiments, problems arose with tryethylene glycol mixtures heating up; therefore, the temperature of the liquid was measured regularly. Figure 2-4 contains the plots showing the viscosity dependence on temperature.

2.3 Laser Doppler Velocimetry (LDV)

LDV is a non-intrusive method of measuring instantaneous velocities, which was first used by Yeh and Cummings (1964). This method was used to measure mean and instantaneous velocities throughout the stirred tank. LDV was used because it has many advantages in chaotic flow systems like a stirred tank (Fingerson and Menon, 1998):

- Small measuring region for approximate point measurements
- High accuracy
- Can measure any desired velocity component
- Accurate measurement of high intensity turbulence with flow reversal
- No velocity calibration required
- Non-intrusive method of measurement

The system used was an Argon ion Laser Doppler Velocimeter (LDV) and the requisite software was purchased from Aerometrics (now TSI). It is a dual beam system that is capable of measuring one velocity component at a time. The measuring volume is created when the two beams cross at a point within the flow system. For a velocity measurements to occur a particle must pass through the measuring volume. This particle scatters the light at a frequency proportional to the velocity it is traveling. For the particles to be representative of the fluid velocity they have to be small enough not to interfere with the flow and match the fluctuating velocities in the flow.

A schematic of the LDV used is shown in Figure 2-5 and consists of many components: an argon laser, a polarization filter and beam splitter, a Bragg cell, focusing lenses, photodetectors, amplifiers and a signal processor. The process of how to measures velocities is described below.

First, beam of blue green light from the Argon Laser is directed to the transmitting optics through a fiber optic cable, where the light is polarized and split into two beams (specifications are given in Table 2-5). The two beams created are of equal intensity and size. They leave the transmitting optics and cross at the beam waist to create a measuring volume. The measuring volume is a set of virtual fringes consisting of consecutive light and dark lines (Figure 2-6). The fringe spacing (δ_f) based on the wave length of the light (λ_o) and the angle at which the two beams cross (θ) is given by:

$$\delta_f = \frac{\lambda_o}{2\sin(\theta/2)} \tag{2.1}$$

Several beam separations are possible with the Aerometrics PDPA, as given in Table 2-6. The fringes are equally spaced and are used to determine the distance a particle has traveled. When a particle passes through the measuring volume, it deflects the light at a frequency proportional to the velocity of the particle. The direction that the velocity is measured is perpendicular to the fringes as seen in Figure 2-6. The Doppler frequency (f_D) and the corresponding velocity (V) as a particle passes through the fringes is:

$$f_D = \frac{V}{\delta_f} \tag{2.2}$$

The difficulty with measuring the velocity in this manner is that there is no way to determine the direction of the flow because the fringes are stationary and non-directional. Because of this, some means of directional discrimination is needed. This is accomplished using a Bragg cell, which induces a frequency shift in one of the two beams causing the fringes to move at a frequency f_S. When a particle passes through the fringes, the light is scattered at a frequency corresponding to a fluid velocity plus the shift frequency:

$$f_d = f_S + f_D \quad (2.3)$$

Particle motion in the direction of fringe movement reduces the frequency f_d while motion in the opposite direction of the fringe movement increases f_d.

The frequencies are collected by a receiver which is focused at the point where the beams cross. When a particle passes through the measuring volume, the photodetectors collect the frequency of the scattered light (f_d). The analog signal is then amplified and sent to the signal processor. During experiments the receiver was set in forward scatter mode at an angle of approximately 20° to the beam angle bisector (ψ) as shown in Figure 2-5.

Two types of signal processors were used throughout the investigation: a Doppler Signal Analyzer (DSA) and a Real Time Signal Analyzer (RSA). Both are frequency domain burst detection signal processors capable of measuring signals with low signal to noise ratios. The DSA and RSA differ primarily in the manner in which the time series is taken, and the implementation of signal processing through software (DSA) or hardware (RSA). Both accurately reproduce mean and RMS velocities from other reported studies (Grgic, 1998). The processors receive the amplified analog signal from the photodetectors, which is converted to a digital signal. The processor, in conjunction with the software, converts the signal to a velocity measurement and records the time of measurement. The velocity time series is averaged to determine mean and RMS velocities.

2.4 Experimental Reproduceability

This section describes measures taken to ensure reproducable LDV measurements. Two areas of concern for the repeatability of the measurements are the accurate positioning of the measuring volume and the accuracy of the velocity measurements.

To ensure repeatability of the positioning and to minimize the optical effect of the laser light entering at a cylindrical surface, the cylindrical tank was placed inside a square tank. Light refraction decreases significantly when first entering the fluid at a plane that is perpendicular to the light surface. Since only axial velocity measurements were taken, the beams did not enter the tank at two different points of curvature. The curvature must be considered when measuring radial and tangential velocities because the laser may enter the tank at two different points of curvature, which can affect the position of the measuring volume.

Macro-scale instabilities in a stirred tank can affect the repeatability of the velocity measurements if the measurement time is insufficient. If measurements are taken over a long enough period, a quasi-stationary average velocity is obtained. The minimum sampling time needed for a repeatable velocity measurement was determined from:

$$\text{sampling time} \geq \frac{120}{N \times N_b} \tag{2.4}$$

This equation, recommended by Zhou (1996), is based on 120 blade passages. N_b represents the number of blades on the impeller and N is the impeller rotational speed. All velocity measurements were taken over a length of time greater than or equal to the recommended sampling time to ensure repeatability. In addition, Zhou (1996) suggested a minimum sample size of 4000 velocity determinations is required for repeatable measurements.

Based on for the minimum number of points and the minimum amount of time needed for repeatable measurements, the velocities reported here require sample sizes of 8000 measurements with sampling times ranging from 14s to 45s, and a mean sampling time of 20s (Zhou 1996). This is sufficient for regions close to the impeller but in regions near the top of the tank measuring times of one minute and a larger sample size are required. The increased record length is due to the effect of the macro-instabilities (MI) or large-scale velocity fluctuations that occur in the stirred tank and the lower data rate in the top of the tank. These MI's occur every 0.1 to 1 Hz (Bruha et. al., 1996). It is important to capture enough of these large-scale fluctuations during the sample period to ensure that the measured mean velocity is representative of the flow. The DSA the sample size ranged from 10 000 to 50 000 points while for the RSA the sample size varied from 90 000 to 125 000 points. As might be expected, the longer record time and the large number of samples reduced the error and improved the repeatability of the measurements.

2.5 Trouble Shooting with Experiments and Data Analysis

This section outlines some simple tricks and solutions to problems that have arisen while performing experiments and data analysis. Although this section is not necessarily directly related to the experimental results, it may help analysis and experiments for future researchers.

The RSA program, the program that acquires velocity data, contains some problems that can potentially lead to errors. The program requires the Enter key to be pressed after changing the settings; therefore, if another box is activated with the mouse, problems may arise. If the Enter key is not used the changed value will revert to the original value. This problem occurred once when entering the fringe spacing and beam separation. If they are entered incorrectly, the velocity is miscalculated, resulting in inaccuracies equivalent to the ratio of the correct fringe spacing to the incorrect fringe spacing. However, the data does not have to be retaken; the velocity measurements can be recalculated once the error has been found.

Another limitation of the RSA program is the number of data points it can process in each run. This is limited by the amount of RAM memory on the computer and, according to the manual, the maximum amount of data it can take is:

Max # of Samples=(Free Expanded Memory (EMS)-Memory to run Data View(4 M))*5000 (2.5)

If more than the maximum amount of data points is required, multiple runs can be taken.

In the RSA program, six traverses can be used. The system currently used has only two traverses automated, in the horizontal direction. The other four traverses can be set to manual, so other information can be entered: z position, RPM, impeller diameter and impeller clearance. When transferring the data to text form at each of these traverses can be printed out with the any of the required information. Many different types of information can be gathered from the RSA: mean velocity, RMS velocity, run time, velocity attempts, velocity reading, traverses, data rate, and percent valid and individual velocity readings including times at which they were taken.

2.6 Conclusion

This chapter examined the basis of all experiments competed during the course of the Ph.D. work. Details of experimental runs are given in each chapter. The runs vary in terms of rotational speed, impeller diameter, and measurement locations.

2.7 Nomenclature

C	off bottom clearanc (m)
D	impeller diameter (m)
f_D	Doppler frequency (Hz)
f_d	shifted plus Doppler frequency (Hz)
f_s	shifted frequency (Hz)
H	liquid level (m)
N	rotational speed (1/s)
N_b	number of blades
r	radial coordinate
T	tank diameter (m)
V	velocity (m/s)
x	horizontal coordinate
y	horizontal coordinate
z	axial coordinate

Greek

δ_f	fringe spacing (nm)
λ_0	wave length (nm)
θ	beam angle (°)
ψ	receiver angle (°)

2.8 References

Bruha O., I. Fort, P. Smolka, and M. Jahoda, 1996, Experimental study of turbulent macroinstabilities in an agitated system with axial high-speed impeller and with radial baffles. *Collect. Czech. Chem. Commun.* **61**, 856-867.

Fingerson L.M. and R.K. Menon, 1998, Laser Doppler Velocimetry, *The Handbook of Fluid Dynamics,* pp 35-1 to 35-18, R.W. Johnson ed., CRC Press, New York.

George W.K., 1988, Quantitative measurement with the burst-mode Doppler anemometer, *Exptl. Thermal and Fluid Sci.,* **1**, 29-40.

Grgic B., 1998, *Influence of the impeller and tank geometry on low frequency phenomena and flow stability.* M.Sc. thesis, University of Alberta, Edmonton, Canada.

Yeh Y. and H.Z. Cummings, 1964, Localized fluid flow measurements with an HE-NE laser spectrometer, *Appl. Phys. Lett.,* **110**, 176-178.

Zhou G., 1996, *Characteristics of turbulence energy dissipation and liquid-liquid dispersions in an agitated tanks,* Ph.D. thesis, University of Alberta, Edmonton, Canada.

Table 2 - 1: PBT and RT Impeller Configuration

Impeller	Blade width	Blade Length	Blade Thickness	Hub size	Disk Size
PBT					
D=120 & 80mm	D/5	N/A	0.8mm	12.7mm	N/A
D=60 & 45mm	D/5	N/A	1.0mm	12.7mm	N/A
RT D=80mm	D/5	D/4	0.9mm	12.7mm	0.7D

Table 2 - 2: Motor Specifications

	Power Requirement	Max Torque	Max RPM
Heller HST20	90 W	3.2	2500
Lightnin L5U08F	75 W	N/A	550
Lightnin L1U08	75 W	N/A	1800
Caframo 3030	150W	6.0	3000

Table 2 - 3: Traverse Specification

Horizontal Traverses	Computer controlled Accuracy = ±0.5mm
Vertical Traverse	Manual Accuracy = ±1.0 mm
Off-Bottom Clearance Adjustment	Manual Accuracy = ±1.0 mm

Table 2 - 4: Liquid Properties at Room Temperature

Liquid	Viscosity (cp)	Specific Gravity	Seeding
Water	1	1	Naturally occurring 1μm particles
Bayol	2.6	0.78	$TiO_2 \leq 5\mu m$ particulate
TEG and Water			
Mixture 1	15.9	1.10	Naturally occurring 1μm particles
Mixture 2	7.7	1.09	

Table 2 - 5: Laser Specifications

Output power	300mW
Focal length	500mm
Wave length of light	514.5nm
Bragg cell frequency shift	40MHz

Table 2 - 6: Fringe Spacing

Track	Beam Separation (mm)	Fringe Spacing (nm)
1	16.9	15.2
2	33.8	7.6
3	63.4	4.1

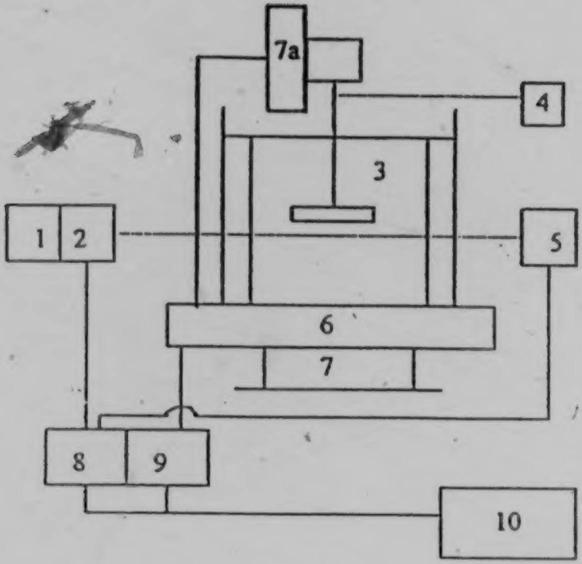

Figure 2 - 1: Experimental Apparatus (Zhou, 1997):

(1) laser, (2) transmitting optics, (3) cylindrical tank, (4) tachometer, (5) receiving optics, (6) x-y traverses, (7) z traverse (7a) clearance adjustment, (8) Doppler signal analyzer, (9) x-y traverse controller and (10) computer.

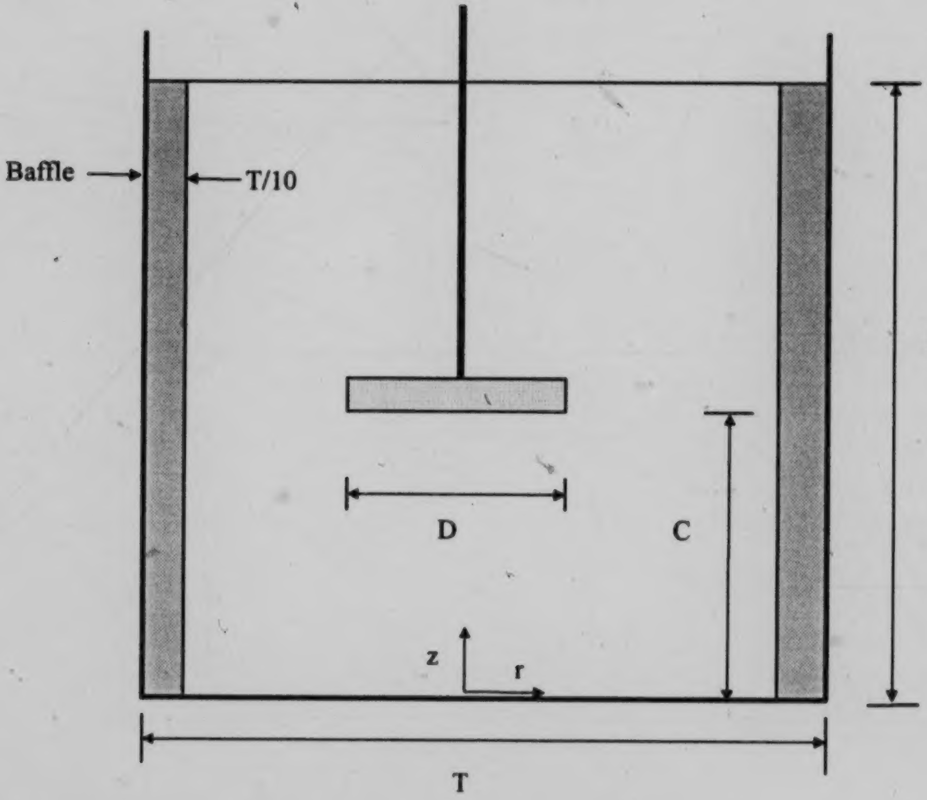
Baffle
T/10
H
D
C
z
r
T

Figure 2 - 2: Tank configuration showing geometric nomenclature.

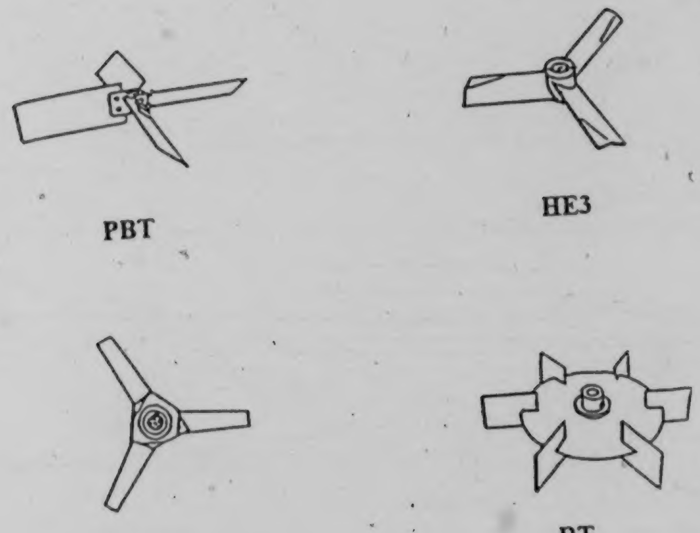

PBT

HE3

A310

RT

Figure 2 - 3: The Four Impellers Used in this work:

- 45° pitched blade turbine (PBT – axial flow)
- high efficiency impeller by Chemineer (HE3 – axial flow)
- airfoil impeller by Lightnin (A310 – axial flow)
- Rushton turbine (RT – radial flow)

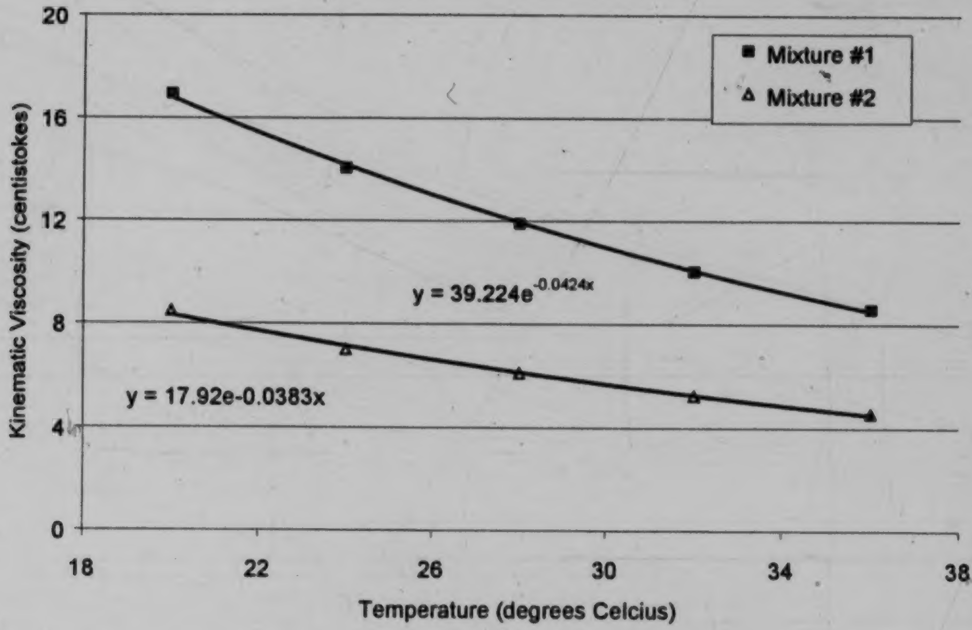

Figure 2 - 4: **Dependence of viscosity on temperature for triethylene glycol and water mixtures. This show the range of viscosities used in Chapter 5. Because of the strong dependence and variable composition, viscosities were measured independently for each run.**

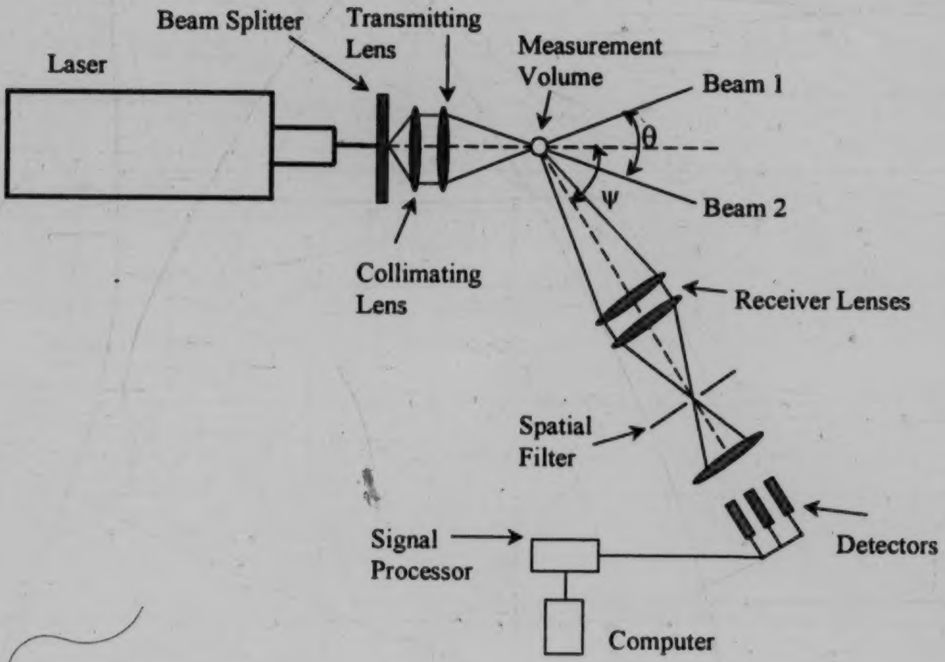
Laser
Beam Splitter
Transmitting Lens
Measurement Volume
Beam 1
θ
ψ
Beam 2
Collimating Lens
Receiver Lenses
Spatial Filter
Signal Processor
Detectors
Computer

Figure 2 - 5: Schematic of the laser Doppler velocimeter (LDV) optical configuration

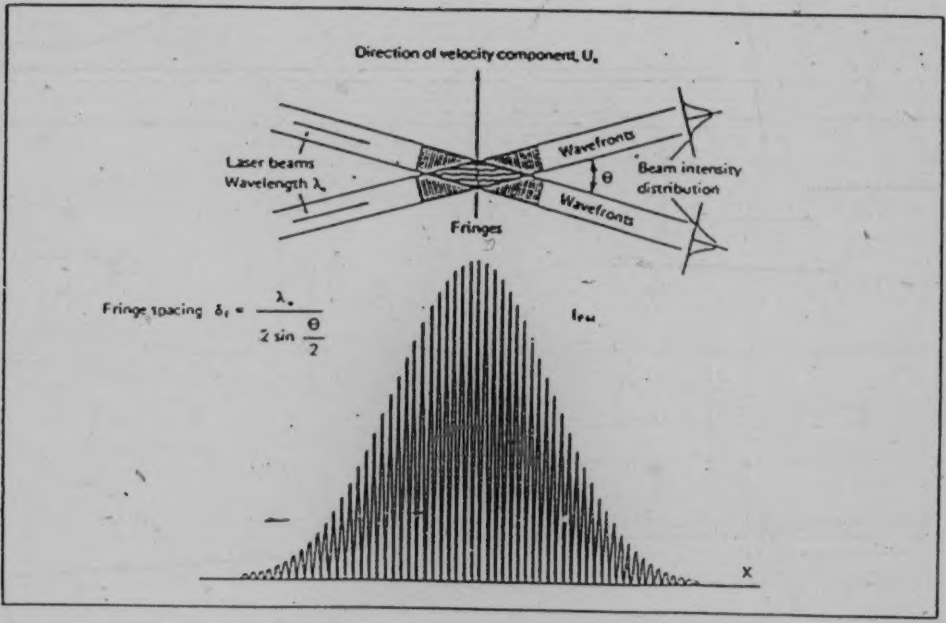
Direction of velocity component, U_x
Laser beams
Wavelength λ_o
Wavefronts
θ
Beam intensity distribution
Wavefronts
Fringes
Fringe spacing $\delta_f = \dfrac{\lambda_o}{2\sin\dfrac{\theta}{2}}$
I_{su}
x

Figure 2-6: LDV measuring volume (George, 1988). The intensity of light is a a maximum at the center of the measuring volume, leading to the Doppler pedestal (bottom) As the two beams cross, virtual fringes are formed (top) and it is the light scatterd from these fringes which gives the Dopper frequency.

Chapter 3

Internal Annular Wall Jets: application to stirred tanks agitated with Rushton turbines

3.1 Introduction

Wall jets have been extensively examined in the literature and wall jet theory has been well established since Glauert's solution was presented in 1956. Key characteristics of wall jets include similarity of velocity profiles, predictable decay of maximum velocity, and linear expansion of the jet due to entrainment of surrounding fluid. In this paper the characteristics of a wall jet are extended to the case of an internal annular wall jet, for which no previous solutions were available. This idealized flow is then used to further our understanding of the complex flow field in stirred tanks.

A two dimensional plane jet can originate from either a line source or a point source. The similarity solution for a wall jet originating from a line source was initially examined by Glauert (1956), who separated the similarity solution into two components: the inner (boundary) layer and the outer (jet) layer. The inner layer is treated as a boundary layer while the similarity profile for the outer layer is modeled as a free jet. Bakke (1957) was the first person to perform experiments on a two dimensional plane wall jet. He confirmed many of Glauert's theoretical results. Since this time Chao and Sandborn (1966) and Launder and Rodi (1981 & 1983) have examined the turbulence, the shear stress at the wall, and the decay and expansion of the plane wall jet. Launder and Rodi (1981 & 1983) further developed the inner layer profile showing that it can be described by a logarithmic function. Recent studies from Abrahamsson et al. (1994), Eriksson et al. (1998) and Venas et al. (1999) have refined the results for the inner layer and the turbulent properties, and have provided additional confirmation of the decay and expansion of the plane wall jet.

There have also been investigations of wall jets that form on the outside of cylinders (Starr and Sparrow, 1966, Rajaratnam, 1976, and Rodman et al. 1989) and the outside of a cone (Sharma, 1981). Rajaratnam(1976) and Starr and Sparrow (1966) derived expressions for the decay of a wall jet on the outside of a cylinder: an external annular wall jet. They showed that the decay depends on the diameter of the cylinder ($d_{cylinder}$) relative to the half width of the jet (b). If $d_{cylinder} >> b$ then the decay of the jet velocity (U_m) is inversely proportional to the *square root* of the distance traveled (i.e. $U_m \propto z^{-0.5}$). If $d_{cylinder} < b$ then the decay of the jet velocity is proportional to the distance traveled (i.e. $U_m \propto z^{-1}$).

This paper progresses from the work on two dimensional wall jets and cylindrical wall jets to develop the equations for an internal annular wall jet. This type of jet has not been of interest until now because most cylindrical systems with internal flow are either small diameter pipes; where annular jets do not exist; large diameter columns; where it is desirable to distribute the flow evenly over the full cross section; or wetted wall columns where the annular flow ends at the gas-liquid interface. The system examined in this work is a stirred tank agitated with a radial impeller. In this geometry, internal annular wall jets are formed due to a large combination of the large diameter of the vessel and the recirculating nature of the flow.

Figure 3-1A shows an internal annular wall jet with an open end and a free stream velocity of zero. It is important to note the axes in the figure because the y-axis (distance from the wall) and the r-axis (radial coordinate) are both used in the derivations which follow. In order to develop and maintain a wall jet with zero free stream velocity, the diameter of the vessel must be significantly larger than the thickness of the jet. As the jet expands, it will eventually penetrate to the center of the pipe. At this point, the internal annular jet will be destroyed.

A second system, shown in Figure 3-1B, was examined for the case of recirculating flow with a negative free stream velocity in this geometry, the end of the cylinder is closed. Under steady flow conditions, the upward and downward volumetric flow rate along any traverse must be equal, since the flow entering the system is equal to the flow leaving the system. Since the flow is symmetrical, the velocity profile is always at a minimum at the center of the tank. The major limitation on this jet is the acceleration of the reverse flow which is required as the jet expands. It is not clear to what extent this is physically realizable in the stirred tank.

In this paper, the equations for internal annular wall jets with zero free stream velocity and with reverse flow are developed and tested in the context of a stirred tank. The first section is devoted to developing the relevant equations for a general internal annular jet and to deriving the jet decay and expansion coefficients. The second section extracts the velocity profiles for the two cases of zero free stream velocity and for reverse flow. The final section examines the experimental data for a stirred tank in the context of the theoretical development.

3.2 Theory

The equations for the internal annular wall jet are based on a two dimensional formulation of the RANS (Reynolds Averaged Navier Stokes) equations. The section begins with the general equations for the decay and expansion functions, followed by development of velocity profiles for the two boundary conditions of interest: zero free stream velocity and flow reversal.

3.2.1 Wall Jet Decay and Expansion

The derivation of the internal annular wall jet begins with the reduction of the RANS equations in cylindrical coordinates. The assumptions used in the reduction of the equations are as follows:

- The flow is fully turbulent; hence, the viscous shear stress can be neglected relative to the turbulent stresses.
- Body forces are balanced by static pressure.
- The jet is axi-symmetric ($\partial/\partial\theta=0$).
- Tangential velocities within the jet are taken to be zero ($W=0$).
- The boundary layer approximations are applied, i.e.:
    - The length scale in the radial direction is much smaller then the length scale in the axial direction; $\partial/\partial r >> \partial/\partial z$.
    - The velocity in the axial direction is much larger then the velocity in the radial direction; $U>>V$.

These assumptions are discussed in detail by Schwarz and Cosart, (1960), Newman et al. (1972), and Rajaratnam and co-authors, (1970, 1974 & 1976). The V (radial) component equation reduces to show that the dynamic pressure gradient is balanced by the Reynolds stress. The W (angular) component is of little interest, since there is no angular variation. The remaining U (axial) component equation and continuity equation in cylindrical coordinates are:

$$U\frac{\partial U}{\partial z}+V\frac{\partial U}{\partial r}=-\left[\frac{1}{r}\frac{\partial}{\partial r}r\overline{u'v'}\right] \tag{3.1}$$

$$r\frac{\partial}{\partial z}U+\frac{\partial}{\partial r}rV=0 \tag{3.2}$$

The next step is based on the assumption that the jet will be self-preserving. Three similarity variables will be used: these are the streamwise velocity (f), the Reynolds stress (g) at a given cross-stream position and the cross-stream distance (η). For the cross stream position the r coordinate is not convenient: the distance from the cylindrical wall, ($y=d_{cylinder}-r$) is used instead. Equation 3.3 gives the similarity variables:

$$\eta=\frac{y}{b} \qquad f(\eta)=\frac{U}{U_m} \qquad g(\eta)=\frac{\overline{u'v'}}{U_m^2} \tag{3.3}$$

Here U_m is the maximum velocity at z, and b is the y location where $U=0.5U_m$. The jet thickness b must be much less than $d_{cylinder}$ to avoid the development of pipe flow. Through substitution of Equation 3.3 into Equation 3.1 the equations of motion become:

$$g'\frac{U_m^2}{b}=\eta f f'\frac{U_m^2 b'}{b}-f^2U_mU'_m+f'V\frac{U_m}{b} \tag{3.4}$$

Here: $f'=df/d\eta$, $g'=dg/d\eta$, $b'=db/dz$ and $U'_m=dU_m/dz$. The continuity equation (Equation 3.2) is used to solve for the radial velocity, V, and is substituted into Equation 3.4, resulting in:

$$g' = b'\left(\eta f f' + f'\int \eta f' d\eta\right) - \frac{b U'_m}{u_m}\left(f^2 + f'\int f d\eta\right) \tag{3.5}$$

If the jet is self-similar, the velocity and the expansion rate must scale with the distance traveled (z), so functions of the form:

$$U_m \propto z^p \qquad b \propto z^q \tag{3.6}$$

are expected. Here p and q are constants to be determined by substituting the expressions of Equation 3.6 into Equation 3.5 and looking only at the variables that vary with z. The result is:

$$z^0 \propto z^{q-1} \tag{3.7}$$

Since the left-hand side of Equation 3.7 is a constant, the right-hand side of Equation 3.7 must also be a constant. For this to occur q must equal 1. To find p, we use the integral of the momentum integral constraint, which is:

$$\frac{d}{dz}\int \rho U^2 2\pi r dr = -2\pi d_{cylinder} \rho \overline{u'v'} \tag{3.8}$$

Substituting the variables of Equation 3.3 into Equation 3.8 and assuming that the Reynolds stress is negligible gives (Rajaratnam 1976):

$$\frac{d}{dz}\int b U_m^2 f^2 d\eta = 0 \tag{3.9}$$

The solution to the integral in Equation 3.9 must be a constant. Using the variables defined in Equation 3.6 and separating the z dependent variables:

$$b U_m^2 \propto z^{2p} z^q \propto z^0 \tag{3.10}$$

Since the right hand side of the equation is a constant and q is 1, p must be equal to –0.5. The results for the velocity decay and the jet expansion for the internal annular wall jet thus become:

$$\frac{U_m}{U_{nozzle}} \propto \frac{1}{\sqrt{z/d_{nozzle}}} \tag{3.11}$$

$$\frac{b}{d_{nozzle}} \propto \frac{z}{d_{nozzle}} \tag{3.12}$$

Here, U_{nozzle} is the nozzle velocity, which is also the maximum velocity in the jet, d_{nozzle} is the size of the nozzle opening, and z is the distance the jet has traveled.

The results derived in Equations 11 and 12 are consistent with external cylindrical wall jet results for a large diameter cylinder, $d_{cylinder}>>b$ (Starr and Sparrow, 1967 and Rajaratnam, 1976). Note that since no boundary conditions have been applied up to this point, the expansion and decay functions will apply to both free stream boundary conditions of interest.

3.2.2 Self-similar Velocity Profiles

A new similarity solution for the velocity profile is now derived for the internal annular jet with flow reversal. The derivation is similar to that for a wall jet with zero free stream velocity, except that the boundary condition for large η is changed. The traditional boundary condition away from the wall has the jet slowly approaching a velocity of zero ($U/U_m=0$ at $\eta=\infty$); however, in a finite cylinder with flow reversal, the velocity quickly goes to zero and then reverses in order to preserve a constant total mass flow across the cylinder. This leads to the boundary condition U/U_m=finite and negative at η=center of the cylinder. Figure 3-2 shows an internal annular wall jet profile from the wall to the center of the tank. This figure illustrates the key points in the velocity profile for a system with recirculating flow. Before moving to the specific solution of this problem, the general velocity profile equations for an annular jet are considered.

Most derivations for wall jets consider the jet in two parts: the boundary layer and the outer layer. The outer layer solution is based on the similarity solution for a free jet while the inner layer is based on boundary layer theory. The primary concern for this study is the outer layer or the free jet solution because this governs the flow in the bulk of a stirred tank. First the jet solution for the outer layer in a stagnant fluid is reviewed in order to show the assumptions made and the form of the original solution. In the context of this classical solution, the similarity profile for a jet in a flow reversal is developed.

The similarity profile for a two dimensional jet begins with the equations of motion in their reduced two-dimensional form:

$$U\frac{\partial U}{\partial z}+V\frac{\partial U}{\partial y}=\frac{1}{\rho}\frac{\partial \tau}{\partial y} \tag{3.13}$$

This equation is valid for internal annular wall jets as long as the tank diameter is much greater than the jet width, as shown in Figure 3-1A. The similarity solution for the jet profile is derived using the Goertler approximation. Goertler (1942) used Prandtl's approximation for the turbulent shear stress:

$$\tau=\rho\varepsilon\frac{\partial U}{\partial y} \tag{3.14}$$

Here, ε is the kinematic eddy viscosity and it is assumed that $\rho\varepsilon >> \mu$. Goertler further assumed that the eddy viscosity is proportional to the local maximum velocity and the half width of the jet:

$$\varepsilon \propto U_m b \qquad \varepsilon = kU_m b \tag{3.15}$$

Here, k is a proportionality constant. From this, Goertler assumed the dimensionless velocity was a function of the distance traveled as well as the transverse location in the jet:

$$\frac{U}{U_m} = F'\left(\sigma\frac{y}{z}\right) = F'(\xi) \tag{3.16}$$

Here, σ is a constant, y is the distance from the center of the jet and z is the distance the jet has traveled. Substituting this information into the equations of motion (Equation 3.16) the integrated form becomes:

$$F^2 + F' = \text{Constant}$$

Here, F' is the first derivative and F is the solved form. Using the boundary conditions in Table 3-1 for a jet in a stagnant fluid Goertler 's (1942) similarity solution in Rajaratnam (1976) is obtained:

$$F'=\frac{U}{U_m}=1-\tanh^2(\xi) \tag{3.17}$$

This solution works very well for jets in stagnant fluid (Rajarnatam, 1976).

We now consider the similarity solution for a two dimensional internal annular system. The derivation is similar to the Goertler solution, but the boundary conditions have changed. The flow does not exist in an infinite medium, but in the presence of recirculation. The new boundary conditions are given in Table 3-2. The differences between the boundary conditions for a recirculating flow (Table 3-2) and a jet in a stationary fluid (Table 3-1) are in boundary conditions IV and V at the center of the tank (R) werhe the velocity is negative. Based on these boundary conditions, the similarity solution becomes:

$$\frac{U}{U_m} = 1 - B\tanh^2(\xi) \qquad (3.18)$$

where B is the difference between the maximum dimensionless velocity and the minimum velocity at the center of the tank (y=T/2).

$$B = 1 - \left(\frac{U}{U_m}\right)_{@y=\frac{T}{2}} \qquad (3.19)$$

For a jet in a stagnant fluid, $U/U_m = 0$ and B=1, reducing Equation 3.18 to the same similarity solution as Equation 3.17 for zero free stream velocity.

Equation 3.18 is the basis of the self similar velocity profile for the internal annular wall jet. The internal annular wall jet profile will change with distance traveled and the constant B will increase as the jet progresses in the system. Figure 3-4 shows dimensionless profiles determined by Equation 3.18 for five different values of B. The profiles for the annular wall jet shown in the figure are for a fixed cylinder size where the upward volumetric flow rate is equal to the downward volumetric flow rate. The lower values of B are near the start of the jet and they increase as the jet progresses. Notice that the similarity profiles aere almost identical from the maximum velocity in the jet up to the half width of the jet. After this point, the minimum velocity determines the velocity profile.

3.2.3 Determination of B Through Application of Continuity Constraint

Unlike a free jet, the velocity profile of an internal annular wall jet depends on the distance the jet has traveled, as shown in Figure 3-3. As the jet travels it expands, forcing the fluid in the center of the tank to accelerate in order to maintain the mass continuity constraint in the streamwise direction. The shape of the velocity profile is defined by

Equation 3.18, and there are two points in the annular wall jet where the velocity is defined a priori: at the wall, and at the half width of the jet. At the wall, the no slip condition applies and the velocity is zero ($U/U_m=0$ at $\eta=0$). At b, the velocity is half the local maximum velocity of the jet ($U/U_m=0.5$ at $\xi=\Phi$ or $\eta=1$) by definition. At the center of the tank, the velocity is at its lowest point (U/U_m =minimum at $\xi=\Phi R/b$ or $\eta=R/b$), but the value of B as a function of streamwise location is needed. This is determined by integrating the volumetric flow over the cross section of the jet.

Figure 3-2 shows the key parameters in the integration: the tank radius ($R=T/2$), the half width of the jet (b), and the net volumetric flow rate ($Q_{up}=Q_{down}$). Figure 3-2 also shows the variables to be solved: the minimum dimensionless velocity (1-B), and the point at which the velocity becomes negative (P). Once b is set, the variables B and P are fixed by the similarity solution. Two conditions are needed in order to solve for B and P:

i. Continuity: in this case upflow is equal to downflow at all z cross sections.

ii. Momentum conservation in the upflow of the jet is constant: Q increases as the jet progresses; however, the upflow and downflow at any cross section are equal .

The volumetric flow rate is given by:

$$Q=\int \text{velocity } dA = 2\pi\int U\, r dr \quad \textbf{(3.20)}$$

Since the similarity profile (U/U_m) is defined with its origin at the tank wall, the integral is restated as:

$$r=R-y \qquad dr=-dy \quad \textbf{(3.21)}$$

$$Q=2\pi\int(Uy-UR)dy \quad \textbf{(3.22)}$$

The volumetric flow rate from the wall of the tank to the position at which the velocity is zero, P, equals the volumetric flow rate from the position P to the center of the tank, R:

$$Q_{up}\Big|_0^P = Q_{down}\Big|_R^P \quad \textbf{(3.23)}$$

The upflow has two parts which are accounted for seperately: the outer portion of the jet and the inner boundary layer.

Outer Layer

To determine the volumetric flow rate in the jet and the recirculating flow, the similarity profile must be defined in a solvable form. The dimensionless velocity similarity profile is not useful in its current form because it relies on the variable ξ. The variable ξ can be modified so that it is a function of the jet half width, b:

$$\xi = \sigma \frac{y}{z} = \sigma \frac{y}{b \cdot \mathrm{const}} = \Phi \frac{y}{b} \qquad \textbf{(3.24)}$$

The similarity profile constant, Φ, accounts for the expansion of b in the outer layer of the jet, the expansion of the inner boundary layer, and applies the necessary conversion from dimensionless distance to radians. Equation 3.18 is now redefined:

$$\frac{U}{U_m} = 1 - B\tanh^2\left(\Phi \frac{y}{b}\right) \qquad \textbf{(3.25)}$$

When y/b=1, U/U_m=0.5, so the similarity constant Φ can be calculated using the half width of the jet;:

$$0.5 = B\tanh^2(\Phi) \qquad \textbf{(3.26)}$$

This is the first of three equations that are used to determine B. The second equation allows solution for the position P where the velocity passes through zero:

$$\frac{1}{B} = \tanh^2\left(\Phi \frac{P}{b}\right) \qquad \textbf{(3.27)}$$

The final equation is based on volumetric flow rate of the outer layer of the jet and the recirculating flow. From Equations 22 and 25, the volumetric flow rate is defined:

$$Q = 2\pi U_m \int y - R + (R - y)B\tanh^2\left(\Phi \frac{y}{b}\right) dy \qquad \textbf{(3.28)}$$

The integral of the equation is:

$$Q = 2\pi U_m \left(Ry(B-1) + 0.5y^2(1-B) + 2B\frac{by}{\Phi} \right) +$$

$$2\pi B \left(\frac{2b(R-y)}{\Phi\left(\cosh\left(2\Phi \frac{y}{b}\right) + \sinh\left(2\Phi \frac{y}{b}\right) + 1\right)} - \frac{b^2}{\Phi^2} \ln\left(\cosh\left(2\Phi \frac{y}{b}\right) + \sinh\left(2\Phi \frac{y}{b}\right) + 1\right) \right) \textbf{(3.29)}$$

With the appropriate limits applied, the volumetric flow rate can be calculated for both the recirculating flow and the outer layer of the jet. Since this equation only accounts for the flow in outer regions of the jet, another set of equations is required to determine the volumetric flow in the inner region or boundary layer of the wall jet.

Inner Layer

The flow in the boundary layer can be dealt with in one of three ways: it can be ignored, it can estimated using a linear profile, or it can be estimated using a model based on boundary layer behavior in other flows. Each of these methods has advantages and disadvantages Ignoring the boundary layer leads to inaccuracies in the calculation of B because part of the flow is ignored; although, its thickness is small, it is at the maximum radius, so the total effect can be significant. The next two methods require knowledge of the boundary layer thickness (δ) in the jet.

First, assuming a linear velocity decay from the peak of the wall jet to the wall, the volumetric flow rate in the boundary layer (Q_{BL}) is estimated as:

$$Q_{BL} = 2\pi\int_0^{\delta} 0.5U_m(R-y)dy = \pi\delta U_m\left(R-\frac{\delta}{2}\right) \qquad \textbf{(3.30)}$$

This method requires the thickness of the boundary layer (δ) and the local maximum velocity U_m. In reality, some curvature in the boundary layer velocity profile exists, so some inaccuracies result from using this method.

The second method requires both the shear stress values along the wall and the boundary layer thickness making the volumetric flow rate more difficult to calculate. Abrahamsson et al. (1994) measured the velocity profile and determined that it follows a logarithmic function:

$$u^+ = 2.44\ln y^+ + 5.0 \qquad \textbf{(3.31)}$$

This equation is valid from a range of $y^+=10$ to $y=\delta$ (or $y^+=u^*\delta/v$). Gerodimos and So (1997) showed that Equation 3.31 is valid in the boundary layer of a wall jet. To complete the profile in the inner layer, a linear relationship is used to determine the profile for values of $y^+<10$:

$$u^+ = y^+ \tag{3.32}$$

Here y^+ is the dimensional distance and u^+ is the dimensionless velocity:

$$y^+ = \frac{u^* y}{\nu} \qquad u^+ = \frac{u}{u^*} \qquad u^* = \sqrt{\frac{\tau_o}{\rho}} \tag{3.33}$$

The shear stress τ_o is required to calculate the velocity u^*, which in turn is required to determine the dimensionless distance, y^+, and dimensionless velocity, u^+. A concern with this method lies in estimating the shear stress; however, it can be estimated if the skin friction coefficient, c_f, at the wall is known:

$$c_f = \frac{\tau_o}{\frac{1}{2}\rho U_{Nozzle}^2} \tag{3.34}$$

The skin friction coefficient is a function of nozzle Reynolds number (Abrahamsson et al., 1994):

$$c_f = 0.0315\mathrm{Re}_{max}^{-0.182} \tag{3.35}$$

This correlation matches data from Eriksson et al. (1998). From Equations 31-35 the volumetric flow rate can be calculated:

$$Q_{BL} = 2\pi u^*\left(\int y^+ dr + \int \left(2.44 \ln y^+ + 5.0\right) dr\right) \tag{3.36}$$

The limits of integration are based on the values calculated from Equation 3.23 and 3.33. When there is no way to calculate the shear stress required for Equation 3.36, Equation 3.30 can be used to estimate the volumetric flow.

Complete Volumetric Flow

All the required equations are now available to equate the upward and downward volumetric flow rates, and solve for B. The upward flow consists of two parts: the boundary layer as described by Equation 3.30 or 3.36 and the outer jet flow as described by Equation 3.28 (for $\delta<y<P$). The recirculating flow for $P<y<R$ is also given by Equation 3.28. Equating the volumetric flow rates and using the limits from Equation 3.23, the integral from Equation 3.28 becomes:

$$Q_{BL}\Big|_0^{\delta} + U_m \int_{\delta}^{P} y - R + (y-R)B\tanh^2\left(\Phi\frac{y}{b}\right)dy = U_m \int_{P}^{R} y - R + (y-R)B\tanh^2\left(\Phi\frac{y}{b}\right)dy \quad (3.37)$$

This is the third equation required to determine B for a given half width (Equations 26 and 27 are the other two).

Equations 26, 27 and 29 are required to determine the three unknowns B, P and Φ. These equations can be solved analytically once the variables R, b, and δ are defined. Figure 3-5 shows the solution for B, P and Φ versus R/b for $\delta/b=0.1$.

In principle, the internal annular jet is now defined for all positions z where P is sufficiently smaller than R to allow reverse flow. If this condition is met, all of the variables can be solved and a profile defined. Consideration of a momentum balance will provide some additional insight regarding the range of z positions where the internal annular jet can be maintained.

3.2.4 Momentum Balance

A momentum balance can be applied to find the point at which the system changes from jet dominated to recirculation dominated. Once the dominant momentum in the flow shifts from the jet to the recirculating flow, the assumption that the diameter of the tank is much greater than the half width of the jet is clearly violated. Figure 3-4 shows the point at which the momentum in the recirculating flow becomes greater than the momentum in the jet. The locus of equal momentum is calculated by equating the upward and downward momentum fluxs. Momentum flux is defined as the integral of mass flow rate with respect to the change in volumetric flow:

$$Mo = \int \rho U dQ = 2\pi\rho \int U^2 r dr \quad (3.38)$$

The coordinate system for the integration of the momentum flux must be changed from dr to dy as was done for volumetric flow rate (Equation 3.21). The velocity, U, is based upon Equation 3.18. Determination of P for the position at which $Mo_{jet}=Mo_{recirc}$, is accomplished by equating Equation 3.38 at two sets of limits.

$$\int_0^P U^2(R-y)dy = \int_P^R U^2(R-y)dy \quad (3.39)$$

Substituting the appropriate equations for velocity and determining P establishes the point in the recirculating flow at which the velocity becomes large enough to match the momentum in the jet. The variables P, B, and b when $Mo_{jet}=Mo_{recirc}$ are as follows:

Given Parameters	$R=1$ and $\delta/b=0.1$
The position at which the flow reverses	$P/R=0.30$
The half width of the jet	$b/R=0.19$
Minimum velocity (1-B)	$\frac{U}{U_m}=-1.1$
Inner Layer	Equation 3.30

When the momentum flux is equated, the jet has expanded to a width of $P/R=0.3$ and the condition of $d_{cylinder}>>b$ no longer holds. A mathematical solution can be attained given the system of equations, but the full solution is of questionable validity after the jet has expanded beyond $P/R>0.3$.

3.2.5 Summary of Similarity Profile Results

The similarity profile, Equation 3.25, has three unknown variables (B, P and Φ) and one parameter based on jet development (b). In this section, a method to determine the variables B, P and Φ was established using the volumetric flow rate in the jet and the recirculating flow. These results will now be applied to the flow in a stirred tank where the half width of the jet (b) is measured and the values of B ($B=1-U/U_m$) are determined from the velocity profile. Both the classical similarity solution for zero free stream velocity and the new solution for recirculating flow are examined. The results will show that the flow at the wall of a stirred tank agitated with a Rushton turbine can be modeled as an internal annular wall jet.

3.3 Experimental

The discharge from a Rushton turbine impinges on the wall of the stirred tank, as shown in Figure 3-5. Two annular wall jets result: one above the impeller and one below. The experiments were designed to measure the velocity profile, decay of maximum velocity, and expansion of the wall jets in this region of the stirred tank. A transparent 240mm cylindrical stirred tank enclosed in a square tank filled with water was used in all experiments. A diagram of the set-up is shown in Figure 3-6A, with the measurement locations shown in Figure 3-6B. Note that the z=0 position is defined relative to the midpoint of the impeller. Mean and fluctuating axial velocities were measured using a Laser Doppler Velocimeter (LDV) as described in Bittorf and Kresta (2000). The equipment settings and experimental parameters are summarized in Table 3-3. The experimental procedure and validation is discussed in detail in Bittorf and Kresta (2000) and Zhou and Kresta (1996).

3.4 Results

The experimental results are examined in several parts. The objective is to determine how closely the flow follows the model of an internal annular jet. First, the variation in the angular direction at several axial positions is used to test for axisymmetry. Next, the velocity profiles in the jet are examined for collapse onto either a single similarity profile, or onto a family of profiles with B changing as a function of z. Both the upward and downward flow are assessed. Where similarity exists, the next test of the model is the decay of the maximum velocity, which is expected to follow a $1/z^{0.5}$ decay. Finally, the fluctuating velocity profiles in the jet are examined for similarity. This last test is the more difficult, since similarity in the fluctuating velocities will not appear until after similarity in the mean velocity is well established. If all of these conditions are met, the hypothesis that the flow at the wall of a stirred tank can be modelled as an internal annular wall jet will be satisfied.

3.4.1 Axisymmetry

First, the assumption of a two dimensional flow was examined in a traverse over the θ direction progressing away from the baffle (Figure 3-6B, Traverse B). The velocities are made dimensionless with the local maximum velocity. The axial velocity measurements are shown in Figure 3-7. The velocities are within 10% of the local maximum velocity at all positions with no clear trends. Based on these results, the model of a two-dimensional system was accepted. The implication of this is that the baffles serve a somewhat different purpose in a radial flow than in an axial flow. For an axial impeller, the baffles concentrate the upward flow in a 3 dimensional jet (Bittorf and Kresta, 2000), but for a radial impeller the baffles simply damp out the remaining tangential motion in the impeller discharge stream.

3.4.2 Similarity Profile

In Equations 11 and 12, the velocity and half width were scaled with the gap width of the nozzle. Since no clear nozzle diameter exists in a stirred tank, the nozzle diameter is replaced by some constant fraction of the tank diameter. This scaling is equivalent to scaling with the baffle width, and was successfully used for the three-dimensional wall jet in axial flow (Bittorf and Kresta, 1999). The resulting scaling equations are:

$$\frac{U_m}{U_{core}} \propto \frac{1}{\sqrt{z/T}} \qquad \frac{b}{T} \propto \frac{z}{T} \qquad \eta = \frac{y}{b} \tag{3.40}$$

The similarity profiles for the Rushton turbine are shown in Figures 3-8 A and 3-8B. The profiles in Figure 3-8A were taken above the impeller for a clearance of C/D=0.75 and the measurements in Figure 3-8B were taken below the impeller for a clearance of C/D=1.75. In each of the similarity profiles, U_m is the local maximum velocity, z/T=0 at the center of the impeller and η=0 is at the tank wall. In Figures 3-8A and 3-8B, the results are compared to the Glauert wall jet profile for a zero free stream velocity. While the Glauert profile does not account for the recirculating flow, it shows a good match with the experimental data up to η=1. Since the velocity profiles exhibit self-similar behavior far beyond this point, it is worthwhile to consider the recirculating condition.

Equation 3.28 was developed to account for the impact of recirculating flow on the annular jet using the similarity constant B. In Figures 3-9B and 3-9B the values of B were fit to the experimental data to give the best fit to each of the measured velocity profiles. The values from the fitted curves in Figures 3-9B and 3-9B are shown in Table 3-4. Next the best fit values of the similarity constant B were compared to the theoretical values of B based on the measured jet half width (from Figure 3-4). The best fit values of

B are plotted on Figure 3-4, allowing a comparison between the theoretical and experimental results. The experimentally determined values of B agree very well with the theoretical profile until the momentum of the jet drops below the momentum in the recirculating flow. As stated earlier, the annular wall jet properties will be difficult to sustain once the momentum in the recirculating flow exceeds momentum the in the wall jet. This is when the jet may start to show three dimensional characteristics. After this point, determination of the velocity profile based on B is essentially a curve fitting exercise with some theoretical basis. There is still value in this approach if the decay of the maximum velocity can be accurately predicted using the similarity scaling, and thus a strong basis for scaling the velocity profile can be established. With this in mind, the decay and expansion of the jet are examined next.

3.4.3 Jet Decay and Expansion Rate

The similarity scaling in Equation 3.40 specifies a velocity decay proportional to $1/z^{0.5}$ in the annular wall jet. The experimental data shown in Figure 3-10 agree very well with this result for absolute values of z/T ranging from 0.3 to 0.55. Below z/T=0.3, the jet is developing. The size of the development zone is independent of the off-bottom clearance of the impeller, as it was for the three-dimensional wall jet reported for axial impellers (Bittorf and Kresta 2000). The decay is the same above and below the impeller, and the annular jet scaling is obeyed.

The wall jet produced by the Rushton turbine has a much slower decay of axial velocity than the 3D wall jet for axial impellers. In addition, the Rushton turbine is often placed at C=T/2, sot the annular jet often traverses only 0.5T, rather than the full height of the tank as is the case for down pumping axial impellers. This supports the general observation that the Rushton turbine induces much stronger circulation throughout the tank than axial impellers, and goes beyond this to allow calculation of the circulation at various heights in the vessel. The most important implication of these results is that the annular wall jet will penetrate further into the volume of the tank than the 3D wall jet before becoming ineffective for bulk circulation.

To complete the jet decay and expansion analysis, the location of the virtual origin and the expansion of the half width of the jet were determined. These are reported in Table 3-5. The internal annular wall jet can be described as originating at a ring source of mass and momentum. Since a jet originating from a theoretical point source always spreads faster than a jet originating from a continuous or line source (Rajaratnam 1976), the annular jet is expected to expand at a much slower rate than the 3D wall jet due to the axial impeller. The data is in agreement with this result. The virtual origin of the jet is approximately 3.5 baffle widths below/above the centerline of the impeller for the upper/lower jets respectively.

3.4.4 Turbulent Intensities

The final property examined for the internal annular wall jet was the turbulent intensities, shown in Figure 3-11. The results from this figure are similar to the results attained from the three dimensional wall jet in a stirred tank (Bittorf and Kresta, 1999). As was the case for the axial impeller, similarity in the fluctuating velocities does not occur until the decay of the mean velocity is well established. This is at a distance of $z/T=0.41$ from the impeller. A longer distance is generally required to establish similarity fluctuating velocities in a wall jet as compared to the mean velocity (Padmanabham and Gowda, 1991b, Swamy and Bandyopadhyay, 1975, and Newman et al., 1972). Because of the limited extent of the flow in a stirred tank, much of the turbulent flow is in the developing part of the jet. Nonetheless, this data establishes a level of turbulence at the wall for the Rushton turbine, which was not previously available in the literature.

3.5 Conclusions

In this paper, equations were developed for an internal annular wall jet with and without recirculating flow. The resulting models were compared to the flow at the wall of a stirred tank: specifically, for a Rushton turbine impeller at two different off bottom clearances. Three important results come from the theoretical developments in this work:

- The decay of velocity in the internal annular wall jet is proportional to the square root of the distance traveled. This is contrasted with axial impellers, where the velocity decays with 1/z. This means that, given the same core velocity, the annular wall jet generated by the Rushton turbine will penetrate further into the volume of the tank than the 3D wall jet generated by axial impellers.
- The similarity solution under recirculating conditions depends on the half width of the jet. Once b is known, and the net volumetric flow is specified, the full profile can be calculated.
- The full similarity solution is only valid as long as the momentum in the annular jet is greater than or equal to the momentum in the recirculating flow, but the decay of the maximum velocity with $1/z^{0.5}$ and the similarity scaling of the velocity profiles over the upwards portion of the jet persist for much longer.

Comparison of the model with experimental results from the stirred tank showed good agreement with the model characteristics:

- the jet is 2 dimensional
- the velocity profiles are self similar
- the velocity decay and expansion agree with the model
- the turbulent intensities develop similarity, but only after the mean velocities are self similar

The strong similarity characteristics of the velocity profiles at the wall of the tank allow a significant simplification of the flow in a stirred tank and provide increased understanding of the differences between axial and radial impellers. With the approximation of an internal annular wall jet, a better formulation of averaged zone models of stirred tanks is possible. These results also provide a good test case for the development of CFD protocols for simulation of stirred tank flow fields.

3.6 Nomenclature

b	distance to $U_m/2$ (L)
B	similarity constant $B=1-(U/U_m)_{minimum}$
C	clearance (L)
c_f	firction coeficient
$d_{cylinder}$	diameter of the cylinder (L)
d_{nozzle}	diameter of the nozzle (L)
D	impeller diameter (L)
F	solved form of the dimensionless velocity derivative
F'	dimensionless velocity derivative
f	dimensionless velocity
g	dimensionless Reynolds stress
N	impeller speed (t^{-1})
k	proportionality constant for eddy viscosity model
P	position at which velocity is zero (L)
p	exponent in similarity solution
Q	volumetirc flow rate (L^3t^{-1})
q	exponent in similarity solution
Re	Reynolds number (ND^2/v)
R	tank radius R=T/2 (L)
T	tank diameter (L)
r	radial coordinate
U_{core}	core velocity ($L\ t^{-1}$)
U_{nozzle}	nozzle velocity ($L\ t^{-1}$)
u	axial velocity component ($L\ t^{-1}$)
U_m	local maximum velocity ($L\ t^{-1}$)
u^+	dimensionless velicty
u^*	shear velocity ($L\ t^{-1}$)
V	y or r velocity component ($L\ t^{-1}$)
V_{tip}	impeller tip speed (πND) ($L\ t^{-1}$)

W	**x or θ velocity component ($L\ t^{-1}$)**
x, y, z	**Cartesian coordinates (L)**
y	**distance from tank wall (L)**
z	**axial coordinate (L)**

Greek

α	**constant from Glauert (1956)**
δ	**boundary layer thickness (L)**
ε	**kinimatic eddy viscosity ($L^2\ t^{-1}$)**
Φ	**similarity constant**
η	**dimensionless distance**
μ	**viscosity ($M\ L^{-1}\ t^{-1}$)**
ν	**kinematic viscosity ($L^2\ t^{-1}$)**
θ	**tangential coordinate (degrees)**
ρ	**density ($M\ L^{-3}$)**
τ	**turbulent stress**
τ_o	**shear stress**
ξ	**similarity constant**

3.7 References

Abrahamsson H., B. Johansson, and L. Fofdahl, 1994, A turbulent plane two-dimensional wall-jet in a quiescent surrounding, *Eur. J. Mech., B/Fluies,* **13**, 533-556.

Bakke P., 1957, An experimental investigation of wall jet, *J. Fluid. Mec.*, **2**, 467-472.

Bittorf K.J. and S.M. Kresta, under review 1999, Three dimensional wall jets driven by axial impeller, *AIChE J.*

Bittorf K.J. and S.M. Kresta, 2000, Active Volume of Mean Circulation for Stirred Tanks Agitated with Axial Impellers, *Chem. Eng. Sci.*, **55**, 1325-1335.

Chao J.L. and V.A. Sandborn, 1966, Evaluation of the momentum equation for a turbulent wall jet, *J. Fluid Mech.*, **26**, 818-828.

Eriksson J.G., R.I. Karlsson, and J. Persson, 1998, An experimental study of a two-dimensional plane turbulent wall jet, *Experiments in Fluids,* **25**, 50-60.

Gerodimos G. and R.M.C. So, 1997, Near-wall modeling of plane turbulent wall jets, *J. Fluids Eng.*, **119**, 304-313.

Glauert M.B., 1956, The wall jet, *J. Fluid Mech.* **1**, 625-643.

Goertler V.H., 1942, Berechnung von Aufgaben der frein Turbulenz auf Grund eines neuen Naherungsansatzes, *Z.A.M.M.*, **22**, 244-254

Kresta S.M. and P.E. Wood, 1991, Prediction of the three dimensional turbulent flow in stirred tanks, *AIChE Journal* **37**, 448-460.

Launder B.E. and Rodi W. 1981 The turbulent wall jet, *Prog. Aerospace Sci.* **19**, 81-128.

Newman B.G., R.P. Patel, S.B. Savage and Tjio H.K., 1972, Three-dimensional wall jet originating from a circular orifice, *Aero. Quarterly* **23**, 188-200.

Padmanabham G. and B.H. Gowda, 1991, Mean and turbulence characteristics as a class of three-dimensional wall jets – Part 1: Mean flow characteristics, *J. of Fluids Engineering* **113**, 620-628.

Rajaratnam N. and B.S. Pani, 1970, Three-dimensional turbulent wall jets *Technical Report, Department of Civil Engineering*, University of Alberta, Edmonton.

Rajaratnam N. and B.S. Pani, 1974, Three-dimensional wall jets, *Proc. ASCE J. Hydraulics Div.* ***100*, *69-83*.**

Rajaratnam N., 1976, *Developments in water sciences, Turbulent Jets,* Elsevier Scientific Publishing Company, New York.

Rodman L.C., N.J. Wood and L. Roberts, 1989, Experimantal investigation of straight and curved annular wall jets, *AIAA J.*, **27**, 1059-1067.

Schwarz W.H. and W.P. Cosart, 1960, The two-dimensional wall-jet, *J. Fluid Mech.* **10**, 481-495.

Sharma R.N., 1981, Experimental Investigation if Conical Wall jets, *AIAA J.*, **19**, 28-33.

Starr J.B. and E.M. Sparrow, 1967, Experiments on a turbulent cylindrical wall jet, *J. Fluid Mech.*, **29**, 495-512.

Swamy N.V. and P. Bandyopadhyay, 1975, Mean and turbulence characteristics of three-dimensional wall jets, *J. Fluid. Mech.* 71, 541-562.

Zhou G. and S.M. Kresta, 1996, Distribution of energy between convective and turbulent flow for three frequently used impellers, *Trans IChemE* **74**, 379-389.

Table 3-1: Boundary conditions for a jet in a stagnant fluid.

I)	$y=0$	$\xi=0$	$U/U_m = F'(0) = 1$
II)	$y=0$	$\xi=0$	$\tau=0$
III)	$y=0$	$\xi=0$	$V=0$
IV)	$y=\infty$	$\xi=\infty$	$F'=0$
V)	$y=\infty$	$\xi=\infty$	$\tau=0$

Table 3-2: Boundary Conditions for a Jet in recirculating flow

I)	$y=0$	$\xi=0$	$U/U_m = F'(0) = 1$
II)	$y=0$	$\xi=0$	$\tau=0$
III)	$y=0$	$\xi=0$	$V=0$
IV)	$y=R$	$\xi=\Phi R/b$	$\left.\frac{dF'}{d\xi}\right\|_{\xi=\Phi R/b} = 0$
V)	$y=R$	$\xi=\Phi R/b$	$\tau=0$

Table 3-3: Equipment Specifications

Argon Laser	Output power = 300mW Beam separation = 0.0340m. Focal length = 500mm Wave length of light = 514.5nm Bragg cell frequency shift = 40MHz Fringe spacing = 7.6μm Velocity Variability = ± 5%
Horizontal Traverses	Computer controlled Accuracy = ±0.25mm
Vertical Traverse	Manual Accuracy = ±1.0 mm
Off-Bottom Clearance Adjustment	Manual Accuracy = ±0.5 mm
Seeding	In tap water - Naturally occurring 1μm particulate
Impeller: Rushton Turbine	D/T=0.33, T=240mm C/D=0.75 and 1.75 Re= 5.33×10^4 Blade Thickness =0.9mm

Table 3-4: Measured Values of B for Equation 3.28 to Fit the Similarity profiles in Figures 3-8B & 3-9B

Distance from the Impeller (z/T)	Jet Half Width (b/R or 2b/T)	Fitted Value of B for the similarity profiles
Low Clearance Case C/D=0.75		
0.10	0.18	1.70
0.21	0.19	1.67
0.31	0.25	1.85
0.42	0.29	1.98
0.52	0.31	1.95
High Clearance case C/D=1.75		
-0.40	0.27	2.04
-0.29	0.23	1.90
-0.19	0.19	1.76
-0.08	0.19	1.85

Table 3-5: Expansion and Virtual Origin of a the Wall Jet in a Stirred Tank

Experiment	Expansion ($\Delta b/\Delta z$)	Virtual Origin (mm)	Core Velocity (U_{core}/V_{tip})
RT D/T=0.33 C/D=1.75	0.19	-79	-0.272
RT D/T=0.33 C/D=0.75	0.18	86	0.244
Absolute Average	**0.19**	**82.5**	**0.258**

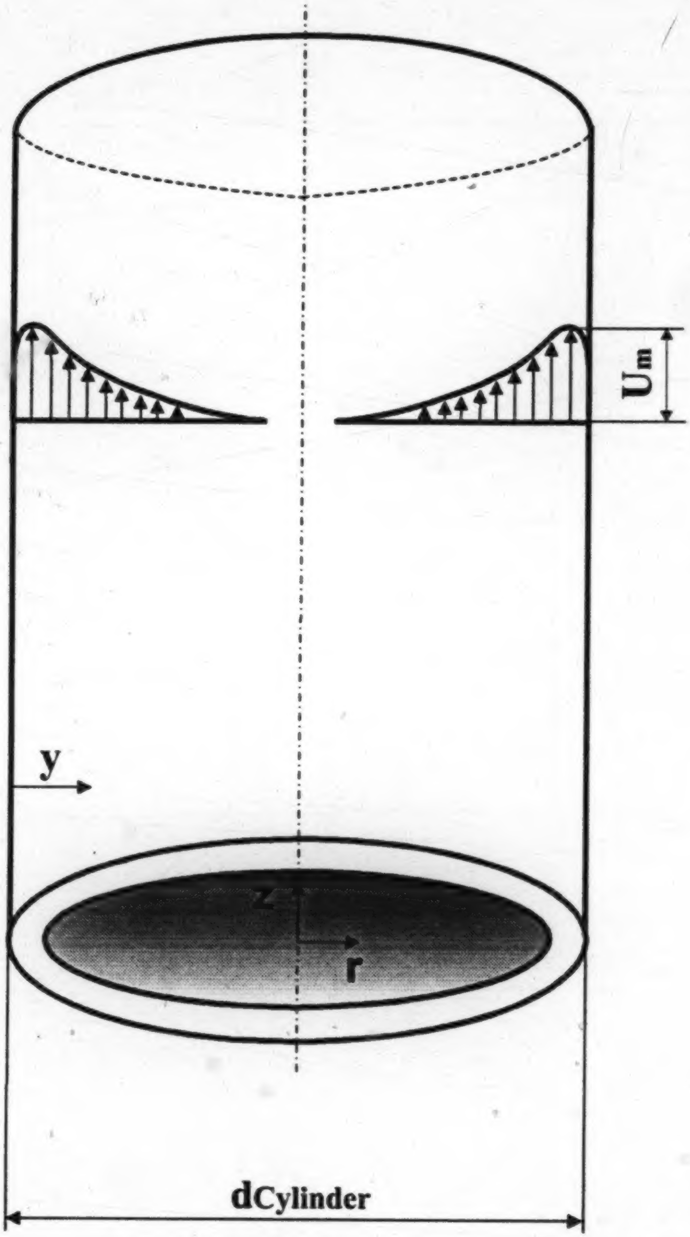

Figure 3 - 1A: Wall jet produced by an annular nozzle inside a cylinder with stagnant fluid. $d_{cylinder}$ is large relative to the nozzle opening and the end of the cylinder is open.

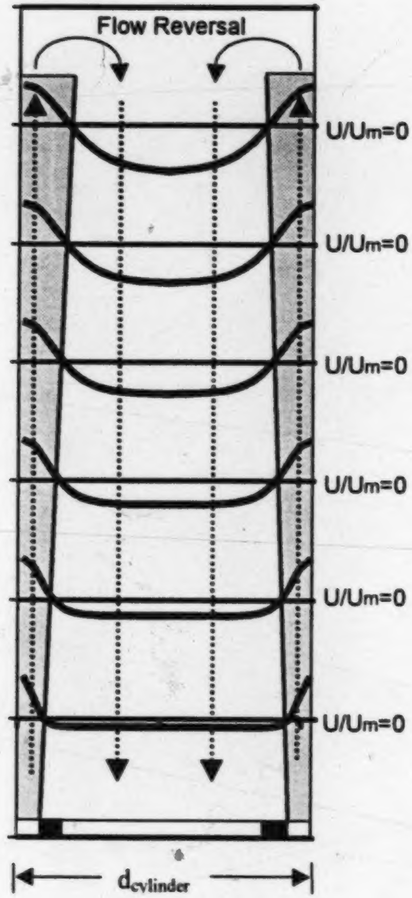
Flow Reversal
U/Um=0
U/Um=0
U/Um=0
U/Um=0
U/Um=0
U/Um=0
$d_{cylinder}$

Figure 3 - 1B: Wall jet produced by an annular nozzle inside a cylinder with recirculating fluid. $d_{cylinder}$ is large relative to the nozzle opening (d_{nozzle}) . The top of the cylinder is closed and the bottom of the cylinder is open.

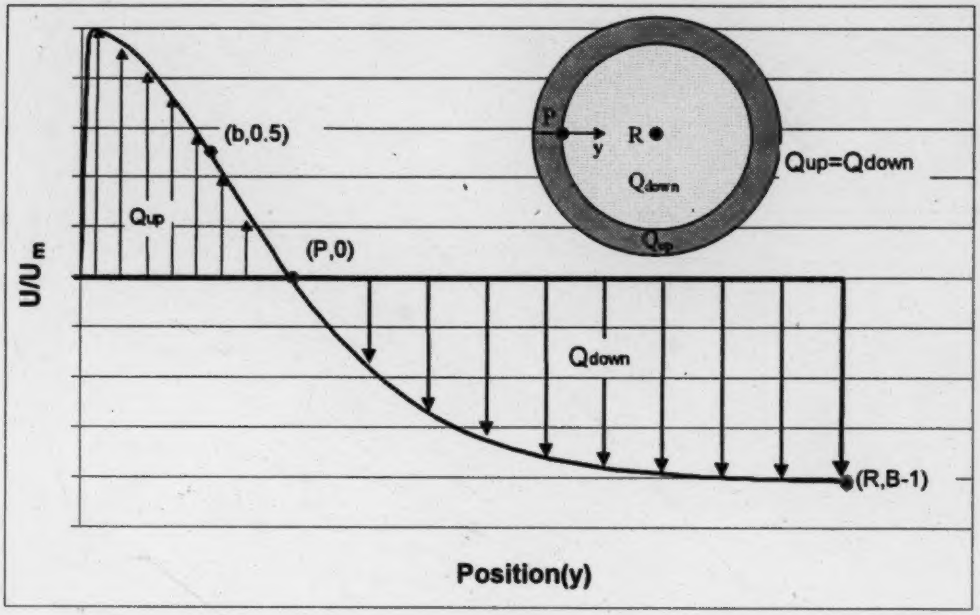
U/U_m
Position(y)
(b,0.5)
(P,0)
(R,B-1)
Qup
Qdown
P
y
R
Qdown
Qup
Qup=Qdown

Figure 3 - 2: Wall jet profile produced by an annular nozzle inside a cylinder with recirculating fluid. This figure shows the area for the upward and downward flows and the nomenclature (b, P, R, and B)

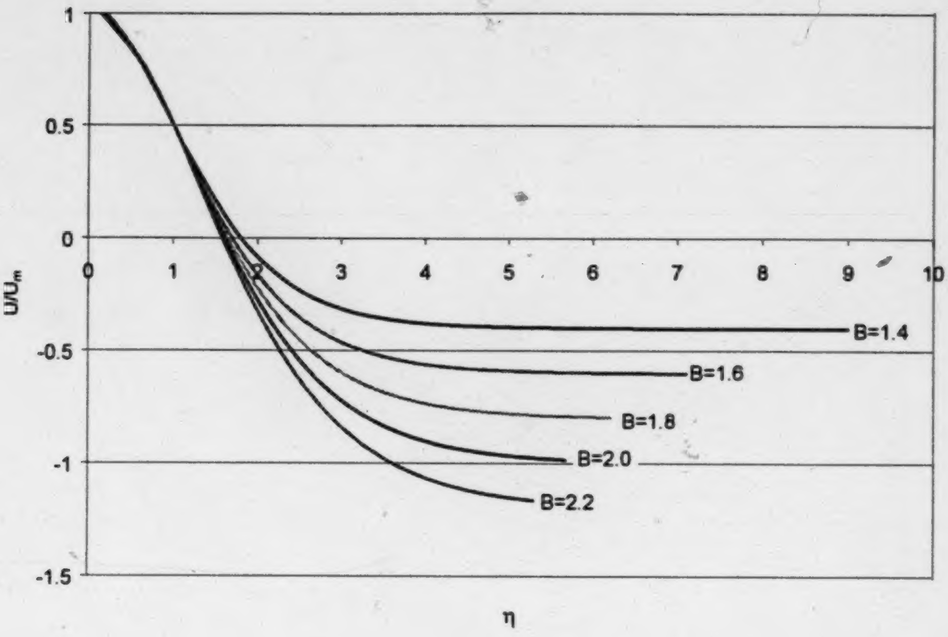

Figure 3 - 3: Jet profiles for various values of B. As the minimum velocity becomes larger the value of B increase.

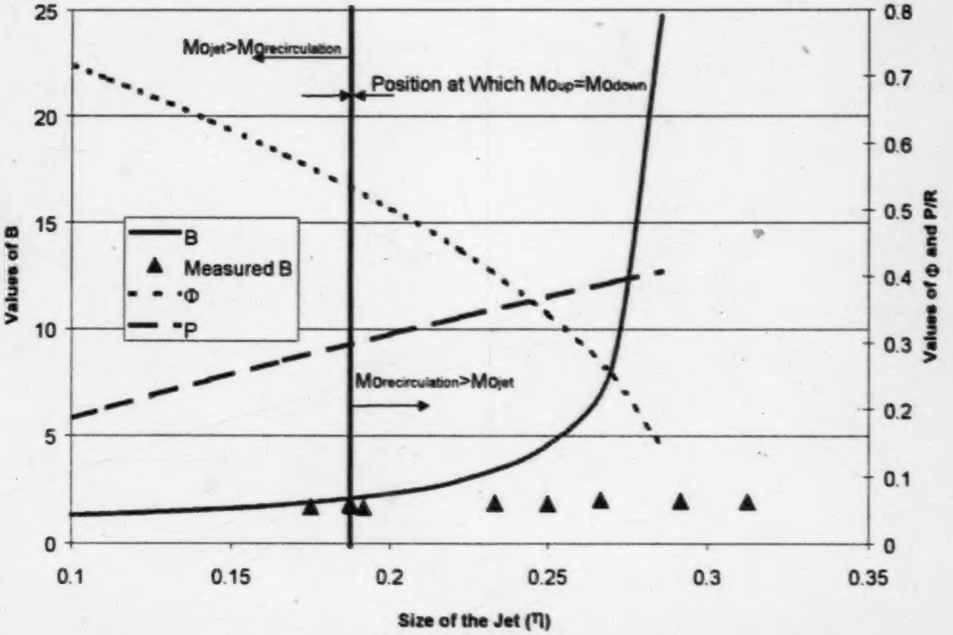

Figure 3 - 4: Solution to variables B, P/R and Φ and experimental values obtained for B. The upward momentum and downward momentum are equal at b/R=0.19. For the experimental data b/R=0.19 occurs at a z/T=0.16.

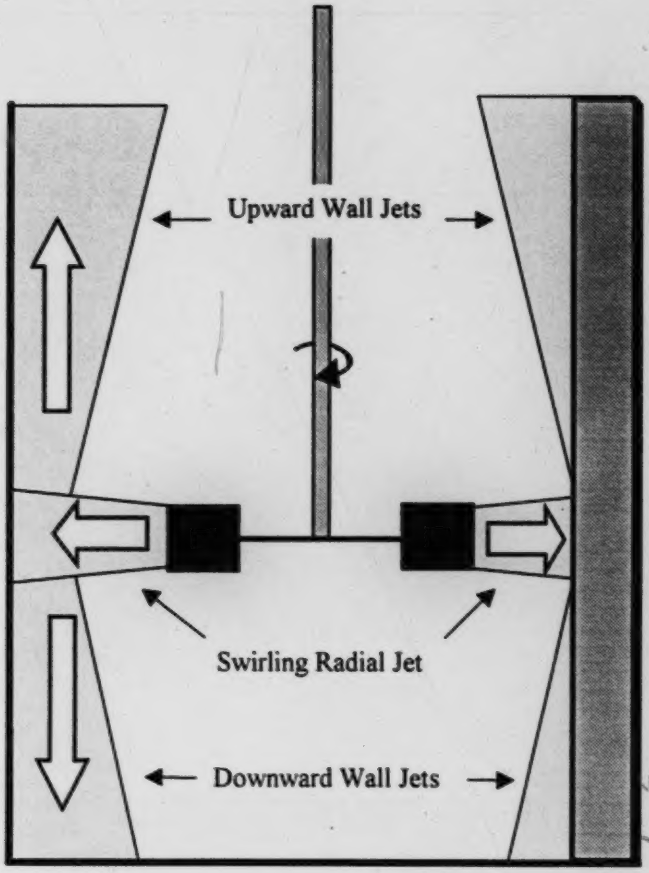
Upward Wall Jets
Swirling Radial Jet
Downward Wall Jets

Figure 3 - 5: Location of the jets in a Rushton Turbine stirred tank.

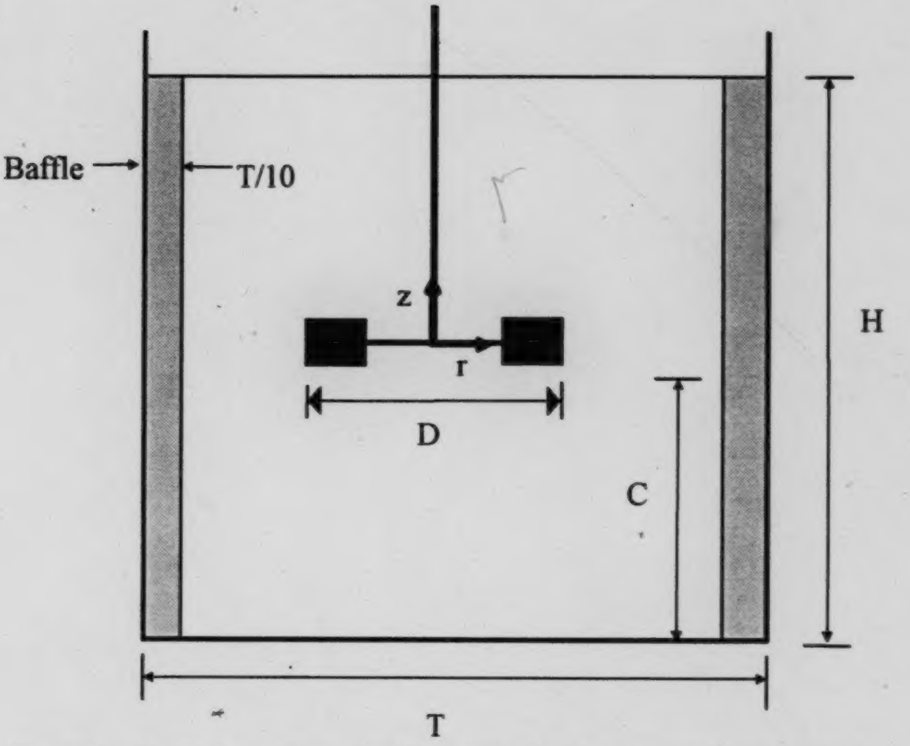
Baffle
T/10
z
r
D
C
H
T

Figure 3 - 6A: Tank configuration (side view) showing geometric nomenclature.

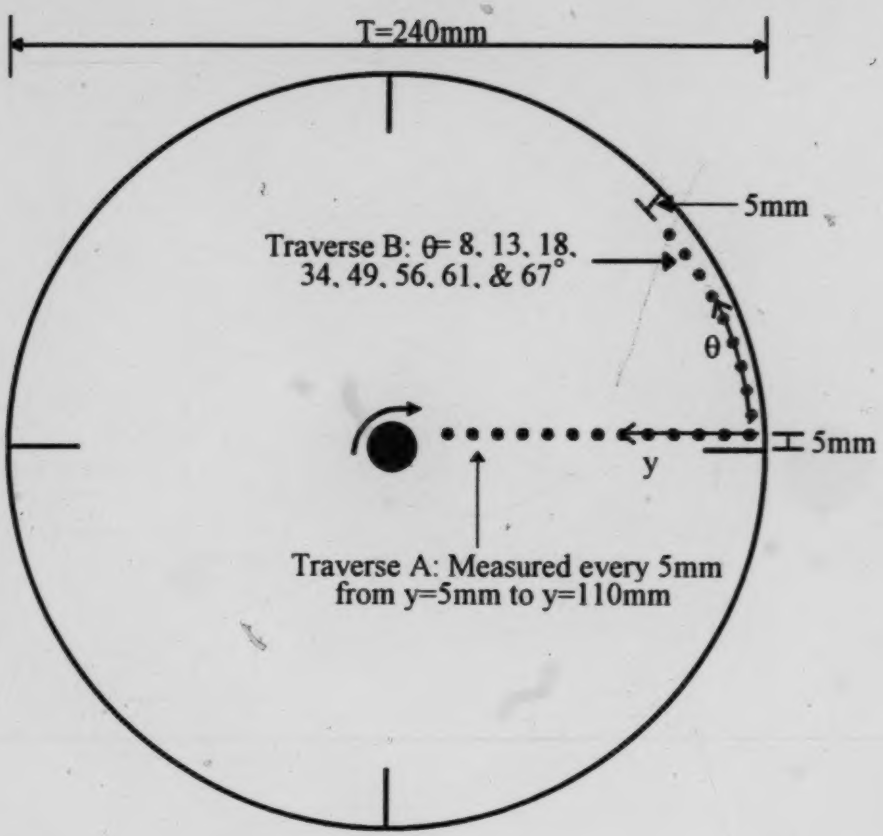
T=240mm
5mm
Traverse B: θ= 8, 13, 18, 34, 49, 56, 61, & 67°
θ
5mm
y
Traverse A: Measured every 5mm from y=5mm to y=110mm

Figure 3 - 6B: Position of measurements (top view)

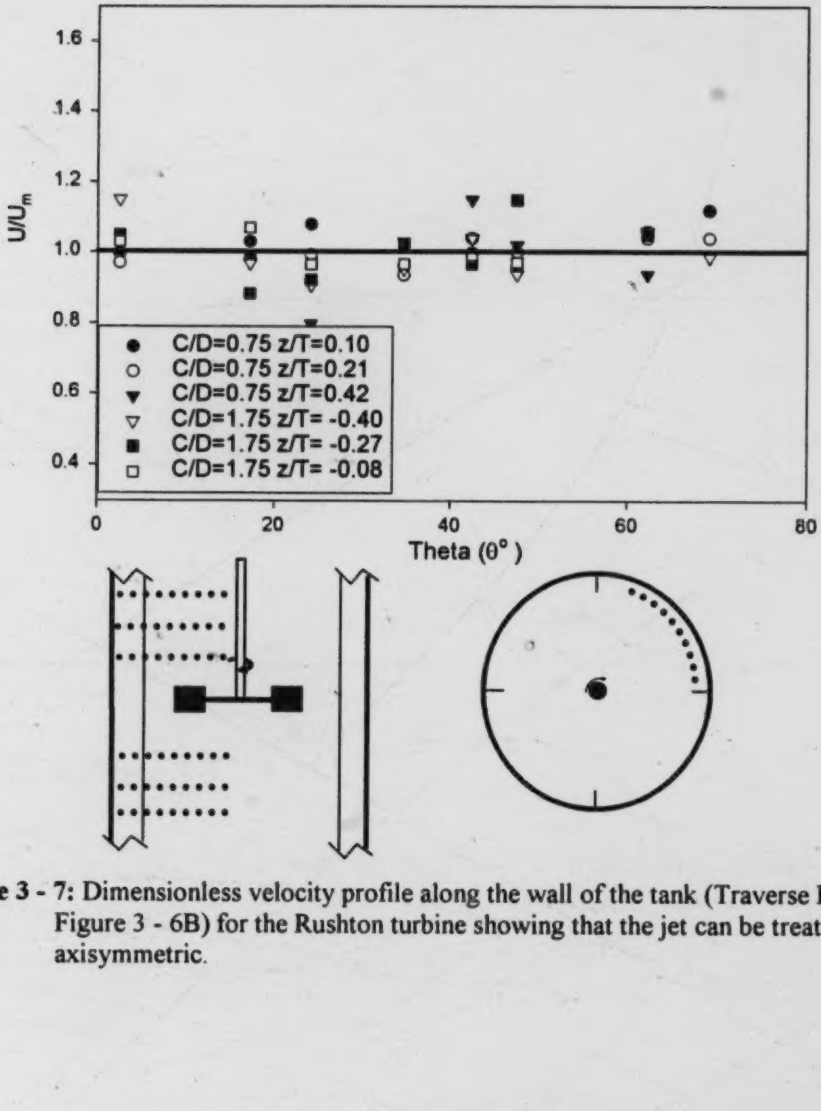

Figure 3 - 7: Dimensionless velocity profile along the wall of the tank (Traverse B in Figure 3 - 6B) for the Rushton turbine showing that the jet can be treated as axisymmetric.

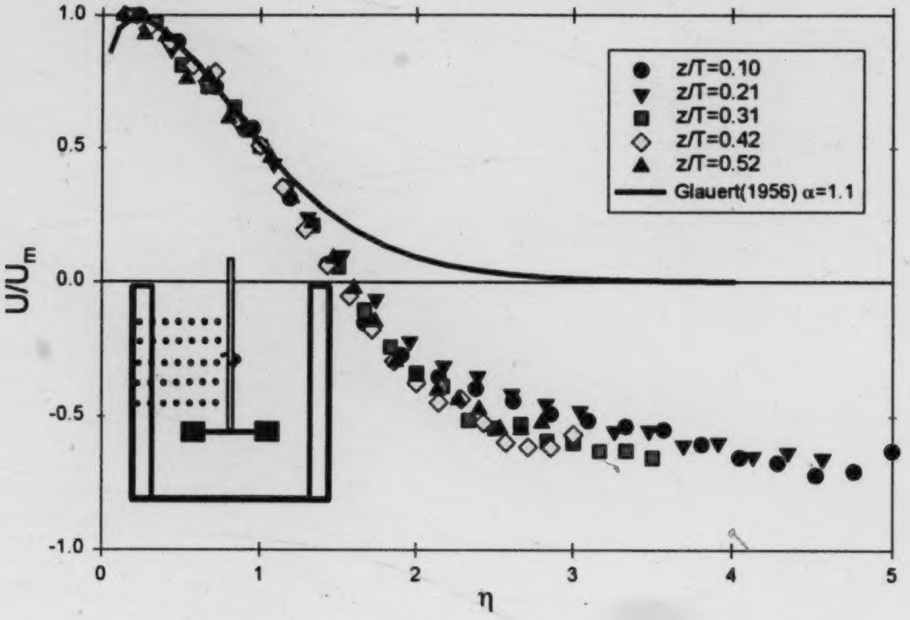

Figure 3 - 8A: Dimensionless velocity distribution for the Rushton turbine at C/D=0.75 and Re=5×10^4. The velocity distributions match Glauert's theory to η_y=1.2 after which recirculation affects the profiles. The recirculating annular jet matches the data well up to U/U_m=-0.2 with little variation between the profiles

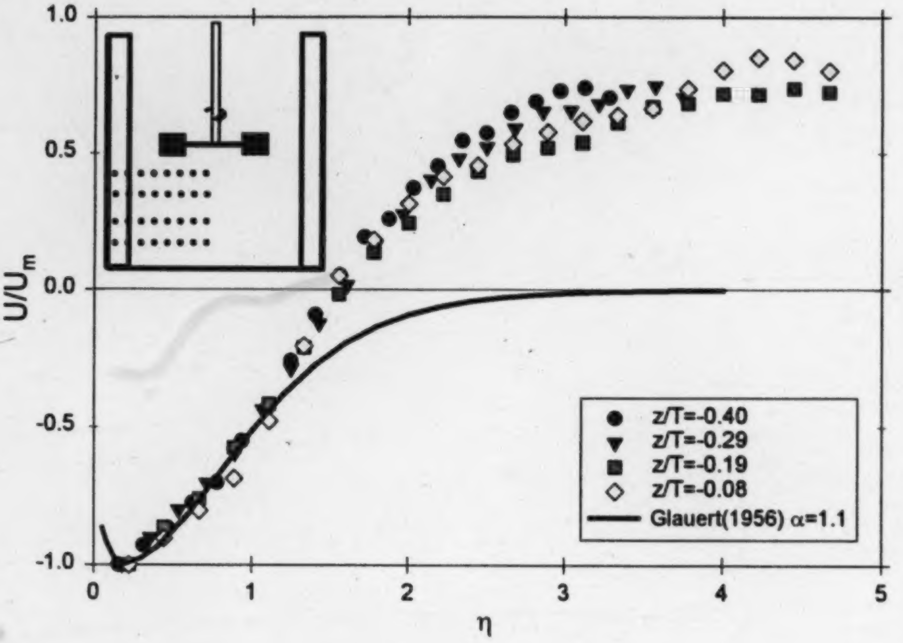

Figure 3 - 8B: Dimensionless velocity distribution for the Rushton Turbine at C/D=1.75 and Re=5×10^4. The velocity distributions match Glauert's theory to η_y=1.2 after which recirculation affects the profiles. The recirculating annular jet matches the data well up U/U_m =0.2 with little variation between the profiles.

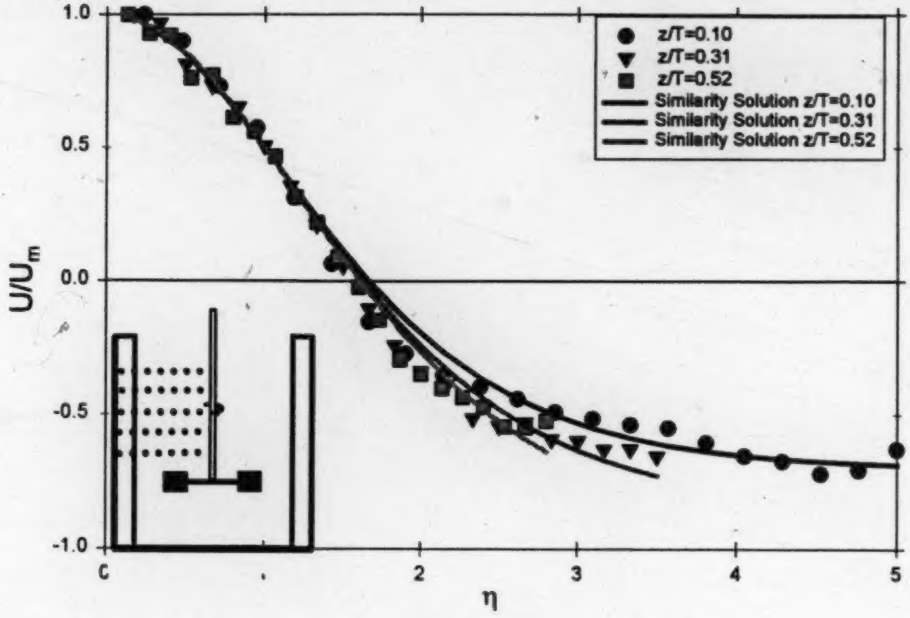

Figure 3 - 9A: Dimensionless velocity distribution for the Rushton turbine at C/D=0.75 and Re=5×10^4. Similarity is maintained beyond $U/U_m = 0$ and the profiles match new similarity solution well.

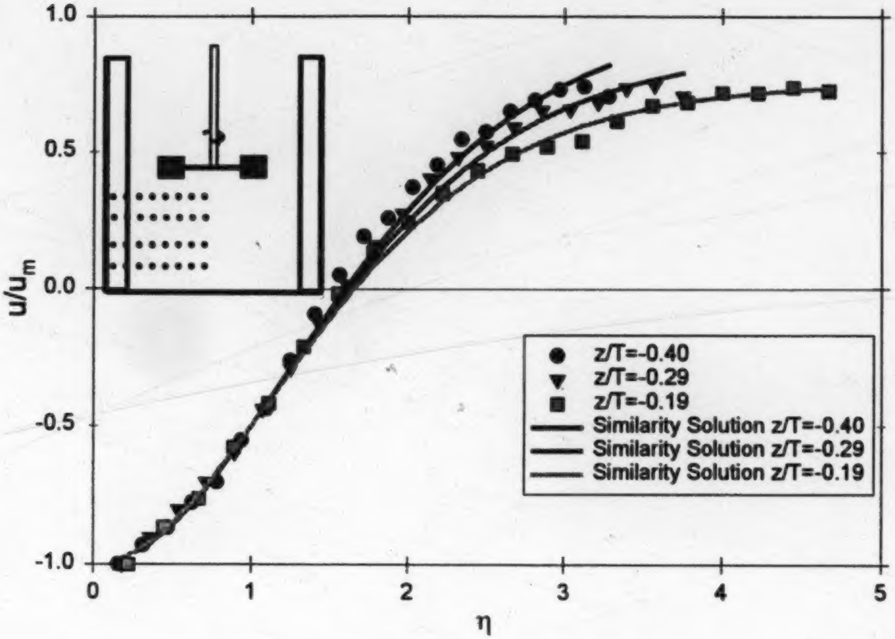

Figure 3 - 9B: Dimensionless velocity profiles for the Rushton Turbine at C/D=1.75 and Re=5×10^4. Similarity is maintained beyond U/U_m =0 and the profiles match new similarity solution well.

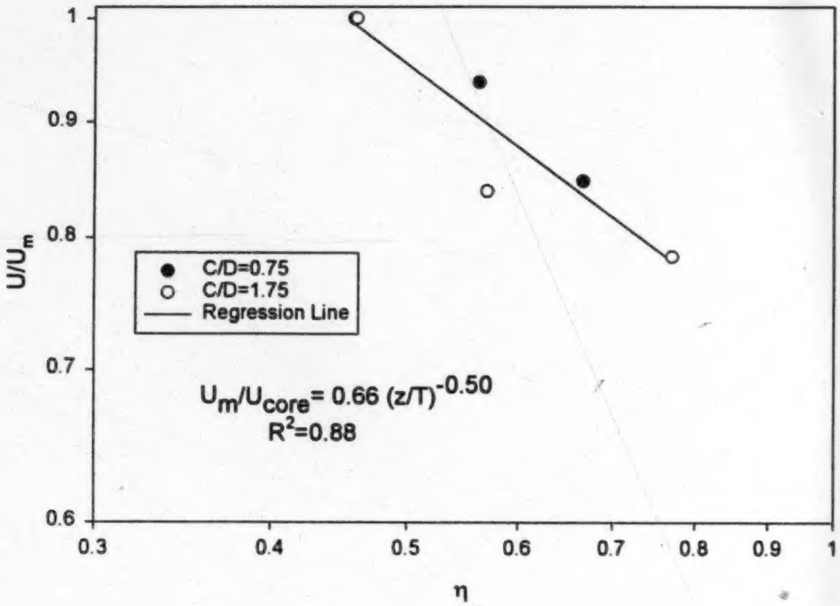

Figure 3 - 10: Decay of maximum velocity for a wall jet produced by the Rushton turbine impeller. The decay of velocity closely matches the similarity scaling.

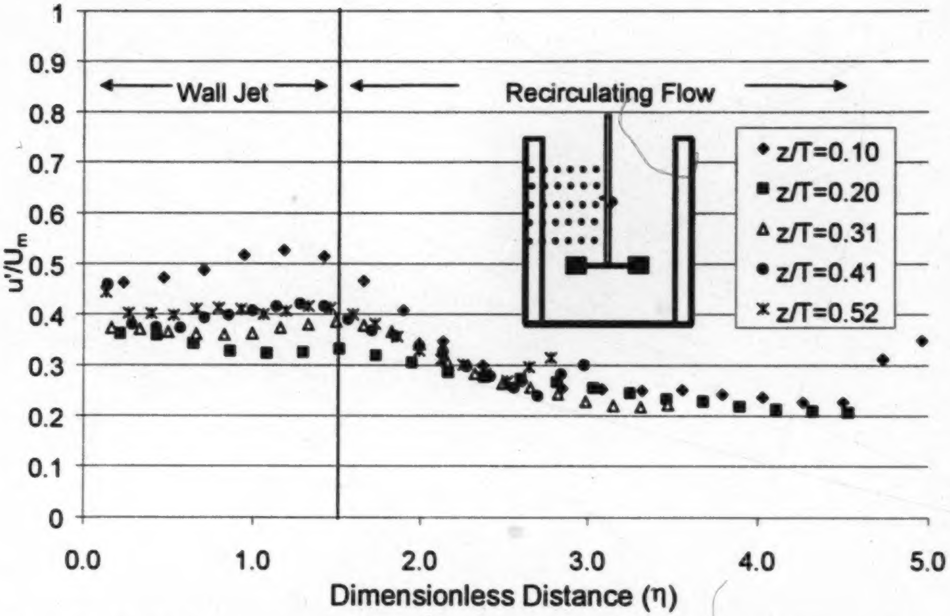

Figure 3 - 11: Turbulence in the internal annular wall jet produced by an RT impeller (D/T=0.33, C/D=0.75, N=500 rpm). After a z/T=0.41 the fluctuating velocities show similarity.

Chapter 4

Three Dimensional Wall Jets Driven by Axial Impellers

4.1 Introduction

Wall jets have been extensively examined in the literature and wall jet theory has been well established since Glauert's solution was presented in 1956. Key characteristics of wall jets include similarity of velocity profiles, predictable decay of maximum velocity, and a linear expansion of the jet due to entrainment of surrounding fluid. In this paper the characteristics of a wall jet are used to further our understanding of the flow field in stirred tanks. Other work in the literature has shown that jets can be successfully applied to model aspects of the flow in a stirred tank. The discharge from a Rushton turbine impeller can be modeled as a swirling radial jet (see review in Kresta and Wood, 1991), while a marine propellor creates a circular swirling free jet (Per et al., 1996). Along with the impeller jet, Fort (1986) suggested that there are a total of three jets in a tank stirred by an axial impeller: a swirling jet produced by the impeller, a radial wall jet at the bottom of the tank and an annular wall jet at the walls of the tank. The objective of this work is to take these ideas further and, in particular, to examine the flow at the wall of the tank in detail. The wall jets generated by axial impellers are classified using their similarity profiles, jet decay, jet expansion and turbulence properties. These results are compared with wall jet theory and with other experiments.

The similarity solution for a wall jet was initially examined by Glauert (1956), who separated the similarity solution into two components: the inner (boundary) layer and the outer jet. The inner layer is treated as a boundary layer while the similarity profile for the outer layer is modeled as a free jet. Figure 4-1 shows the velocity profiles for a wall jet originating at a square nozzle and flowing along the intersection of two walls. (The nomenclature for the derivation of the velocity decay and expansion is shown in this figure. There is an inner and outer layer along each of the walls)

While the configuration in Figure 4-1 is similar to the geometry in a stirred tank at the intersection of the baffle and the tank wall, three dimensional wall jets can be generated using various configurations: jets originating from orifices of various shapes and progressing along a single wall were reported by Rajaratnam & Pani, (1970 & 1974), Newman et al. (1972), Swamy and Bandyopadhyay, (1975), and Venas et al., (1999). Baines (1985) used multiple walls. Although each of these studies had different configurations, they all found that the jet half width (b) expands linearly and the local maximum velocity (U_m) decays inversely with the distance traveled ($U_m/U_{core} \propto 1/x$). This suggests that a three dimensional wall jet will give consistent properties, independent of configuration, making it a good candidate for application to the complex flow in a stirred tank.

The inner layer of the wall jet has been examined extensively to determine wall friction or shear stress at the wall and the turbulent properties of the inner layer. Schwarz and Cosart (1960) report one of the first investigations of the inner layer; Launder and Rodi (1981) review the turbulent wall jet results up to 1981; Abrahamsson et al. (1994), Eriksson et al. (1998), and Venas et al.(1999) provide more recent experimental results, and Gerodimos and So (1997) examine and review the near wall modeling of wall jets. Most of this work concentrates on the inner boundary layer flow and the turbulent scaling of wall jets while this study will focus on the bulk fluid motion in the outer layer.

The outer layer of a wall jet is modeled as a free jet (Glauert (1956), Rajaratnam and co-authors (1970, 1974, & 1976)). The decay of the jet is broken into three zones: a core close to the nozzle where the velocity and turbulence are at a maximum with little decay, a characteristic decay zone which is characteristic for the shape of the nozzle, and a radial decay zone where the expansion of the jet is purely radial (Swamy and Bandyopadhyay (1975)). The characteristic decay zone is dependent on the experimental configuration while the radial decay zone is general for all jets. The scaling for radial decay is easily derived from the RANS (Reynolds averaged Navier Stokes) equations of motion. Padmanabham and Gowda (1991) provide a recent review of the decay and expansion coefficients measured for three dimensional wall jets.

Shifting focus from the classical results for wall jets to the stirred tank, it is possible to model the flow in a stirred tank as a series of jets (Figure 4-2). Flow visualization shows that a discharge stream from the impeller impinges on either the wall or the bottom of the tank, depending on the impeller geometry and placement in the tank. The discharge stream from a radial impeller impinges on the wall of the tank, driving an annular wall jet (examined in detail in Bittorf and Kresta, 2000). The discharge from an axial impeller generally impinges on the bottom of the tank, driving a vertical wall jet along the intersection of the tank wall and the vertical baffle, as shown in Figure 4-2. In jet terminology, this is best described as a three dimensional wall jet along two perpendicular walls originating from a theoretical point source.

In the remainder of this paper, the wall jet properties are tested for application in a stirred tank. Axial velocities are measured in front of the baffle and along the wall of the tank. The velocity decay, jet expansion, virtual origin, and turbulent properties of the jet are compared to values predicted by theory, and to values found in the literature. As a basis for this comparison, the pertinent equations are addressed in the next section.

4.2 Theory

A three dimensional wall jet along two perpendicular walls issuing from a square nozzle is shown in Figure 4-1. Only a summary of the derivation of the expansion and decay is given here, as details are available elsewhere (Rajaratnam and co-authors, 1970, 1974 & 1976).

The Reynolds Averaged Navier-Stokes (RANS) equations in rectangular coordinates are reduced using the following assumptions:

- The flow field is fully turbulent; hence, the viscous shear stress is much smaller than the turbulent shear stress.
- Body forces are balanced by static pressure.
- The boundary layer approximations are:
    - The length scale in the x and y directions is much smaller than the length scale in the direction of flow hence, $\partial/\partial x \cong \partial/\partial y >> \partial/\partial z$.
    - The velocity in the direction of flow is much larger than the velocity in the perpendicular directions hence, $V \cong W << U$.

Given these assumptions the Navier-Stokes equations reduce to:

$$U\frac{\partial U}{\partial z}+V\frac{\partial U}{\partial y}+W\frac{\partial U}{\partial x}=-\left[\frac{\partial\overline{u'v'}}{\partial y}+\frac{\partial\overline{u'w'}}{\partial x}\right] \tag{4.1}$$

The V (or W) component of the equation reduces to show that the dynamic pressure gradient is balanced by the Reynolds stress. From this point a variety of dimensionless distance, velocity and shear stress variables are used to determine the similarity solution (See Rajaratnam and co-authors 1970, 1974 & 1976). The solution found from the dimensionless form of Equation 4.1 is:

$$U_m \propto z^p \qquad b \propto z^q \tag{4.2}$$

The other equation required to attain the similarity solution for the exponents, p and q, is the integral momentum equation which must remain constant at any point in the jet:

$$\frac{d}{dz}\int_0^\infty\int_0^\infty U^2 dydx \tag{4.3}$$

From this equation, the variables p and q are solved. Based on the derivation by Rajaratnam (1970, 1974 & 1976) the expansion and decay rates for a three dimensional wall jet along two perpendicular walls are:

velocity decay: $$\frac{U_m}{U_{nozzle}} \propto \frac{1}{z/d_{nozzle}} \tag{4.4a}$$

jet expansion: $$\frac{b}{d_{nozzle}} \propto \frac{z}{d_{nozzle}} \tag{4.4b}$$

Where U_m is the local maximum velocity (a function of z), U_{nozzle} is the core velocity of the jet (the global maximum at the nozzle outlet), $b_{1/2}$ is the half width of the jet, d_{nozzle} is the diameter of the nozzle, and z is the distance the jet has traveled.

The equations for the wall jet are now placed in the context of a stirred tank. The three major zones (core, characteristic and radial decay) are defined as follows. The potential core is where the wall jet initially develops and in this region, the velocities have little decay. In the case of a stirred tank the potential core is the region close to the bottom of the tank where the vertical flow develops. The core velocity is defined as the global maximum velocity in the jet. The characteristic decay region is where the decay exponent depends on the tank configuration. The region of radial decay is where the maximum velocity decays according to Equation 4.4, independent of impeller geometry and placement in the tank.

In the wall jet equations, the nozzle diameter is used to make the cross stream and stream wise directions dimensionless. Since there is no nozzle in a stirred tank, the tank diameter (T) is used as the characteristic length scale. Other possible length scales, the impeller diameter and the baffle width, were discarded. The experiments showed no dependence of the jet width on the impeller size, so D is not the characteristic length scale. While the baffle width may be an equally valid length scale, in these experiments the baffles are a constant fraction of T, so the tank diameter and the baffle width are indistinguishable as length scales. For the characteristic velocity, the wall jet equations use the nozzle velocity for U_{core}. In the stirred tank, there is no nozzle and the local maximum axial velocity in the jet may increase from its initial value at the bottom of the tank as the vertical circulation is incorporated into the jet. As a result, U_{core} for the stirred tank is defined as the global maximum axial velocity in the wall jet. The resulting dimensionless jet equations for an axial impeller are:

$$\frac{U_m}{U_{core}} \propto \frac{1}{z/T} \qquad \frac{b}{T} \propto \frac{z}{T} \qquad \eta_y = \frac{y}{b} \tag{4.5}$$

Here U_m is the local maximum velocity at a fixed height z, z is the axial distance from the bottom of the tank, y is the distance from the tank wall, b is the position where the velocity is equal to half of the local maximum velocity, and η is the dimensionless distance from the wall.

4.3 Experimental Conditions

Experiments were designed to measure the decay and expansion of wall jets in a stirred tank. Axial velocities were measured using a Laser Doppler Velocimeter (LDV) as described in Bittorf and Kresta (1999) and Zhou and Kresta (1996). The system parameters are summarized in Table 4-1. A transparent 240mm cylindrical stirred tank enclosed in a square tank was agitated using four different impellers: a 4 bladed 45° pitched blade turbine (PBT), a Chemineer HE-3 (HE-3), and Lightnin A310 (A310), all of standard geometry as obtained from the manufactures. The impeller diameter, the rotational speed and the off-bottom clearance were varied. Water was used as the test fluid in all experiments. A complete list of experiments is given in Table 4-2. A cross section of the tank is shown in Figure 4-3A and the measurement locations are shown in Figure 4-3B. Note that the z=0 position is at the bottom of the tank.

4.4 Results

The application of jet theory to a stirred tank may result in significant mismatch due to the effects of tank curvature, the finite width of the baffle, and the low frequency disturbances which have been reported as "surface welling at the baffle" (Brůha et al., 1995) and "macroinstabilities" (Roussinova et al., 2000). In spite of these aspects of the flow, experimental results in this section will show that the three dimensional wall jet generated by an axial impeller follows theory very closely. Two criteria are used to assess the validity of the wall jet model:

1. collapse of axial mean and fluctuating velocities onto a single similarity profile characteristic of wall jets;
2. agreement of the velocity decay and jet expansion with literature values.

These criteria require that the effect of tank curvature be negligible, and that in spite of the relatively complicated origin of the wall jet in a stirred tank, the expansion of the jet be linear.

4.4.1 Similarity Profile

For the flow to be considered a jet, the velocity profiles must collapse onto a single similarity profile as the jet proceeds upward in the tank. Figures 4 A, B, & C show the collapsed similarity profiles for wall jets produced by the A310, HE3 and PBT. The data in these figures were taken on Traverse A (shown in Figure 4-2B) at various axial positions. In the similarity profiles U_m is the local maximum velocity in each of the profiles, $z/T=0$ at the bottom of the tank and $\eta_y=0$ at the tank wall. Given the similarity of the profiles it can be concluded that the first criteria for the flow to be considered a wall jet is satisified.

The similarity profile from Figures 4 A, B & C are averaged and compared to a classical wall jet similarity profiles attained from Glauert (1956, $\alpha=1.3$) in Figure 4-5. In Glauert's solution, alpha is a function of the boundary layer thickness. For this data set, alpha is determined using the location of the maximum velocity at each z in combination with Glauert's Figure 4-3. Because the outer layer of the jet is of greatest interest, the experiments focus on the profile from $U/U_m=1$ to $U/U_m=0$. The velocity profiles match Glauert's results very well up to $U/U_m\approx+0.4$. After this point, the results stray from the classical wall jet results due to the recirculating flow in the tank. This is to be expected, since the wall jet in a stirred tank ends as a shear layer begins, whereas the classical wall jet results were obtained using a free stream velocity of zero.

Perhaps even more useful than the agreement with established characteristics of wall jets is the fact that the wall jet profiles collapse exactly for all three axial impellers. The exact match of the profiles from $U/U_m=1$ to $U/U_m= -0.4$ is extremely useful for the modeling of these flows. This allows a complete characterization of the vertical circulation using only U_{core} and the decay of U_m for *all* axial impellers. The collapse of the profiles can be attributed to the continuity of shear stress at the interface between the two shear layers (the wall jet and the impeller suction). The viscosity in the two shear layers is the same, hence the slopes must be equal, which is what the data in Figure 4-5 shows.

4.4.2 Jet Decay

The size of the development zone and the velocity decay are examined next. Figures 6 A, B, & C show the development and decay of the local maximum velocity in the wall jet for an A310, a PBT and an HE3 as a function of distance along the jet. Both axes use log scales in order to determine the exponent of the decay of U_m with z. The x-axis is the dimensionless distance (z/T) from the bottom of the tank and the y-axis is the dimensionless velocity (U_m/U_{core}): here U_{core} is the global maximum velocity.

Figure 4-6A shows the development zone for an A310 impeller. For this impeller, the development of the potential core extends from z/T=0 to 0.28 as the radial flow impinges on the wall of the tank and is converted to vertical circulation. This is in good agreement with Fort et al. (1993), who showed that the height of the radial flow at the bottom of the tank is z/T=0.2 for a four bladed airfoil impeller. After the impingement height, the jet needs another 0.10 z/T before it starts to decay. The development zone is similar for all 5 cases in this figure extending to z/T=0.28, in spite of the fact that the off bottom clearance varies from $0.32<C.D<0.68$.

Figures 6 B, & C show the characteristic decay and the radial decay regions of the wall jet produced by a PBT and HE-3. The scatter in these figures is within experimental error. The slope of the velocity decay (exponent on x) was determined for each set of data using linear regression. The results, given in Table 4-3, show the range of slopes for both decay regions. The average slopes for the characteristic and radial decay are also given for all three impellers. The characteristic decay zone has an average decay exponent of –0.48. The range of values for individual impellers is quite large due to the short length of this region (approximately 0.1z/T), and the limited amount of data. The average values correspond to a square orifice geometry, for which characteristic decay exponents ranging from 0.16 to 0.61 (Padmanabham and Gowda, 1991) have been observed. The decay of the local maximum velocity for a three dimensional wall jet is proportional to the inverse of the distance traveled. The average slope in the radial decay region differs slightly from this theoretical exponent of –1. This is common for three dimensional wall jets, as shown by Rajaratnam and Pani (1970), who found values ranging from –1.0 to –1.14; Swamy and Bandyopadhyay (1975), who found a value of –1.1, and Padmanabham and Gowda (1991), who found values in the literature ranging from -1.0 to -1.27. Launder and Rodi (1981) have shown that the friction along the wall leads to a more rapid decay due to the influence of the inner layer and the shear stress at the wall. Given this information, the average slope of −1.15 in the radial decay zone for axial impellers can be considered a very good match to the classical three dimensional wall jet.

4.4.3 Three Dimensional Characteristics

The third dimension of the jet was determined by taking axial velocity measurements in the theta direction as shown in Figure 4-3B, Traverse B. These profiles, reported in Figure 4-7, were examined to test for similarity and for a small boundary layer at the baffle wall. Similarity in the θ direction appears later than similarity in the z direction because of the continuity constraint near the bottom of the tank. The flow upwards must match the flow from the impeller discharge, and the only upward flow is near the walls of the tank. To minimize the energy required to satisfy continuity, the flow spreads out in the theta direction. In spite of this distribution in the volumetric flow, the jet does not extend along the whole wall of the tank. The axial velocities terminate their upward climb at different points. This was also shown by Roussinova (1996). In a jet formed by a ring source, the velocities would all terminate at the same point; hence, one may conclude that the jet induced by axial impellers is best modeled as issuing from a point source. Beginning at $z/T=0.67$, traverse B also shows evidence of a three dimensional similarity profile.

4.4.4 Jet Expansion and its Originating Position

Once it is established that the jet starts from a theoretical point source, the origin of the point source and the expansion rate of the jet can be determined. The virtual origin of the jet for each of the axial impellers is given in Table 4-4. The average virtual origin is located approximately one baffle width below the bottom of the tank as shown in Figure 4-2. The expansion of the wall jet ($\Delta b/\Delta z$) is also given in Table 4-4: the half width of the jet spreads with a slope of 0.38, or 20° in the y direction. Bains (1985) predicted the spreading rate for a three dimensional wall jet along two perpendicular walls to be 20°. The spreading rate is dependent on the environment of the jet, because this environment determines the profile of the jet. Moving away from the baffle in the theta direction, the expansion of the jet driven by the PBT has a slope of 0.19, or 10.7°. Although it is not uncommon for the expansion of a jet to be different in these two directions (Bains, 1985), the curvature of the tank may retard the spreading of the jet in a stirred tank. If this is the case, the jet may spread faster in a larger tank where the curvature is not as significant. This aspect of the jet behavior requires further investigation.

4.4.5. Turbulent Intensities

The final characteristic of the jet to be examined for similarity is the fluctuating velocities in the jet. The RMS velocities in the stream-wise direction were measured and compared to those reported elsewhere. In general, fluctuating velocities take longer to develop a similarity profile than mean velocities (Padmanabham and Gowda, 1991b, Swamy and Bandyopadhyay, 1975, and Newman et al., 1971). Figure 4-9 shows the RMS velocity (u') made dimensionless with the local maximum velocity (U_m) for the A310 impeller. It takes a distance of z/T=0.66 from the bottom of the tank before the profiles start to show similarity. Similarity occurs at z/T=0.56 for $\eta > 0.8$. This suggests that full similarity occurs between z/T=0.56 and z/T=0.66. The similarity of turbulent intensities satisfies the final criterion used to determine the existence of a three dimensional wall jet in stirred tanks agitated with axial impellers.

4.5 Conclusions

This study has shown that the vertical circulation along the baffle of a stirred tank agitated with an axial impeller is self similar and decays like a three dimensional wall jet. Five major characteristics of the wall jet can be summarized from this work:

- The local maximum velocity decays inversely with the distance traveled ($U_m \propto z^{-1}$)
- The jet expansion in the y direction is proportional to the distance traveled ($b_{1/2} \propto z$)

- The mean velocity profiles exhibit similarity beyond z/T=0.354 in the y direction (away from the wall), and beyond z/T=0.67 in the angular direction (away from the baffle)
- Similarity is maintained in the recirculating flow beyond $U/U_m=0$, up to $U/U_m=-0.4$ in the y direction
- The fluctuating velocity profiles exhibit similarity in tbe y direction beyond z/T=0.67

The strong similarity characteristics of the velocity profiles at the wall of the tank are somewhat surprising, given the complexity of the flow, but agree very well with jet theory. These results provide simplified models and an increased understanding of the characteristics of axial flow in a stirred tank. With the ability to approximate the flow at the wall with a jet and a potential core region, better models of solids distribution and averaged zone models of the tank may be possible. Finally, these results provide a set of test data for development of CFD simulation protocols in stirred tanks.

4.6 Nomenclature

b	distance to $U_m/2$ (L)
C	clearance (L)
d_{nozzle}	nozzle diameter of the wall jet(L)
D	impeller diameter (L)
H	tank height H=T (L)
N	impeller speed (t^{-1})
p	exponent in similarity solution
q	exponent in similarity solution
Re	Reynolds number (ND^2/v)
T	tank diameter (L)
r	radial coordinate
U_{core}	core velocity ($L\ t^{-1}$)
U_{nozzle}	nozzle velocity ($L\ t^{-1}$)
U	axial velocity component ($L\ t^{-1}$)
U_m	local maximum velocity ($L\ t^{-1}$)
u', v', w'	fluctuating velocity ($L\ t^{-1}$)
V	y or r velocity component ($L\ t^{-1}$)
W	x or θ velocity component ($L\ t^{-1}$)
x, y, z	Cartesian coordinates (L)
y	distance from tank wall (L)
z	axial coordinate (L)

Greek

α	constant from Glauert (1956)
θ	tangential coordinate (degrees)
ν	kinematic viscosity ($L^2\ t^{-1}$)
η	dimensionless distance
ρ	density ($M\ L^{-3}$)

4.7 References

Abrahamsson H., B. Johansson, and L. Fofdahl, 1994, A turbulent plane two-dimensional wall-jet in a quiescent surrounding, *Eur. J. Mech., B. Fluids,* **13**, 533-556.

Bains D.W., 1985, Entrainment by a buoyant jet flowing along vertical walls, *Journal of Hydraulic Research* **23**, 221-228.

Bittorf K.J. and S.M. Kresta, 2000, Active Volume of Mean Circulation for Stirred Tanks Agitated with Axial Impellers, *Chem. Eng. Sci.*, **55**, 1325-1335.

Bruha, O., I. Fort, & P. Smolka, 1995, Phenomenon of turbulent macroinstabilities in agitated systems, *Collect. Czech. Chem. Commun.* **60,** 85-94.

Eriksson J.G., R.I. Karlsson, and J. Persson, 1998, An experimental study of a two-dimensional plane turbulent wall jet, *Experiments in Fluids,* **25**, 50-60.

Fort I., 1986, Flow and turbulence in vessels with axial impellers, in the book: *Mixing: Theory and Practice*, Vol. III, V.W. Uhl and J.B. Gray ed., New York: Academic Press Inc., 133-197.

Fort I., M. Vozny, and T. Makovsky, 1993, Flow and turbulence in a baffled system with impeller with inclined blades, *ACTA Polytechnica*, **33**, 31-44.

Gerodimos G. and R.M.C. So, 1997, Near-wall modeling of plane turbulent wall jets, *J. Fluids Eng.*, **119**, 304-313.

Glauert M.B., 1956, The wall jet, *J. Fluid Mech.* **1**, 625-643.

Kresta S.M. and P.E. Wood, 1991, Prediction of the three dimensional turbulent flow in stirred tanks, *AIChE Journal* **37**, 448-460.

Kresta S. M., 1996, Boundary Conditions Required for the CFD Simulation of Flows in Stirred Tanks, in the book: *Advances in Fluid Mechanics: Multiphase Reactor and Polymerization System Hydrodynamics*, N. P. Cheremisinoff ed., Houston: Gulf Publishing Company, 297-316.

Launder B.E. and Rodi W. 1981 The turbulent wall jet, *Prog. Aerospace Sci.* **19**, 81-128.

Newman B.G., R.P. Patel, S.B. Savage and Tjio H.K., 1972, Three-dimensional wall jet originating from a circular orifice, *Aero. Quarterly* **23**, 188-200.

Padmanabham G. and B.H. Gowda, 1991, Mean and turbulence characteristics as a class of three-dimensional wall jets – Part 1: Mean flow characteristics, *J. of Fluids Engineering* **113**, 620-628.

Per P., L. Magnus, and J. Lennart, 1996, Measurements of the velocity field downstream of an impeller, *J. of Fluids Engineering* **118**, 602-610.

Rajaratnam N. and B.S. Pani, 1970, Three-dimensional turbulent wall jets *Technical Report, Department of Civil Engineering*, University of Alberta, Edmonton.

Rajaratnam N. and B.S. Pani, 1974, Three-dimensional wall jets, *Proc. ASCE J. Hydraulics Div.* ***100**, 69-83.*

Rajaratnam N., 1976, *Developments in water sciences, Turbulent Jets,* Elsevier Scientific Publishing Company, New York.

Roussinova V., 1996, Comparison of detailed LDV-measurements with numerical simulation on turbulent flow-fields within stirred tank reactors, MSc Thesis, Lehrstuhl fur Stromungsmechanik, Germany.

Roussinova, V., B. Grgic and S. Kresta, 2000, Study of macro-instabilities in stirred tanks using a velocity decomposition technique, in press.

Schwarz W.H. and W.P. Cosart, 1960, The two-dimensional wall-jet, *J. Fluid Mech.* **10**, 481-495.

Swamy N.V. and P. Bandyopadhyay, 1975, Mean and turbulence characteristics of three-dimensional wall jets, *J. Fluid. Mech.* **71**, 541-562.

Venas B., and H. Abrahamsson, P.A. Krogstad, and L. Lofdahl, 1999, Plused hot-wire measurements in two and three-dimensional wall jets, *Experiments in Fluids*, **27**, 210-218.

Zhou G. and S.M. Kresta, 1996, Distribution of energy between convective and turbulent flow for three frequently used impellers, *Trans IChemE* **74**, 379-389.

Table 4-1: Equipment Specifications

Argon Laser	Output power = 300mW Beam separation = 0.0340m. Focal length = 500mm Wave length of light = 514.5nm Bragg cell frequency shift = 40MHz Fringe spacing = 7.6μm Velocity Variability = ± 5%
Horizontal Traverses	Computer controlled Accuracy = ±0.25mm
Vertical Traverse	Manual Accuracy = ±1.0 mm
Off-Bottom Clearance Adjustment	Manual Accuracy = ±0.5 mm
Seeding	In tap water - Naturally occurring 1μm particulate

Table 4-2: Experimental Conditions

Impeller	Diameter (D/T)	Reynolds #'s Examined	Clearances (C/D)	Dimensionless Core Velocity for a given Clearace (U_{core}/V_{tip})
A310	0.58	6.53×10^4 1.96×10^5	0.32 0.50 0.68	0.290 0.255 0.230
HE3	0.50	6.00×10^4 2.40×10^5	0.50 0.67	0.226 0.210
PBT	0.33	5.33×10^4 1.07×10^5	0.40 1.0	0.326 0.298

Table 4-3: Decay Coefficients of the Wall Jet for Axial Impellers

	Characteristic Decay Zone			
Impeller	Range of Slopes	Average Slope	Average Intercept	R^2 of the Average Slope
A310	-0.27 to -0.86	-0.48	-0.31	0.76
PBT	-0.47 to -0.66	-0.59	-0.35	0.88
HE3	-0.29 to - 0.44	-0.30	-0.19	0.73
Overall Average		-0.49	-0.30	0.73
	Radial Decay Zone			
Impeller	Range of Slopes	Average Slope	Average Intercept	R^2 of the Average Slope
A310	-0.95 to -1.12	-1.00	-0.54	0.97
PBT	-1.08 to -1.29	-1.13	-0.61	0.97
HE3	-1.19 to -1.48	-1.30	-0.60	0.90
Overall Average		-1.15	-0.56	0.94

Table 4-4: Expansion and Virtual Origin of a the Wall Jet in a Stirred Tank

Experiment	Expansion ($\Delta b/\Delta z$)	Virtual Origin (mm)
PBT D/T=0.33 C/D=0.40	0.38	-20
A310 D/T=0.58 C/D=0.68	0.36	-16
HE-3 D/T=0.50 C/D=0.50	0.39	-29
Average For Axial Impellers	**0.38**	**-22**

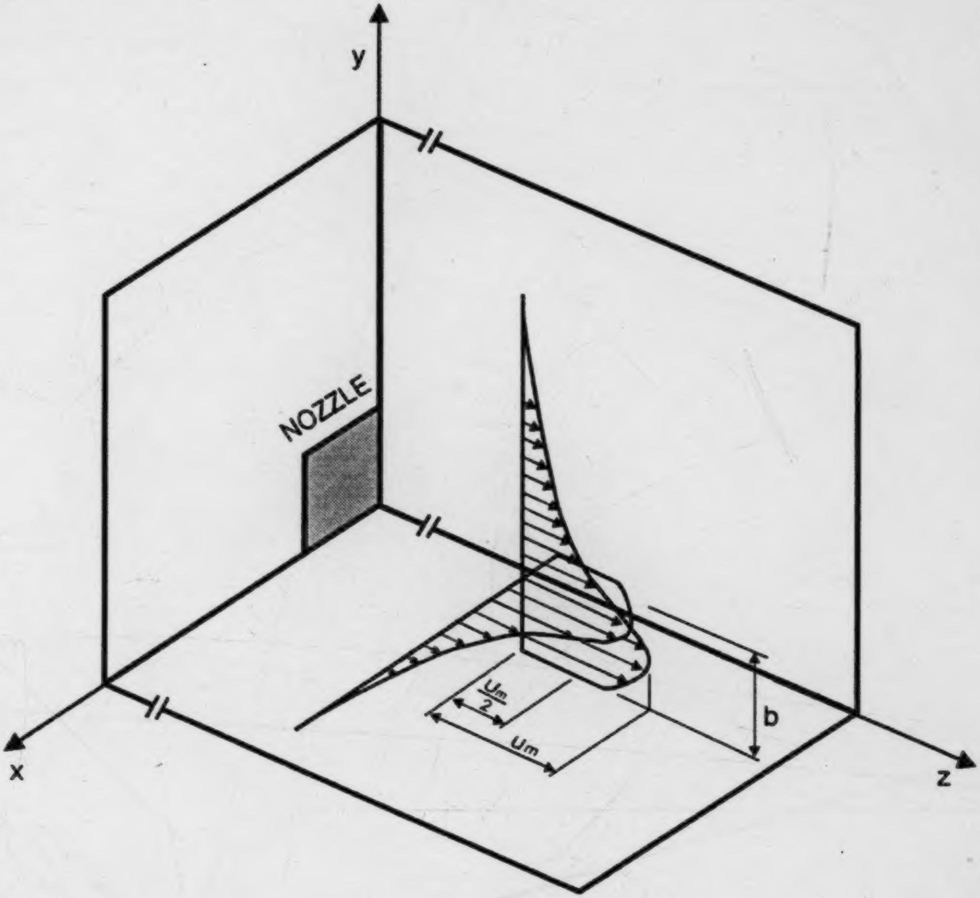
y
NOZZLE
$\frac{U_m}{2}$
U_m
b
x
z

Figure 4 - 1: Three dimensional wall jet produced by a square nozzle. b is the half width of the jet in the y direction. In the tank the baffle is in the y-z plane and the tank wall is in the x-z plane.

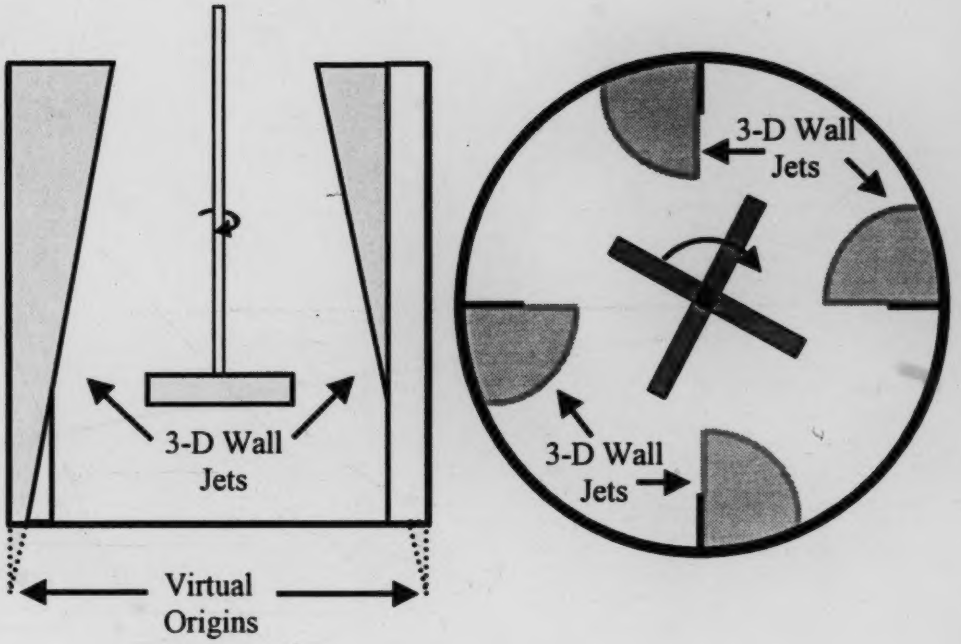
3-D Wall Jets
Virtual Origins
3-D Wall Jets
3-D Wall Jets

Figure 4 - 2: Location of the virtual origins for a three dimensional wall jet driven by an axial impeller system. The virtual origins are located approximately one baffle width below the tank.

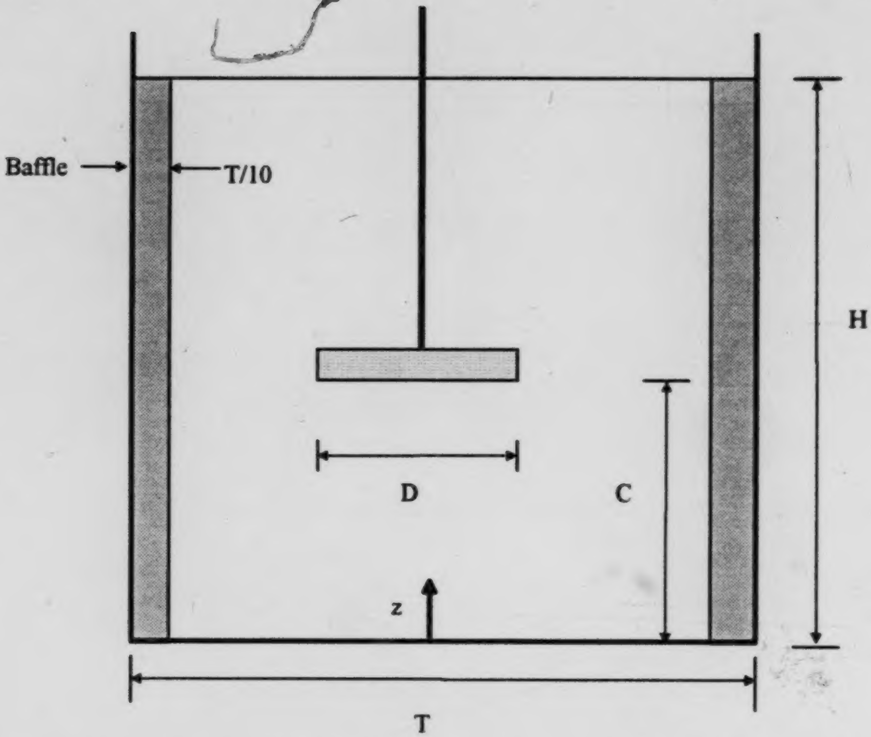
Baffle
T/10
H
D
C
z
T

Figure 4 - 3A: Tank configuration (side view) showing geometric nomenclature.

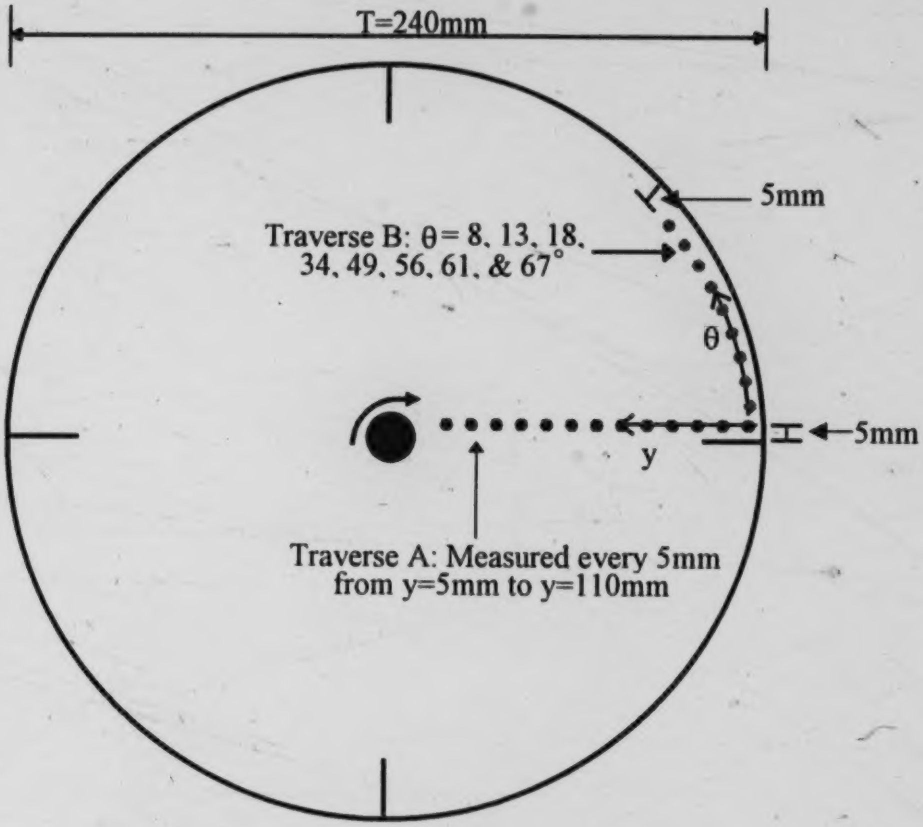
T=240mm
5mm
Traverse B: θ= 8, 13, 18, 34, 49, 56, 61, & 67°
θ
5mm
y
Traverse A: Measured every 5mm from y=5mm to y=110mm

Figure 4 - 3B: Position of measurements (top view)

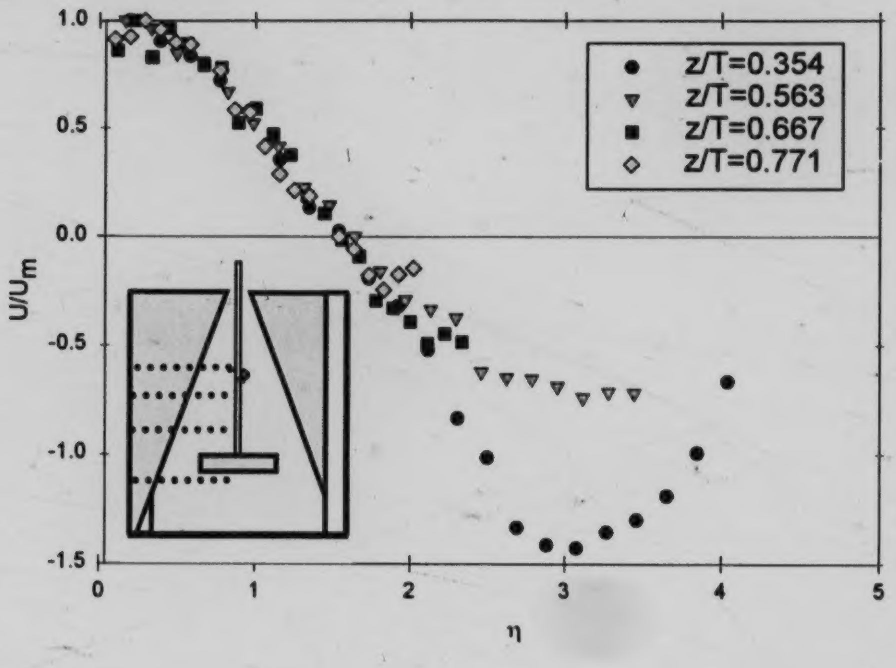

Figure 4 - **4A:** Dimensionless velocity distribution for the A310 impeller at C/D=0.68 and Re=1.96×10^5. Profile fits U/U$_m$=0.5 and at 1.0 by definition. Similarity is maintained beyond the end of the jet model (U/U$_m$ =0) except for one traverse below the impeller (z/T=0.354) where additional momentum is injected into the flow.

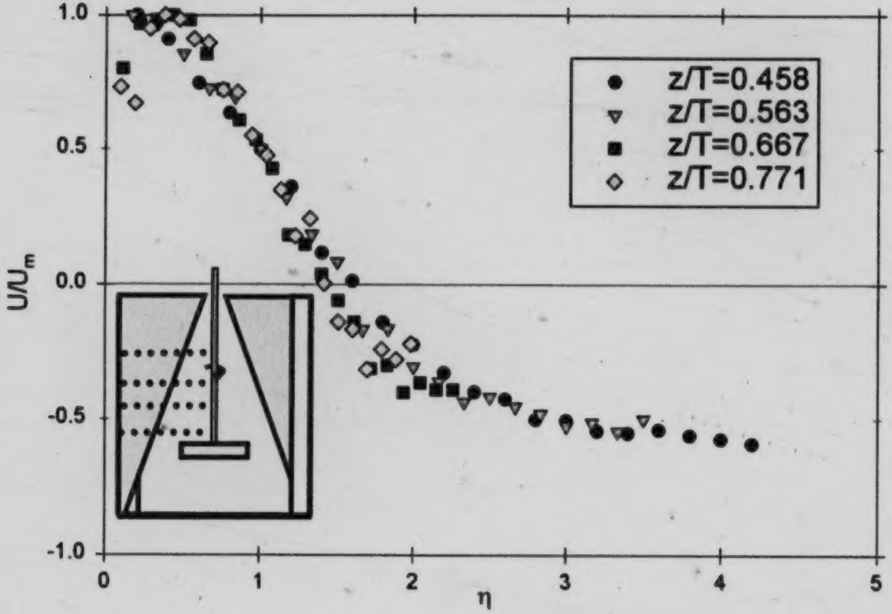

Figure 4 - 4B: Dimensionless velocity distribution for the PBT impeller at C/D=0.4 and Re=5.33×10^4. Profile fits at U/U_m =0.5 and 1.0 by definition. Similarity is maintained beyond U/U_m =0 for all profiles.

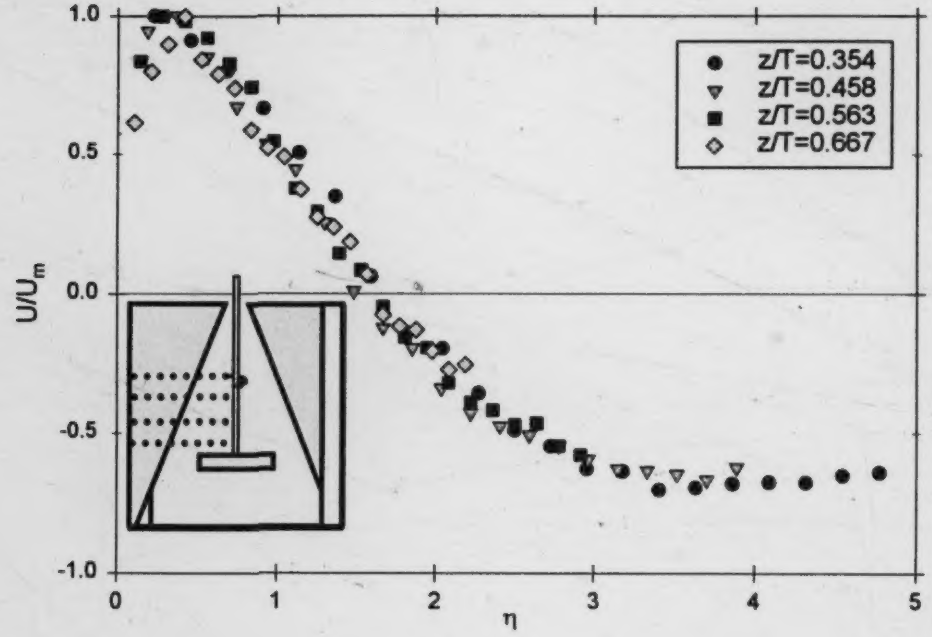

Figure 4 - 4C: Dimensionless velocity distribution for the HE3 impeller at C/D=0.5 and Re=2.40×10^4. Profile fits at U/U_m =0.5 and 1.0 by definition. Similarity is maintained beyond U/U_m =0 for all profiles.

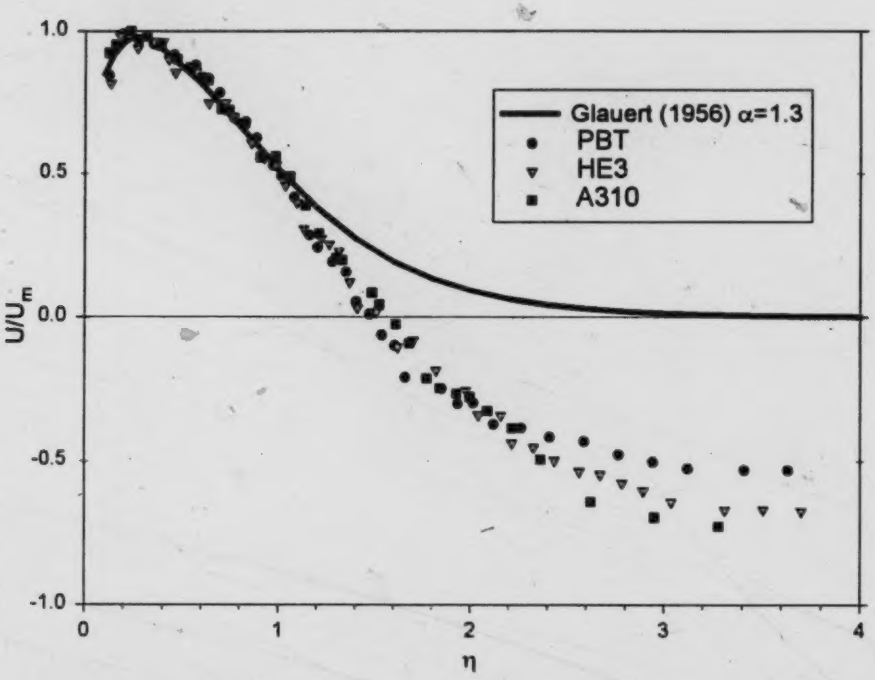

Figure 4 - 5: Comparison of velocity distributions for the three axial impellers with the theoretical wall jet model. The velocity distributions match Glauert's theory to η=1.2 after which recirculation affects the profiles. Similarity between all three impellers is maintained up to η=2.3.

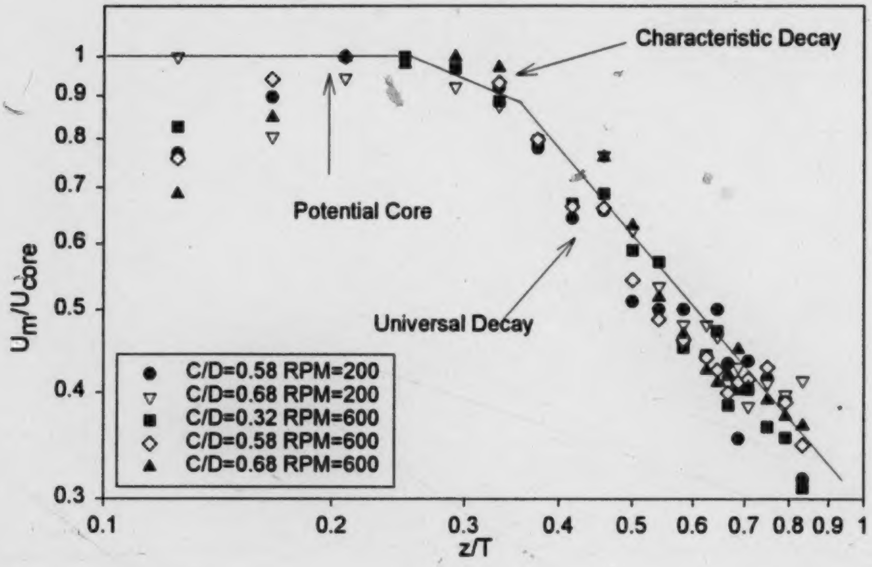

Figure 4 - 6A: Decay of maximum velocity for the wall jet produced by the A310 impeller for various dimensionless clearances (C/D) and rotational speeds.

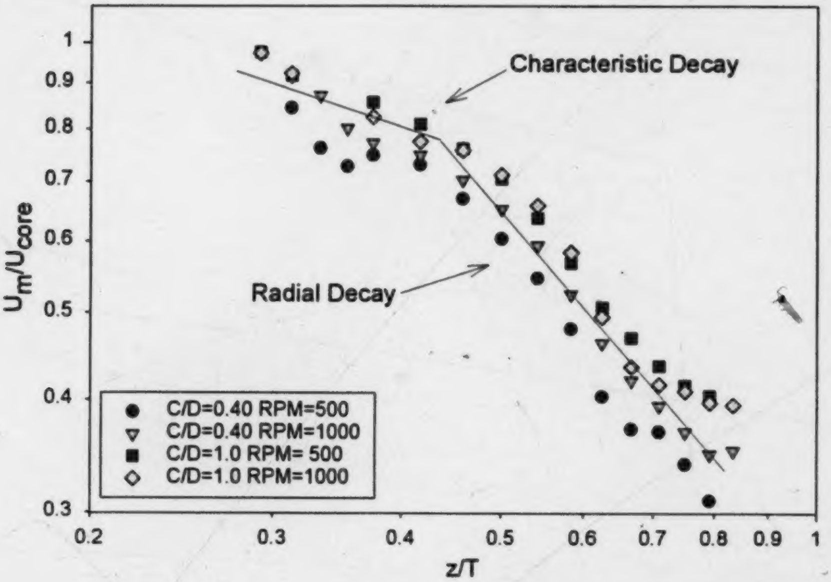

Figure 4 - 6B: Decay of maximum velocity for the wall jet produced by the PBT impeller for various dimensionless clearances (C/D) and rotational speeds.

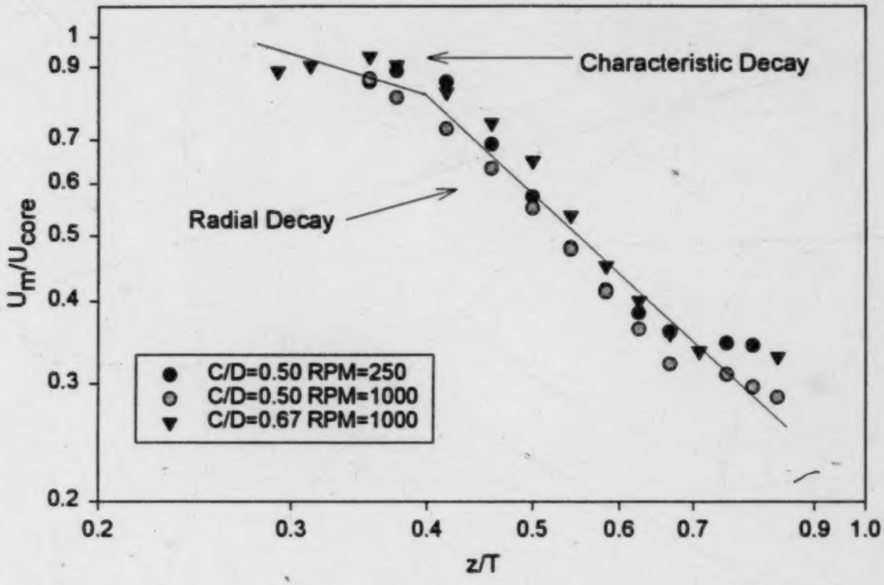

Figure 4 - 6C: Decay of maximum velocity for the wall jet produced by the HE3 impeller for various dimensionless clearances (C/D) and rotational speeds.

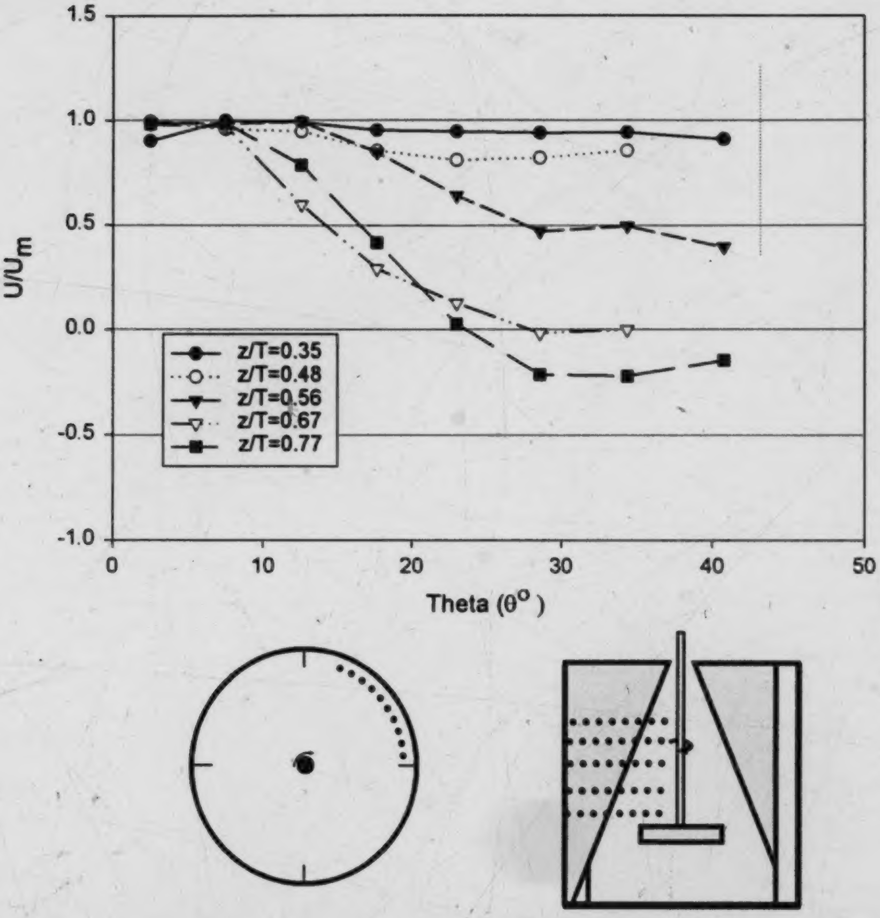

Figure 4 - 7: Velocity profile along the wall of the tank (Traverse B in Figure 4 - 3B) for the PBT impeller at C/D=1. The jet becomes the dominant flow in the theta direction only after a dimensionless height of z/T=0.67.

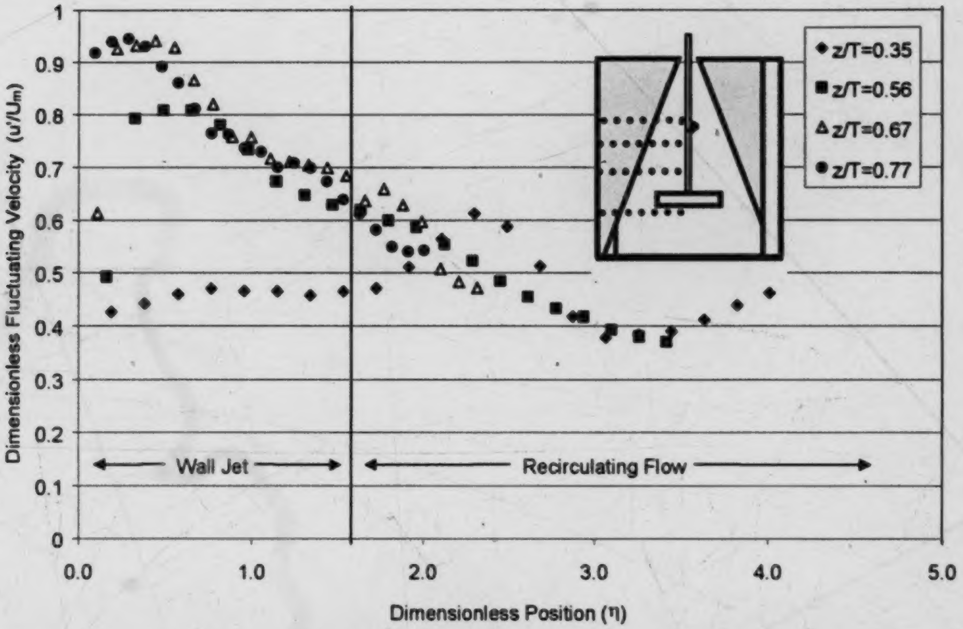

Figure 4 - 8: Turbulence in the three dimensional wall jet produced by an A310 impeller (D/T=0.58, C/D=0.68, N=600 rpm). It takes a distance of z/T=0.67 before fluctuating velocities show similarity.

Chapter 5

Active Volume of Mean Circulation for Stirred Tanks Agitated with Axial Impellers

5.1 Introduction

Stirred tanks are used in a variety of applications including blending, reactions, liquid-liquid dispersions and solids suspension. Although our understanding of these vessels has improved substantially over the last 35 years, many important design principles and limits are still poorly defined. This chapter is directed at a better definition of the active volume of mean circulation in the tank.

At present the whole tank volume is treated as active and is assumed to be equally involved in the mixing operations. The tank turnover time is defined as the volume of the tank divided by the primary pumping capacity of the impeller. However, attempts to correlate blend time to the tank turnover time have failed (Grenville et al., 1995). This study shows that, for axial impellers, only a fraction of the tank is actively involved in mean circulation. This has implications for solids distribution in the tank, spacing between multiple impellers, and understanding the function of draft tubes. It is also important information for the development of Eulerian zone averaged models of the tank, such as that proposed by Bourne and Yu (1994).

If the axial velocity is measured in front of the baffle, where it is at a maximum, both flow visualization and LDV measurements show a point where the fluid ends its upward climb. This is characterized by zero gradient in the axial velocity. Because the axial circulation is driven by a wall jet (Chapter 4 and 5), when the velocity gradient approaches zero in this jet, the dispersion of momentum is essentially complete and the wall jet is no longer effective for driving mean circulation. The volume above this point is not actively involved in the mean circulation, although there is exchange between this volume and the rest of the tank due to macro-instabilities in the flow field (Bruha et al., 1995).

The experiments reported here show that the wall jet extends over a constant fraction of the tank, implying that the active volume of mean circulation is constant. This hypothesis was tested for three different axial impellers over a range of impeller speeds and off bottom clearances. It held for these conditions and for changes in the tank diameter and fluid viscosity. The results allow definition of general design principles for the off bottom clearance of axial impellers, and suggest limits of separation between impellers when multiple impellers are used.

5.1.1 Mean Circulation Patterns

Various authors have studied flow fields for axial impeller stirred tanks; however, the only papers which will be discussed here are those where authors show complete or nearly complete flow fields. Flow throughout the tank has been reported in papers by Ranade and Joshi (1989) Jaworski et al. (1991), Kresta and Wood (1993), Fort et al. (1993), Mavros et. al. (1996), Bakker et. al. (1996) , Hockey and Nouri (1996), Myers et. al. (1996), Mao et. al. (1997), Sheng et. al. (1998), Mishra et. al.(1998), Schafer et. al. (1998), and Fentiman et. al. (1998). Although each used a different axial impeller and different experimental set-ups, the flow fields observed were similar in one respect: the impeller discharge stream proceeds towards the bottom of the tank and then upward along the tank wall.

Jaworski et al. (1991) examined the 6 bladed 45° pitched blade turbine at two different clearances. For the lower impeller clearance (C=T/4), the impeller discharge stream hits the bottom of the tank, then proceeds up along the tank wall. The jet along the wall decays as it proceeds. For the higher clearance (C=T/2), the impeller stream does not reach the bottom of the tank but hits the wall of the tank. In this case, the wall jet starts at a point above the bottom of the tank. Through flow visualization, Kresta and Wood (1993) also showed the effect of impeller clearance on the flow pattern for a pitched bladed turbine. Ranade and Joshi (1989) displayed the effect of impeller blade angle on the discharge stream and Myers et. al. (1996) and Bakker et. al. (1996) used DPIV and LDV to show that the discharge stream from a 45° PBT can impinge on the wall and not the bottom of the tank. Sheng et. al.(1998) used DPIV and CFD to study the flow pattern for a PBT. Mao et. al. showed how the mean flow field changed due to impeller size and spacing. Hockey and Nouri (1996) used a 4 bladed 60° PBT at C=T/3. In their data, the discharge from the impeller reaches the bottom of the tank. The flow patterns in the articles mentioned, all show a limited volume of mean circulation for pitched blade impellers.

Jaworski et al. (1996) compared the mean velocity fields for a Prochem Maxflo T and a Chemineer HE3 impeller. The Maxflo T impeller is used for gas dispersion while the HE3 is designed for solids suspension. Jaworski et al. (1996) compared the flow patterns for the two impellers, concentrating on radial and axial velocities. Their vector plots clearly show that the upward axial velocity drops to zero and returns to the impeller at a distance of 2T/3 from the bottom of the tank. Several other types of impellers show the same characteristics: the wide bladed hydrofoil impeller (Mishra et. al., 1998); a profiled blade impeller (Fentiman et. al., 1998); and an airfoil impeller with four inclined blades (Fort et al., 1993). In all of these studies, the impeller discharge stream reaches the bottom of the tank and the jet decays along the tank wall, giving the same active volume for all cases.

Although the mean circulation may not reach the top of the tank, it is known that the tank is well mixed throughout. Through flow visualization, it can be seen that the fluid periodically surges to the top of the tank. This can also be observed as surface welling (Bruha et al., 1995). This surface welling is due to macro-scale instabilities, which have been observed by: Grgic (1998), Montes et al. (1997), Myers et al. (1997), Bakker et al. (1996), Bruha and co-authors (1996, 1995, 1994 & 1993), Chapple and Kresta (1994), Kresta and Wood (1993) and Haam et al. (1992). This is important information: if the mean circulation zone is constant and does not fill the whole tank, there must be an alternate mechanism (e.g. large scale structures) which mixes the rest of the fluid in the tank.

In previous work, authors have focused on the properties of the impeller: power numbers, circulation, flow and turbulence characteristics. The goal of this study is to find characteristics which characterize the flow in the bulk of the tank and which are common for all axial impellers.

5.1.2 Active Volume or Penetration Height

The active region for axial impellers in a baffled tank is defined as the volume of the tank where the mean flow contributes to bulk circulation. The active volume of the stirred tank was defined using velocity measurements taken at the baffle. These measurements show a three-dimensional (3-D) jet along the wall and baffle as discussed in Chapter 4. The wall jet is 3-D in two respects: the velocities vary in the axial and radial directions as one would expect with a two dimensional wall jet, but the jet also varies in the theta direction due to the influence of the baffles. In this work, the penetration of the wall jet into the top half of the tank was measured and was used to define the active volume. Figure 5-1 shows the progression of the jet along the wall and the baffle. Notice that the jet is much stronger at z/T=0.375 and as it progresses up to z/T=0.771 it flattens out.

The gradients of the 3-D wall jet near the baffle were examined and for generality, the results were made dimensionless. There is a large difference in the velocity gradients between the top and bottom of the tank. The jet near the top of the tank has a gradient close to zero, while the one near the bottom of the tank has a fairly large gradient. The dimensionless gradients along the z-axis were used to determine where the active volume of the tank starts and ends. In the dimensionless gradient the velocities were made dimensionless with respect to tip speed ($V_{Tip}=\pi ND$) and radial positions were made dimensionless with respect to tank diameter (T). The velocity gradient in the wall jet is thus defined as:

$$\text{Velocity Gradient} = \frac{\Delta V_z}{V_{Tip}} \bigg/ \frac{\Delta r}{T} \qquad (5.\ 1)$$

The conventional approach for determining the velocity gradient is to use a variable Δr, which would measure the same point along the jet profile each time. This measurement is usually made at the half width of the jet ($b_{1/2}$). $b_{1/2}$ is a linear function of z as shown is Chapter 3 and 4, so to have a constant position in the expanding jet, Δr must vary:

$$b_{1/2} \propto z \quad \frac{\Delta r}{b_{1/2}} = \text{Constant} \quad \therefore \quad \Delta r \propto z \qquad (5.2)$$

Similarly, the axial decay of the axial velocity component scales with 1/z for axial impellers (Chapter 4):

$$V_z \propto \frac{1}{z} \quad V_{tip} = \text{Constant} \quad \therefore \quad \frac{\Delta V_z}{V_{tip}} \propto \frac{1}{z} \qquad (5.3)$$

Therefore, the dimensionless velocity gradient would be:

$$\frac{\Delta V_z}{V_{Tip}} \bigg/ \frac{\Delta r}{b_{1/2}} \propto \frac{1}{z} \qquad (5.4)$$

For a variable Δr.

In this work, a constant Δr was used and T was used as a scaling variable since $b_{1/2}$ was unknown. With these variables, the expected decay of the dimensionless slope is:

$$\Delta r = \text{const.} \quad T = \text{const.} \quad \therefore \quad \frac{\Delta V_z}{V_{Tip}} \bigg/ \frac{\Delta r}{T} \propto \frac{1}{z} \qquad (5.5)$$

5.1.3 Effect of Off-Bottom Clearance

The discharge angle from the pitched blade turbine and the off bottom clearance of the impeller determine if the discharge stream will impinge on the bottom of the tank or on the tank wall. It can be shown through a momentum balance that the angle of discharge is dependent on the angle of the blade. For a blade at 45° to the horizontal plane, the discharge is at 45° to the horizontal plane. For a 45° discharge angle, the vector in the horizontal plane $\left(\sqrt{V_r^2 + V_\theta^2}\right)$ is equal to that in the vertical plane (V_z). The relative magnitudes of the two vectors in the horizontal plane (radial and tangential) determine the direction the fluid takes relative to the tank wall. Figure 5-2A shows a projection of the discharge stream (W) in the horizontal plane of a stirred tank. The distance to the wall is determined by the angle of discharge in the horizontal plane(α). The shortest possible distance to the wall occurs when there is no tangential component (α=0°). Figure 5-2A also shows a range of angles ($0^\circ \le \alpha \le 100^\circ$) at which the jet could be directed in the horizontal plane, based on all available data for velocities at the impeller discharge.

For the general case, the known variables are the distance from the center of the tank to the tank wall (T/2), and the distance from the center of the tank to where the discharge stream originates, x_o. The discharge angle, α, will be the independent variable and the distance to the wall, W, the dependent variable. Given this information and using the variables in Figure 5-2A we can say that:

$$(x_o + a)^2 + b^2 = (T/2)^2 \tag{5. 6}$$

$$a = W\cos\alpha \quad b = W\sin\alpha \tag{5. 7}$$

Alpha, α, is found experimentally and is determined by measuring the radial and tangential velocity components under the impeller blade.

$$\alpha = \tan^{-1}\left(\frac{V_\theta}{V_r}\right) \tag{5. 8}$$

W can than be determined as follows: expand Equation 5.6, substitute in Equation 5.7 and solve the result solved by the quadratic equation:

$$W = \frac{-2x_o \cos\alpha \pm \sqrt{(2x_o \cos\alpha)^2 - 4(x_o^2 - (T/2)^2)}}{2} \qquad (5.9)$$

The only physically meaningful results occur when there is plus sign in front of the square root because the negative sign will give a negative number which is not physically possible.

Given W and the blade angle, the off bottom clearance at the transition point can be found. Figure 5-2B shows the w-z plane, where w is the slice through the vertical plane as determined by α. The maximum clearance at which the impeller discharge stream hits the bottom of the tank before coming into contact with the tank wall is:

$$C = W \tan\phi \qquad (5.10)$$

Where ϕ is the angle of the blade. This assumes that the discharge stream comes from a point source and does not spread. If the impeller discharge stream is treated as a free jet, which expands at 10° from the center plane, a different maximum clearance emerges, as is shown in Figure 5-1B. Since the stream from the impeller is expanding, the jet comes into contact with the tank wall sooner than Equation 5.10 predicts. If the impeller discharge stream has a width of 0.1D (Kresta and Wood, 1993), one must add 0.05D to x_o and 10° to the angle of the blade. Equations 5.9 and 5.10 are proposed as tools to determine whether a given clearance is low enough for the discharge stream to impinge on the bottom of the tank. The application of these equations is discussed further in the results and conclusion.

For purely axial impellers like the A-310 and HE3, the effect of off bottom clearance is somewhat different. The expansion of the jet created by a marine impeller is 7.6° (Per et al., 1996) from center. To be conservative a free jet expansion rate of 10°

is taken for the A310 and the HE3. For the discharge stream to impinge on the tank wall would require C>2T for D=T/2. However, at clearances this high, the momentum in the discharge stream will be fully dispersed before the stream impinges on the bottom of the tank. Continuity and the tangential velocity will drive the limits of the active mean circulation loop in this case. For this work, it will be assumed that the discharge from the A310 and HE3 is purely axial because all clearances examined are low enough to ensure that the active zone begins at the bottom of the tank.

5.2 Experimental Set-up

To determine the penetration height of the 3-D wall jet for mean circulation, and the generality of the results, three axial impellers, two fluids and two scales of tank were studied. Within these major variations, subsets of dimensionless off bottom clearance (C/D), impeller diameter (D/T) and rotational speed (N) were examined. Axial velocities were measured using a laser doppler velocimeter (LDV) and the tank was mounted on an automated traverse system. The details of the equipment used, the experimental conditions and the repeatability of the measurements follows.

Three axial impellers were used: a 4 bladed, 45° pitched blade turbine (PBT), a Chemineer HE3 and a Lightnin' A310. The impeller diameters ranged from D=0.19T to D=0.58T. While most experiments used water ($\nu=1\times10^{-6}$ m^2/s); Bayol-35 ($\nu=3\times10^{-6}$ m^2/s) was used to test the effect of viscosity. Two fully baffled flat bottom tanks of diameters T=240mm and T=140mm, as shown in Figure 5-3A, were filled with liquid. A free liquid surface was used to eliminate any possible effects due to the presence of a lid. The 240mm tank was filled to a liquid height equivalent to the tank diameter. The

140mm tank was filled to a height of 1.21T to minimize air entrainment. Since an LDV was used, the optical effect due to the curvature of the tank had to be minimized. To accomplish this, the cylindrical tank was placed within a square tank filled with the working fluid.

Instantaneous axial velocities were measured using an Argon ion Laser Doppler Velocimeter (LDV). The specifications of the laser and the other equipment used are given in Table 5-1. The LDV was used in forward scatter mode and the signal processor used frequency domain burst detection to convert signals to velocity measurements. These velocity measurements have a standard error of 0.01m/s for the velocity ranges measured. The validation of the equipment is described in Zhou and Kresta (1996).

Positioning of the tank was both automated and manual. An automated traverse system was used for the x-y (horizontal) plane, while manual positioning was used in the z (vertical) direction and to adjust the off-bottom clearance of the impeller. The accuracy of the traversing equipment is given in Table 5-1.

Axial velocity measurements were taken in front of the baffle as shown in Figure 5-3B. This is where the upward flow and the 3-D wall jet are the strongest, as the tangential momentum is converted to axial momentum by the baffle. Six axial velocity measurements were taken and these were used to determine the velocity profile in the jet. The same traverse was repeated at up to 35 axial positions along the baffle for each set of experimental conditions. The z spacing between the traverses varied from 10mm to 3mm, starting near the bottom of the tank and ending near the top of the tank. Three to five clearances and two rotational speeds were tested for each impeller.

A complete list of the 66 experimental configurations is given in Table 5-2. The Reynolds numbers ($Re=ND^2/\nu$) ranged from 1.35×10^4 to 1.96×10^5, with the majority of the experiments done at a Reynolds number above 2.00×10^4.

Macro-scale instabilities in a stirred tank can affect the repeatability of the velocity measurements if the measurement time is too short. If measurements are taken over a long enough period of time; however, a quasi-stationary average velocity is obtained. This velocity is repeatable and is representative of the flow. The minimum sampling time needed for a repeatable velocity measurement was determined from:

$$\text{sampling time} \geq \frac{120}{N \times N_b} \tag{5. 11}$$

This equation, recommended by Zhou (1996), is based on 120 blade passages. N_b is the number of blades on the impeller and N is the impeller rotational speed. All of the velocity measurements were taken over a length of time greater than or equal to the recommended sampling time to ensure repeatability. In addition, Zhou (1996) suggested that a minimum sample size of 4000 velocity determinations is required for repeatable measurements. Since Zhou's work was done close to the impeller, the minimum sample time and size were confirmed for the region examined in this study. Taking into account the minimum number of points and the minimum amount of time needed for repeatable measurements, the velocities reported here are based on sample sizes of 8000 measurements with sampling times ranging from 14s to 45s, and a mean sampling time of 20s.

The velocity gradient is used to characterize the wall jet to reduce the error and give results that are more meaningful then V_{max}. Using six velocity measurements to calculate the velocity gradient further reduces the standard error. Chapter 4 showed that the wall jet has a relatively linear slope and that the slope does not taper out as it would for a wall jet in a stagnant fluid. The linearization of the slope is due to the downward flow in the center of the tank both above and below the impeller. In this work, three slopes are calculated for each traverse, so the standard error of the velocity gradient $\left(s/\sqrt{n}\right)$ is reduced by a factor of 1.8.

5.3 Results and Discussion

All experimental results from this work show that the active height of the time averaged flow field in a stirred tank with an axial impeller is 2/3T. The active height is defined as the point where the 3-D wall jet becomes ineffective for driving the time averaged circulation. Once the slope of the wall jet drops to zero, the momentum dispersion is essentially complete. The active height does not depend on the speed, clearance, size, or type of axial impeller. The active height was also found to be independent of both the fluid viscosity and the scale of the equipment. The data presented in the figures discussed below covers a representative cross section of all experimental runs. The results are compared to flow fields measured by other authors where available and the possible implications of the work are discussed.

5.3.1 Experimental Data

The active volume was determined by examining the velocity gradient of the 3-D wall jet. The 3-D wall jet produced by three different sizes of PBT impellers and two styles of airfoil impellers was examined in water. The 3-D wall jet produced by the

PBT impeller was also examined in a fluid with a higher viscosity (Bayol-35), and in a different scale of tank to ensure the generality of the results. When the dimensionless velocity gradient in the jet is less then 0.1, the jet is deemed to be ineffective for gross circulation. This number represents velocity gradient less then five percent of the velocity gradient at the impeller.

First, the effect of impeller size (D/T) on the active volume is examined. Figures 5-4, 5-5 and 5-6 show how the gradient of the 3-D wall jet changes with dimensionless height for impeller diameters (D/T) of 0.188, 0.33 and 0.50. The effect of off-bottom clearance is shown in all of the figures. Notice that most of the axial velocity gradients decay in a similar way. In Figures 5-4, 5-5 and 5-6, the velocity gradients start approaching zero at z/T=0.55, and that all gradients approach zero by z/T=0.70. On average, the velocity gradients approach zero at z/T=0.67. This remains true as long as the impeller discharge stream reaches the bottom of the tank. This is true for the data except the clearance in Figure 5-6 corresponding to a C/D=0.67. This is a case where the impeller discharge steam does not reach the bottom of the tank and will be discussed later in the paper.

Several different axial impellers were compared to test the generality of the active height. The impellers used were the Lightnin' A310 impeller, with a diameter of 0.58 T and the Chemineer HE3 impeller, with a diameter of 0.33 T. The results are shown in Figures 5-7A&B. The gradients approach zero between z/T =0.55 and 0.73. Within experimental error this coincides with an active height of z/T = 0.67.

The next step in the investigation was to determine if the maximum active height of z/T =0.67 held true in a more viscous fluid. The fluid used was Bayol-35, which has a kinematic viscosity of 3×10^{-6} m^2/s. A D = 0.33 T PBT impeller was used and the data obtained is shown in Figure 5-8. The point where the jet flattens out starts at z/T= 0.56 and the last curve flattens out by z/T=0.70. Again, this range corresponds to a height which includes z/T= 0.67, confirming what was shown in the previous experiments.

Finally, the scale of the tank was reduced from 240mm to 140mm. The liquid used was water and the impellers used were two PBT impellers with a size of D=0.32T and D=0.43T. At this scale, there were problems with air entrainment. To eliminate this problem the tank was filled with liquid to a height of z/T =1.21. Figure 5-9 shows how the jet reacted in the smaller system. Most of the 3-D wall jets became inactive at a height of z/T=0.65 to 0.70. The jets which do not flatten out by z/T=0.70 have impeller clearances of C/D =1.5 and 2.0 will be discussed later in the paper.

When the impeller discharge stream impinges on the bottom of the tank, all of the data for the average active zone height falls within one standard deviation of z/T=0.67, as shown in Table 5-3. Figure 5-10 shows a sample run from each set of experiments. Notice that all of the data approaches zero at a z/T between 0.64 and 0.70.

Figures 5-6 and 5-9 show cases where the impeller discharge stream does not reach the bottom of the tank. In Figure 5-6 the data that corresponds to a clearance of C/D=0.67 does not come to zero at the same place as the data corresponding to the clearances for C/D<0.67. The data for C/D =0.67 approaches zero between z/T = 0.77 and 0.80. It must be noted that the velocity does not start going upwards until z/T=0.15; before this, the velocity is negative. In Figure 5-9 the clearances corresponding to C/D =1.5 and 2.0 were the largest clearance to tank diameter ratio used, and in these cases the impeller discharge stream does not reach the bottom of the tank. In fact, the velocities did not start going upwards until z/T=0.35-0.45 from the bottom of the tank, hence, there are two inactive zones. This agrees with observations from Kresta and Wood (1993), Mao et. al. (1997) and Myers et. al. (1997). The range of clearances where the impeller discharge stream will not impinge on the bottom of the tank, based on a 20° expansion of the jet is listed in Table 5-4, along with all possible angles of the radial/tangential (r-θ) vector as shown in Figure 5-2A. The range can be narrowed if the angle of the radial/tangential vector is known. From Kresta and Wood (1993) the direction of the r-θ vector for a T/2 impeller is 45° and the direction of the r-θ vector for a T/3 impeller is 95°; the range of clearances based on these angles is also shown in Table 5-4. Notice that there is a different discharge angle for the D=T/2 and the D=T/3 impeller. This is due to the interactions of the impeller discharge stream with the wall of the tank. The D/T at which the wall starts to influence the discharge stream is not known. Due to the influence of the wall, the impeller discharge stream may not go to its expected destination, as defined by Equations 5.9 and 5.10. The jet may attach itself to the tank wall earlier than expected, hence a range of values is given in Table 5-4. While our experimental data in the third column shows the range of values between the last point where the discharge was known to reach the bottom of the tank and the first value where it was known to impinge on the wall of the tank. The experimental range falls within the range given in first two columns of Table 5-4. The range of clearances is very broad and the data are not extensive enough to tightly define the transition point.

From the data shown, the active zone of mean circulation for an axial impeller covers a height of 2T/3. This active height is constant and does not depend on the impeller diameter (0.2T<D<0.6T) or the speed. Increasing the impeller speed only increases the magnitude of the velocity, not the dimensionless slope.

5.3.2 Comparison to What Other Authors Have Shown

Experimental flow fields reported by other authors are consistent with the finding that the active height of mean circulation is constant. The only articles examined were ones that showed complete flow fields. Very few authors examine flow fields near the top of the tank. Jaworski et al. (1996 Figures 11 and 12), used two different impellers at two different clearances. They show a mean circulation which ends at approximately z/T= 0.67 for both of the impellers. Data from Hockey and Nouri (1996, Figure 3) also shows the jet dying out at z/T=0.67, this time for a 60° PBT. Various other authors show the same trend, namely that the velocity profile becomes flat at a height of 2T/3: Jaworski et al. (1991), Kresta and Wood (1993, Figures 1 & 2), Mavros et. al. (1996, Figure 7b & 7c), Myers et. al. (1996, Figure 1), Mao et. al. (1997, Figures 4-15), Mishra et. al. (1998, Figure 3), Sheng et. al. (1998, Figure 2a), Fentiman et. al. (1998, Figures 6 & 7), and Schafer et. al. (1998, Figure 3).

CFD simulations have also shown that the top 1/3 of the tank is inactive compared to the bottom. Fokema et al.(1994, Figures 1 and 4) report CFD simulations for a PBT impeller. Their flow pattern shows the 1/3 of the tank being relatively inactive . Armenante and Chou (1996, Figure 8) show the velocity distribution calculated using the software package FLUENT. The inactive volume is approximately one third of the total tank volume. Xu and McGrath (1996, Figure 2) show simulations for a PBT impeller in a dish-bottomed tank, also with a mean circulation zone in the bottom 2/3 of the tank. Kresta (1996, Figure 2a) showed results of the impeller discharge stream not reaching the bottom of the tank. In these cases, the inactive zone was the bottom of the tank. Kresta (1996, Figure 2b) shows another example where the impeller discharge stream does reach the bottom of the tank. The flow patterns predicted by all simulations run by the aforementioned authors show the same results as the experiments in this study: the top third of the tank is inactive when the impeller discharge stream reaches the bottom of the tank, and a portion of the bottom is inactive when the discharge stream does not reach the bottom of the tank.

5.3.3 Possible Implications

This work can be used for further development of solids dispersion designs, feed location, and impeller spacing design principles. A figure from Harnby et al. (1993), show solids concentration as a function of height for A310 and PBT impellers. In examining their figure there is an inflection point at a z/T=0.6 - 0.7. This is supported by Oldshue (1983), who recommends an optimum liquid height for solid suspensions between z/T=0.6 - 0.7. Above this height solids dispersion is probably due to the large-scale instabilities within the tank (Grgic 1998, Montes, 1997, Bruha et al., 1996 & 1995), and the solids concentration is not uniform.

Feed locations near the top of the tank will not reach the major circulation loop; hence, it is better to feed below a height of 0.67T, preferably close to the impeller (Gholap et al. (1994)). Reduction of the height of the fluid to 2/3T is *not* recommended based solely on the active zone results. If the liquid height is reduced with a free liquid surface, there may be problems with air entrainment. This was observed experimentally in the smaller tank. If a high residence time is needed, reducing the volume will also decrease the residence time. If a reacting system with fast competitive reactions is used the product distribution may depend on how well the system is mixed on the micro-scales, so a high volumetric turnover rate and low residence time may be needed. The reduction of the volume may be worthwhile in this case. Every system should be examined for its specific *process* needs before changing the volume of the tank.

This work helps explain the complex interactions between impellers in a multiple impeller system. Baudou et. al. (1997) showed there are three types of interactions between two impeller systems depending on the impeller separation (ΔC). The first two zones have the impellers interacting with each other to different extents; however, when the clearance between the impellers is $\Delta C > 2T/3$ the circulation loops do not interact. This indicates that the impellers will only interact if the impellers are within each others active volumes. If the clearance between the impellers is greater than the height of the active volume, there is no interaction between impellers, and a dead zone may develop between the impellers. Mavros and Baudou (1997) also confirm this.

5.4 Conclusions

The active volume or mean circulation zone for axial impellers is two-thirds the tank volume. The primary tank used had a liquid height equal to the tank diameter, leaving 1/3 of the tank to be governed by macro-instabilities. The size of the active volume for mean circulation was found to be independent of impeller diameter, rotational speed and off bottom clearance.

The location of the active volume was dependent on the clearance for the PBT impeller but not for the A310 or the HE3. The dependence on clearance is due to the discharge angle of the PBT impeller and subsequent possible impingement of the discharge stream on the tank wall. The impeller clearance at the transition point is dependent on the direction of the r-θ vector as well as on the impeller blade angle. Once the impeller discharge stream impinges on the tank wall, the clearance determines the location of the mean circulation zone. The impingement of the impeller discharge and the location of the mean circulation loop should be taken into account when designing any system using a PBT. The height of the active volume should also be considered when designing systems with multiple impellers.

5.5 Nomenclature

a	radial distance to tank wall(m)
b	tangential distance to tank wall(m)
$b_{1/2}$	half width of a jet (m)
C	clearance (m)
D	impeller diameter (m)
N	impeller speed (s^{-1})
N_b	number of impeller blades
T	tank diameter (m)
Re	Reynolds number ($Re=ND^2/\nu$)
r	radial coordinate (m)
V	velocity ($m\ s^{-1}$)
W	distance from impeller discharge to tank wall in the horizontal plane(m)
w	r-θ coordinate
x_o	distance to impeller discharge (m)
z	axial coordinate

Greek

α	discharge angle in the horizontal plane (°)
ϕ	impeller blade angle (°)
θ	tangential coordinate
ν	kinematic viscosity ($m^2\ s^{-1}$)

5.6 References

Armenante P.M. and C.C. Chou, 1996, Velocity profiles in a baffled vessel with single or double pitched-blade turbines. *AIChE J.* **42**, 42-54.

Bakker A., K. J. Myers, R.W. Ward and C.K. Lee, 1996, The laminar and turbulent flow pattern of a pitched blade turbine. *Trans. I. Chem. E. Part A* **74**, 485-491.

Baudou C., C. Xuereb and J. Bertrand, 1997, 3-D hydrodynamics generated in a stirred vessel by a multiple-propeller system. *Can J. Chem. Eng.* **75**, 653-663.

Bourne, J.R. and S. Yu, 1994, Investigation of Micromixing in Stirred Tank Reactors Using Parallel Reactions, Ind. Eng. Chem. Res., **33**, 41-55.

Bruha O., I. Fort, and P. Smolka, 1993, Large scale unsteady phenomenon in a mixing vessel. *Acta Polytechnica, Czech Tech. Univ. Prague* **27**, 33.

Bruha O., I. Fort, and P.Smolka , 1994, Flow transition phenomenon in an axially agitated system. *Proceedings of the Eighth European Conference on Mixing, IChEME Symposium series* **136**, 121-128.

Bruha O., I. Fort, and P.Smolka , 1995, Phenomenon of turbulent macroinstabilities in agitated systems. *Collect. Czech. Chem. Commun.* **60**, 85-94.

Bruha O., I. Fort, P. Smolka, and M. Jahoda, 1996, Experimental study of turbulent macroinstabilities in an agitated system with axial high-speed impeller and with radial baffles. *Collect. Czech. Chem. Commun.* **61**, 856-867.

Chapple, D. and S.M. Kresta, 1994, The effect of geometry on the stability of flow patterns in stirred tank. *Chem. Eng. Sci.* **49**, 3651-3660.

Fentiman N.J., N.ST. Hill, K.C. Lee, Paul and M. Yianneskis, 1998, A novel profiled blade impeller for homogenization of miscible liquids in stirred vessels. *Trans IchemE* **76**, 835-842.

Fokema M.D., S.M. Kresta, and P.E. Wood, 1994, Importance of using the correct impeller boundary conditions for CFD simulations of stirred tanks. *Can. J. of Chem. Eng.* **72**, 177-183.

Fort I., M. Vozny, and T. Makovsky, 1993, Flow and turbulence in a baffled system with impeller with inclined blades. *ACTA Polytechnica* **33**, 31-44.

Gholap R.V., S. Petrozzi, and J.R. Bourne, 1994, Influence of viscosity on the product distribution of fast competitive chemical reactions. *Chem. Eng. Technol.* **17** 102-

107.

Grenville R., S. Ruszkowski, and E. Garred, 1995, Blending of miscible liquids in the turbulent and transitional regimes. *Mixing XV, Banff Alberta, June 20-25*.

Grgic B., 1998, *Influence of the impeller and tank geometry on low frequency phenomena and flow stability*. M.Sc. thesis, University of Alberta, Edmonton, Canada.

Haam S., R.S. Brodkey, and J. Fasano, 1992, Local Heat Transfer in a Mixing Vessel Using Heat Flux Sensors. *Ind. Eng. Chem. Res.* **31**, 1384-1391.

Harnby N., M.F. Edwards and A.W. Nienow, 1993, *Mixing in the Process Industries, 2nd ed.*, pp. 364-393 Butterworth Heinemann, Toronto.

Hockey R.M. and J.M. Nouri, 1996, Turbulent flow in a baffled vessel stirred by a 60° pitched blade impeller. *Chem. Eng. Sci.* **51**, 4405-4421.

Jaworski Z., A.W. Nienow, K.N. Dyster, and W. Bujalski, 1991, An LDA study of turbulent flow in a baffled vessel agitated by a pitched blade turbine. *Trans IChemE* **60**, 313-320.

Jaworski Z., A.W. Nienow and K.N. Dyster, 1996, An LDA study of the turbulent flow field in a baffled vessel agitated by an axial, down-pumping hydrofoil impeller. *Can. J. of Chem. Eng.* **74**, 3-15.

Kresta S.M., and P.E. Wood, 1993, The mean flow field produced by a 45° pitch blade turbine: changes in the circulation pattern due to off bottom clearance. *Can. J. of Chem. Eng.* **71**, 42-53.

Kresta S.M., 1996, Boundary conditions required for the CFD simulation of flows in stirred tanks, *Advances in fluid mechanics: Multiphase Reactor and Polymerization System Hydrodynamics*, pp. 297-316, N. P. Cheremisinoff ed., Gulf Publishing Company, Houston.

Mao D., L. Fang, K. Wang, and Y. Li, 1997, The mean flow field generated by a pitched blade turbine: changes in the circulation pattern due to impeller geometry. *Can J. Chem. Eng.* **75**, 307-316.

Mavros P., C. Xuereb and J. Bertrand, 1996, Determination of 3-D flow fields in agitated vessels by laser-doppler velocimetry: Effect of impeller type and liquid viscosity on liquid flow patterns. *Trans I ChemE* **74**, 658-668.

Mavros P. and C. Baudou, 1997, Quantification of the performance of agitators in stirred vessels: Definition and use of an agitation index. *Trans I ChemE* **75**, 737-

745.

Mishra V.P., K.N. Dyster, Z. Jaworski, A.W. Nienow and J. McKemmie, 1998, A study of an up- and down- pumping wide blade hydrofoil impeller: Part I LDA measurements. *Can J. Chem. Eng.* **76**, 577-588.

Montes J.L., H.C. Boisson, I. Fort, and M. Jahoda, 1997, Velocity field macro-instabilities in an axial agitated mixing vessel. *Chem. Eng. J.* **67**, 139-145.

Myers K.J., A. Bakker, and R.R. Corpstein, 1996, The effect of flow reversal on solids suspension in agitated vessels. *Can. J. Chem. Eng.* **74**, 1028-1033.

Myers K.J., R.W. Ward, and A. Bakker, 1997, A digital particle image velocimetry investigation of flow field instabilities of axial flow impellers. *J. Fluids Eng.* **119**, 623-632.

Oldshue J.Y. *Fluid Mixing Technology* McGraw-Hill Publications Co., New York, N.Y.

Per P., L. Magnus and J. Lennart, 1996, Measurements of the velocity field downstream of an impeller, *J. of Fluids Engineering* **118**, 602-610.

Ranade V.V. and J.B. Joshi, 1989, Flow generated by pitched blade turbines I: Measurements using laser doppler anemometer. *Chem. Eng. Comm.* **81**, 197-224.

Schafer M., M. Yianneskis, P. Wachter, and F. Durst, 1998, Trailing vortices around a 45° pitched-blade impeller. *AIChE J.* **44**, 1233-1246.

Sheng J., H. Meng, and R.O. Fox, 1998, Validation of CFD simulations of a stirred tank using particle image velocimetry data. *Can J. Chem. Eng.* **76**, 611-625.

Xu Y. and G. McGrath, 1996, CFD Prediction of Stirred Tank Flows. *Trans. I. Chem. E. Part A* **74**, 471-475.

Zhou G. and S.M. Kresta, 1996, Distribution of energy between convective and turbulent flow for three frequently used impellers. *Trans IChemE* **74**, 379-389.

Zhou G., 1996, *Characteristics of turbulence energy dissipation and liquid-liquid dispersions in an agitated tanks*, Ph.D. thesis, University of Alberta, Edmonton, Canada.

Table 5 - 1: Equipment Specifications

Argon Laser	Output power = 300mW Beam separation = 0.03404m Focal length = 500mm Wavelength of light = 514.5nm Bragg cell frequency shift = 40MHz Fringe Spacing = 3.79μm
Horizontal Traverse System	Computer Controlled Accuracy = ±0.25mm
Vertical Traverse	Manual Accuracy = ±1.0 mm
Off-Bottom Clearance Adjustment	Manual Accuracy = ±0.5 mm
Seeding installation	Water - Naturally occurring 1μm particulate Bayol-35 – $TiO_2 \leq 5\mu m$ particulate

Table 5 - 2: Experimental Runs

Impeller Diameter (mm) & Type	Impeller Speed (RPM)	Impeller Clearances (c/D)	Liquid	Tank Diameter (mm)
45 PBT	400 & 800	0.70, 1.0, 1.5, 2.0, 3.0	Water	240
60 PBT	400 & 800	0.60, 0.80, 1.0, 1.5, 2.0	Water	240
80 PBT	170 & 400	0.4, 0.60, 0.80, 1.0, 1.5	Water	240
120 PBT	200 & 400	0.33, 0.50, 0.67	Water	240
80 PBT	580 & 700	0.40, 0.80 , 1.0	**Bayol-35**	240
45 PBT	400 & 800	0.67, 1.0, 2.0	Water	**140**
60 PBT	350 & 650	0.50, 1.0, 1.5	Water	**140**
80 **HE3**	400 & 1100	0.40, 0.80, 1.0	Water	240
140 **A310**	200 & 600	0.33, 0.50, 0.68	Water	240

Table 5 - 3: Maximum Active Volume

Experimental Run	Mean (z/T)	Standard Deviation(z/T)
D/T=0.19 PBT	0.66	0.03
D/T=0.25 PBT	0.64	0.03
D/T=0.33 PBT	0.64	0.03
D/T=0.50 PBT	0.66	0.03
D/T=0.33 Bayol-35	0.65	0.04
D/T=0.58 A310	0.64	0.03
D/T=0.33 HE3	0.66	0.01
Tank D=140mm	0.68	0.02
Average Active Volume	**0.65**	**0.03**

Table 5 - 4: The Range of Clearances at which the Discharge Stream Reaches the Tank Wall Before the Bottom of the Tank

	C/D Based on Figure 3-2A		C/D Based on measured α		Experimental range of C/D where the impeller jet no longer impinges on the tank bottom	
D/T	Minimum α = 0°	Maximum α = 100°	Minimum	Maximum	Last observed bottom impingement	First observed wall impingement
0.50	0.38	1.42	0.44	1.03	0.5	0.67
0.43	0.50	1.68	N/A	N/A	1.0	1.5
0.33	0.73	2.17	1.04	2.13	1.5	Not found
0.32	0.74	2.19	1.05	2.15	1.0	2.0
0.19	1.55	3.86	N/A	N/A	3.0	Not found

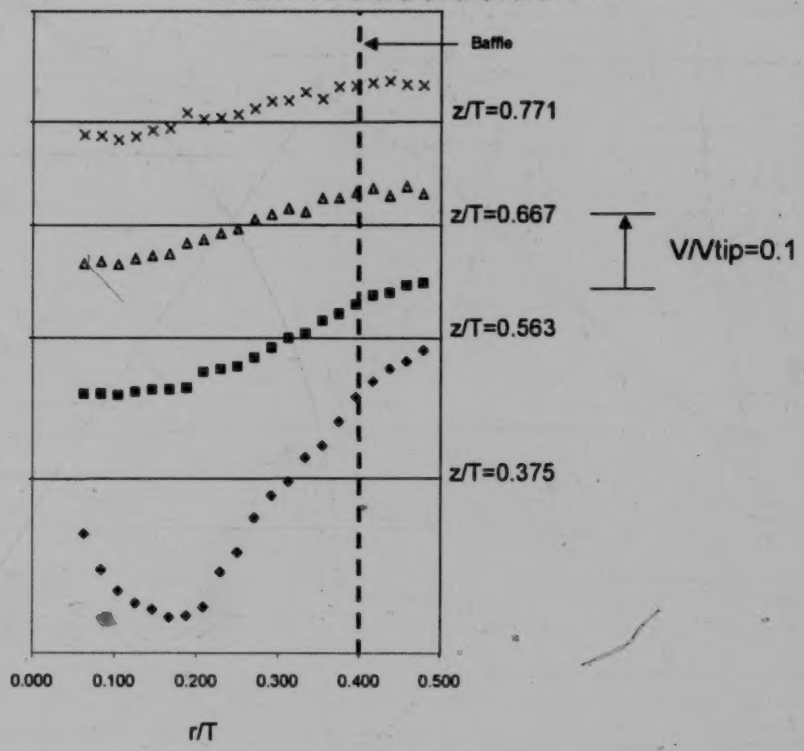

Figure 5 - 1:Axial Velocity Measurements for an A310 D/T=058 C/D=0.68

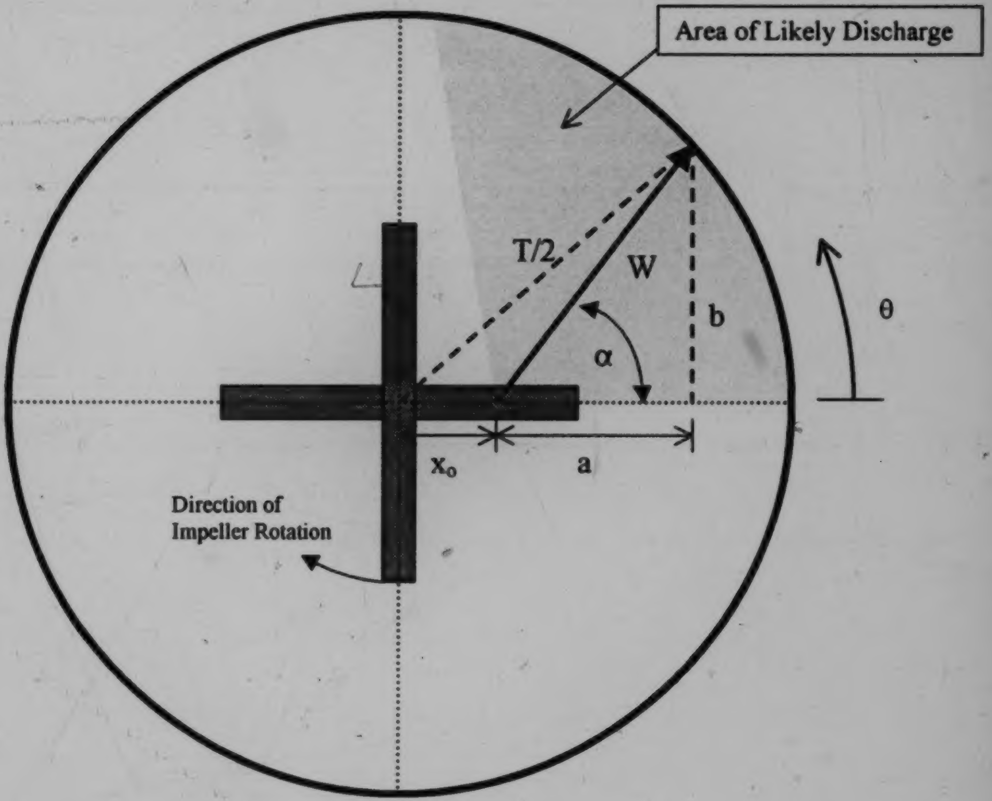
Area of Likely Discharge
T/2
W
b
θ
α
x_o
a
Direction of
Impeller Rotation

Figure 5 - 2A: Discharge of a PBT in the Horizontal Plane

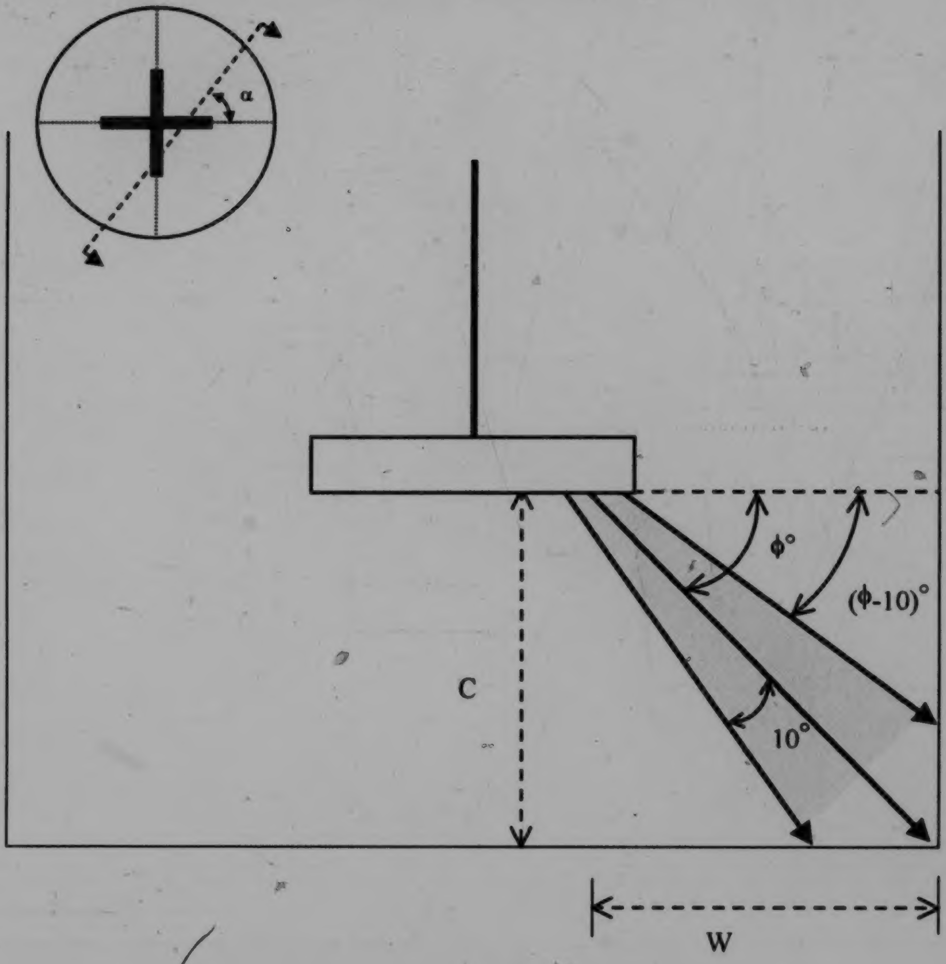

Figure 5 - 2B: Discharge of the impeller jet in the Vertical Plane.

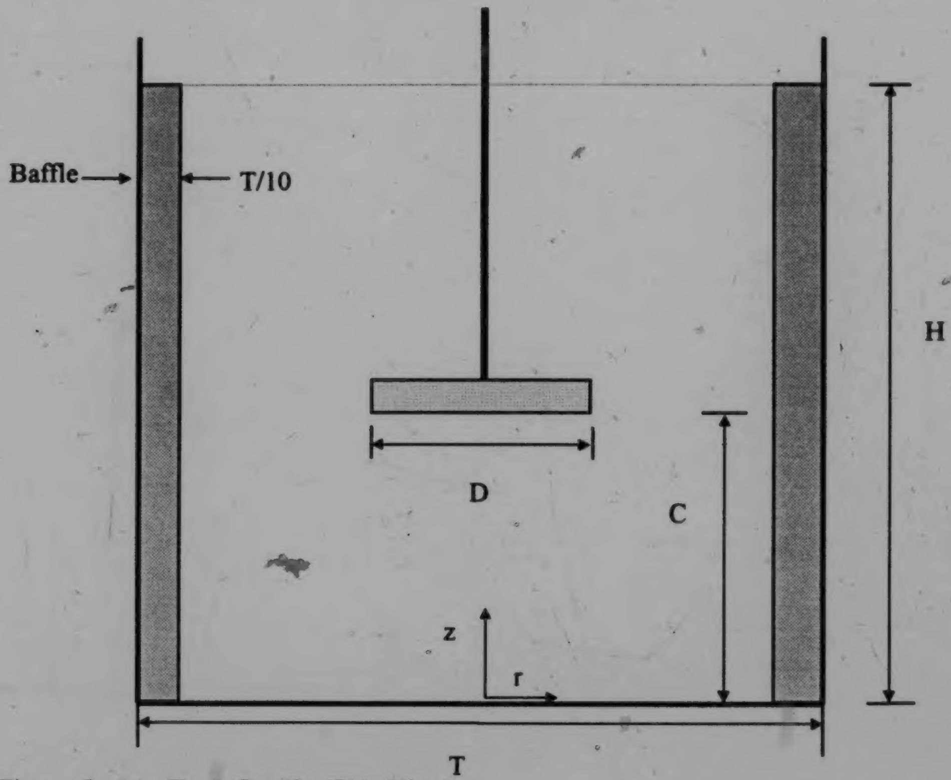
Baffle
T/10
H
D
C
z
r
T

Figure 5 - 3A: Tank Set-Up (Side View)

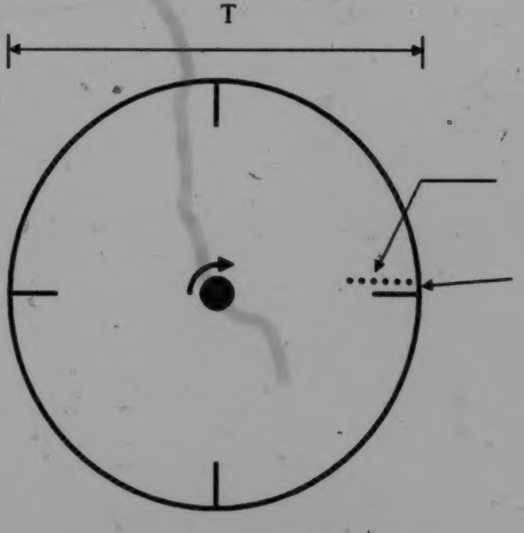

Measured Points r= 90, 95, 100,105,110 &115mm
T=240mm

Distance from baffle 5mm

Figure 5 - 3B: Position of Measurements (Top View)

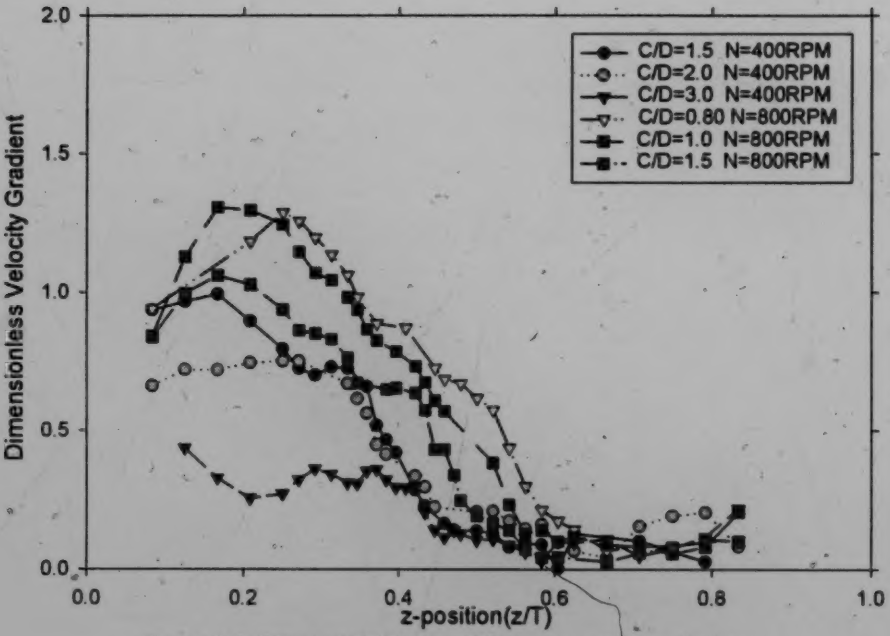

Figure 3-5: Effect of Off-Bottom Clearance on Dimensionless Velocity Gradient for a D=0.19T PBT Impeller

Figure 5 - 4: Effect of Off-Bottom Clearance on Dimensionless Velocity Gradient for a D=0.19T PBT Impeller

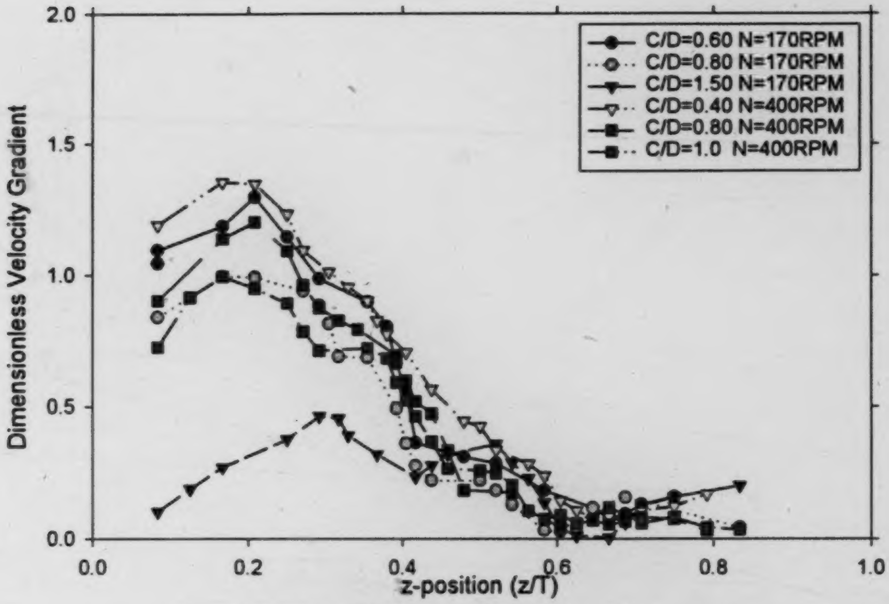

Figure 5: Effect of Off-Bottom Clearance on Dimensionless Velocity Gradient for a D=0.33T PBT Impeller

Figure 5 - 5: Effect of Off-Bottom Clearance on Dimensionless Velocity Gradient for a D=0.33 PBT Impeller

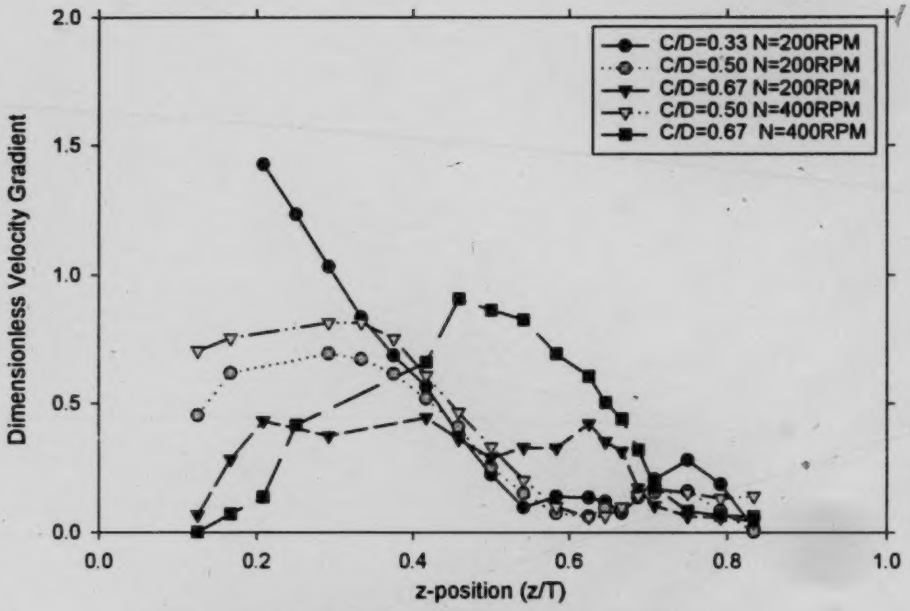

Figure 6: Effect of Off-Bottom Clearance on Dimensionless Velocity Gradient for a D=0.50T PBT Impeller

Figure 5 - 6: Effect of Off-Bottom Clearance on Dimensionless Velocity Gradient for a D=0.50T PBT Impeller

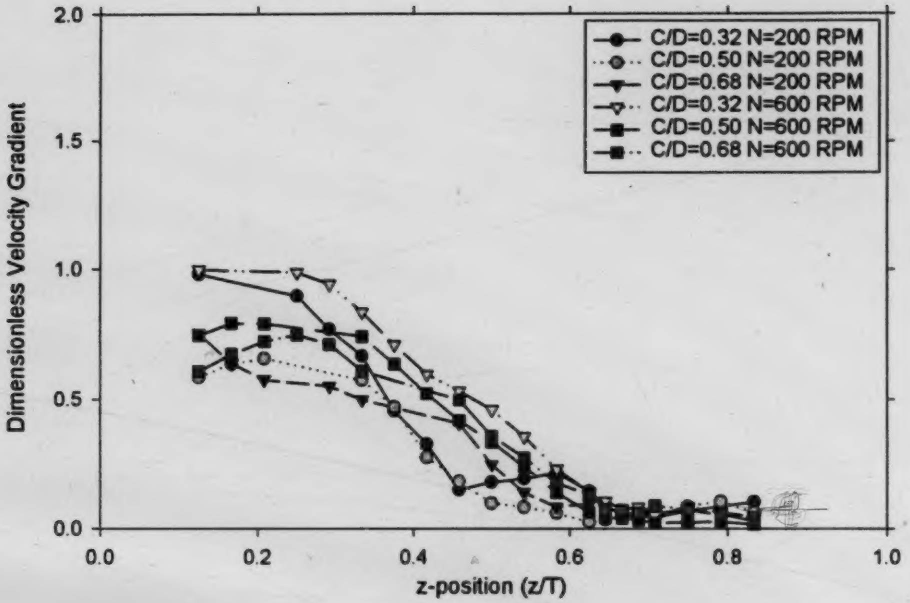

Figure 7A: Effect of Off-Bottom Clearance on Dimensionless Velocity Gradient for a D=0.58T Lightnin' A310 Impeller

Figure 5 - 7A: Effect of Off-Bottom Clearance on Dimensionless Velocity Gradient for a D=0.58T Lightnin A310 Impeller

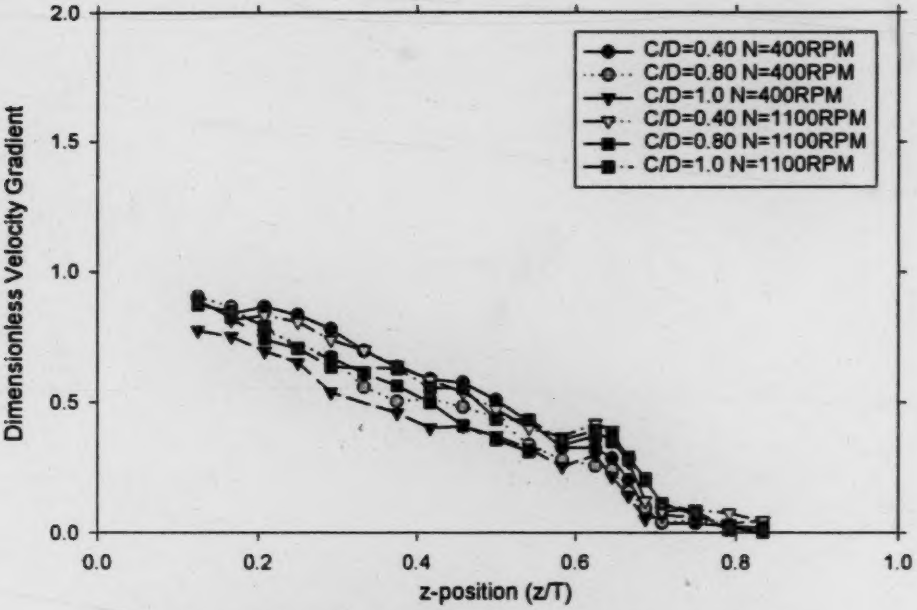

Figure 7B: Effect of Off-Bottom Clearance on Dimensionless Velocity Gradient for a D=0.33T Chemineer HE-3 Impeller

Figure 3-7B: **Effect of Off-Bottom Clearance on Dimensionless Velocity Gradient for a D=0.33T Chemineer HE3 Impeller**

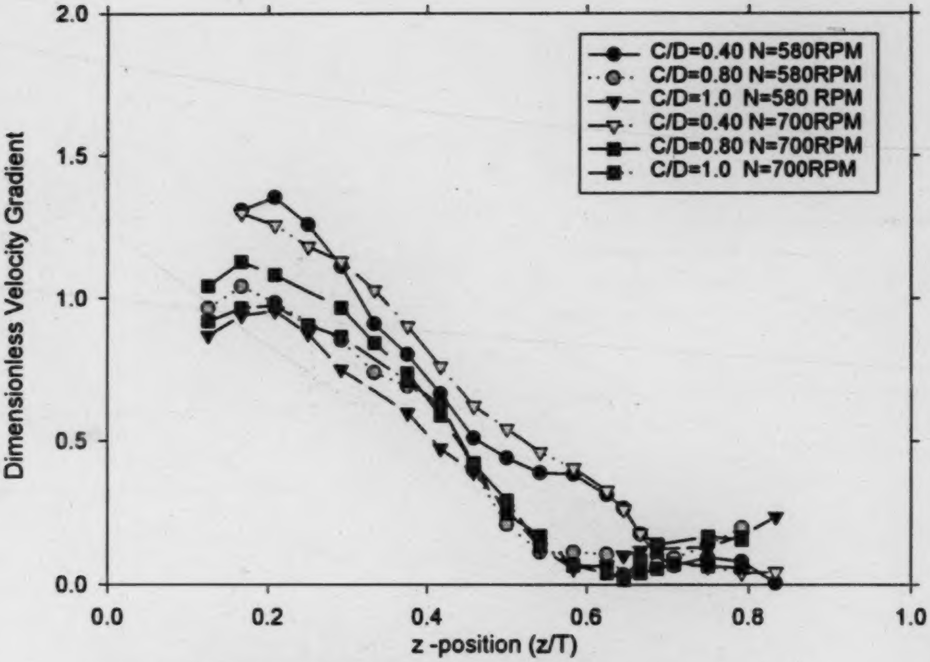

Figure 8: Effect of Off-Bottom Clearance on Dimensionless Velocity Gradient for a D=0.33T PBT Impeller in Bayol-35

Figure 5 - 8: Effect of Off-Bottom Clearance on Dimensionless Velocity Gradient for a D=0.33 PBT Impeller in Bayol-35

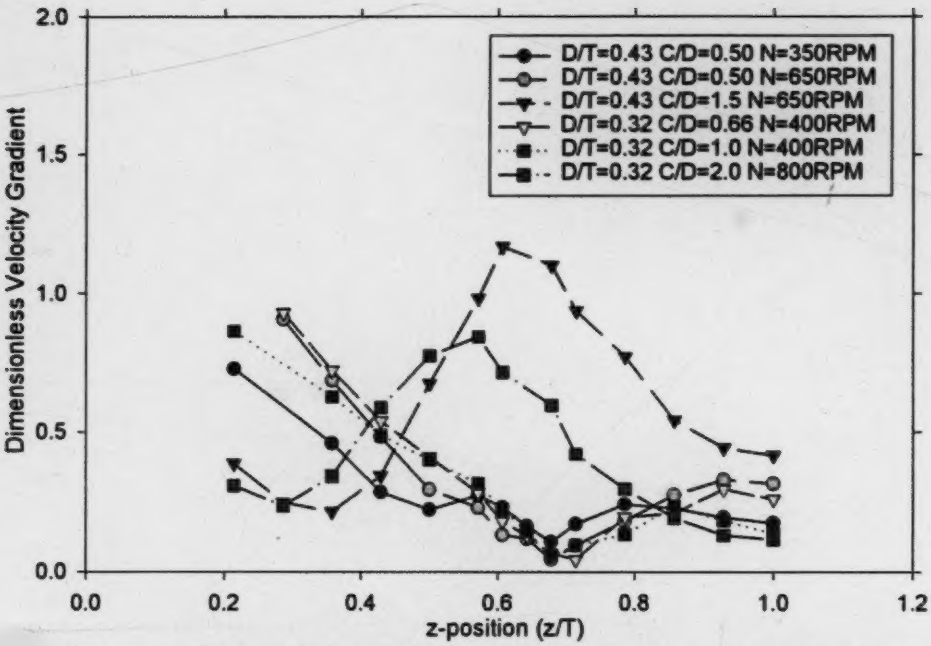

Figure 9: Effect of Off-Bottom Clearance on Dimensionless Velocity Gradient With a Reduction of Scale (T_{small}/T_{large}=0.58) using PBT Impellers

Figure 5 - 9: Effect of Off-Bottom Clearance on Dimensionless Velocity Gradient with a Reduction of Scale(T_{small}/T_{large}=0.58) using PBT Impellers.

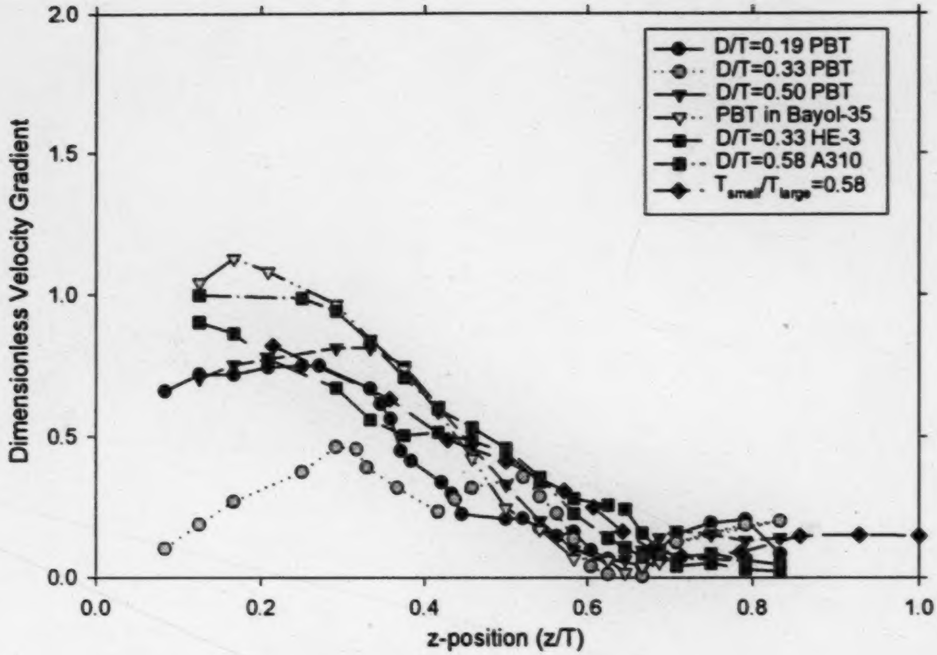

Figure 10: Comparison of Data from Different Experimental Configurations

Figure 5 - 10: Comparison of Data from Different Experimental Configurations

Chapter 6

Fully Turbulent Flow in a Stirred Tank with Axial Flow

6.1 Introduction

Turbulence in a stirred tank was defined by Rushton and co-authors (1946 & 1950) in terms of the power consumed by the impeller. Their measure of fully turbulent flow, the power number (Po), considers only the size of the impeller, D, not the size of the tank, T. When D<<T the impeller region may be fully turbulent without the penetration of fully developed turbulence throughout the tank. In this chapter, the point in the tank to which fully developed turbulence penetrates is examined for the pitched blade turbine, Chemineer HE3 and the Lightnin A310.

The transition from laminar flow to fully turbulent flow occurs over a range of Reynolds number. The Reynolds number is a ratio of inertial forces to viscous forces based on the characteristic length and velocity scales in the system under investigation:

$$\mathrm{Re} = \frac{\text{Inertial Forces}}{\text{Viscous Forces}} = \frac{\dot{m} \cdot U}{\tau \cdot A} = \frac{L_C \cdot U_C}{\nu} \qquad \textbf{(6.1)}$$

The inertial force scales with the mass flow rate ($\dot{m}$) and the velocity at which it travels (U), while the viscous forces scale with the shear stress (τ) and the area over which the shear stress affects the system (A). Through simplification, the Reynolds number becomes a ratio of a characteristic length scale (L_C) and characteristic velocity scale (U_C) to the kinimatic viscosity (ν) of the fluid in the system. A Reynolds number can be defined for any flow field in which the characteristic scales are defined.

The Reynolds number length and velocity scales are well defined for classical flows, like pipe flow (L_C=pipe diameter and U_C=superficial velocity), jet flow (L_C=half width of the jet and U_C=local maximum velocity) and a falling sphere (L_C=diameter of the sphere and U_C=velocity of the sphere). For the impeller region in a stirred tank, the characteristic velocity and length scales are the impeller diameter (D) and impeller tip speed (ND), giving the Reynolds number:

$$\mathrm{Re} = \frac{ND^2}{\nu} \tag{6.2}$$

Although U_C for the impeller flow is not a fluid velocity, the discharge velocity scales with the impeller tip speed (Ranade and Joshi, 1989 and Nouri et al. 1987).

For any system, fully developed turbulence occurs when the inertial forces in the system are so large that the viscous forces become negligible. The value of the Reynolds number at which the flow becomes fully turbulent is dependent on the system of interest. One way to determine the point at which the viscous forces become much greater than the inertial forces is to plot the Reynolds number against a variable that accounts for the drag in the system. This variable is always dimensionless, for example, the drag coefficient (C_D) for a falling sphere (Gerhart et al. 1992):

$$C_D = \frac{\mathrm{Drag}}{0.5\rho U_C^2 L_C^2} \tag{6.3}$$

pipe loss coefficient or friction factor (C_f) (Gerhart et al. 1992):

$$C_f = \frac{\tau_{\mathrm{wall}}}{0.5\rho U_C^2} \tag{6.4}$$

When the variable that accounts for the drag in the system becomes constant with increasing Reynolds numbers the system is considered fully turbulent: the effect of viscosity is overwhelmed by inertia. This is clearly illustrated in the Moody charts for friction coefficient in pipe flow (Figure 7.9 Gerhart et al. 1992) and drag coefficient (C_D) for a falling sphere in a stagnant fluid (Figure 8.10 Gerhart et al. 1992).

In the impeller region of a stirred tank, the results are analogous. The drag is characterized by the power number (Po):

$$\mathrm{Po} = \frac{P}{\rho N^3 D^5} \tag{6.5}$$

The denominator is the drag ($\rho U_c^2 L_c^2 = \rho N^2 D^4$) multiplied by velocity ($U_c = ND$) and the numerator is force multiplied by velocity; hence, the power number is analogous to the friction and drag coefficients. The flow in the impeller region is considered fully turbulent when the power number becomes constant with increasing Re (Rushton and co-authors, 1946 & 1950). It is usually stated that fully developed turbulence based on impeller drag exists for $Re \geq 2\times10^4$. In some instances, fully turbulent flow persists to lower Re, as shown in Rushton et al. (1950).

The power number and friction factor are used to define the onset of fully turbulent flow for their respective systems; however, the onset of fully turbulent flow can also be determined using dimensionless velocity profiles. In fully turbulent flow, and in laminar flow the dimensionless velocity profiles will collapse to a single similarity profile if the proper characteristic velocity and length scales are used. For pipe flow, the characteristic length is the pipe radius and the characteristic velocity is the maximum velocity at the center of the pipe. In the impeller discharge stream the characteristic velocity is the impeller tip speed ($V_{TIP} = \pi ND$), and the characteristic length is the impeller radius (D/2). The dimensionless velocity profile is self-similar if the flow is fully turbulent for all common impellers (Ranade and Joshi, 1989 and Nouri et al. 1987). This criterion is the basis of the work in this chapter. It will be used to determine the limits of fully turbulent flow in the outer regions of a stirred tank.

In the transitional regime, both inertial and viscous forces influence the velocity profiles and similarity no longer holds. For the purposes of this chapter, the onset of transitional flow is the point when the dimensionless velocity profile deviates from the turbulent profile. The point at which this occurs in the outer regions of the tank does not necessarily correspond to the point at which the impeller region becomes fully turbulent.

In laminar flow, the viscous force is dominant; however, laminar scaling is based on the same ideas as fully turbulent scaling. The friction factor and drag coefficient in laminar flow are inversely proportional to the Reynolds number. This is also the case in comparing the impeller power number to Re. In a pipe, the same characteristic length and velocity scales are used for laminar and turbulent flow but the dimensionless laminar velocity profile is significantly different from the turbulent velocity profile.

6.1.2 Scaling in the Bulk of the Tank

To determine when the flow is fully turbulent mean velocity scaling is used. Mean velocity scaling does show the point at which the flow is fully turbulent because as the Reynolds number in a system increases a point at which the mean velocity profile becomes constant, which does not vary at higher Reynolds numbers. Jet flow exhibits this characteristic and is used to determine the point at which the flow is considered fully turbulent.

The mean flow in the bulk of the tank was examined to determine the dominant flows and from this possible characteristic velocity and length scales were extracted. It is shown in Chapter 4 that a three-dimensional wall jet is formed along each of the baffles for axial flow impellers, as shown in Figure 6-1. The three dimensional wall jet is the only mean flow structure in the bulk of the tank and it dominates both the active volume of mean curculation (Chapter 5) and the height to which solids are suspended in the tank (Chapter 7). Its characteristics are now used to determine if the flow in the bulk of the tank is fully turbulent.

Figure 6-2 shows the velocity profile in a three dimensional wall jet along two walls. Scaling for wall jets has been widely examined (Glauert 1956, Newman et al. 1972, Padmanabham & Gowda 1991), and the characteristic velocity and length scales are the local maximum velocity (U_m) and the half width of the jet (b). The half width of the jet (b) is the point at which $U/U_m=0.5$ on the dimensionless velocity profile (U/U_m).

These characteristic scales will still apply in a stirred tank; however, the velocity profile differs slightly.

Figure 6-3 shows two similarity profiles: the first profile is that of a jet in a stagnant fluid as defined by Glauert 1956, the second profile is for a jet in a system with recirculating flow as defined in Chapter 3. The distance from the wall is made dimensionless with the half width of the jet ($\eta=y/b$) and is plotted against the dimensionless velocity (U/U_m) to complete the similarity profile for the wall jet. The dimensionless velocity profile retains similarity at any stream wise (z/T) position as long as the flow remains fully turbulent. This scaling is used to examine the limits of fully developed turbulence in the bulk of the tank.

6.2 Experimental

The limits of fully turbulent flow were examined for a fully baffled cylindrical tank with a diameter of T=240mm agitated by a pitched blade turbine (PBT) Chemineer HE3 and Lightnin A310. The fluids examined were water, Bayol, and solutions of triethylene glycol (TEG) in water, with viscosities ranging from 1cP to 16 cP. The full range of experimental conditions is given in Table 6-1.

During the experiments, it was noticed that the TEG solution heated up significantly. The temperature fluctuations were recorded and the effect of temperature on the viscosity of the TEG solutions was measured and the dependence is shown in Chapter 2. The viscosities rarely varied by more then 2cP. The viscosity at the point where transitional flow first occurs is the viscosity used to calculate the Re at the last known point of turbulence.

Using LDV, velocity profiles were measured throughout the tank. Each traverse passes through the three-dimensional wall jet as shown in Figure 6-1 in both plan and profile views. The specifications of the experimental equipment are given in Table 6-2, with a more detailed description of the equipment is found in Chapter 2. The measurement duration of each point along the traverse was one minute and the number of points in each record varied from 80,000 to 100,000 to insure the accuracy of the measurement.

6.3 Results

The wall jet was used to determine the location at which the flow changes from fully turbulent to transitional flow for two reasons. The velocities in the top of the tank are much smaller than those at the impeller. In a jet, the velocities are made dimensionless with the local maximum velocity; this scales the velocity so the same scale can be used throughout the jet decay regardless of axial location. By using a local velocity scale, a more accurate comparison can be made between the velocity profiles with higher and lower U_m. The jet model also forces the profiles to collapse at $\eta=1$. If a profile deviates from similarity in spite of a forced fit at $\eta=1$, it is clear that similarity is violated and the flow is no longer in the fully turbulent regime.

Sample velocity profiles just above and below the impeller blade were made dimensionless with the impeller tip speed and the impeller radius in Figures 4A and 4B. The velocity profile just below the impeller, in the impeller discharge, scales within experimental error. In contrast, the profiles in Figure 6-4B have a similar shape but do not collapse when made dimensionless with the tip speed and impeller radius. This shows that either the flow is not fully turbulent or that the impeller no longer dominates the velocity profile. Wichterle et al. (1988) showed that the friction along the wall of a stirred tank is Reynolds number dependent from $6,000 < Re < 110,000$). Normalized friction plots showed that as the Reynolds number increased so did the normalized friction. The friction at the wall of the tank is directly related to the wall jet, suggesting the use of jet similarity to collapse the velocity profiles and determine the onset of transitional flow.

6.3.1 Criteria for Assessing Fully Developed Turbulence

Figure 6-5 shows the dimensionless similarity profile for the three-dimensional wall jet in a stirred tank. In this figure, the x-axis is the dimensionless distance from the wall ($\eta=y/b$) and the y-axis is the axial velocity made dimensionless with the local maximum velocity in the wall jet (U/U_m). The classical exponential profile could not be used here because the velocity in this wall jet passes through zero, whereas the classical profile developed for a stagnant surrounding fluid asymptotically approaches zero. A cubic regression is required to account for both the inflection point and the maximum at $U/U_m=1$. Over 200 data points from various experimental configurations were used to ensure an accurate similarity profile. The resulting cubic regression has an $R^2=0.99$:

$$U/U_m=0.925 + 0.779\eta - 1.778\eta^2 + 0.574\eta^3 \tag{6.6}$$

This regression is valid from the maximum velocity to the point at which the dimensionless velocity passes through zero. Beyond this point, the jet is no longer examined for similarity because it is affected by the impeller intake and discharge streams. The region from $\eta=0$ to $\eta=0.28$ is also neglected in this analysis. It is the boundary layer of the wall jet and is expected to exhibit similarity but limited data were taken in this region and a regression could not be accurately completed.

The regression residuals were used to determine the 99% confidence interval of the similarity profile. Any measurement with a deviation from the regression curve larger than ±0.010 indicates one of two things: a) the point is an outlier and should be discarded or b) the velocity profile violates similarity and the flow is no longer turbulent. If multiple points deviated from the 99% confidence interval, the traverse was classified as transitional.

6.3.2 Limits of Fully Developed Turbulence

This is examined in detail for two configurations, PBT D=T/3 and C/D=1 and the A310 D=T/2 and C/D=0.5. The complete figures for the other configurations listed in Table 6-1 can be found in Appendix A. The analysis shown below was repeated for several other geometries with similar results. In cases where the fully turbulent flow reaches z/T=0.92, the wall jet is about to impinge on the top of the tank. Impingement marks the end of the wall jet, so jet similarity will be violated by definition beyond this point, although fully turbulent flow may well persist to z/T=1.0.

PBT D=T/3

Beginning close to the impeller at z/T=0.46, all 7 traverses in Figure 6-6A obey similarity from Re=2×10^4 to 1.7×10^5 and up to η=1.5. Beyond η=1.5, the influence of the impeller becomes apparent, and the appropriate scaling changes to the impeller tip speed and radius. Continuing upwards in the tank, similarity is obeyed for all Re up to z/T=0.58, as shown in Figure 6-6B. Figure 6-7A shows the first failure of similarity at z/T=0.71. In this case, 2 traverses must be discarded, and similarity is obeyed for Re>3×10^4, as shown in Figure 6-7B. The same condition exists for z/T=0.83, as shown in Figures 8A and 8B. In Figures 9A and 9B the last traverses examined are at z/T=0.92, where the limiting Re is 6.6×10^4. Note that the first occurrence of transitional flow for an impeller Reynolds number in the fully turbulent range occurs between 0.58<z/T<0.71, the same range identified as the limit of the active zone for mean circulation (Bittorf and Kresta, 2000a).

Table 6-3 shows all of the results for the PBT D=T/3. There is some effect of C/D, but this is difficult to define with the available data. The Re required to attain fully turbulent flow clearly increases with z/T for both clearances examined.

A310 D=T/2

The lowest traverse for the A310 (Figure 6-10A) did not show similarity for all of the profiles examined. Two traverses at Re=2.0×10^4 are eliminated in Figure 6-10B. Continuing up the tank to z/T=0.58 (Figures 11A and 11B), similarity is obeyed for Re>1.7×10^4. The progression through the tank proceeds much like the previous case; as the traverses were taken higher in the tank more of them were eliminated (Figures 12A

& B and 13A & B). The final traverse shown in Figures 14B & A indicates that Re $\geq$ 1.2×10^5 for the entire tank to be turbulent.

Table 6-4 shows the locations for the last measured position of fully developed flow for the D=T/2 A310. Tables 3 and 4 show that at lower Reynolds numbers the PBT maintains the flow fully turbulent longer than the A310.

Combined Results

Figure 6-15 shows the average Reynolds number versus its last known location of turbulence. The average Re is taken from all of the experimental runs described in Tables 6-3 to 6-7. In Figure 6-15 the error bars in the x direction account for the standard error of the mean which is 20% of the mean value. The error bars in the y direction take into consideration the gaps of 20 to 30mm between measurements. There is a linear relationship between the Re and the turbulent height of the fluid in a stirred tank:

$$\text{Dimensionless Fully Turbulent Height} = 4.23\times10^{-6}\,\text{Re} + 0.377 \qquad (6.7)$$

Notice that a very large Reynolds number is needed to maintain turbulence throughout the tank. For the PBT cases Re $\geq 6.6\times10^4$ and for the A310 case Re $> 1.2\times10^5$. The amount of power to induce Re's this high is significant because power is proportional to the rotational speed cubed. If a second impeller is added the power required only doubles at most (Oldshue, 1983). Assuming that fully turbulent flow throughout the tank can be induced by 2 impellers at Re=30 000 (at this Re, one impeller induces fully developed flow in ½ the tank based on Equation 6.7) or one impeller at Re=150 000, the single impeller system uses more than 50 times as much power as the dual impeller system. This suggests consideration of a dual impeller design if fully turbulent flow is required through out the entire tank.

6.4 Conclusion

The objective of this work was to examine the limits of fully developed turbulence in the bulk of a stirred tank. Similarity profiles of axial velocity were examined in the wall jet at the baffle, and it was shown that for three axial impellers, the upper third of the tank drops into the transitional flow regime at $Re=2\times10^4$. This result agrees well with a previous study which examined the active volume of mean circulation and determined that the limit of this volume occurred close to a $z/T=0.667$.

This result has implications for many industrial applications with surface feed or with dip pipes in the top third of the tank. It shows that similarity rules will not necessarily be obeyed in the top of the tank on scale-up or on changing the fluid, even if $Re>2\times10^4$. The appearance of transitional flow should also be an important consideration for those researchers wishing to model the flow and turbulence in the bulk of the tank.

6.5 Nomenclature

A	area (m^2)
b	y location at $U=U_m/2$ (m)
C	clearance (m)
C_D	drag coefficient
C_f	friction coefficient
D	impeller diameter (m)
H	liquid depth
L_C	characteristic length (m)
$\dot{m}$	mass flow rate (kg s^{-1})
N	impeller speed (s^{-1})
P	power (W)
Po	power number $Po=P/N^3D^5\rho$
Re	Reynolds number
T	tank diameter (m)
r	radial coordinate (m)
U_{core}	core velocity (m s^{-1})
U_C	characteristic velocity (m s^{-1})
U	axial velocity component (m s^{-1})
U_m	local maximum velocity (m s^{-1})
V_{Tip}	impeller tip speed(m s^{-1})
y	distance from tank wall (m)
z	axial coordinate (m)

Greek

η	dimensionless distance ($\eta=y/b_{1/2}$)
ν	kinematic viscosity (m^2 s^{-1})
ρ	density (kg m^{-3})
τ	shear stress (Pa)

6.6 References

Bittorf K.J., 2000, *Wall Jets in Stirred Tanks With Applications to Turbulent Limits and Solids Distribution*, University of Alberta, Ph.D. Thesis.

Bittorf K.J. and S.M. Kresta , 2000a, Active Volume of Mean Circulation for Stirred Tanks Agitated with Axial Impellers, *Chem. Eng. Sci.*, **55**, 1325-1335.

Bittorf K.J., and S.M. Kresta, 1999a, Wall Jets in Stirred Tanks, *accepted AIChE J.*

Gerhart P.M., R.J. Gross and J.I. Hochstein, 1992, *Fundamentals of Fluid Mechanics 2nd edition.* Addison-Wesley Publishing Company, New York.

Glauert M.B. 1956 The wall jet, *J. Fluid Mech.* **1**, 625-643.

Newman B.G., R.P. Patel, S.B. Savage and H.K. Tjio, 1972, Three-dimensional wall jet originating from a circular orifice, *Aero. Quarterly* **23**, 188-200.

Nouri J.M., J.H. Whitelaw, and M. Yianneskis, 1987, The scaling of the flow field with impeller size and rotational speed in a stirred reactor. *Second International Conference on Laser Anemometry – Advances and Applications,* Strathclyde, UK, (Sept.)

Oldshue J.Y. *Fluid Mixing Technology* McGraw-Hill Publications Co., New York, N.Y.

Padmanabham G. and B.H. Gowda, 1991, Mean and turbulence characteristics as a class of three-dimensional wall jets – Part 1: Mean flow characteristics, *J. of Fluids Engineering* **113**, 620-628.

Ranade V.V. and J.B. Joshi, 1989, Flow generated by pitched blade turbines I: measurements using Doppler anemometer, *Chem. Eng. Comm.*, **81**, 197-224.

Rushton J.H., 1946, Technology of Mixing *Can. Chem. Process. Ind.*, **30**, 55-61.

Rushton J.H., E.W. Costich, and H.J. Everett, 1950, Power characteristics of mixing impellers, *Chem. Eng. Progress* ,**46**, 395-467.

Wichterle K., P. Mitschke, J. Hajek, and L. Zak, 1988, Shear stress on the walls of vessels with axial impellers, *Trans. IChemE.*, **66**, 102-106.

Zhou G. and S.M. Kresta, 1996, Distribution of energy between convective and turbulent flow for three frequently used impellers, *Trans IChemE* **74**, 379-389.

Table 6- 1: Experimental Variables

Impellers	
PBT*	***D = 80mm = T/3 **** & D = 120mm =T/2
Lightnin A310*	D = 80mm = T/3 & ***D = 120mm =T/2***
Chemineer HE3	D = 60mm = T/4
Clearances	C_1= T/3 C_2= D/2
z traverses	z = 110, 140, 170, 200, 220 mm or z/T=0.46, 0.58, 0.71, 0.83, 0.92
Liquids	
Water	$\nu=1.0 \times 10^{-6}\ m^2/s$
Bayol	$\nu=3.0 \times 10^{-6}\ m^2/s$
TEG and Water (Mix 1)	$\nu=6.2 \times 10^{-6}\ m^2/s$
(Mix 2)	$\nu=14.5 \times 10^{-6}\ m^2/s$

** Conditions presented here in detail. The other results can be found in Appendix A.*

Table 6- 2: Equipment Specifications

Argon Laser	Output power = 300mW Beam separation = 34mm Focal length = 500mm Wavelength of light = 514.5nm Bragg cell frequency shift = 40MHz Fringe spacing = 7.6μm Velocity variability = ± 5%
Horizontal Traverses	Computer controlled Accuracy = ±0.25mm
Vertical Traverse	Manual Accuracy = ±1.0 mm
Off-Bottom Clearance Adjustment	Manual Accuracy = ±0.5 mm
Seeding	Tap Water - Naturally occurring 1μm particulate Bayol-35 – $TiO_2 \leq 5\mu m$ particulate

Table 6- 3: Last Known Turbulent Height (z/T) Compared to Re (PBT D=T/3)

Fluid	Water	Bayol	TEG mix2	Bayol	Bayol	Water	Water
Re	2.0×10^4	2.0×10^4	2.7×10^4	6.4×10^4	6.6×10^4	1.0×10^5	1.7×10^5
C/D=0.5	0.58	0.71	0.83	0.92	0.92	0.92	0.92
C/D=1.0	0.58	0.58	0.83	0.83	0.92	0.92	0.92

Table 6- 4: Last Known Turbulent Height (z/T) Compared to Re (A310 D=T/2)

Fluid	Water	Bayol	TEG mix2	Water	Bayol	Bayol	Water
Re	2.0×10^4	2.0×10^4	4.0×10^4	1.0×10^5	1.0×10^5	1.2×10^5	3.1×10^5
C/D=0.5	<0.46	<0.46	0.58	0.58	0.83	0.83	0.92
C/D=0.67	0.58	0.46	0.58	0.71	0.71	0.71	0.83

Table 6- 5: Last Known Turbulent Height (z/T) Compared to Re (PBT D=T/2)

Fluid	Water	Bayol	Bayol	Water	Water
Re	2.0×10^4	2.0×10^4	5.6×10^4	1.0×10^4	1.6×10^4
C/D=0.67	0.71	0.68	0.92	0.71	0.92
C/D=0.5	0.46	0.83	0.92	0.92	0.92

Table 6- 6: Last Known Turbulent Height (z/T) Compared to Re (A310 D=T/3)

Fluid	Water	Bayol	TEG Mix 1	TEG Mix 2	Bayol
Re	**2.0×10^4**	**2.0×10^4**	**2.7×10^4**	**4.5×10^4**	**9.8×10^4**
C/D=1.0	<0.46	0.46	0.58	0.58	0.71
C/D=0.5	0.58	0.71	0.58	0.71	0.83

Fluid	Water	Water
Re	**1.0×10^5**	**2.9×10^5**
C/D=1.0	0.71	0.71
C/D=0.5	0.92	0.92

Table 6- 7: Last Known Turbulent Height (z/T) Compared to Re (HE3 D=T/4)

Fluid	Water	Bayol	TEG Mix 2	Bayol	Bayol
Re	**2.0×10^4**	**2.0×10^4**	**2.3×10^4**	**3.6×10^4**	**6.0×10^4**
C/D=1.33	<0.46	0.71	0.71	0.71	0.92
C/D=0.5	0.46	0.46	0.58	0.92	0.92

Fluid	Water	Water
Re	**1.0×10^5**	**1.8×10^5**
C/D=1.33	0.92	0.92
C/D=0.5	0.92	0.92

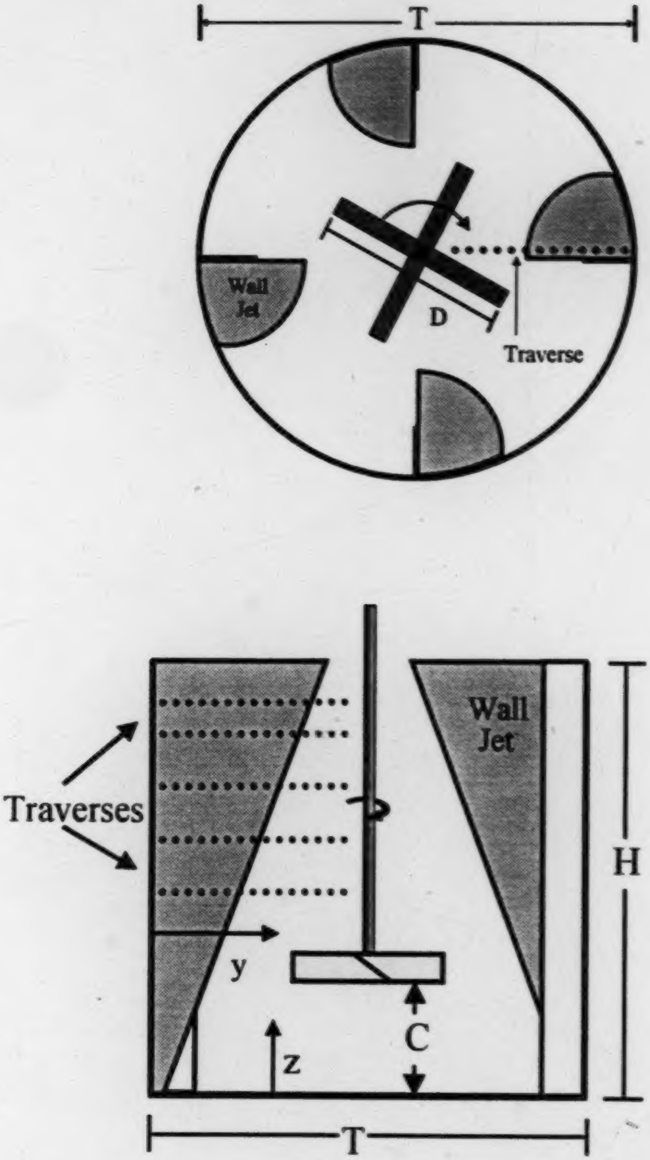
T
Wall Jet
D
Traverse
Traverses
Wall Jet
y
z
C
H
T

Figure 6-1: Experimental configuration, traverse locations and location of the three dimensional wall jets in the stirred tank.

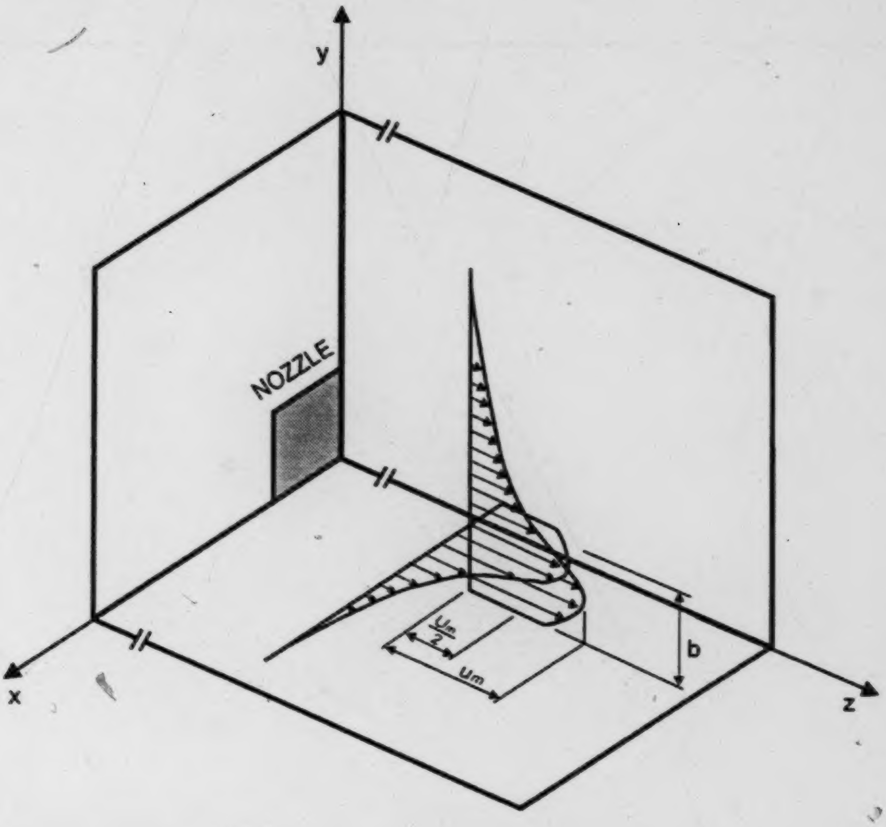
y
NOZZLE
$\frac{U_m}{2}$
U_m
b
x
z

Figure 6-2: Three dimensional wall jet produced by a square nozzle. b is the half width of the jet in the y direction. In the tank the baffle is in the y-z plane and the tank wall is in the x-z plane.

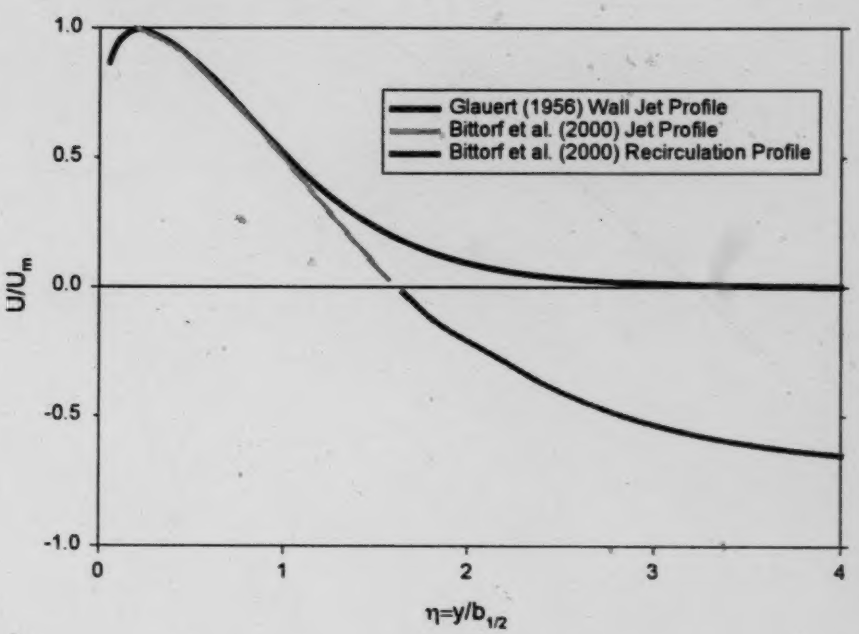

Figure 6-3: Two types of three dimensional wall jet profiles. Glauert's profile is for a jet in a stagnant fluid. Bittorf's profile is for a jet with recirculating flow and is broken into two parts: the wall jet and the recirculating flow.

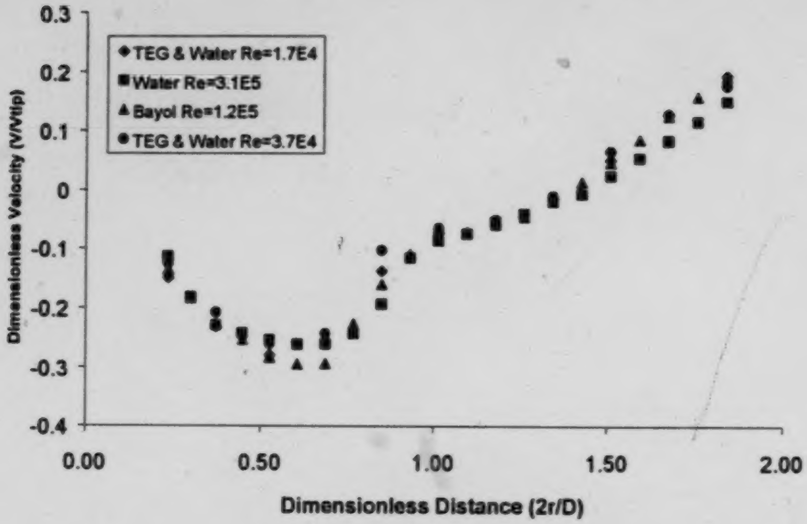

Figure 6-4 A: Dimensionless velocity profile taken below an A310 impeller, (C/T=0.33, D/T=0.5, z/T=0.29) showing that scaling of axial velocity with the tip speed produces a single profile.

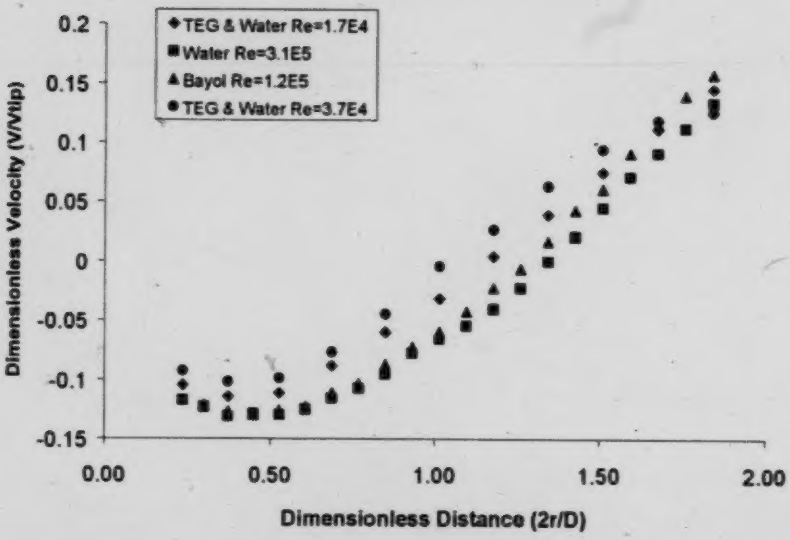

Figure 6-4B: Dimensionless velocity profile taken above an A310 impeller (C/T=0.33, D/T=0.5, z/T=0.46) showing that the profiles no longer collapse.

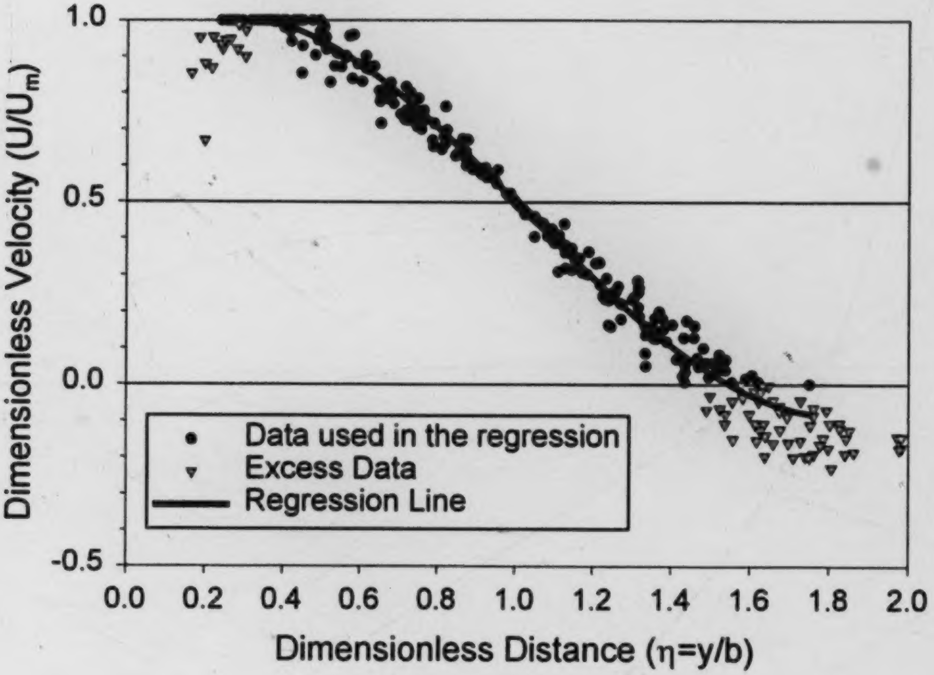

Figure 6-5: Similarity profile for the three dimensional wall jet in based on data from Bittorf 2000. This profile is used to test local velocity profiles for scalability and thus for fully turbulent flow. Note that all data is forced to fit at U/U_m=1.0 and U/U_m =0.5

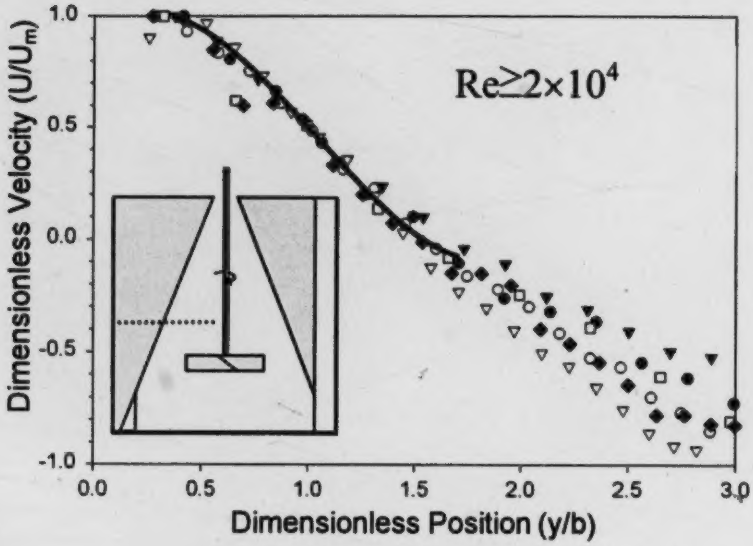

Figure 6-6A: Fully turbulent velocity profiles at z/T=0.46, C=D and D=T/3 for a PBT. All profiles collapse onto the jet profile

Legend for Figures 6-6 to 6-9

	Symbol	Re	Fluid
Profile 1	●	1.7×10^5	Water
Profile 2	○	1.0×10^5	Water
Profile 3	▼	6.6×10^4	Bayol
Profile 4	▽	6.4×10^4	Bayol
Profile 5	■	3.0×10^4	T.G. and Water
Profile 6	□	2.0×10^4	Bayol
Profile 7	◆	2.0×10^4	Water
Equation 6.4	—		

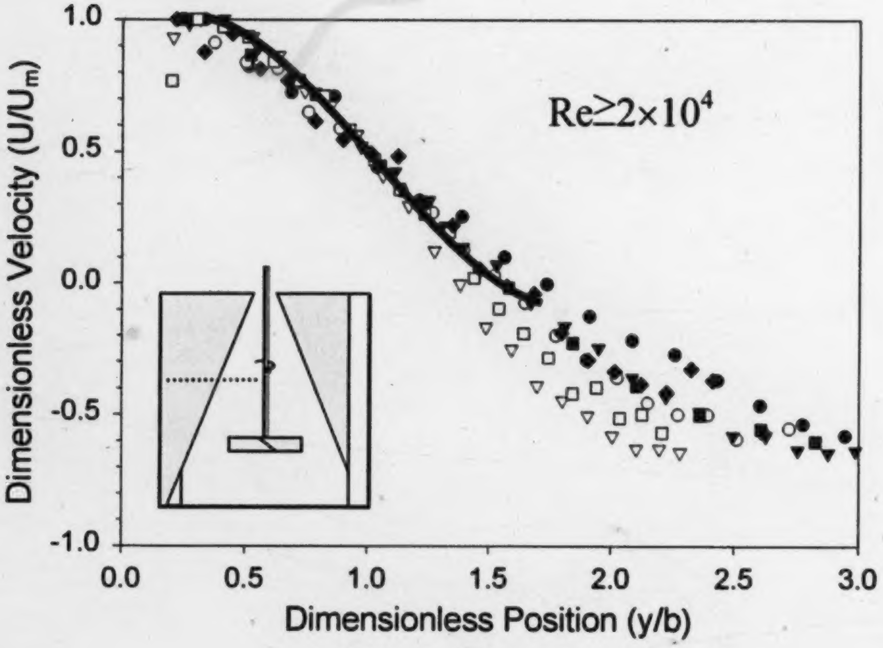

Figure 6-6B: Fully turbulent velocity profiles at z/T=0.58, C=D and D=T/3 for a PBT (see Figure 6-6A for legend). All profiles collapse.

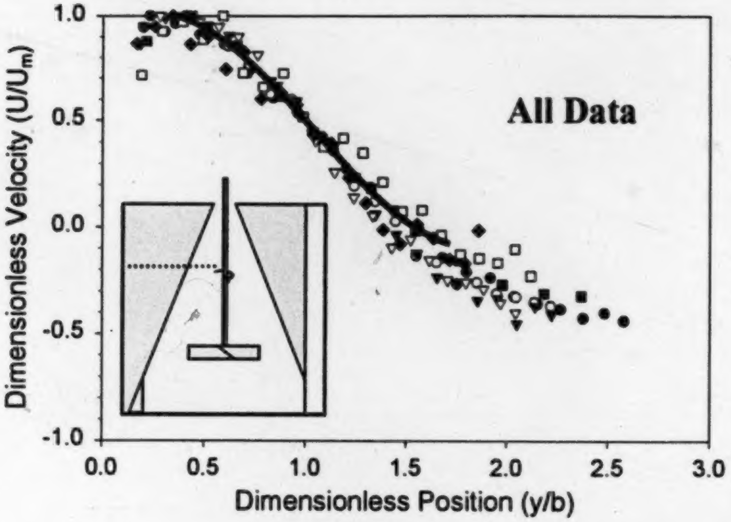

Figure 6-7A: Velocity Profiles at z/T=0.71, C=D and D=T/3 for a PBT (see Figure 6-6A for legend)

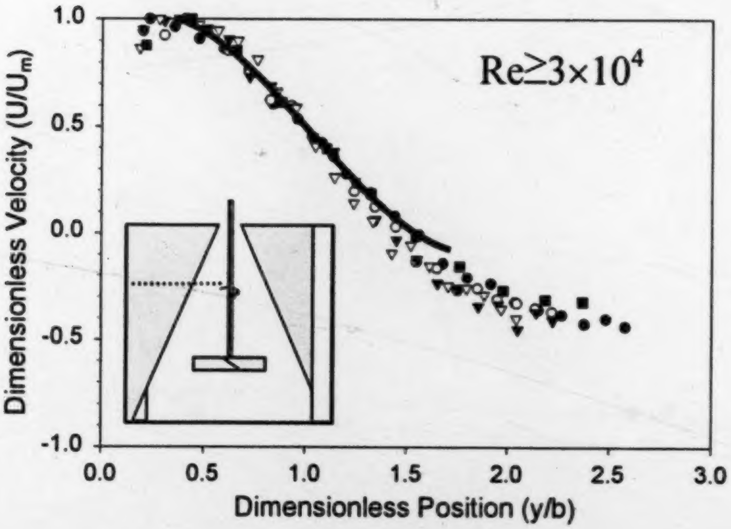

Figure 6-7B: Fully turbulent velocity profiles at z/T=0.71, C=D and D=T/3 for a PBT with Profiles 6 & 7 eliminated (see Figure 6-6A for legend)

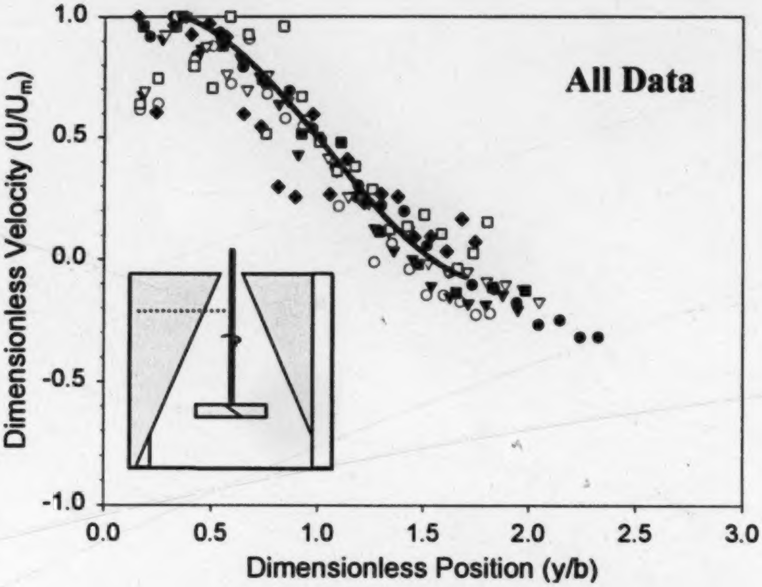

Figure 6-8A: Velocity Profiles at z/T=0.83, C=D and D=T/3 for a PBT (See Figure 6-6A for legend)

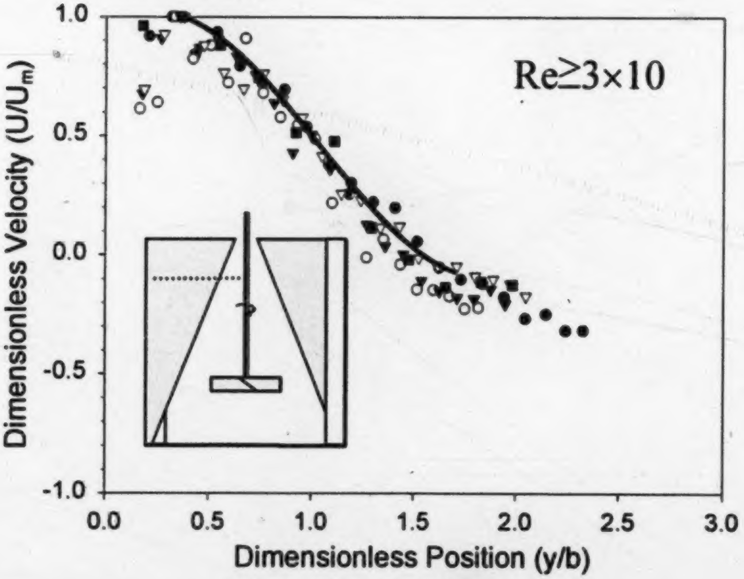

Figure 6-8B: Fully turbulent velocity profiles at z/T=0.83, C=D and D=T/3 for a PBT with profiles 6 & 7 eliminated. (see Figure 6-6A for legend)

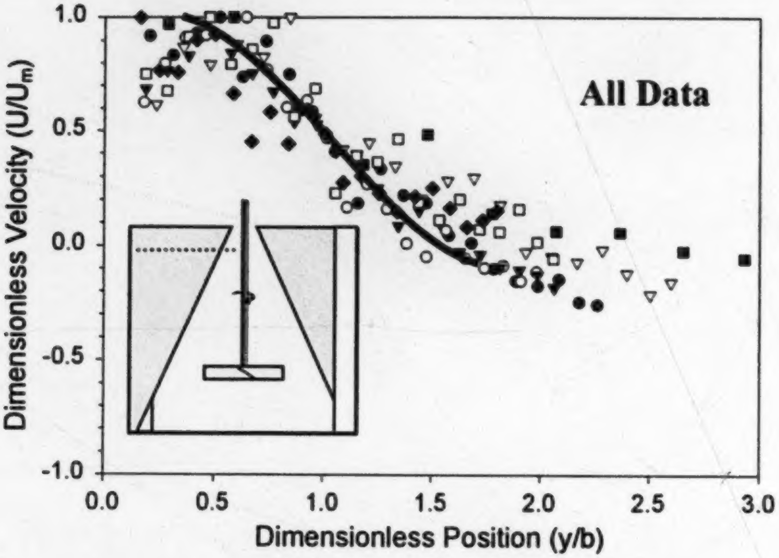

Figure 6-9A: Velocity profiles at z/T=0.92, C=D and D=T/3 for a PBT (see Figure 6-6A for legend)

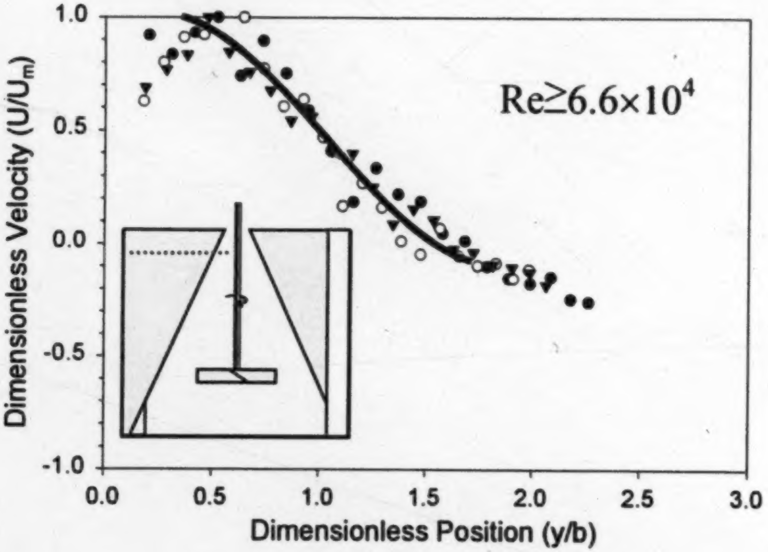

Figure 6-9B: Fully turbulent velocity profiles at z/T=0.92, C=D and D=T/3 for a PBT with profiles 4,5,6, &7 eliminated (See Figure 6-6A for legend)

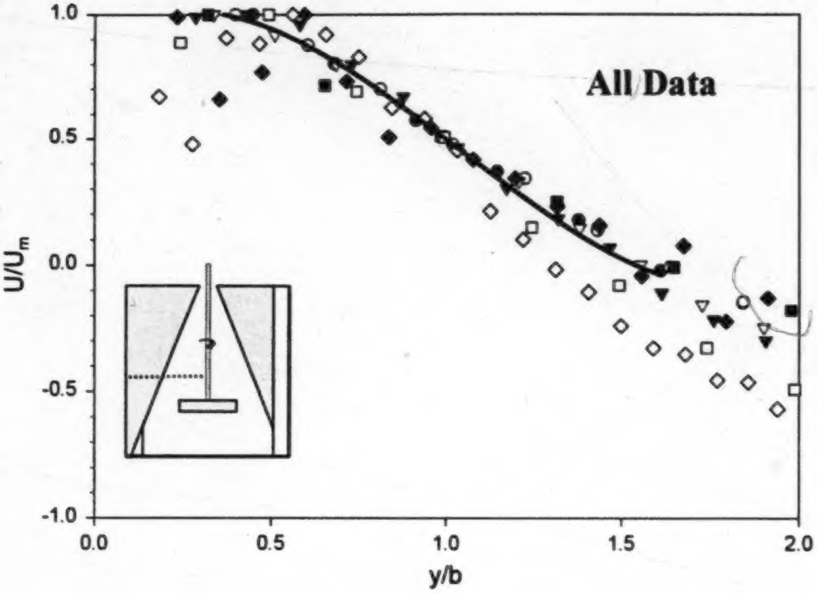

Figure 6-10A: Velocity profiles at z/T=0.46, C=D/2 and D=T/2 for an A310 impeller.

Legend for Figures 6-10 to 6-14

	Symbol	**Re**	**Fluid**
Profile 1	●	3.1×10^5	Water
Profile 2	○	1.2×10^5	Bayol
Profile 3	▼	1.0×10^5	Bayol
Profile 4	▽	1.0×10^5	Water
Profile 5	■	3.7×10^4	T.G. and Water
Profile 6	□	2.0×10^4	T.G. and Water
Profile 7	◆	2.0×10^4	Water
Profile 8	◇	2.0×10^4	Bayol
Equation 6.4	—		

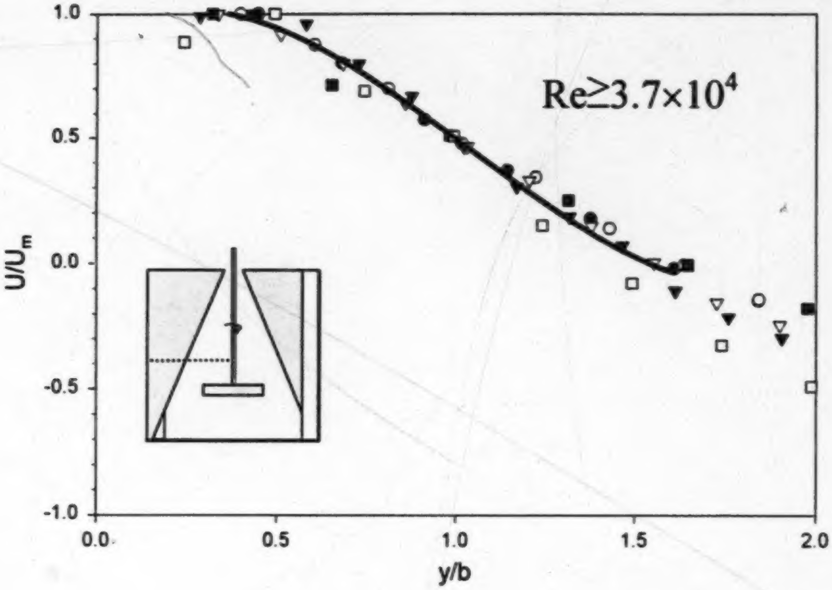

Figure 6-10B: Fully turbulent velocity profiles at z/T=0.46, C=D/2 and D=T/2 for an A310 with profiles 7 & 8 eliminated (see Figure 6-10A for legend).

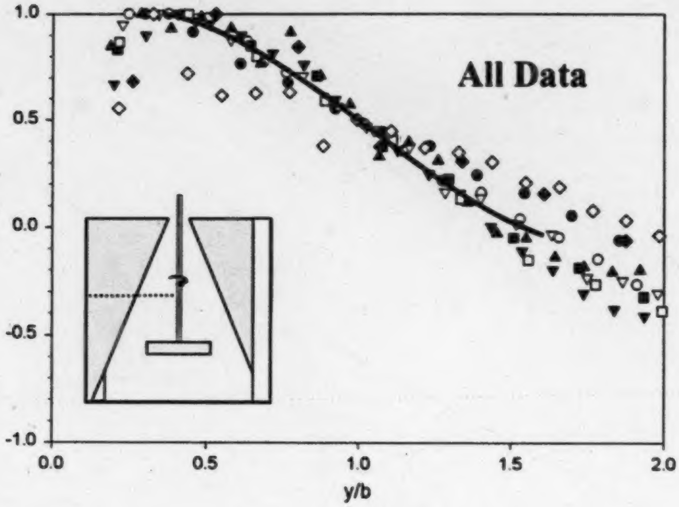

Figure 6- 11A: Velocity profiles at z/T=0.58, C=D/2 and D=T/2 for an A310 (see Figure 5-10A for legend).

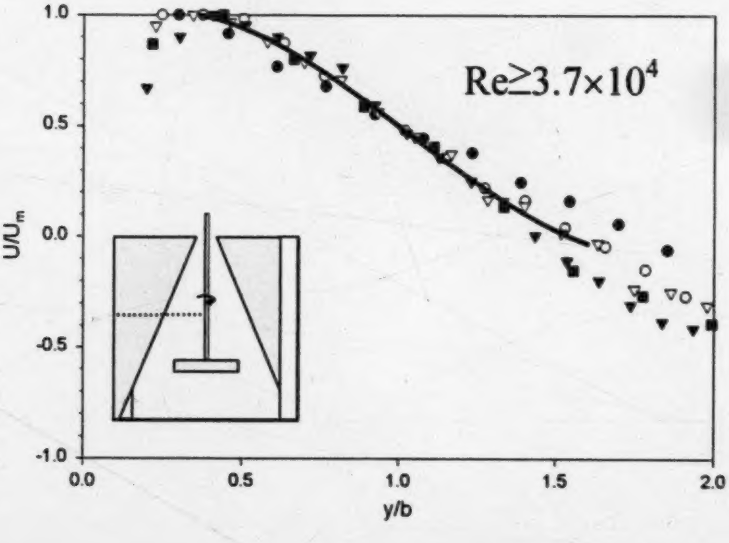

Figure 6-11B: Fully turbulent velocity profiles at z/T=0.58, C=D/2 and D=T/2 for A310 with profiles 6,7& 8 eliminated (see Figure 5-10A for legend).

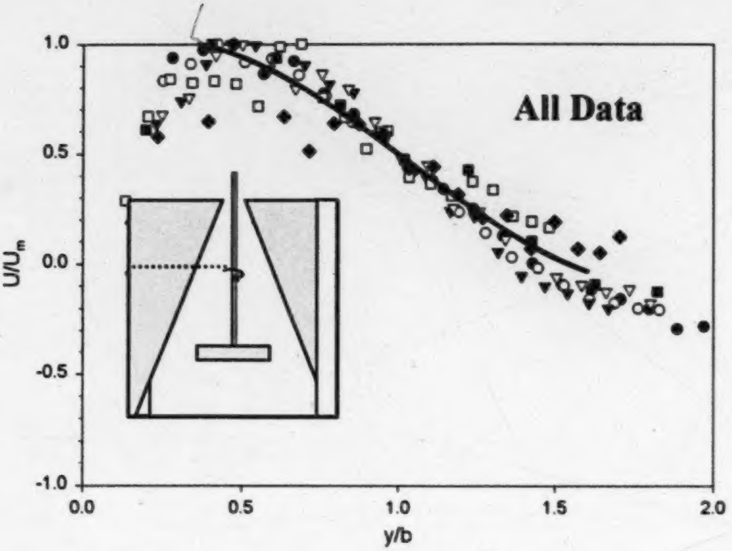

Figure 6- 12A: Velocity profiles at z/T=0.71, C=D/2 and D=T/2 for an A310 (See Figure 5-10A for legend).

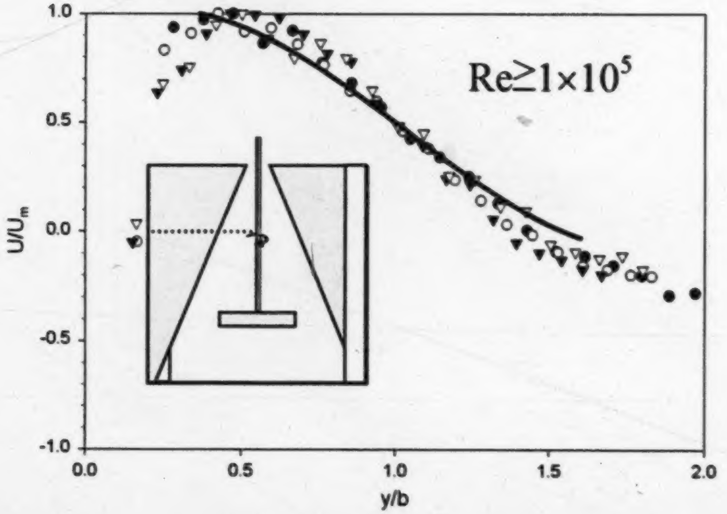

Figure 6-12B: Fully turbulent velocity profiles at z/T=0.71, C=D/2 and D=T/2 for an A310 with profiles 5, 6, 7& 8 eliminated (see Figure 6-10A for legend).

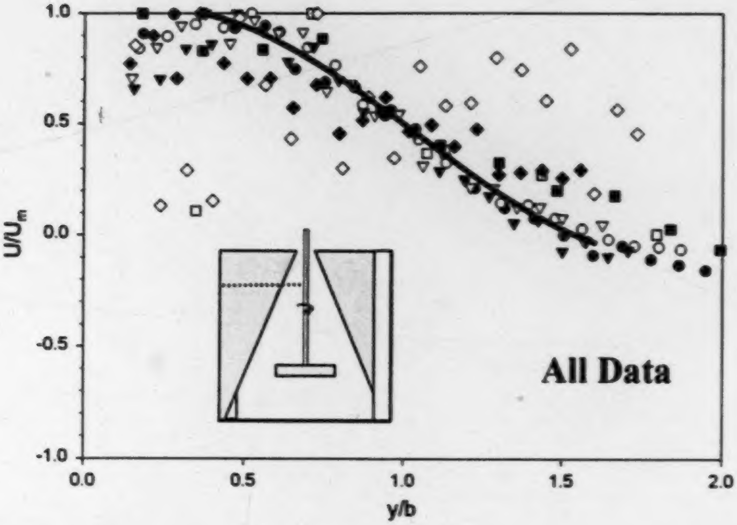

Figure 6-13A: Velocity profiles at z/T=0.83, C=D/2 and D=T/2 for an A310 (see Figure 5-10A for legend).

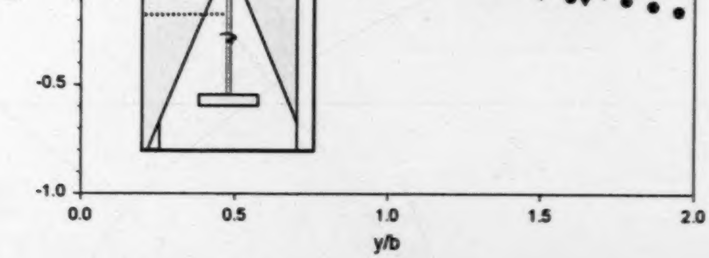

Figure 6-13B: Fully turbulent velocity profiles at z/T=0.83, C=D/2 and D=T/2 for an A310 with profiles 5,6,7& 8 eliminated (see Figure 6-10A for legend)

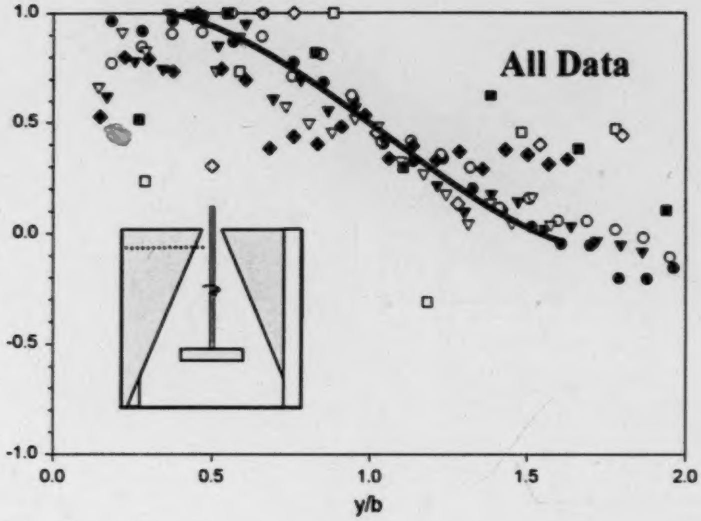

Figure 6-14A: Velocity profiles at z/T=0.92, C=D/2 and D=T/2 for an A310 (see Figure 5-10A for legend).

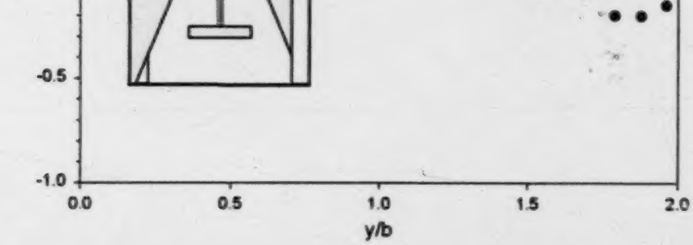

Figure 6-14B: Fully turbulent velocity profiles at z/T=0.92, C=D/2 and D=T/2 for an A310 with profiles 2, 3, 4, 5, 6, 7& 8 eliminated (see Figure 5-10A for legend)

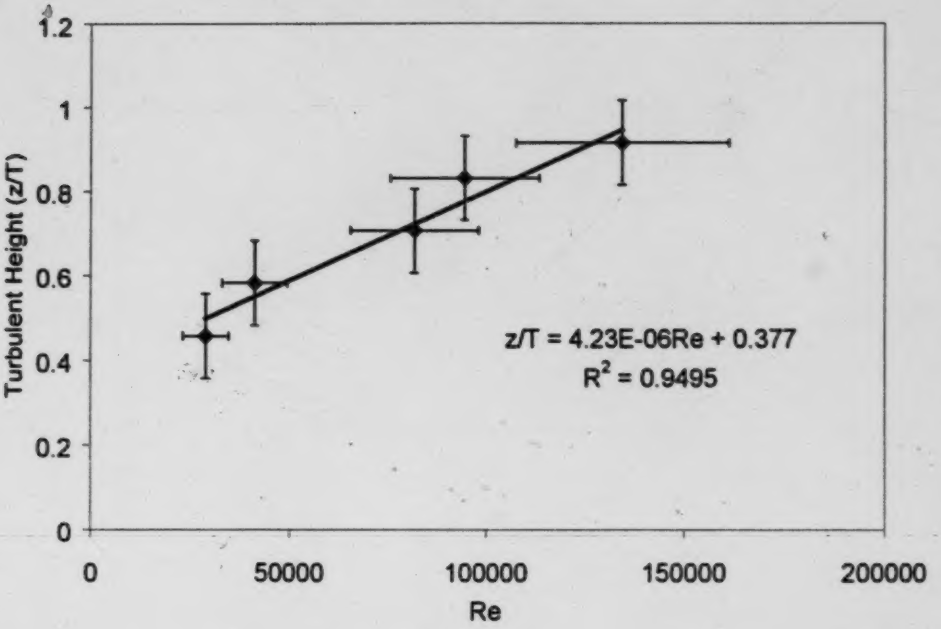

Figure 6-15: Impeller Reynolds number required to achieve fully turbulent conditions as z/T increases. Only at the impeller is $Re=2\times10^4$ sufficient to attain fully turbulent flow.

Chapter 7

Prediction of Cloud Height for Slow Settling Solids in Stirred Tanks

7.1 Introduction

Uniform solids distribution is an important component of mixing theory for both batch and continuous mixing operations in slurry catalyst reactors and in mineral processing. The height to which the solids are suspended, or the cloud height, is not yet fully understood. Investigations of solids suspension conditions have concentrated mostly on the just suspended speed (Njs) (Armenante et al., 1998, Myers and Bakker, 1998, Takahashi and Fujita, 1995, Myers et al., 1994, Tay et al., 1984, Baldi et al., 1978, Nienow, 1968 and Zwietering, 1958) while studies of solids distribution and cloud height are limited by comparison (Bujalski et al., 1999 and Hicks et al., 1997). The prediction of cloud height developed in this paper is based on mean flow patterns in a fully baffled stirred tank mixed with an axial impeller.

The flow structures in a stirred tank determine the solids distribution but the solids in the stirred tank can also influence the flow. Although, the effect of solids on the turbulent characteristics of a pipe flow system has been examined by Gore and Crowe (1989a & b), the effect they have in a stirred tank environment has yet to be determined. With respect to the mean flow and the largest scales of time varying motions there are three structures that can affect the solids distribution and cloud height in a stirred tank: the mean circulation loop, the three dimensional wall jets along the baffles, and the large scale turbulent structures or macro-instabilities (MI). Mak (1992) indicated that constant power per unit volume is the appropriate method to scale solid systems. In general, mean flow patterns produced by axial impellers have a single circulation loop. The size of the mean circulation loop was examined in Chapter 5 and by Bittorf and Kresta (2000), who defined it as the active volume for a stirred tank. The active volume in a stirred tank mixed with an axial impeller is $z=2T/3$ high and is independent of impeller clearance and size (Bittorf and Kresta, 2000). The location of the active zone may change depending on the impingement point of the impeller discharge stream on the tank wall. The lower portion of the tank is mixed by the mean circulation loop, which fills the active volume (Bittorf and Kresta, 2000).

The dominant flow upward flow in a stirred tank is along the front of each of the baffles. This flow can be described as a series of three-dimensional wall jets (Chapter 3). In this chapter it will be shown that the velocities in the jets, in balance with the settling velocity of the solids, determine the solids cloud height particularly at high solids concentration.

Even though a mean circulation pattern can be clearly defined in the stirred tank, at any instant in time the flow is complex. For some geometries, large velocity fluctuations or macro-instabilities have been observed (Grgic, 1998, Myers et al., 1997 and Bruha et al., 1995). Macro-instabilities drive the mixing in the upper portion of the stirred tank and are responsible for the "surface welling". The macro instabilities are more dominant for a system mixed with a pitched bladed turbine (PBT) as compared to a system mixed with fluid foil impellers (Lightnin A-310 and Chemineer HE3) (Grigic 1998).

This investigation concentrates on developing a model for the prediction of the solids cloud height. This model is based upon two essential components: the velocities in the three dimensional wall jet along the baffle of the tank, and the impeller speed required to fully suspend the solids off the bottom of the tank (Njs). The model to predict cloud height assumes that mean velocities are the driving force for solid suspension. For a mean flow model to apply, the macro-instabilities in the flow must not be a major driving force in the suspension of solids. To test this hypothesis, velocity measurements were taken close to the top of the tank to determine the effect that the solids have on the macro-instabilities in the clear liquid layer above the suspension. The model is developed and validated using solids distribution and cloud height data from Bujalski et al. (1997), Hicks et al. (1997) and Mak (1992).

7.1.1 Cloud Height and Solids Distribution

While most solids suspension work has focused on Njs, several papers examine the cloud height and solids distribution. Barresi and Baldi (1997) studied solids dispersion in a torispherical-bottomed tank while Shamlou and Koutsakos (1987) used a tank with a spherical bottom and a tank height equivalent to three tank diameters (H=3T). Bujalski et al. (1999) and Hicks et al. (1997) reported cloud height for various solids, but neither gives a generalized model. Data from Mak (1992) measured concentration profiles at high solids concentrations and from this CH can be calculated. These three studies cover significantly different conditions as summarized in Table 7-1. Bujalski et al. (1999) examined cloud height at high solids concentrations (28 wt.%). The types of solids were varied, but they maintained the tank configuration constant. Hicks et al. (1997) varied the types of solids and experimental configuration but considered only solids concentrations of 10 wt.%. In this work, a generalized model for prediction of cloud height is developed using data from Hicks et al. (1997) and validated with Bujalski et al.'s (1999) data, and additional data from this study. Mak (1992) examined concentration profiles at high solids loading for various tank scales and his data is used to test the model under scale-up conditions.

The cloud height in a concentration profile is defined as the point where the concentration drops sharply to zero. A well defined cloud height appears mainly in suspensions with solids loadings greater than or equal to 10%. Below a solids concentration of 10% no clear liquid interface is apparent and the concentration changes gradually. Barresi and Baldi (1987) gave concentration profiles for low solids loadings ($X \leq 5\%$). In these instances, the concentration changes are so subtle that a definite height below which the concentration is uniform can not be determined.

7.1.2 Effect of Solids Loading

For solids loading greater than 10%, a clear interface forms, and it is assumed that mean flow dominates the solids distribution. The clearly defined cloud height, shown in this work, coincides with the disappearance of macro-instabilities (MI). This may be due to two phenomena observed in other flows: turbulence damping by particles and/or stable stratification due to the presence of a density gradient.

Gore and Crowe (1989a & b) showed that small particles reduce turbulence. "Small" is quantified by a comparison of particle size to turbulence length scales and specifically to the integral length scale of the energy producing eddies. In a stirred tank, the integral length scale is related to the impeller diameter because of the vortices attached to the blades (Kresta, 1998, Zhou and Kresta, 1996, and Van't Riet and Smith, 1975). These vortices are one-tenth the impeller diameter (l=D/10) and are the most energetic eddies within the stirred tank. According to Gore and Crowe (1989a & b) particles with a diameter of less then 10% of the integral length scale may reduce the turbulence in the system. Particles larger then the integral length scale increase the turbulence in the system. The particle generated turbulence is produced in the particle wakes. Although this increases the turbulence in the system, it will not increase the intensity of the large-scale structures within the system. In a stirred tank, particles with a diameter less then D/100 may be expected to damp out the turbulent fluctuations.

The other phenomenon reducing the turbulence in a two-phase system is density stratification. Stratification is relevant for high solids loadings ($X \geq 10\%$) where a clear interface develops. The density of the lower layer can be calculated as long as $N \geq Njs$, but if $N < Njs$ the calculation of the slurry density would be more difficult since the amount of solids at rest must be known. To break through a stratified layer there must be enough momentum to break through the stratification. Larson and Jonsson (1994) showed that increasing the nozzle speed of a jet in a two-layer stratified fluid increased the jet's penetration distance into the second layer. This is much like the stirred tank where an increase in impeller speed raises the interface height (provided the solids are in a fully suspended state). This is also an indication that the wall jet is penetrating higher into the tank.

7.1.3 Just Suspended Speed (Njs)

Cloud height must be clearly distinguished from Njs, since the two characteristics are related but quite distinct. Njs has been regularly investigated since 1958 when Zwietering formed the correlation:

$$Njs = S \cdot \left(\frac{g \cdot \Delta\rho}{\rho_L} \right)^{0.45} \frac{X^{0.13}\, d_p^{0.2}\, \nu^{0.1}}{D^{0.85}} \qquad (7.1)$$

This is still the best available prediction of Njs. Variations on the Njs correlation since Zwietering have expanded the correlation for conditions not previously examined (Armenante et al., 1998, Myers and Bakker, 1998, Takahashi and Fujita, 1995, Myers et al., 1994, Tay et al., 1984 and Neinow, 1968). Baldi et al. (1978) derived an expression similar to Zwietering's correlation using turbulent scaling arguments:

$$Njs = \underset{\text{I}}{\left(\frac{g \cdot \Delta\rho}{\rho_L} \right)^{1/2}} \underset{\text{II}}{\frac{d_p^{1/6}}{Po^{1/3}}} \underset{\text{III}}{\left(\frac{T}{D} \right)} \underset{\text{IV}}{\frac{1}{D^{2/3} \cdot Z}} \qquad (7.2)$$

Baldi et al. (1978) assumed that there is a critical eddy size at which particles are lifted off the bottom of the tank. The actual eddy size near the bottom of the tank was estimated using the local rate of dissipation of turbulent kinetic energy. Isotropic flow and uniform dissipation within the tank were assumed. Neither of these assumptions are unambiguous; Zhou and Kresta (1996) showed that the dissipation in the impeller region is much higher than in the rest of the tank. The degree of local isotropy in the rest of the tank is still under debate. Nonetheless, Baldi's hypothesis is that the dissipation near the bottom of the tank is proportional to the total energy in the system. If local dissipation near the bottom of the tank could be estimated, Z would not be needed as a fitting constant in Equation 7.2.

The most significant difference between Zwietering's equation and Baldi's is the absence of the viscosity term in Baldi's equation. The viscosity term in Equation 7.1 is only to the power of 0.1, so its significance is small in any case. Baldi took the solids concentration into account in the Z term of his equation and Zwietering took impeller characteristics like the Power number (Po) into account in his constant S. The remaining differences between Baldi's equation and Zwietering's correlation consist of some differences in exponents.

To cast Baldi's equation in a different light, Terms I and II contain the turbulent settling velocity as described by Newton (Perry and Green, 1984):

$$V_T = 1.73\left(\frac{g \cdot \Delta\rho \cdot d_p}{\rho_L}\right)^{1/2} \tag{7.3}$$

If Equation 7.2 is then converted to give the impeller tip speed at Njs in terms of the terminal velocity the following equation results:

$$V_{tip,Njs} = V_T \frac{1.82}{Z \cdot Po^{1/3}}\left(\frac{T}{D}\right)\left(\frac{D}{d_p}\right)^{1/3} \tag{7.4}$$

This equation will be used as the characteristic velocity for solids suspension in a given tank configuration. Three key factors are accounted for in $V_{tip,Njs}$: the particle characteristics, as described by the terminal velocity (V_T); impeller and geometric characteristics, as given by the power number (Po) and Z; and relative length scales, as given by the two dimensionless groups, impeller to tank diameter ratio (T/D) and the impeller to particle diameter ratio (D/d_p). The impeller tip speed at Njs will be used to scale the suspension velocity in later sections.

7.2 Model Development

The development of a model for the prediction of cloud height is the main objective of this paper. The model is based on a mean flow assumption, which implies that the dominating driving force for solids distribution is the wall jets along the baffles. The required suspension velocity is related to the local maximum jet velocity at the cloud height. This velocity is made dimensionless with the characteristic impeller speed $V_{tip,Njs}$.

Scale-up of the impeller speed required for a given cloud height based on this model is equivalent to maintaining constant power per unit volume.

7.2.1 Validation of Steady Flow Assumption

The first step in the model development is to confirm that a mean flow model is valid for the system under consideration. The flow in a stirred tank is driven by the mean flow patterns and the large scale macro instabilities. For a mean flow model to apply, the macro-instabilities in the flow must not be a major driving force in the suspension of solids. It is hypothesized that the solids at high concentrations damp out the macro-instabilities, hence the suspension is mean flow driven. To validate this assumption, experiments were conducted to assess the importance of macro-instabilities at high solids concentrations.

Experimental Conditions

A fully baffled, cylindrical, flat-bottomed tank of a diameter T=0.24m and liquid height (H=T), shown in Figure 7-1 and Table 7-1, was examined. Two types of impellers were used: a four bladed 45° PBT and the Lightnin A310. Laser Doppler Velocimety (LDV) was used to measure time series of velocity at the top of the tank, with and without solids. Table 7-2 summarizes the LDV configuration. More information is given in Chapter 2. The location of the measurements in an r-θ plane is shown in Figure 7-2. Velocity measurements were taken over a minimum period of 50s with a minimum record size of 10,000 points per time series.

The solids used for the validation of the steady flow assumption was sand with an average diameter of 300μm, a density of 2550 kg/m^3 and solids concentrations ranging from 24% to 55% weight percent. The velocity measurements during suspended conditions were completed in the clear liquid above the solids cloud height, 220mm from the bottom of the tank. Due to the stability of the cloud height, the solids rarely interfered with the velocity measurements.

Results

The time series data was analyzed to determine the effect of solids on the large-scale structures and the velocity fluctuations within the tank. The analysis consisted of smoothing the data and visually examining the time series data. The smoothing method used was an eleven point smoothing: at each time t the average of the velocity measured at time t plus the five velocity measurements before and after t was recorded. This eliminates the instantaneous velocity fluctuations and makes it possible to see the influence of the macro instabilities on the time series. Figure 7-3A shows a time series for velocity measurement completed without solids and Figure 7-3B shows this signal smoothed to emphasize the large structures. Figure 7-3C shows a smoothed time series for a solids concentration of 24wt.% at the same RPM and location as the clear water case. The velocity fluctuations are approximately one tenth the size of the clear water case; hence proving that high solids loading reduces the magnitude of the large-scale structures in the tank.

The effect of solids on the RMS velocity is shown in Table 7-3. The RMS velocity is reduced by over 75% at high solids concentrations. Finally, the dimensionless RMS velocity at z=220mm and r=95mm for increasing cloud heights is shown in Figure 7-4. This figure shows that the increased impeller speed needed to raise the cloud height does not have an effect on the turbulence in the clear liquid above CH for solids concentrations at or above 24%.

Although the turbulence in the clear liquid is greatly reduced, some fluctuations in the cloud height were observed. Small bursts of solids periodically rise higher in the tank. This seems similar to the behavior of circular jets in a reverse buoyancy setting (Turner, 1966, and Pantzlaff and Lueptow 1999). The reverse buoyancy effect occurs when a jet of a higher density fluid is projected upward in a continuous fluid with a lower density.

Various studies of jets with reverse buoyancy can be used to describe what occurs at high solids concentrations. A jet of fluid which is more dense than its surroundings will have an initial penetration height that is greater than its mean penetration height (Turner, 1966, and Pantzlaff and Lueptow 1999). Once the jet reaches its steady state height it continues to fluctuate various amounts. The fluctuations of the jet are constant and periodic, even though the flow rate of the jet remains constant (Turner, 1966).

7.2.2 Wall Jet Model: determining fluid velocity at the wall

The prediction of cloud height requires the velocity in the wall jet. There are two types of wall jets formed in a stirred tank (Bittorf and Kresta, 1999): one below the impeller along the bottom of the tank and the other along the wall of the tank. The discharge from a purely axial impeller impinges on the bottom of the tank and then spreads radially until wall impingement occurs. The combination of the impeller discharge stream impinging on the wall and swirling tangential flow impinging on the baffle produces a three dimensional wall jet along the baffle. The jet reaches its maximum velocity around z/T=0.3.

There are three distinct regions in a classical three dimensional wall jet: the potential core, where velocities are constant; the characteristic decay region, where velocities decay according to the initial shape of the jet; and the universal decay region, where velocity decay is independent of the initial shape of the jet (Swamy and Bandyopadhyay (1975) call this the radial decay region). Figure 7-5 shows these regions for an A-310 impeller driven flow. The x-axis is the dimensionless height (z/T) while the y-axis is the local maximum velocity, U_m, made dimensionless with the potential core velocity, U_{core}. While in a stirred tank there is a development zone rather than a potential core, it was shown in Chapter 4 that the velocity decay is similar for all axial impellers. The maximum local velocity in the jet U_m is calculated using (Chapter 4):

$$\frac{U_m}{U_{core}} = 0.28\left(\frac{1}{z/T}\right)^{1.15} \qquad (7.5)$$

where U_m is the local maximum velocity, U_{core} is the core velocity, z is the distance from the bottom of the tank and T is the tank diameter.

The next stage required for the cloud height model is to determine the core velocity for various geometries. The core velocity can be correlated with the distance the impeller discharge stream travels before wall impingement. This distance depends on the impeller type, the off-bottom clearance, and the blade angle. Two methods for calculating the core velocity are considered, both of which depend on the geometric configuration.

The model for predicting cloud height upon scale-up is based on the discharge properties of the axial impeller and the properties of the three dimensional wall jet. Predicting the core velocity is dependent on various influences in the stirred tank: impeller discharge angle, impeller clearance, and impeller type (Chapter 6). It is unknown how solids affect these properties, but it is hypothesized that the core velocity is proportional to the tip speed of the impeller for any given configuration (fixed impeller type, impeller clearance, impeller diameter and solids concentration). Given this, the core velocity is:

$$V_{tip} = U_{core} K \qquad \textbf{(7.6)}$$

Here the constant K accounts for the impeller properties and the effect of solids. The distance the discharge travels can be estimated from mean velocity data and it is important to note that the impeller clearance does affect the discharge angle of a PBT impeller (Chapter 6 and Kresta and Wood, 1993). Even though an estimate of the discharge distance can be attained, it does not account for the effect the solids may have on the discharge angle.

Core Velocity Model 1: Purely Axial Discharge Stream

Figure 7-1 illustrates the first method of predicting core velocity. This assumes that the discharge from axial impellers is purely axial; hence, the distance to impingement on the tank wall is equivalent to the impeller clearance, plus the distance from the impeller blade tip to the wall of the tank. The problem with this method is that the PBT impeller is not purely axial; its discharge is influenced by the blade angle, off bottom clearance and impeller to tank diameter ratio (Kresta and Wood, 1993). Model 1 can only be applied in the calculation of distances for purely axial impellers like the HE-3 and A310.

Core Velocity Model 2: Mixed Flow Discharge Stream

Figure 7-6 illustrates the second method, which models the distance traveled by the impeller discharge using the axial, radial, *and* tangential velocities generated by the PBT. The angle between the axial velocity vector and the tangential (V_θ) - radial (V_r) resultant velocity vector (ϕ) is assumed equal to the impeller blade angle (45° for the PBT, 90° for hydrofoils). Figure 7-6 shows an r-z slice through the tank, at the angle α made by the r-θ velocity vector in the impeller discharge stream, as shown in the plan view. Based on this model, the distance the impeller discharge stream travels before impingement on the wall is given by:

$$\alpha = \tan^{-1}\left(\frac{V_\theta}{V_r}\right) \tag{7.7}$$

$$W = C \cdot \tan(90 - \phi) \tag{7.8}$$

$$F = \frac{T}{2} - \left[\frac{(2W + 2x_o \cos\alpha)^2 - (2x_o \cos\alpha)^2}{4} + x_o^2\right]^{1/2} \tag{7.9}$$

$$R = \sqrt{C^2 + W^2} \tag{7.10}$$

The total distance to wall impingement: $G = R + F$ **(7.11)**

Here x_o is the point on the impeller blade where the maximum discharge velocity is located, and where ϕ is measured. The r-θ discharge angles for T/3 and T/2 PBT impellers are 95° and 45° respectively (Kresta and Wood, 1993).

To compare the two methods of predicting distance to wall impingement, the measured core velocity is made dimensionless with the impeller tip speed and the impingement distance is made dimensionless with tank diameter. A regression was completed on Model 1, purely axial discharge, and it was found that this assumption leads to significant inaccuracies ($R^2 = 0.50$). Incorporation of the blade angle (Model 2) improves the accuracy to that shown in Figure 7-7 ($R^2 = 0.60$). Although the second method predicts the velocity more accurately, there is still significant variability that needs to be resolved. Based on Figure 7-7 the core velocity can be estimated using:

$$U_{core} / V_{tip} = 0.105\,(G/T)^{-1.4} \qquad \textbf{(7.12)}$$

Table 7-4 gives measured values of U_{core} for PBT and A310 impellers used at various C's and D's.

The largest source of error in Model 2 is due to the assumption that the discharge follows a straight path to the wall or the bottom of the tank. The walls of the tank actually tend to deflect the jet, affecting the distance the jet travels to wall impingement. Macro-instabilities in the stirred tank may also affect the distance traveled by the impeller discharge stream. Grgic (1998) showed more macro-instabilities for a system mixed with a PBT impeller than for an airfoil type impeller. Because of the macro-instabilities, the distance the jet travels to the wall may vary with time. CFD may be useful for this problem if accurate prediction of the impingement point, the length of the discharge stream and the core velocity can be achieved for an arbitrary new geometry.

7.2.3 Cloud Height Models

The model proposed for predicting the cloud height applies the properties of the three-dimensional wall jet to solids distribution. Since the velocities in the wall jet and their decay can be calculated, these velocities can be used to determine the height where the upward velocity of the fluid equals the downward velocity of the suspended solids.

The local maximum velocity at the cloud height was calculated for the cloud height measurements reported by Hicks et al. (1997). Figure 7-8 shows the local maximum velocity as a function of cloud height for nine different cases and for solids terminal velocities ranging from 0.0047 to 0.18 m/s. The data series (D/T=0.35 C/T=0.25 Njs=1050 HE3 V_T=0.178 m/s) was eliminated from further analysis because it is the only data set for a fast settling solid and it shows different settling characteristics than the other suspensions. With the exception of this data, the local maximum velocity in the wall jet is constant above z/T=0.6, indicating that as the cloud height rises the fluid velocity at the cloud height is constant. Constant velocity is not expected below a z/T=0.6 because the three-dimensional wall jet is not the dominant flow below this point (Bittorf and Kresta, 1999).

Although the velocity at CH for a single suspension remains constant above CH=0.6, the value of the local maximum jet velocity depends on the suspension and the mixing geometry. A characteristic velocity variable was needed to make the local maximum velocity dimensionless and to collapse the data. Two velocities were considered: the terminal velocity of a single particle and the hindered settling velocity for the suspension. The data for a stirred tank do not follow a hindered settling model. The hindered settling model applies in cases where all of the particles are descending, and was developed for constant flow or no flow systems. The flow in a stirred tank is recirculating and because of this, the particles are forced upward or downward depending on their location in the tank and the dominance of the macro-instability at that location. Since the hindered settling model does not apply here, the terminal velocity was incorporated into the cloud height model without correction.

As discussed earlier, the correlation for Njs can be rearranged so that it contains the particle terminal velocity. The best scaling result was obtained by making the maximum fluid velocity at CH ($U_{m,CH}$) dimensionless with $V_{Tip,Njs}$. Figure 7-9 shows the result of this scaling. The data collapses above CH=0.6 within the estimating error of the core velocity.

The data in Figure 7-9 can be reduced to a model in one of two ways. The first method entails averaging the data from z/T=0.6 to the top of the tank, imposing a constant $U_{m,CH}/V_{tip,Njs}$. The second method uses regression analysis to fit a curve from z/T=0.6 to 1.0. The rationale behind this method is the apparent curvature in the data near the top of the tank. This method will predict the cloud height with more accuracy; however, it will be shown later that the two results are statistically equivalent.

Constant Cloud Height Velocity

All of the cloud height velocities above z/T=0.6 were averaged. The resulting value of $U_{m,CH}/V_{tip,Njs}$ was 0.11 with a standard deviation of 0.04 for cloud heights greater than 0.6. The prediction of the required impeller tip speed for a specified cloud height is then achieved using three equations:

$$U_{m,CH} = 0.11\ V_{tip,Njs} \tag{7.13}$$

giving $U_{m,CH}$ for the suspension and geometry in question;

$$0.56\ U_{core} = U_{m,CH}\ CH^{1.15} \tag{7.14}$$

giving U_{core} and U_m for a specified CH and $U_{m,CH}$; and from Equation 7.12

$$V_{tip} = 9.5\ (G/T)^{1.4}\ U_{core} \tag{7.15}$$

where $V_{tip} = \pi ND$.

Equation 7.13 assumes that the dimensionless local maximum velocity at the cloud height is constant above a cloud height of 0.6. Equations 7.14 and 7.15 are taken directly from Equation 7.5 and Figure 7-7. This method is an excellent starting point, although it does not take into account the surface effects above CH=0.95. Based on Equation 7.15 the constant K is estimated to be:

$$K \approx 9.5\,(G/T)^{1.4} \tag{7.16}$$

However, this equation should only be used as an approximation since it may not account for the effects of the solids on the discharge stream and it assumes the discharge stream is composed of straight lines (See Figure 7.6). The accuracy of K can greatly be increased if a single value of N is known for a given cloud height (CH). The solved form of K starts by combining Equations 7.13 and 7.14 to isolate U_{core}:

$$U_{core} = \frac{0.054\pi N_{js} D\, CH^{1.15}}{0.28} \tag{7.17}$$

From this, the rotational speed required for any given cloud height is calculated by substituting in Equation 7.15. Equation 7.15 is used to minimize the potential error of G for scale-up. From this the rotational speed needed for a given cloud height can be determined:

$$N_{CH} = \frac{0.054\,\pi\ N_{Njs} D\, CH^{1.15}}{0.28\,\pi\, D} K \tag{7.18}$$

$$K = \frac{5.2 V_{tip@CH}}{V_{tip,Njs} CH^{1.15}} \tag{7.19}$$

If K is independent of scale and constant for any particular configuration. The value of K calculated in this manner accounts for all possible effects on the discharge of the impeller discharge stream and on the core velocity in the three dimensional wall jets along the baffles of the tank; as well, K will account for any other effects the solids may have on the jet. The K values calculated for configurations for Hicks et al. (1997) data are shown in Table 7-5. This table shows the average K value calculated above a CH of 0.6 the standard deviation and the 99% confidence interval. These values are only valid to calculate CH>0.6.

Cubic Fit of Suspension Velocity

The cloud height velocity as a function of CH was fit to a cubic equation. All of the calculated velocities at z/T=0.6 were averaged, then all of the velocities at z/T=0.65

were averaged and so on. A regression analysis was performed on the resulting data, returning:

$$\frac{U_{m,CH}}{V_{tip,Njs}} = -0.88 + 3.94CH - 5.14CH^2 + 2.20CH^3 \tag{7.20}$$

The R^2 value for the regression analysis is 0.75 and the average standard deviation for each of the points is 0.007. The regression is cubic due to the two changes in direction that occur between z/T=0.6 and z/T=1. The regression analysis is valid only in the range of CH=0.6 to CH=1. The additional effect considered in this model, is the deflection of the jet at the surface

Validation of Cloud Height Velocity Model

The two methods for predicting cloud height are compared with each other and with data from Bujalski et al. (1999) in Figure 7-10. The average difference between the two models is <3%. Either model is sufficient to predict the cloud height. Bujalski et al.'s data fall within a 99% confidence interval of both models, but the slope of the data is closer to the slope of cubic model. This data was not used in development of the model equations, was collected in a different lab, and different solids were used. Bujalski's data does not extend above a CH=0.80, so the models for CH given U_{core} cannot be tested in this region.

Next, experimental values of K were determined using Equation 7.19 and are shown in Table 7-6. Bujalski et al. (1999) maintained the same clearance and impeller diameter throughout the experiments conducted but varied solids concentration and particle diameter. Table 7-6 shows that there is some effect of particle diameter and concentration on K. This indicates that the type of solids and solids concentrations can affect the impeller discharge stream and the core velocity in the wall jet.

7.2.4 Scale-Up of Cloud Height

The final step in model validation is to test the accuracy on scale-up. Scaling was tested using experimental data from Mak (1992). He used tank diameters of 0.6, 1.9 and 2.67m, which were tank diameters three to ten times larger than the scale used for model development. Mak (1992) measured Njs and reported axial concentration profiles from which cloud heights were estimated. Equation 7.20 was used to determine the K values for the various scales Mak (1992) used. If the values of K are constant and independent of scale for each configuration the model can be applied with confidence on scale-up.

Table 7-6 shows the tabulation of K values for three scales used by Mak (1992). The first two columns (D & $V_{tip,Njs}$) compile data directly from Mak's (1992) data, the third and fourth columns (N & CH) are derived from his solids distribution data. The estimated cloud height and corresponding impeller speed were determined from the point at which solids concentration suddenly jumped from zero to a near uniform concentration. The impeller speed at which concentration jumped to uniformity was recorded along with the cloud height. The data has some error since Mak (1992) recorded solids distribution at only five different heights and only two were above 0.6., K remains constant for all of the experimental configurations. We conclude that the cloud height, CH, for an industrially sized stirred tank can be predicted by building a geometrically similar system, measuring CH and Njs in the bench scale, and calculating K (Equation. 7.18). Once Njs is estimated for the larger system(e.g. using the Zweitering correlation, Equation 7.1) , the impeller speed required for a the specified CH can be calculated using Equation 7.18.

Application of the Model

This model can be used either for predicting the cloud height for a given geometry and tip speed or for predicting the tip speed needed to achieve a specified cloud height. First, the particle settling velocity V_T and Njs need to be measured or estimated. Second, the distance the impeller discharge travels before it impinges on the wall is calculated using Equations 7.6 to 7.10. At this point, one must pick an impeller speed and estimate the cloud height or choose a cloud height and calculate the required impeller speed. If the cloud height is specified, the dimensionless cloud height velocity is calculated using Njs and Equation 7.12. Finally, Equation 7.13 is used to determine the impeller tip speed required to suspend solids to the specified cloud height. The prediction of impeller speed is only accurate to within 25% due to the inaccuracies in predicting the core velocity (Figure 7-7).

The model accuracy can be improved significantly if the cloud height is measured at a given impeller speed and Njs is either measured or predicted. Once these variables are known, U_{core} can be recovered from Equations 7.11 and 7.12. Using Equation 7.11, U_m can be calculated since $V_{tip,Njs}$ is known. From this relationship between V_{tip} and U_{core} one can back calculate the value for K from Equation 7.6. Once the constant K is calculated, the cloud height at any rotational speed can be found without resorting to use of Equations 7.6 to 7.10.

7.3 Conclusions and Recommendations

The goal of this research was to predict the position of the solids liquid interface or the cloud height. The prediction of cloud height requires knowledge of the three-dimensional wall jet along the baffle and its rate of decay. Given the local maximum velocities along the wall jet and the suspension properties of the system, the interface height can be predicted. $U_{M,CH}/V_{tip,Njs}$ is constant for dimensionless cloud heights from 0.6 to 0.95. Due to surface effects, the wall jet is deflected and the velocity no longer remains constant above CH=0.95.

To predict cloud height more accurately, better data for the discharge angles and impingement points of the various impellers are needed. The clearance, diameter and blade geometry of the axial impeller all affect the impeller discharge. The application of CFD may help to predict the angles and impingement points and may be useful to predict velocities within the jet. Accurate CFD solutions could improve the prediction of U_{core} (Equation 7.13) and reduce the scatter in Figure 7-7.

The effect of scale-up is included in the Njs calculation. The most accurate method of scale-up is to measure Njs and cloud height at the bench scale. This method eliminates the dependence on G because it is assumed that G/T remains constant upon scale-up in a geometrically similar system. This method eliminates the need to calculate the distance to wall impingement, thus eliminating the variable with the most inaccuracy. Results of this method agree very well with data from Mak (1992).

7.4 Nomenclature

A	wall jet constant
C	impeller clearance (m)
CH	cloud height (z/T)
D	impeller diameter (m)
d_p	particle diameter (m)
G	distance traveled from impeller discharge to wall impingement (m)
g	acceleration due to gravity 9.81(m/s^2)
K	constant
Njs	impeller rotational speed where solids are fully suspended (1/s)
n	jet decay exponent
Po	power number
r	radial distance from the center of the tank (m)
S	Njs constant
T	tank diameter (m)
U_{core}	core velocity of the jet (m/s)
U_m	local maximum jet velocity (m/s)
$U_{m,CH}$	local maximum jet velocity at cloud height (m/s)
V_r	radial velocity (m/s)
V_{slip}	particle slip velocity (m/s)
V_T	particle terminal velocity (m/s)
V_{tip}	impeller tip speed(m/s)
$V_{tip,\,Njs}$	impeller tip speed at Njs (m/s)
V_θ	tangential velocity (m/s)
W	distance from impeller discharge to tank wall in the horizontal plane (m)
X	solids loading
Y	distance the impeller jet has traveled before impingement (m)
x_o	distance to the maximum velocity in the impeller discharge (m)
z	axial distance (m)
α	angle (°)
ϕ	impeller angle (°)
ρ	density (kg/m^3)
ρ_L	liquid density (kg/m^3)

7.5 References

Armenante P.M., E.U. Nagamine and J. Susanto, 1998, Determination of correlations to predict the minimum agitation speed for complete solid suspension in agitated vessels, *Can. J. Chem. Eng.*, **76**, 413-419.

Baldi G., R. Conti and E. Alaria,1978, Complete suspension of particles in mechanically agitated vessels, *Chem. Eng. Sci.*, **33**, 21-25.

Barrisi A. and G. Baldi, 1987, Solid dispersion in an agitated vessel, *Chem. Eng. Sci.*, **42**, 2949-2956.

Bittorf K.J. & S.M. Kresta, 2000, Active Volume of Mean Circulation for Stirred Tanks Agitated with Axial Impellers, *Chem. Eng. Sci.*

Bittorf K.J., and S.M. Kresta, accepted 1999, Wall Jets in Stirred Tanks *AIChE J.*

Bruha, O., I. Fort, and P. Smolka, 1995, Phenomenon of turbulent macroinstabilities in agitated systems, *Collect. Czech. Chem. Commun.* **60**, 85-94.

Bujalski W., K. Takenka, S. Paolini, M. Jahoda, A. Paglianti, K. Takahashi , A.W. Nienow, and A.W. Etchells, 1999, Suspensions and liquid homogenisation in high solids concentration stirred chemical reactors, *Trans I ChemE,* **77**, 241-247.

Gore R.A. and C.T. Crowe, 1989a, Effect of particle size on modulating turbulent intensity: influence of radial location, *Turbulence modification in dispersed multiphase flows,* ed. by Michaelides E.E. and Stock D.E., p. 31-35 ASME, New York

Gore R.A. and C.T. Crowe, 1989b, Effect of particle size on modulating turbulent intensity, *Int. J. Multiphase Flow,* **15**, 279-285.

Grgic B., 1998, *Influence of the impeller and tank geometry on low frequency phenomena and flow stability*. M.Sc. thesis, University of Alberta, Edmonton, Canada.

Hicks M.T., K.J Myers. and A. Bakker, 1997, Cloud height in solids suspension agitation, *Chem. Eng. Comm.* **160**, 137-155.

Kresta S.M., and P.E. Wood, 1993, The mean flow field produced by a 45° pitch blade turbine: changes in the circulation pattern due to off bottom clearance. *Can. J. of Chem. Eng.* **71**, 42-53.

Kresta S.M., 1998, Turbulence in Stirred Tanks: Anisotropic, Approximate and Applied. *Can J. Chem. Eng.* **76**, 563-576.

Larson and Jonsson, 1994, mixing in a 2-layer stably stratified fluid by a turbulent jet, *J. Hydraul. Res.*, **32**, 271-289.

Mak A., 1992, *Solid-liquid mixing in mechanically agitated vessels*. Ph.D. thesis, University College London, London, England.

Myers K.J. and A. Bakker , 1998, Solids suspension with up-pumping pitched-blade and high-efficiency impellers, *Can. J. Chem. Eng.*, **76**, 433-440.

Myers K.J., J.B. Fasano and R.R. Corpstein, 1994, The influence of solids properties on the just-suspended agitation requirements of pitched-blade and high-efficiency impellers, *Can. J. Chem. Eng.*, **72**, 745-748.

Myers K.J., R.W. Ward, A. Bakker, 1997, A digital particle image velocimetry investigation of flow field instabilities of axial flow impellers, *J. Fluids Eng.*, **119**, 623-632.

Nienow A.W., 1968, Suspension of solid particles in turbine agitated baffled vessels, *Chem. Eng. Sci.*, **23**, 1453-1459.

Pantzlaff L. and R.M. Lueptow, 1999, Transient positively and negatively buoyant turbulent round jets, *Exper. in Fluids*, **27**, 117-125.,

Perry and Green, 1984, *Perry's Chemical Engineers' Handbook 6th edition*. McGraw-Hill, San Francisco.

Shamlou P.A. and E. Koutsakos, 1987, Solids suspension and distribution in liquids under turbulent agitation, *Chem. Eng. Sci.* **44**, 529-542.

Swamy N.V. and P. Bandyopadhyay, 1975, Mean and turbulence characteristics of three-dimensional wall jets, *J. Fluid. Mech.* **71**, 541-562.

Takahashi K. and H. Fuhita, 1995, A study of the agitation speed to just cause complete suspension for non-spherical particles, *J. of Chem. Eng. Of Japan*, **28**, 237-240.

Tay M., B. Deutschlander and G. Tatterson, 1984, Suspension characteristics of large cylinders in agitated tanks, *Chem. Eng. Commun.*, **29**, 89-99.

Turner J.S., 1966, Jets and plumes with negative or reversing buoyancy, *J. Fluid Mech.*, **26**, 779-792.

Van't Riet K., and J.M. Smith, 1975, The trailing vortex system produced by Rushton turbine agitators, *Chem. Eng. Sci.*, **30**, 1093-1105.

Zhou G. & S.M. Kresta, 1996, Distribution of energy between convective and turbulent flow for three frequently used impellers, *Trans IChemE*, **74**, 379-389.

Zwietering Th. N., 1958, Suspending of solid particles in liquid by agitators. *Chem. Eng. Sci.*, **8**, 244-253.

Table 7-1: Description of Experimental Conditions

	Hicks et al. (1997)	**Bujalski et al. (1999)**	**Mak (1992)**	**Bittorf and Kresta (1999)**
Liquids	Water and Salt Water	Water	Water	Water and Bayol
Tank Diameter	0.289m		0.6, 1.9 and 2.67m	0.240 and 0.140m
Impellers				
Type	PBT & HE-3	A310	PBT	PBT, HE-3, A310
Size (D/T)	0.15 - 0.53	0.52	0.5	0.19 to 0.44
Clearances (C/T)	0.10 – 0.40	0.25	0.25	0.13 - 0.4
Solid Properties				
Shape	Rectangular, Cylinders, Spheres Granules	Spheres	Spheres	Spheres
Size (μm)	780- 2950	115-678	150-210	300μm
Loading (wt.)	0.1	0.28	0.30	0.24-0.55
Density (kg/m^3)	1053-2590	2500	2630	2550

Table 7-2: Laser Doppler Velocimeter Specifications

Argon Laser	Output power = 300mW Beam separation = 0.0340m. Focal length = 500mm Wave length of light = 514.5nm Bragg cell frequency shift = 40MHz Fringe spacing = 7.6μm
Seeding	In tap water - Naturally occurring 1μm particulate

Table 7-3: Reduction of RMS due to the addition of solids

(r=95mm z=220mm C=60mm)

Solids Concentration (%wt)	Dimensionless RMS (V_{rms}/V_{tip}) for PBT Impeller	Dimensionless RMS (V_{rms}/V_{Tip}) for A310 Impeller
0	0.0845	0.0522
24	0.0240	0.0091
31	0.0193	0.0093
39	0.0181	0.0080
45	0.0173	0.0085
52	0.0158	0.0086

Table 7-4: Measured U_{core} Values

T (mm)	D/T	C/D	Type	Dimensionless Core Velocity (U_{core}/V_{tip})
240	**0.19**	0.80	PBT	0.33
240	**0.19**	1.00	PBT	0.32
240	**0.19**	1.49	PBT	0.29
240	**0.19**	2.00	PBT	0.27
240	**0.19**	3.00	PBT	0.18
240	**0.33**	0.40	PBT	0.32
240	**0.33**	0.60	PBT	0.30
240	**0.33**	0.80	PBT	0.28
240	**0.33**	1.00	PBT	0.27
240	**0.33**	1.50	PBT	0.17
240	**0.50**	0.33	PBT	0.44
240	**0.50**	0.67	PBT	0.33
140	0.43	0.50	PBT	0.32
140	0.43	1.00	PBT	0.22
140	0.32	0.67	PBT	0.25
140	0.32	1.00	PBT	0.23
240	0.58	0.32	**A310**	0.29
240	0.58	0.50	**A310**	0.25
240	0.58	0.68	**A310**	0.22

Table 7-5: K values calculated for Hicks et al. (1997) data.

Experimental Run From Hicks et al. (1997)	Average K	Standard Deviation	99% Confidence Interval
Data from Figure 6 from Hicks et al. (1997)			
D/T=0.154 Njs=1700	8.01	0.42	±0.37
D/T=0.527 Njs=280	5.24	0.61	±0.48
D/T =0.352 Njs=430	7.69	0.54	±0.39
D/T =0.44 Njs=310	6.80	0.26	±0.21
Data from Figure 9 from Hicks et al. (1997)			
C/T=0.1 Njs=410	7.64	0.64	±0.64
C/T=0.4 Njs=470	6.60	0.30	±0.21
Data from Figure 3 from Hicks et al. (1997)			
PBT, Njs=280	7.60	0.09	±0.07
Data from Figure 4 from Hicks et al. (1997)			
V_T=0.0132 Njs=190	7.94	0.26	±0.17
V_T=0.0904 Njs=1040	7.44	0.30	±0.22
V_T=0.00467 Njs=65	7.93	0.49	±0.48
V_T=0.178 Njs=1050	9.88	0.99	±1.13

*NOTE: C/T=0.25, D/T=0.35, V_T=0.0767 and the impeller is an HE3 unless otherwise specified

Table 7-6:K values calculated for Bujalski et al. (1999) data.

Experimental Run From Bujalski et al. (1999)	Average K	Standard Deviation	99% Confidence Interval
Data from Figure 8 from Bujalski et al. (1999)			
X= 28% d_p=115μm	6.37	0.22	±0.25
X= 28% d_p=255μm	6.40	0.14	±0.17
X= 28% d_p=466μm	5.81	0.13	±0.18
X= 28% d_p=678μm	5.00	0.16	±0.23
Data from Figure 7 from Bujalski et al. (1999)			
X= 20% d_p=255μm	5.33	0.02	±0.02
X= 33% d_p=255μm	6.34	0.13	±0.16
X= 40% d_p=255μm	6.23	0.14	±0.22

Table 7-7: K on scale-up for Mak's (1992) data in Appendices A-E

D=T/2	$V_{tip,Njs}$	N (rpm)	CH (z/T) (±0.08)	K (calculated from Eq. 7.19)
1.33	5.01	40	0.66	4.38
1.33	5.01	50	0.83	4.35
0.915	4.00	40	0.66	3.77
0.915	4.00	60	0.83	4.67
0.6	7.07	120	0.66	4.20
0.6	7.07	150	0.83	4.33
			Average K	4.28
			Standard Error of K	0.12

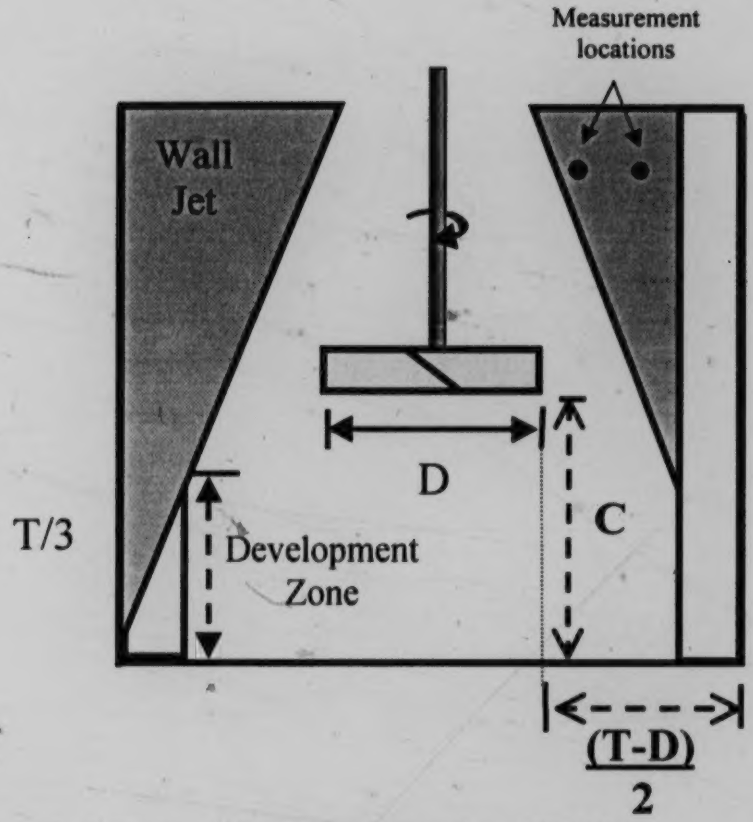
Measurement locations
Wall Jet
D
C
T/3
Development Zone
(T-D)
2

Figure 7 - 1: Tank configuration and Location of Wall Jets

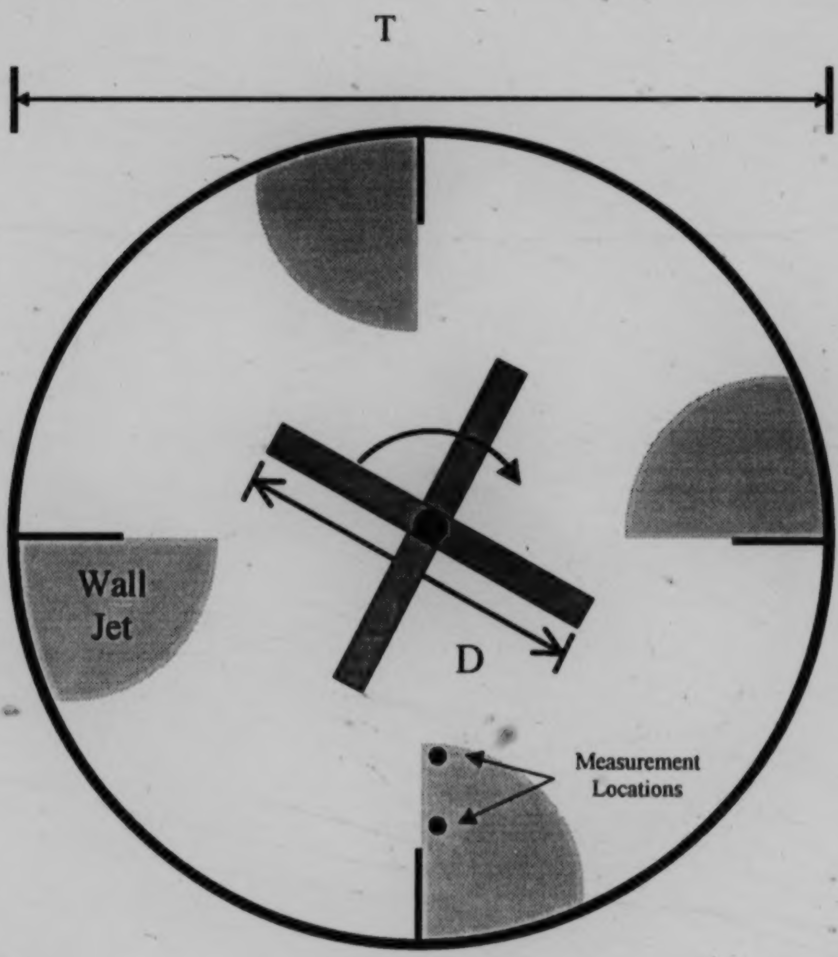
T
Wall Jet
D
Measurement Locations

Figure 7 - 2: Tank cross section at z/T=0.9 showing measurement points for Figures 7-3 and 7-4

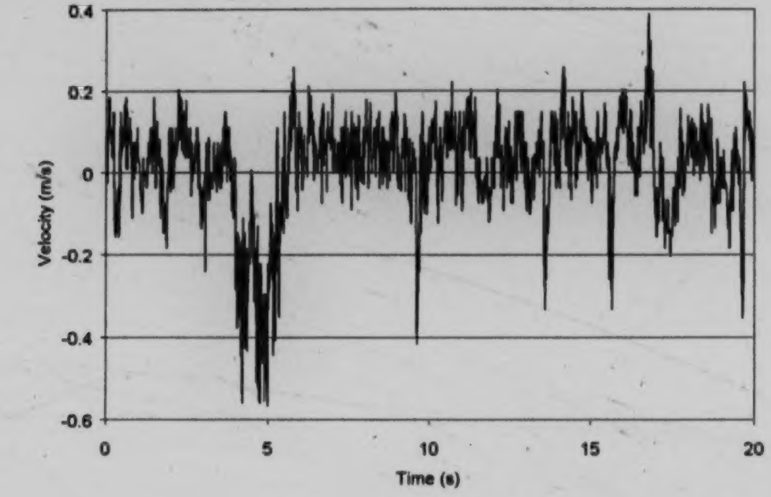

Figure 7 - 3A: Raw time series data for a A310 flow field in clear liquid (z/T=0.9, 2r/D=1.5, C/T=1/6, D/T=0.5, N=530 rpm) Note the intensity of the turbulence and the scale of the macro instability at 5 seconds.

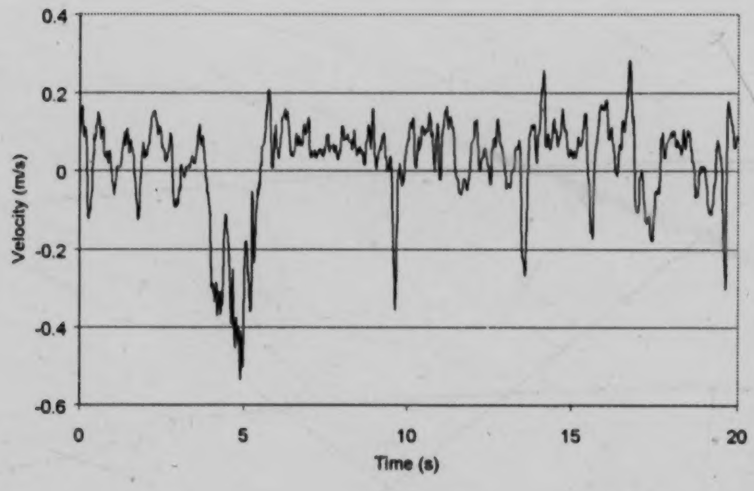

Figure 7 – 3B: Smoothed time series data for a A310 flow field in clear liquid (z/T=0.9, 2r/D=1.5, C/T=1/6, D/T=0.5, N=530rpm)

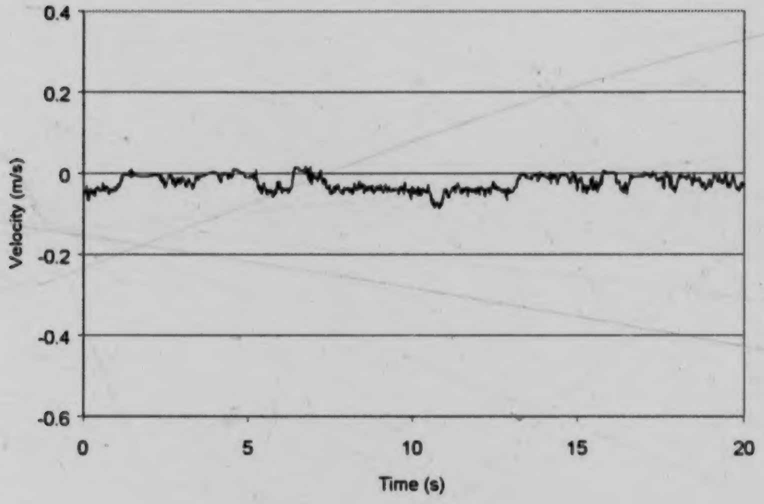

Figure 7 - 3C: Smoothed time series data for an A310 flow field with a solids concentration X=24wt.% and experimental conditions duplicated from Figure 7-3B. Notice the large reduction in turbulent intensity and the absence of macro instabilities.

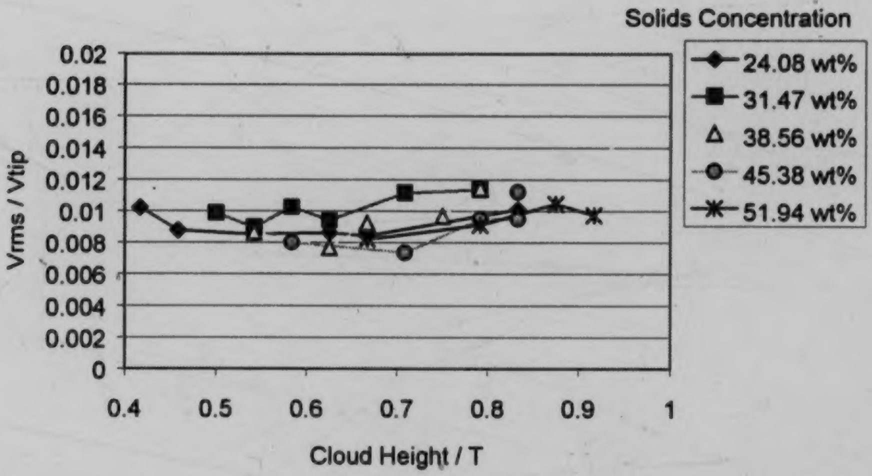

Figure 7 - 4: RMS Velocity as a function of solids cloud height for an A310 impeller. There is no significant difference between the measured RMS velocities at different cloud heights and solids concentrations. (z/T=0.9, 2r/D=1.5, C/T=1/6, D/T=0.5)

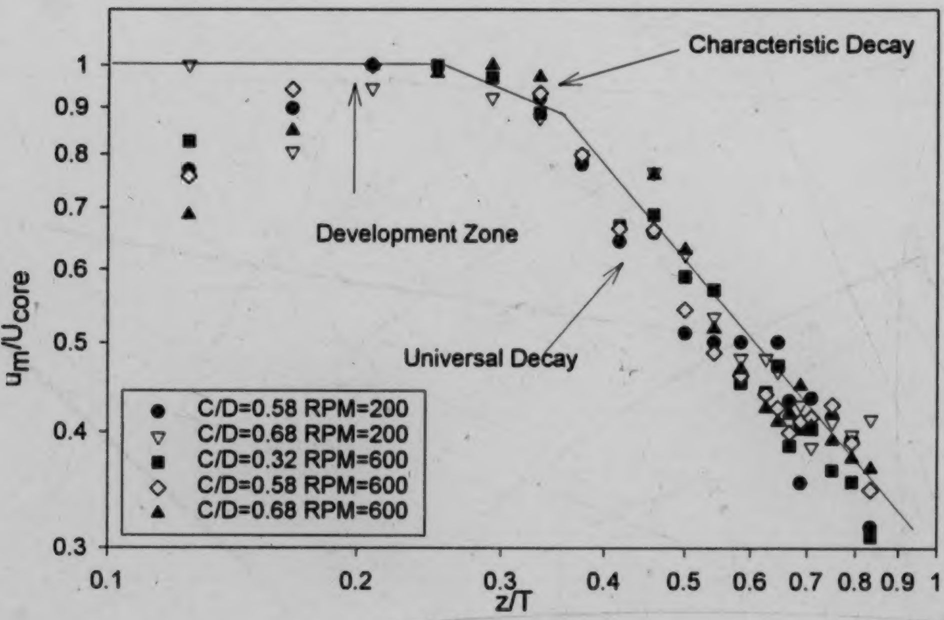

Figure 7 - 5: Decay of maximum velocity for a wall jet produced by an A310 impeller, D/T=0.58, taken from Chapter 4. This decay of maximum velocity is used to predict cloud height

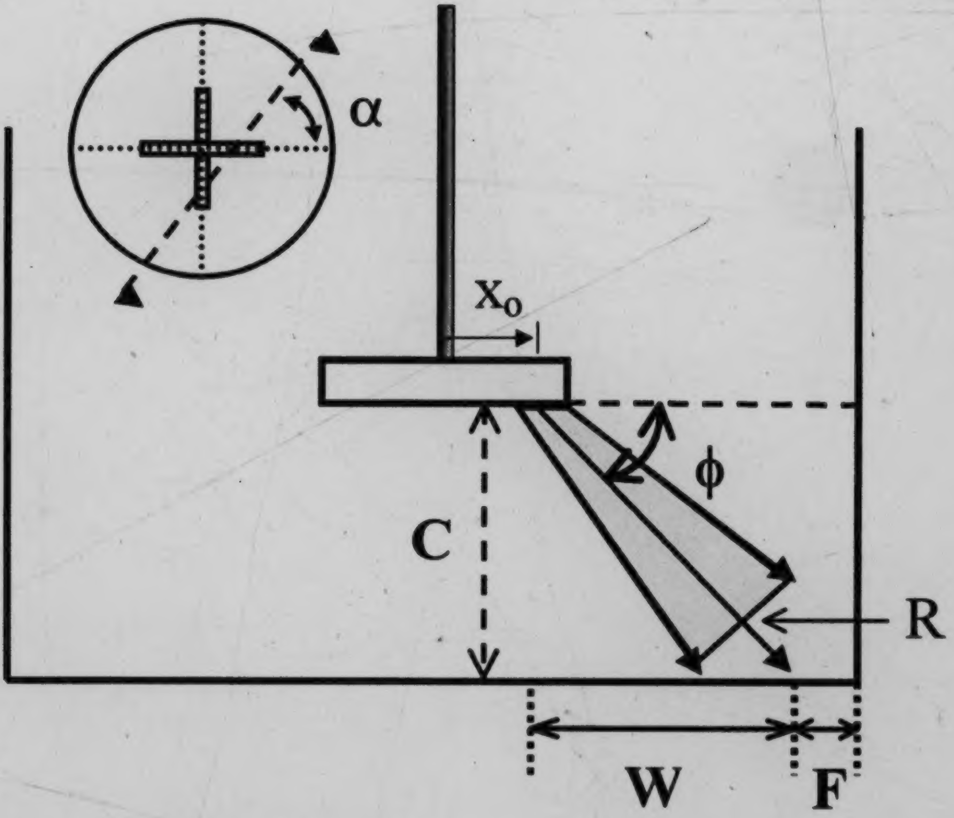

Figure 7 - 6: Direction of the impeller discharge stream assuming an angular discharge. The angle α is the direction of the maximum velocity vector in the horizontal plane.

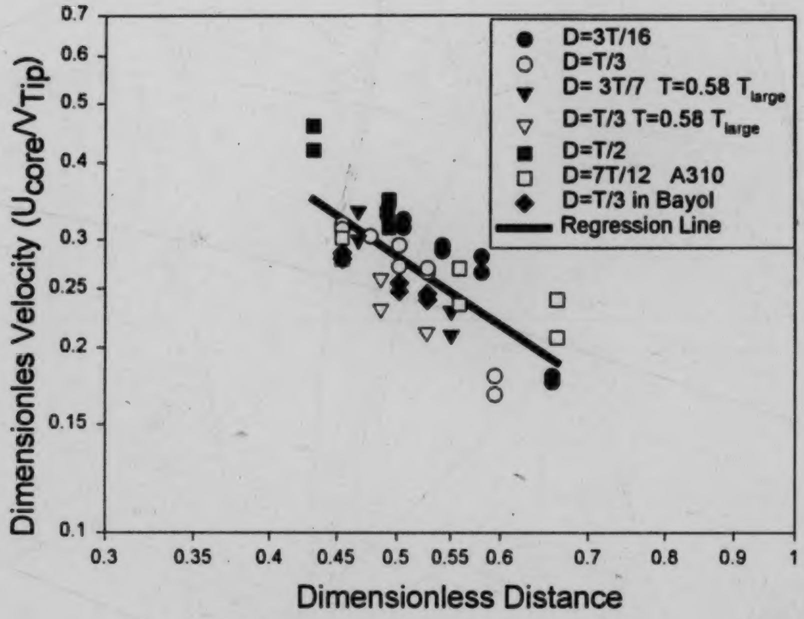

Figure 7 - 7: Prediction of U_{core} using Model 2. Unless otherwise noted the data is for PBT impellers in water for the off-bottom clearances listed in Table 7-1.

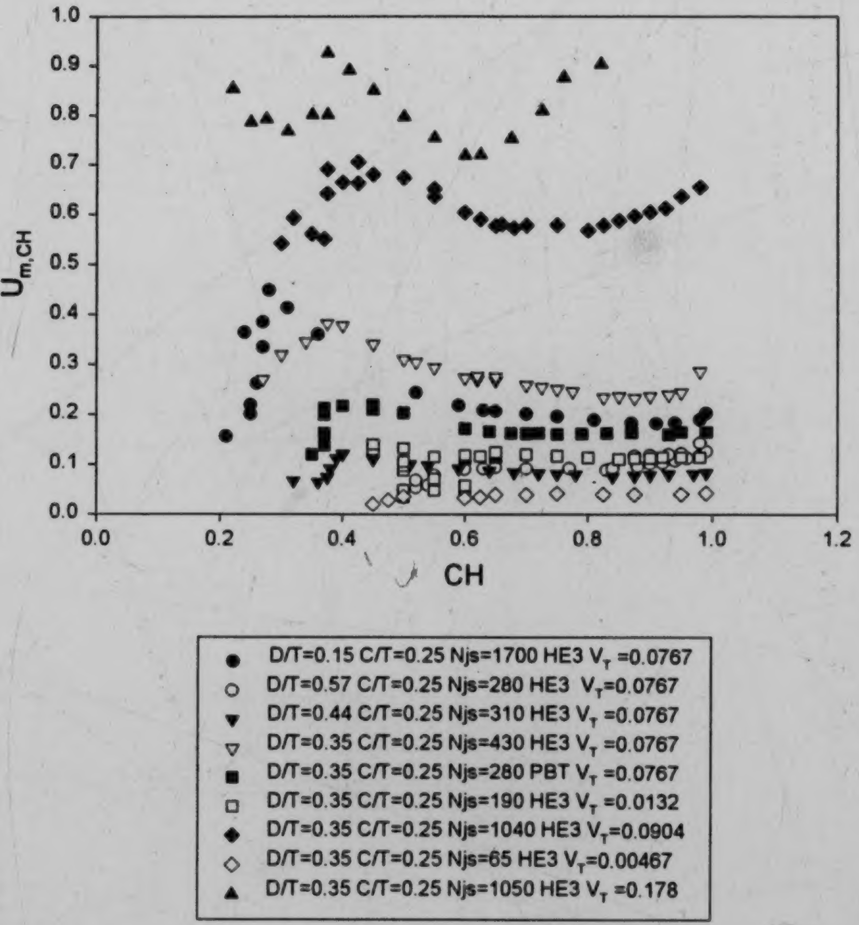

Figure 7 - 8: Local maximum jet velocity at cloud height for nine cases examined by Hicks et al. (1997). The velocities remain constant between a CH=0.6 and CH=0.95. The velocities remain constant between a CH=0.6 and CH=0.95, assuming that the mean fluid velocity is unchanged by the addition of solids.

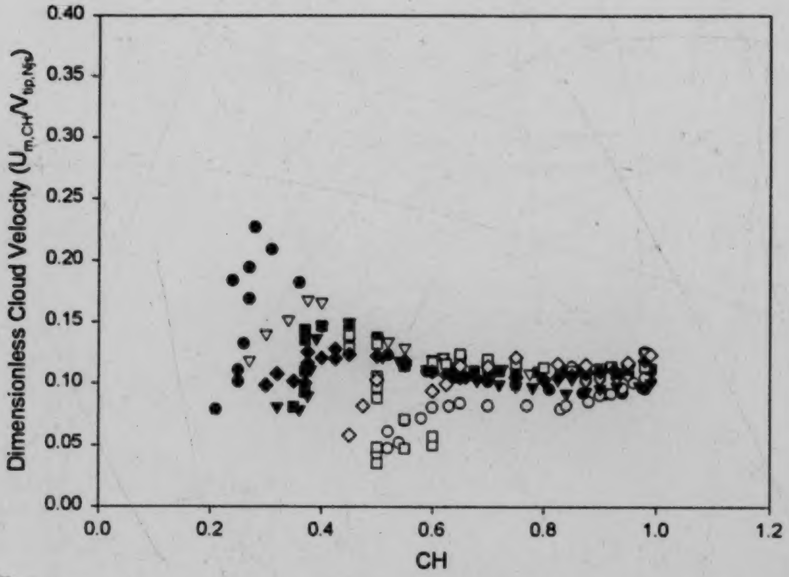

Figure 7 - 9: Velocity st the cloud height made dimensionless with V_{tip} at Njs (see legend in Figure 7-8). The data collapses and remains constant at 0.11 above a cloud height of 0.6.

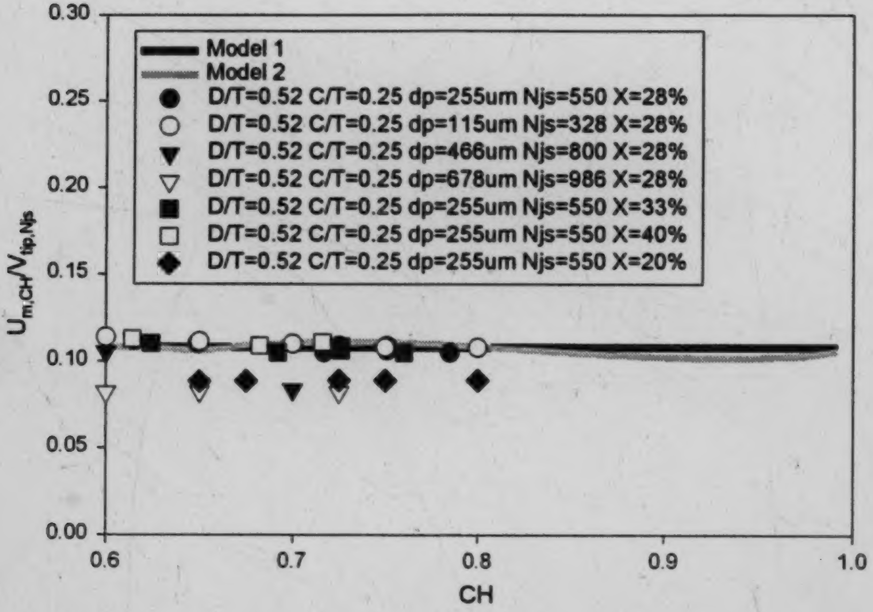

Figure 7 - 10: Validation of the cloud height velocity models using data from Bujalski et al. (1999). (Experiments were completed using a Lightnin A310)

Chapter 8

Conclusions

8.1 Conclusions

The flow field in the bulk of a stirred tank and its application to solids distribution modeling were examined. The following conclusions can be drawn from this study:

- The active height of mean circulation is equivalent to 2/3T, which suggests limits for multiple impeller separation and liquid height, and the core velocity in the jet.
- The discharge angle of the PBT varies depending on the clearance and D/T ratio, this affects the distance to wall impingement.
- The flow in a stirred tank can be modeled as a series of jets: swirling jets from the impeller discharge and wall jets along the tank walls.
- The upward flow along the wall of the tank for an axial impeller can be modeled as a three-dimensional wall jet along two walls. The decay of the local maximum velocity is inversely proportional to the distance traveled and the jet expands linearly: $U_m \propto (z/T)^{-1.15}$; $b \propto x$
- The upward flow and downward flow along the wall of the tank for a radial impeller can be modeled as an axi-symmetric annular wall jet. The decay of the local maximum velocity is inversely proportional to the distance traveled and the jet expands linearly: $U_m \propto (z/T)^{-0.5}$; $b \propto x$

- Turbulence in the impeller region does not guarantee fully turbulent flow throughout the bulk of the tank; however, there is a linear relationship between the impeller Reynolds number and the dimensionless turbulent height, z/T:
  $z/T = 4.23 \times 10^{-6}\,Re + 0.377$

- Macro-instabilities are not a factor in suspending solids at high concentrations; hence the suspension driving force is the wall jet. The damping of the macro instabilities also helps produce a clear liquid interface that does not appear at lower concentrations.

- Solids cloud height at high solids concentrations can be predicted based on a mean flow model using the properties of the three-dimensional wall jet along the baffle of the tank. The local maximum velocity of the wall jet remains constant at any cloud height above z/T=0.6 for all experimental configurations and solids examined.

Appendix A

Additional Data Supporting Chapter 6

Profiles for a PBT Impeller (D/T=0.33 C/D=1.0)

Legend for PBT, D/T=0.33 C/D=1.0

	Symbol	Re	Fluid
Profile 1	●	**1.7×10^5**	**Water**
Profile 2	○	**1.0×10^5**	**Water**
Profile 3	▼	**6.6×10^4**	**Bayol**
Profile 4	▽	**6.4×10^4**	**Bayol**
Profile 5	■	**3.0×10^4**	**T.G. and Water**
Profile 6	□	**2.0×10^4**	**Bayol**
Profile 7	◆	**2.0×10^4**	**Water**
Wall Jet Profile	—		

Note: The legend for each set of figures is located at the figure title page.

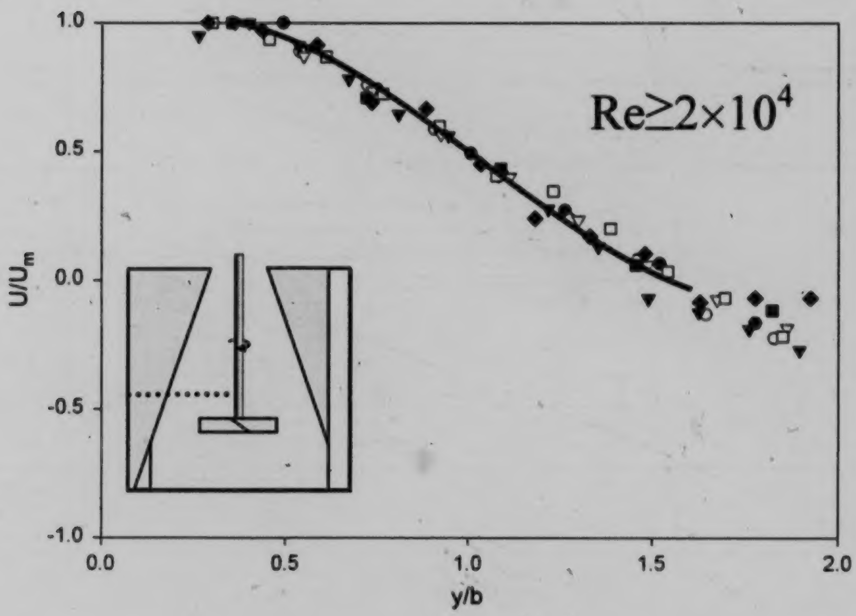

Figure A - 1: Fully Turbulent Profile at z/T=0.46 for a PBT C/D=0.5 D/T=0.33

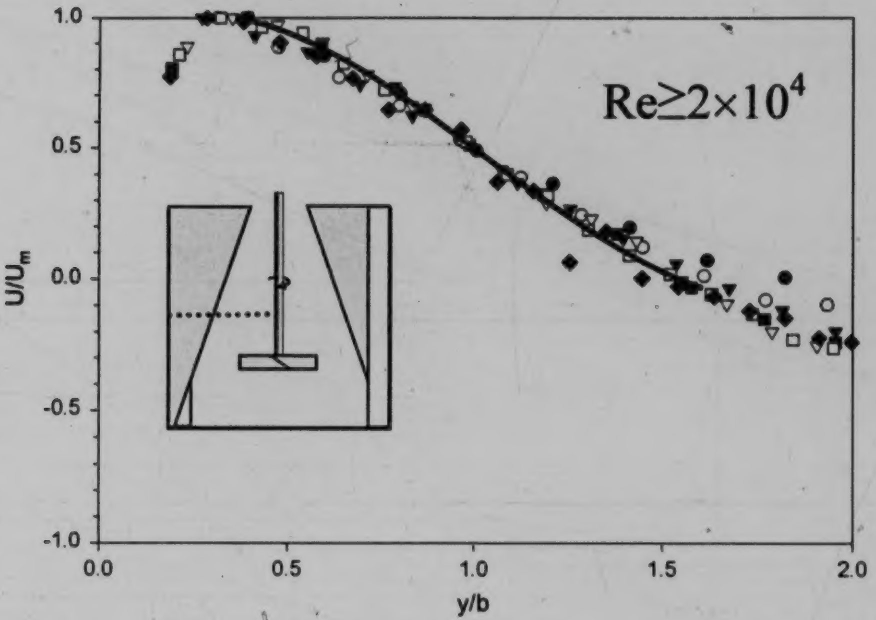

Figure A - 2: Fully Turbulent Profile at z/T=0.58 for a PBT C/D=0.5 D/T=0.33

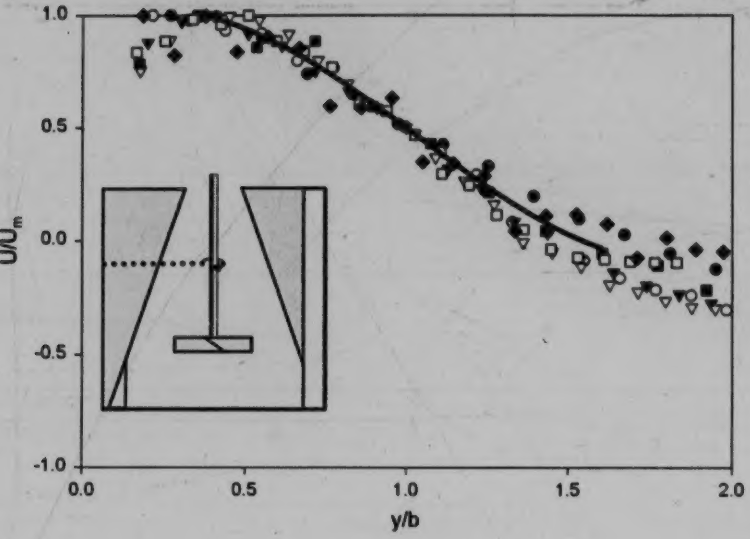

Figure A - 3: Velocity Profile at z/T=0.71 for a PBT C/D=0.5 D/T=0.33

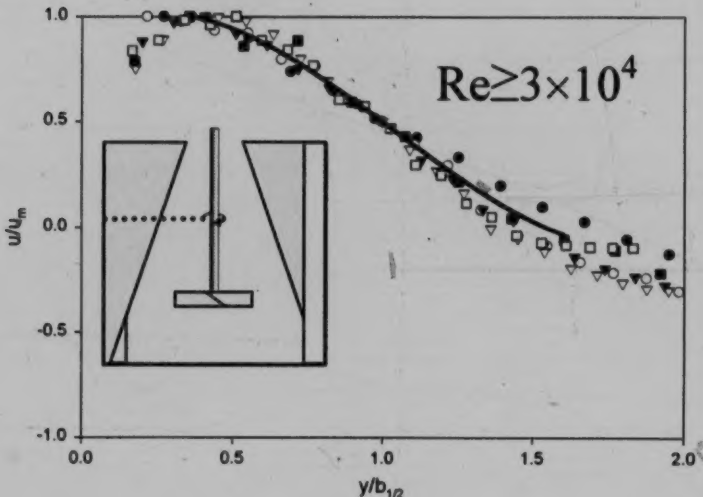

Figure A - 4: Fully Turbulent Profile at z/T=0.71 for a PBT C/D=0.5 D/T=0.33 (Profiles 6 & 7 eliminated)

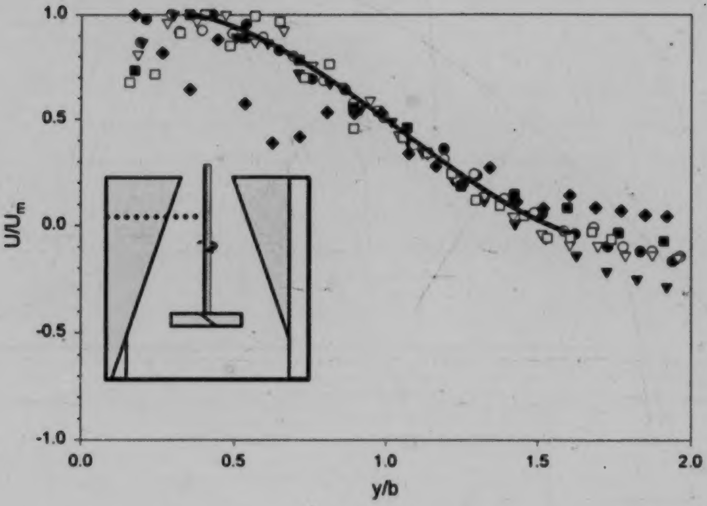

Figure A - 5: Velocity Profile at z/T=0.83 for a PBT C/D=0.5 D/T=0.33

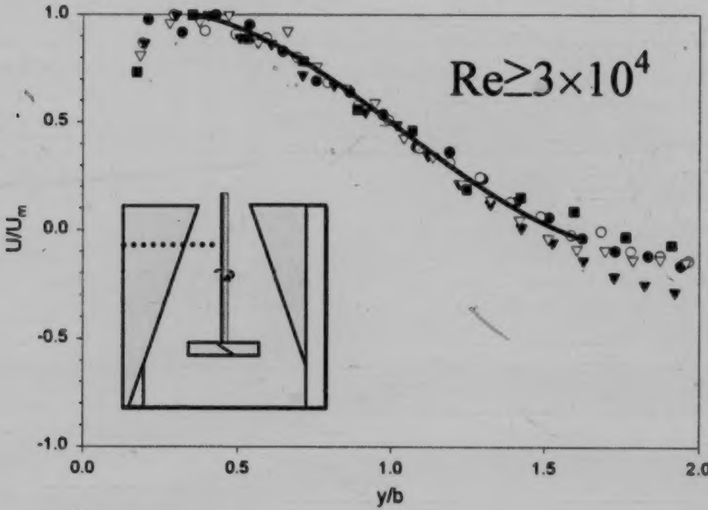

Figure A - 6: Fully Turbulent Profile at z/T=0.83 for a PBT C/D=0.5 D/T=0.33 (Profiles 6 & 7 eliminated)

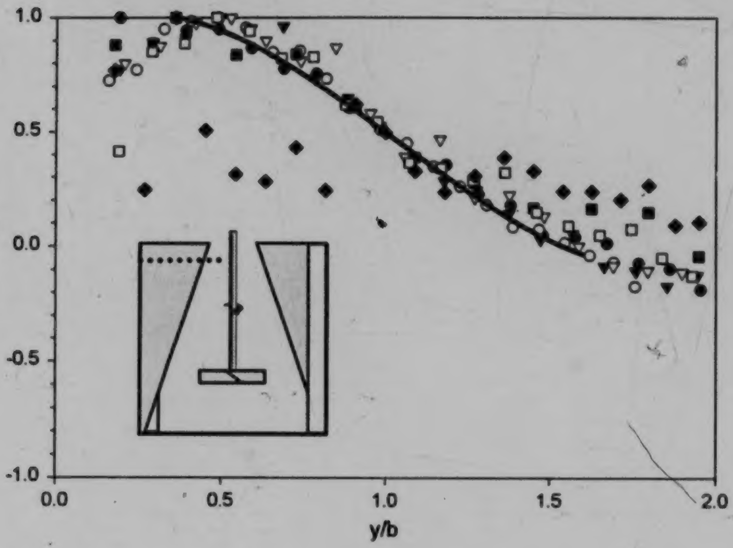

Figure A - 7: Velocity Profile at z/T=0.92 for a PBT C/D=1 D/T=0.33

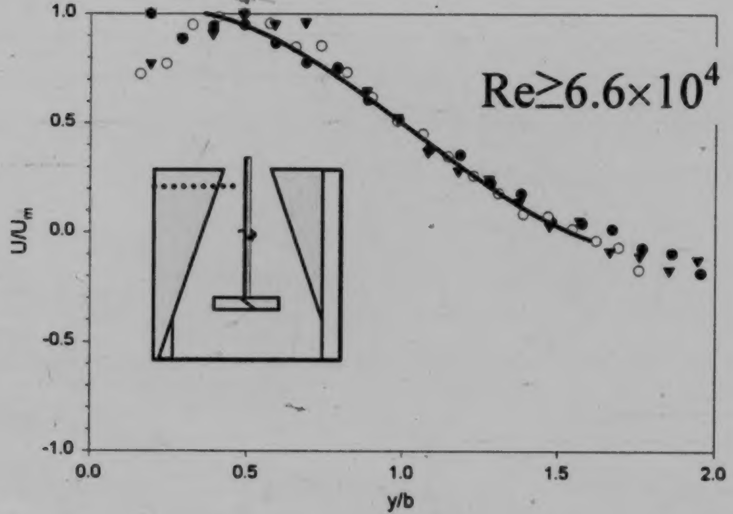

Figure A - 8: Fully Turbulent Profile at z/T=0.92 for a PBT C/D=1 D/T=0.33 (Profiles 4, 5, 6 & 7 eliminated)

Profiles for an A310 Impeller (D/T=0.5 C/D=0.67)

Legend for A310, D/T=0.5 C/D=0.67

	Symbol	Re	Fluid
Profile 1	●	**3.1×10^5**	**Water**
Profile 2	○	**1.2×10^5**	**Bayol**
Profile 3	▼	**1.0×10^5**	**Bayol**
Profile 4	▽	**1.0×10^5**	**Water**
Profile 5	■	**3.7×10^4**	**T.G. and Water**
Profile 6	□	**2.0×10^4**	**T.G. and Water**
Profile 7	◆	**2.0×10^4**	**Water**
Profile 8	◇	**2.0×10^4**	**Bayol**
Wall Jet Profile	—		

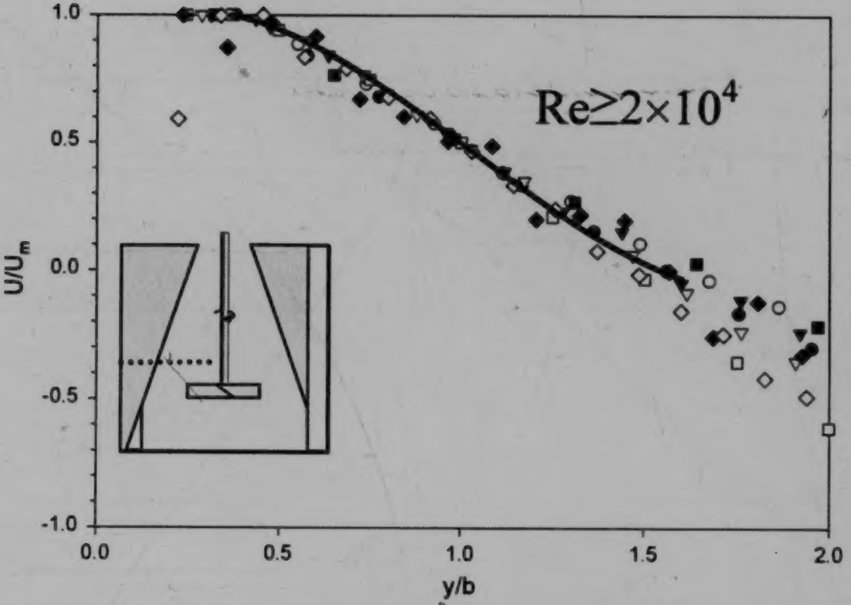

Figure A - 9: Fully Turbulent Profile at z/T=0.46 for a A310 C/D=0.67 D/T=0.5

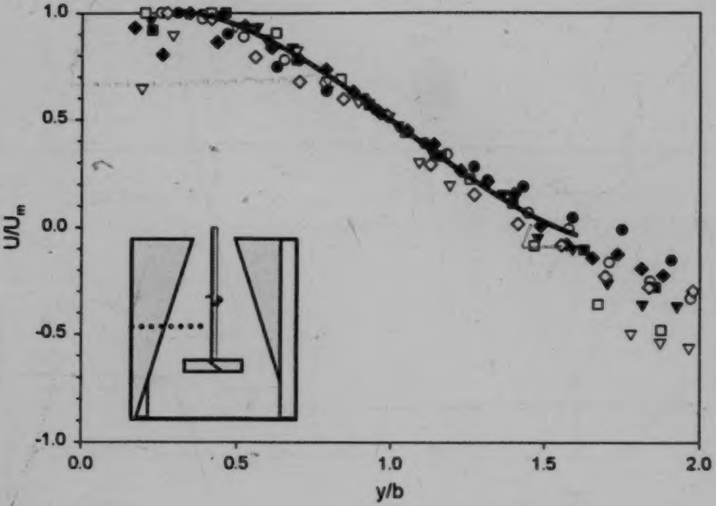

Figure A - 10: Velocity Profile at z/T=0.58 for a A310 C/D=0.67 D/T=0.5

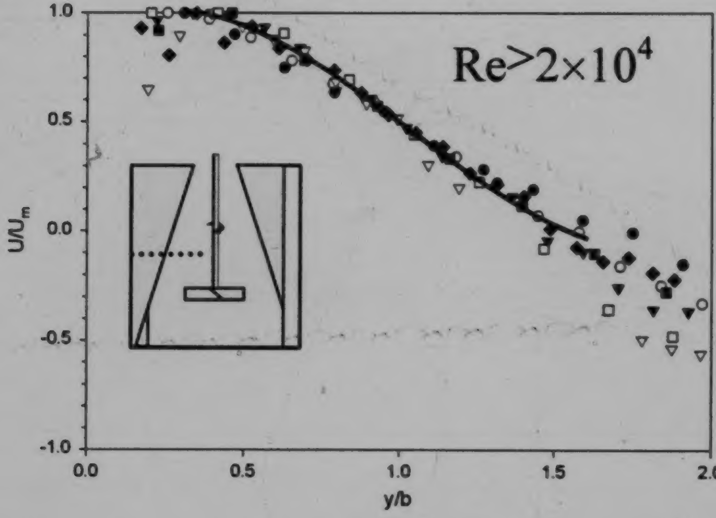

Figure A - 11: Fully Turbulent Profile at z/T=0.58 for a A310 C/D=0.67 D/T=0.5 (Profile 8 eliminated)

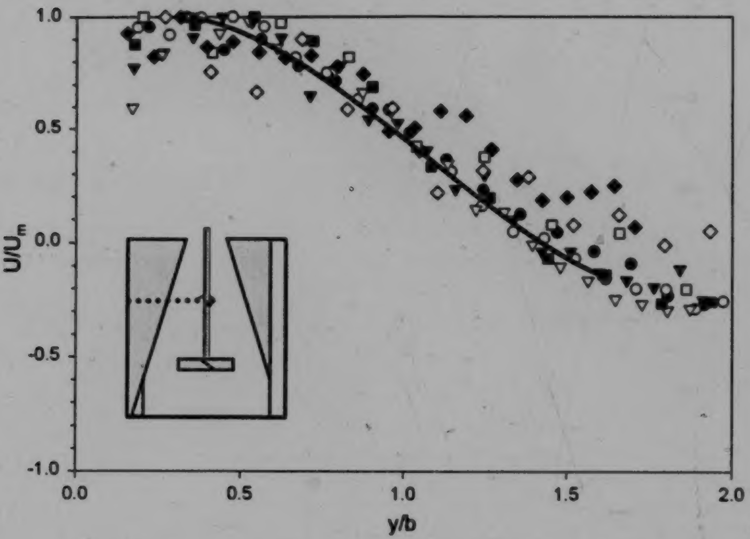

Figure A - 12: Velocity Profile at z/T=0.71 for a A310 C/D=0.67 D/T=0.5

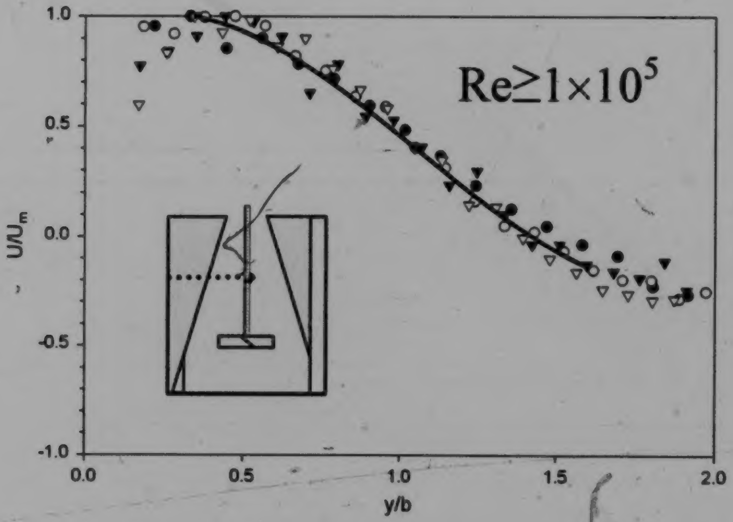

Figure A - 13: Fully Turbulent Profile at z/T=0.71 for a A310 C/D=0.67 D/T=0.5
(Profiles 5, 6, 7 & 8 eliminated)

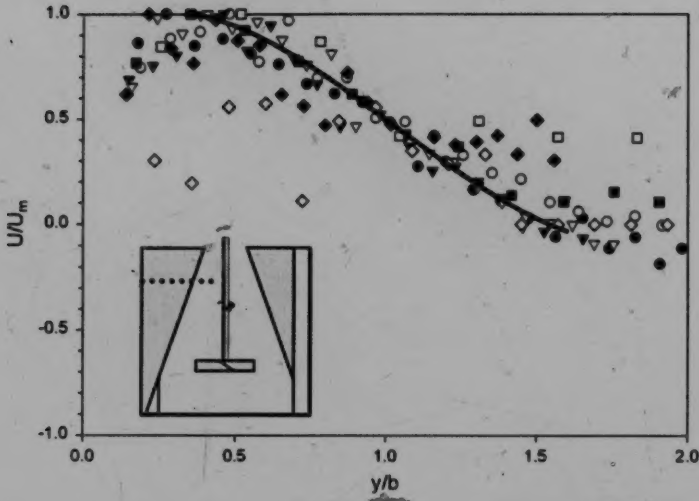

Figure A - 14: Velocity Profile at z/T=0.83 for a A310 C/D=0.67 D/T=0.5

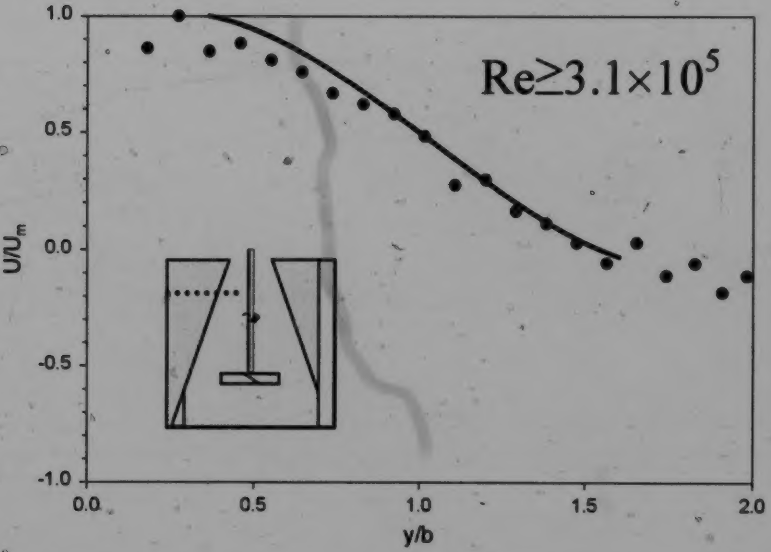

Figure A - 15: Fully Turbulent Profile at z/T=0.83 for a A310 C/D=0.67 D/T=0.5 (Profiles 2, 3, 4, 5, 6, 7 & 8 eliminated)

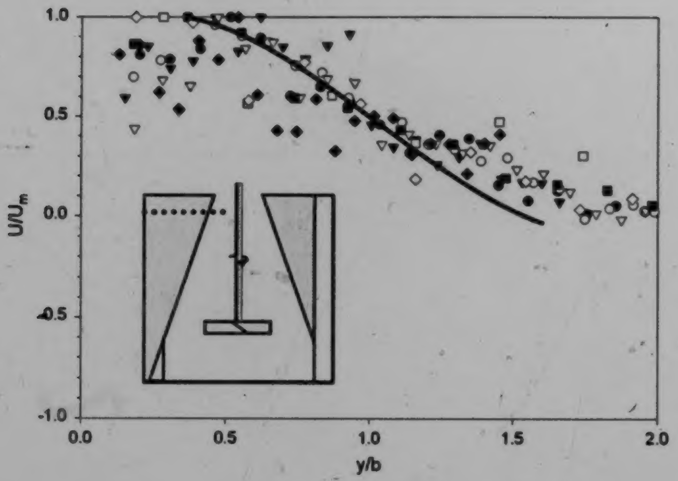

Figure A - 16: Velocity Profile at z/T=0.92 for a A310 C/D=0.67 D/T=0.5

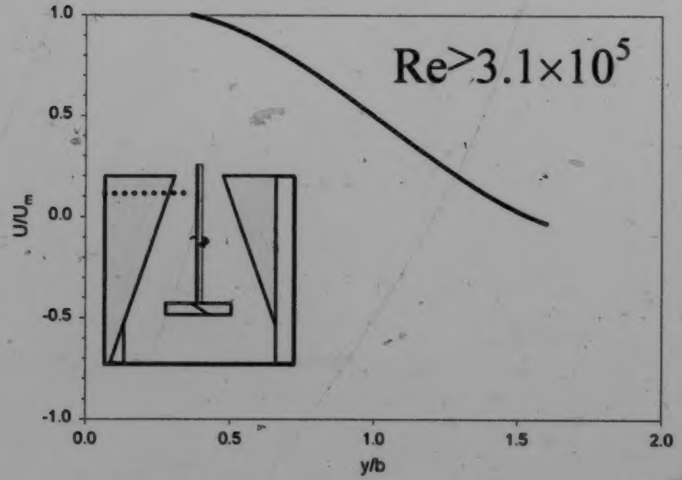

Figure A - 17: Fully Turbulent Profile at z/T=0.92 for a A310 C/D=0.67 D/T=0.5
(Profiles 1, 2, 3, 4, 5, 6, 7, 8 eliminated)

Profiles for an PBT Impeller
(D/T=0.5 C/D=0.50)

Legend for PBT, D/T=0.5 C/D=0.5

	Symbol	Re	Fluid
Profile 1	●	**1.6×10^5**	**Water**
Profile 2	○	**5.6×10^4**	**Bayol**
Profile 3	▼	**1.0×10^5**	**Water**
Profile 4	▽	**2.0×10^4**	**Bayol**
Profile 5	■	**2.0×10^4**	**Water**
Wall Jet Profile	—		

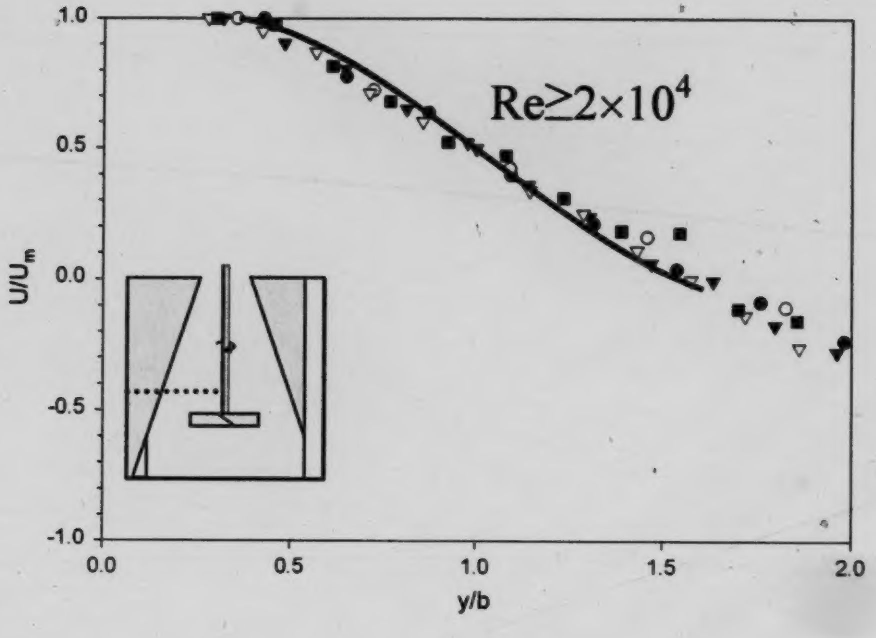

Figure A - 18: Fully Turbulent Profile at z/T=0.46 for a PBT C/D=0.5 D/T=0.5

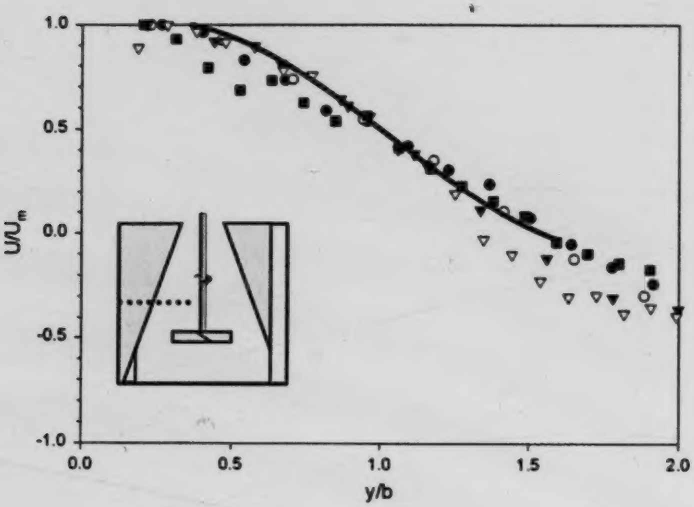

Figure A - 19: Velocity Profile at z/T=0.58 for a PBT C/D=0.5 D/T=0.5

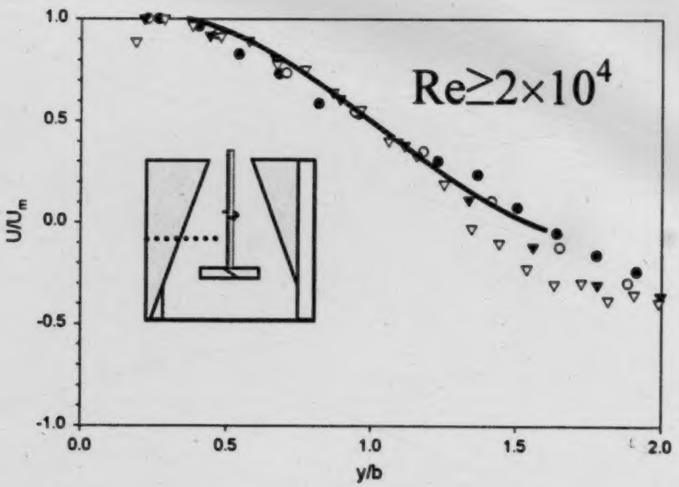

Figure A - 20: Fully Turbulent Profile at z/T=0.58 for a PBT C/D=0.5 D/T=0.5 (Profile 5 eliminated)

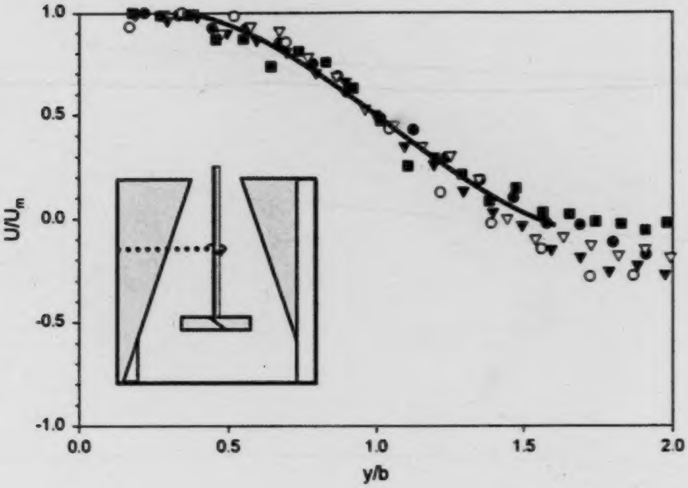

Figure A - 21: Velocity Profile at z/T=0.71 for a PBT C/D=0.5 D/T=0.5

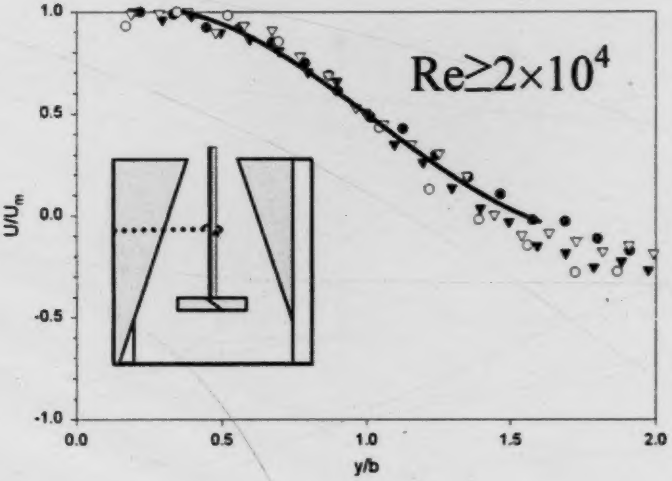

Figure A - 22: Fully Turbulent Profile at z/T=0.71 for a PBT C/D=0.5 D/T=0.5 (Profile 5 eliminated)

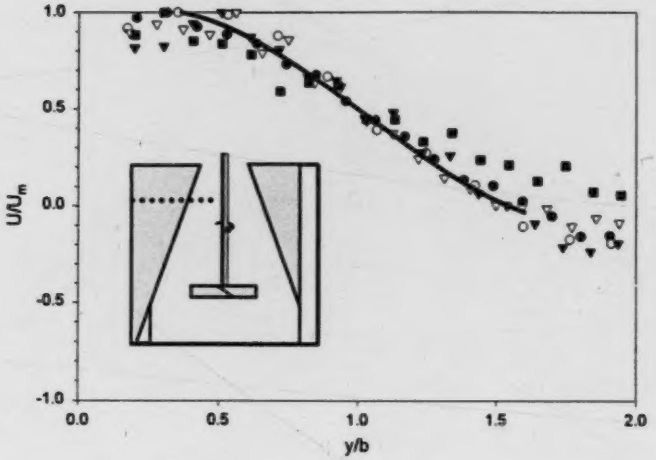

Figure A - 23: Velocity Profile at z/T=0.83 for a PBT C/D=0.5 D/T=0.5

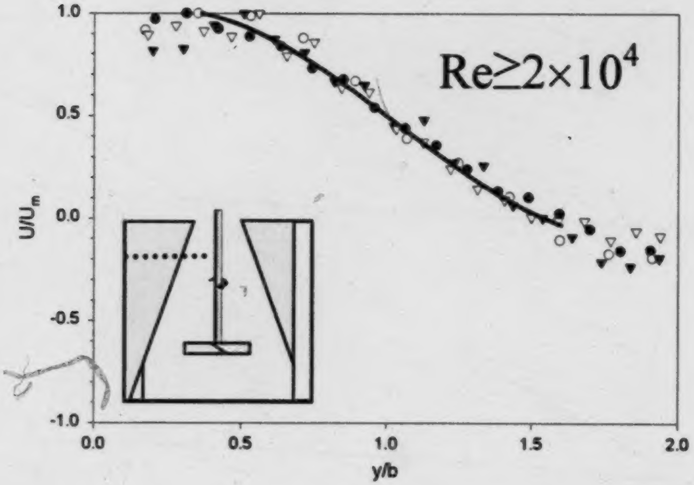

Figure A - 24: Fully Turbulent Profile at z/T=0.83 for a PBT C/D=0.5 D/T=0.5 (Profile 5 eliminated)

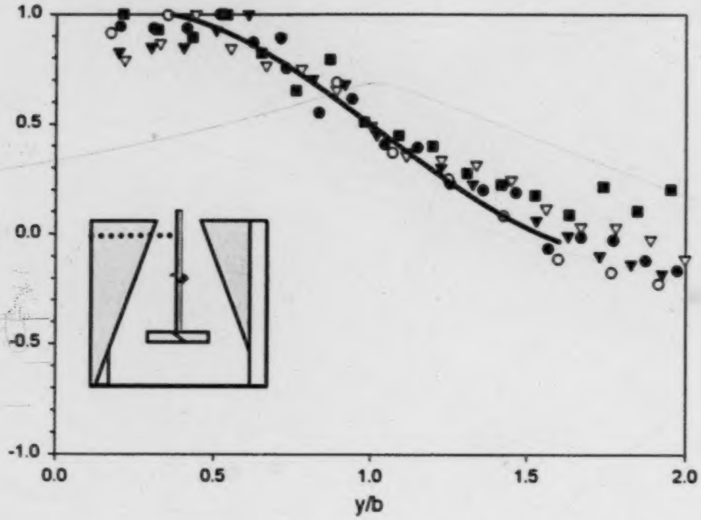

Figure A - 25: Velocity Profile at z/T=0.92 for a PBT C/D=0.5 D/T=0.5

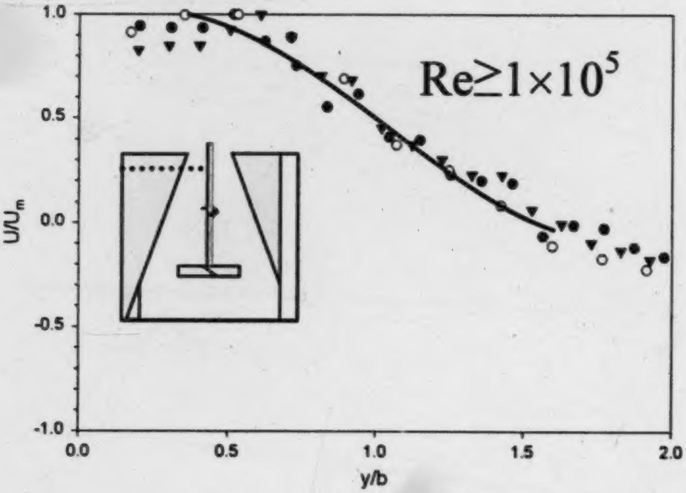

Figure A - 26: Fully Turbulent Profile at z/T=0.92 for a PBT C/D=0.5 D/T=0.5 (Profiles 4 & 5 eliminated)

Profiles for a PBT Impeller
(D/T=0.5 C/D=0.67)

Legend for PBT, D/T=0.5 C/D=0.67

	Symbol	Re	Fluid
Profile 1	●	**1.6×10^5**	**Water**
Profile 2	○	**5.6×10^4**	**Bayol**
Profile 3	▼	**1.0×10^5**	**Water**
Profile 4	▽	**2.0×10^4**	**Bayol**
Profile 5	■	**2.0×10^4**	**Water**
Wall Jet Profile	—		

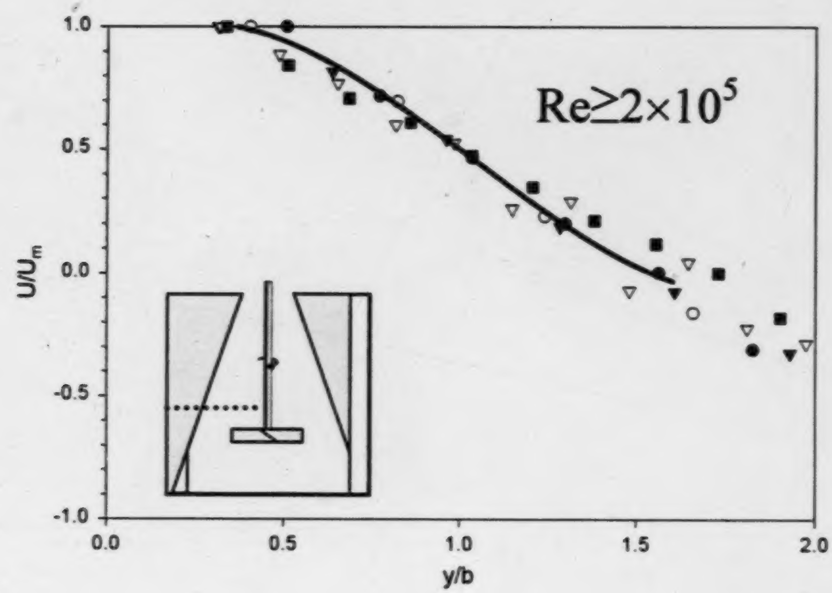

Figure A - 27: Fully Turbulent Profile at z/T=0.46 for a PBT C/D=0.67 D/T=0.5

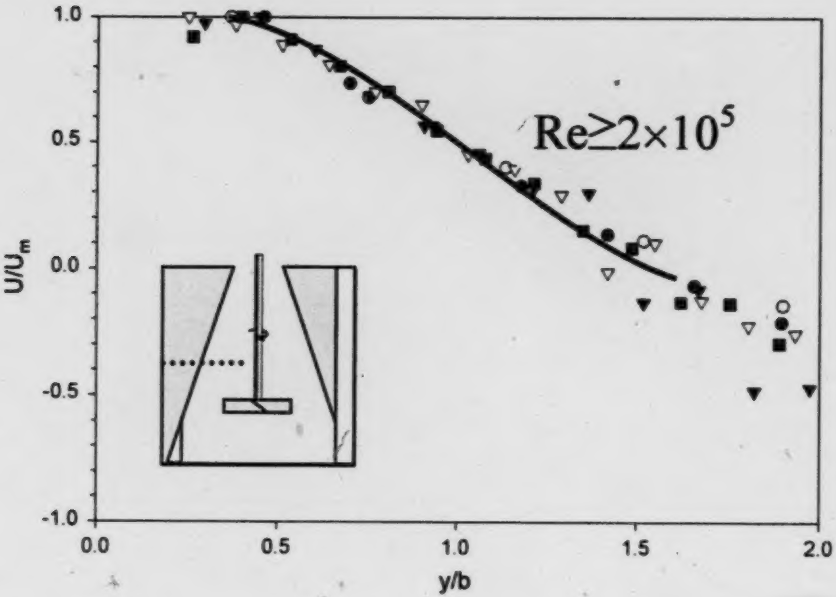

Figure A - 28: Fully Turbulent Profile at z/T=0.58 for a PBT C/D=0.67 D/T=0.5

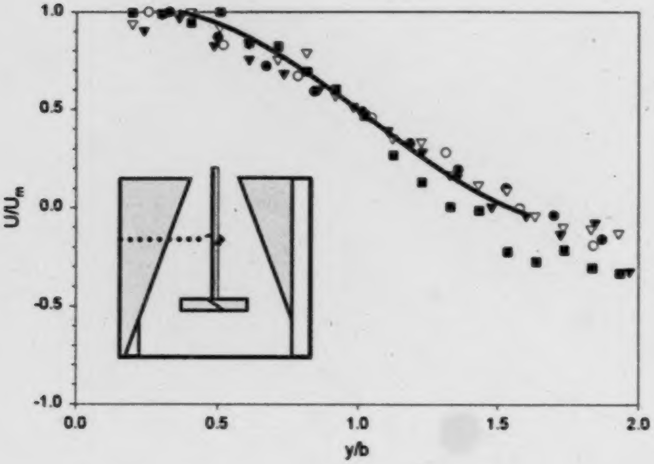

Figure A - 29: Velocity Profile at z/T=0.71 for a PBT C/D=0.67 D/T=0.5

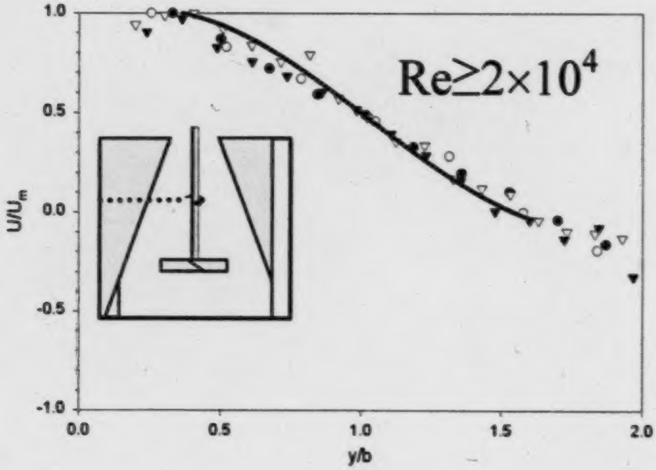

Figure A - 30: Fully Turbulent Profile at z/T=0.71 for a PBT C/D=0.67 D/T=0.5 (Profile 5 eliminated)

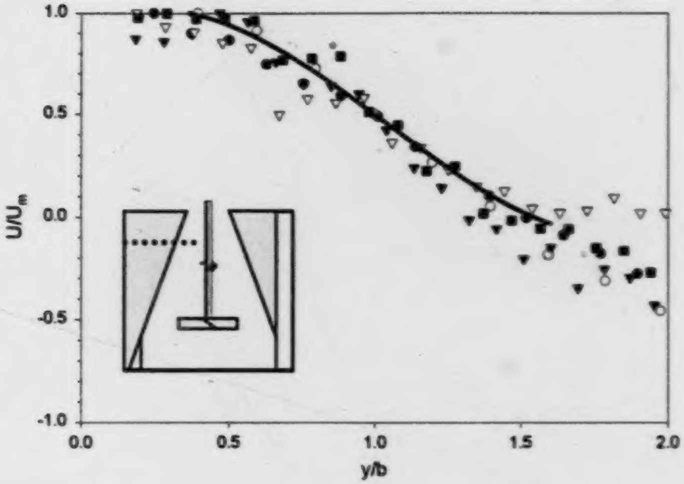

Figure A - 31: Velocity Profile at z/T=0.83 for a PBT C/D=0.67 D/T=0.5

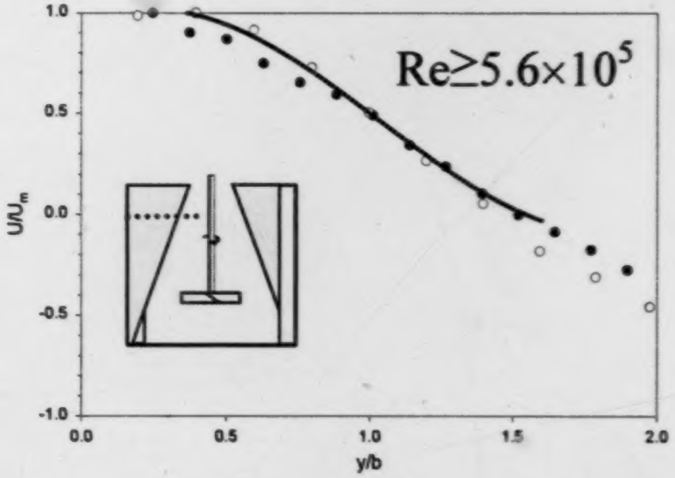

Figure A - 32: Fully Turbulent Profile at z/T=0.83 for a PBT C/D=0.67 D/T=0.5
(Profiles 3, 4 & 5 eliminated)

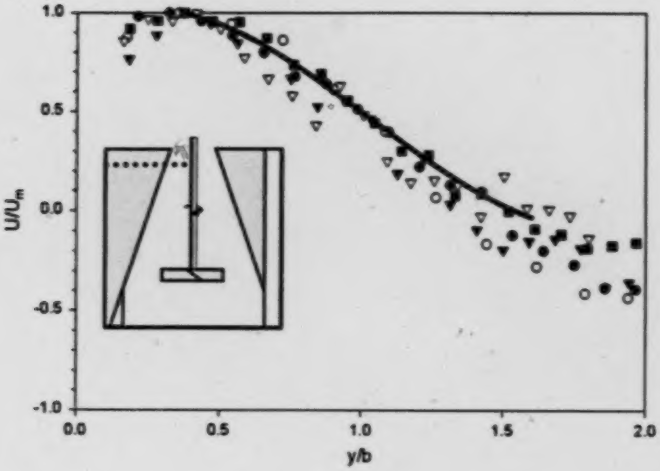

Figure A - 33: Velocity Profile at z/T=0.92 for a PBT C/D=0.67 D/T=0.5

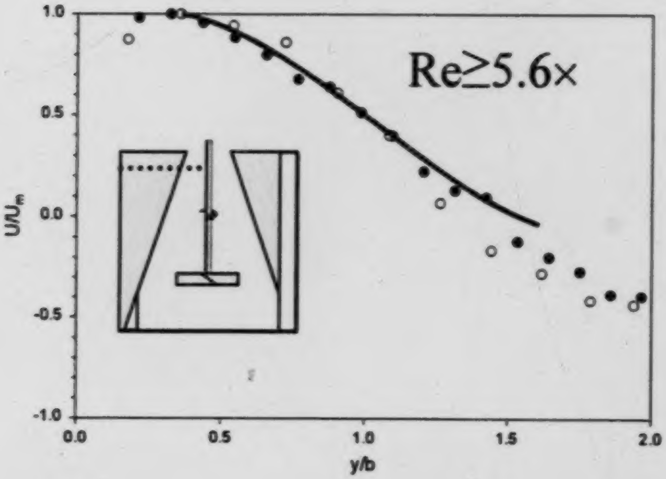

Figure A - 34: Fully Turbulent Profile at z/T=0.92 for a PBT C/D=0.67 D/T=0.5
(Profiles 3, 4 & 5 eliminated)

Profiles for an A310 Impeller
(D/T=0.33 C/D=0.50)

Legend for A310, D/T=0.33 C/D=0.5

	Symbol	Re	Fluid
Profile 1	●	2.9×10^5	**Water**
Profile 2	○	1.0×10^5	**Water**
Profile 3	▼	9.8×10^4	**Bayol**
Profile 4	▽	4.5×10^4	**T.G. and Water**
Profile 5	■	2.0×10^4	**Bayol**
Profile 6	□	2.7×10^4	**T.G. and Water**
Profile 7	◆	2.0×10^4	**Water**
Wall Jet Profile	—		

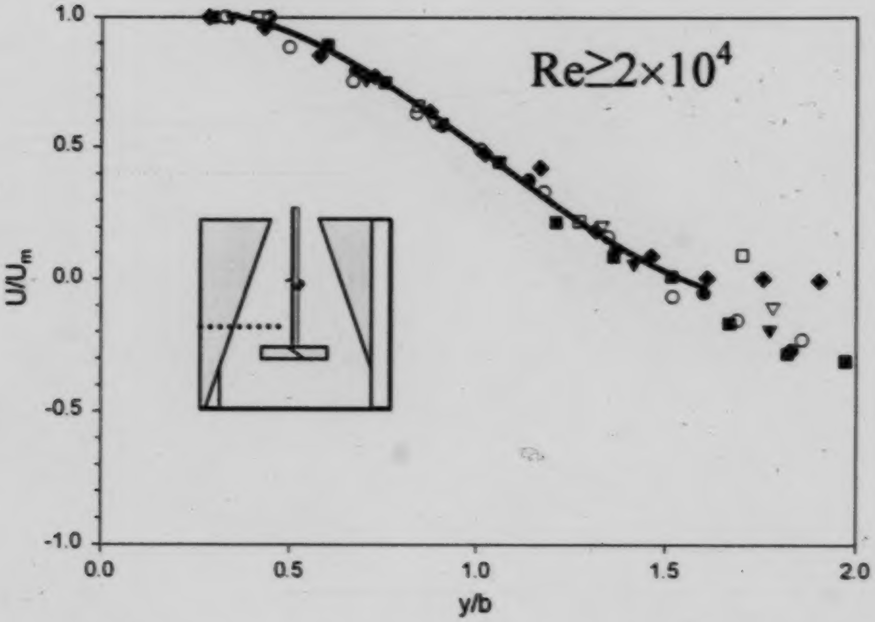

Figure A - 35: Fully Turbulent Profile at z/T=0.58 for a A310 C/D=0.5 D/T=0.33

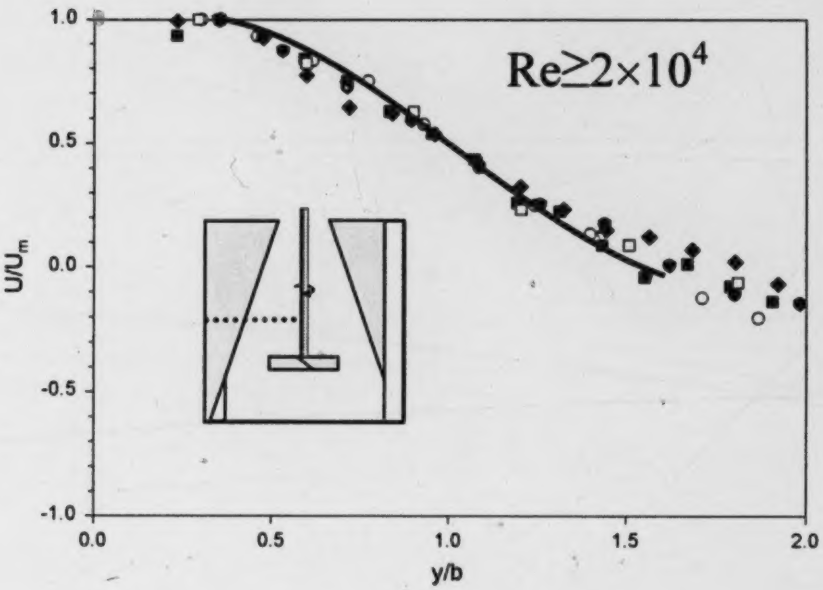

Figure A - 36: Fully Turbulent Profile at z/T=0.58 for a A310 C/D=0.5 D/T=0.33

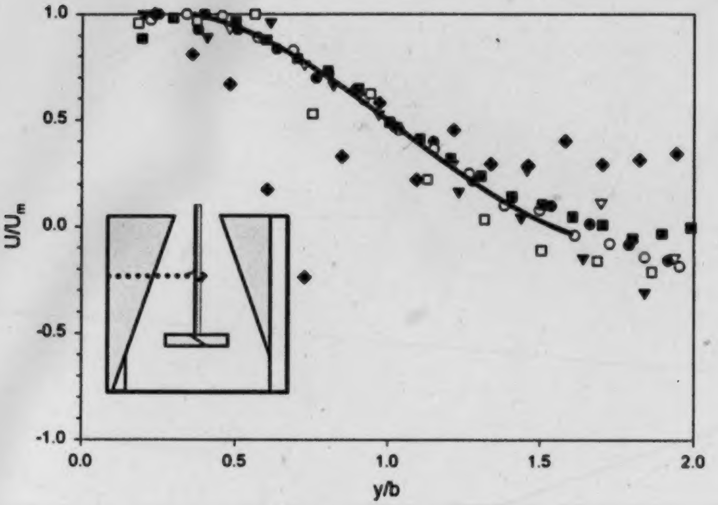

Figure A - 37: Velocity Profile at z/T=0.71 for a A310 C/D=0.5 D/T=0.33

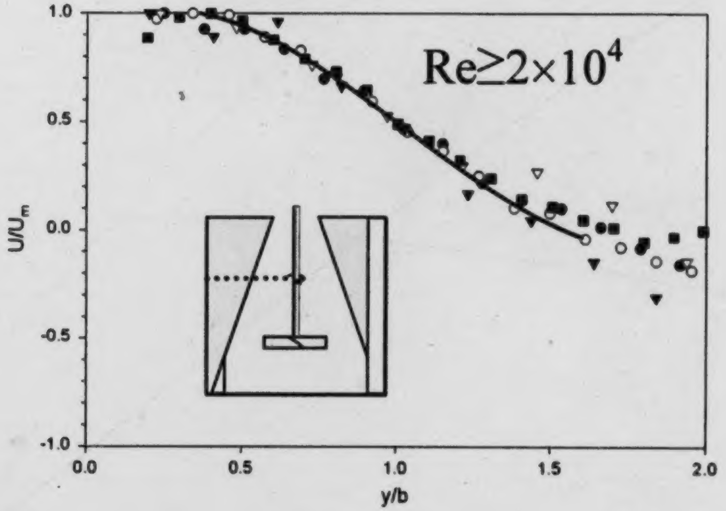

Figure A - 38: Fully Turbulent Profile at z/T=0.71 for a A310 C/D=0.5 D/T=0.33
(Profiles 6 & 7 eliminated)

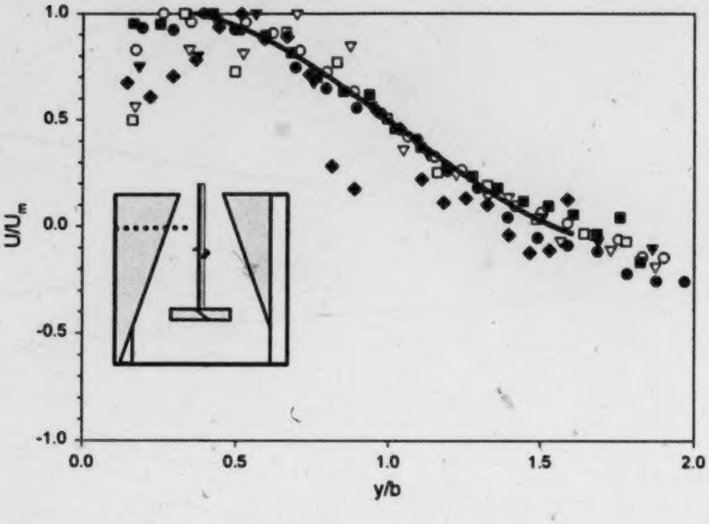

Figure A - 39: Velocity Profile at z/T=0.83 for a A310 C/D=0.5 D/T=0.33

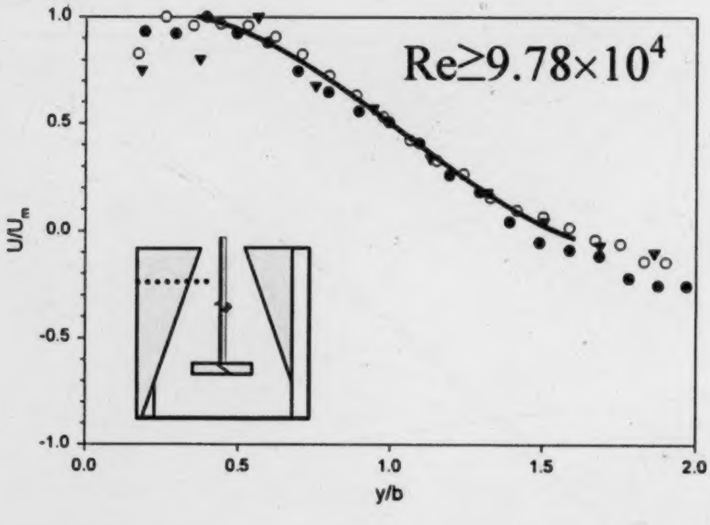

Figure A - 40: Fully Turbulent Profile at z/T=0.83 for a A310 C/D=0.5 D/T=0.33
(Profiles 4, 5, 6 & 7 eliminated)

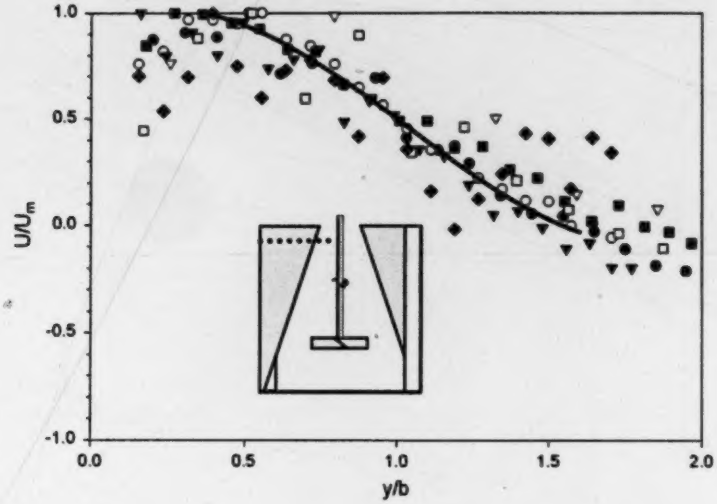

Figure A - 41: Velocity Profile at z/T=0.92 for a A310 C/D=0.5 D/T=0.33

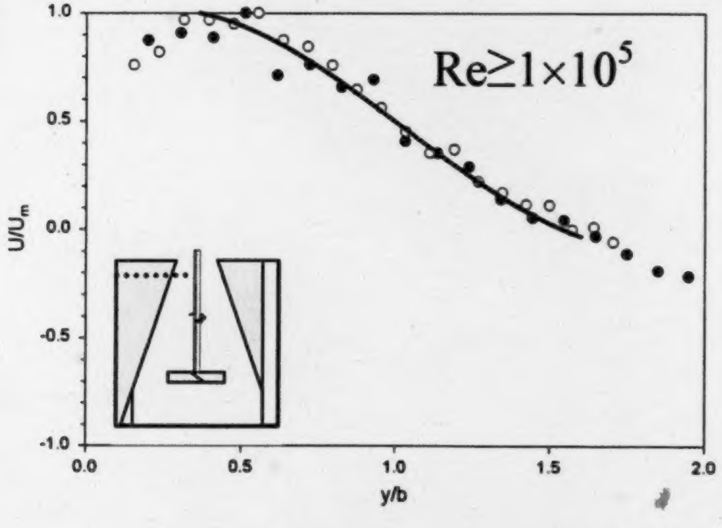

Figure A - 42: Fully Turbulent Profile at z/T=0.92 for a A310 C/D=0.5 D/T=0.33
(Profiles 3,4,5,6 & 7 eliminated)

Profiles for an A310 Impeller (D/T=0.33 C/D=1.0)

Legend for A310, D/T=0.33 C/D=1.0

	Symbol	Re	Fluid
Profile 1	●	2.9×10^5	**Water**
Profile 2	○	1.0×10^5	**Water**
Profile 3	▼	9.8×10^4	**Bayol**
Profile 4	▽	4.5×10^4	**T.G. and Water**
Profile 5	■	2.7×10^4	**T.G. and Water**
Profile 6	□	2.0×10^4	**Bayol**
Profile 7	◆	2.0×10^4	**Water**
Wall Jet Profile	—		

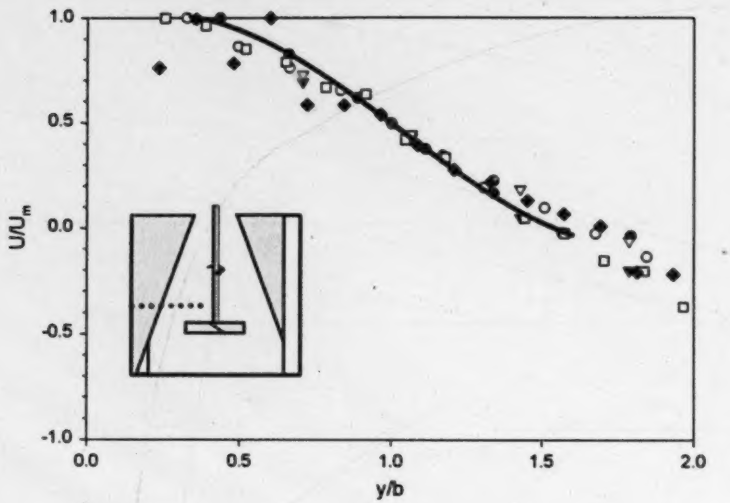

Figure A - 43: Velocity Profile at z/T=0.46 for a A310 C/D=1 D/T=0.33

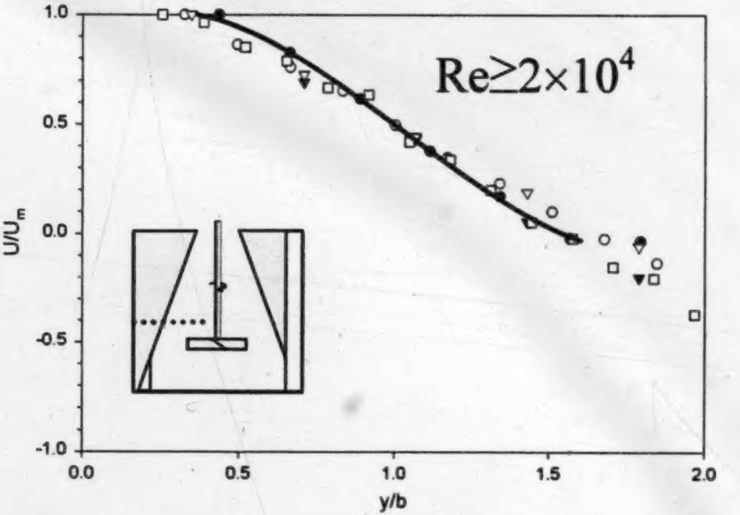

Figure A - 44: Fully Turbulent Profile at z/T=0.46 for a A310 C/D=1 D/T=0.33 (Profile 7 eliminated)

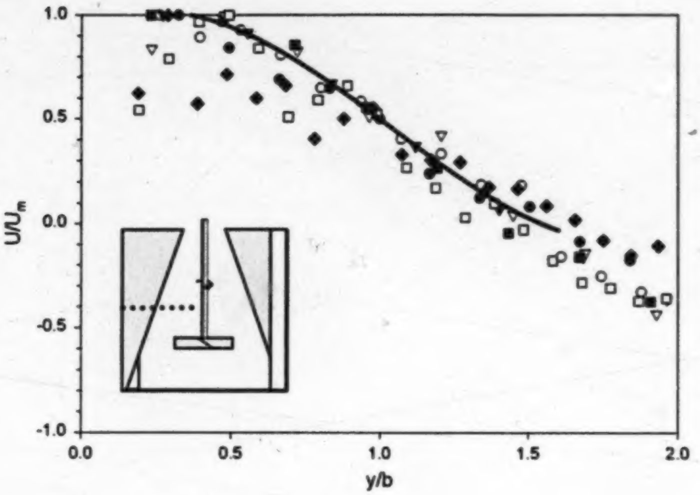

Figure A - 45: Velocity Profile at z/T=0.58 for a A310 C/D=1 D/T=0.33

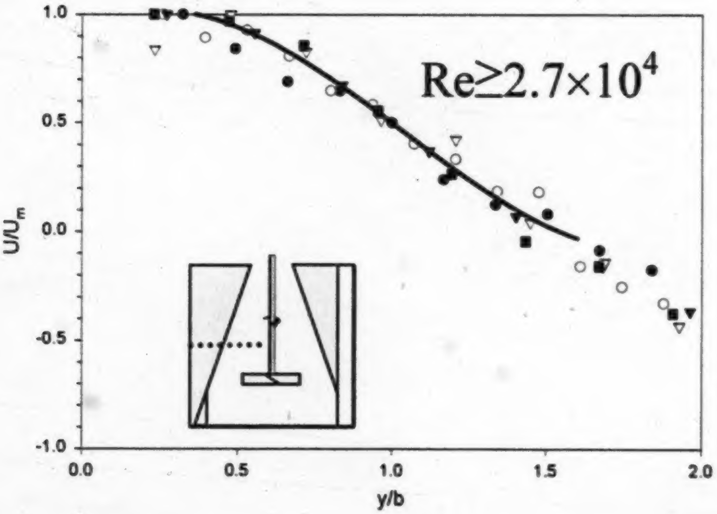

Figure A - 46: Fully Turbulent Profile at z/T=0.58 for a A310 C/D=1 D/T=0.33 (Profiles 6 & 7 eliminated)

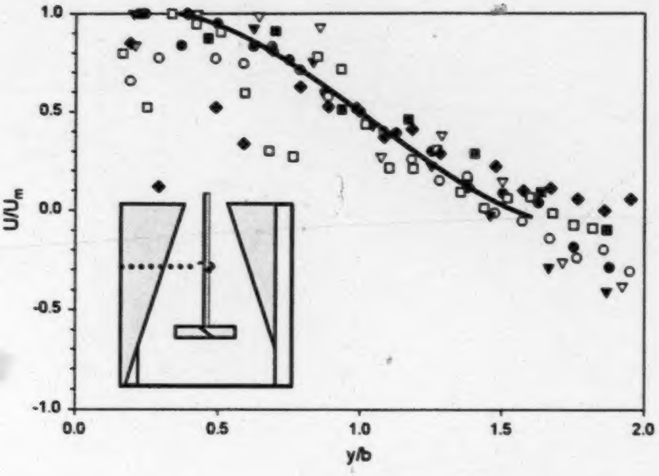

Figure A - 47: Velocity Profile at z/T=0.71 for a A310 C/D=1 D/T=0.33

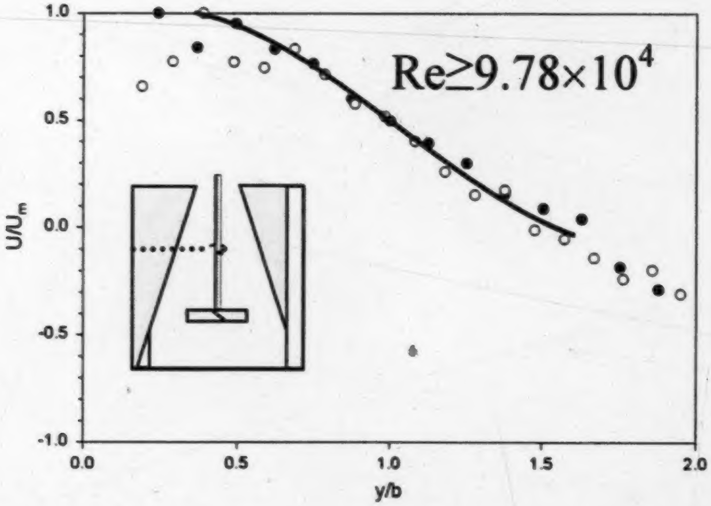

Figure A - 48: Fully Turbulent Profile at z/T=0.71 for a A310 C/D=1 D/T=0.33 (Profiles 4, 5, 6 & 7 eliminated)

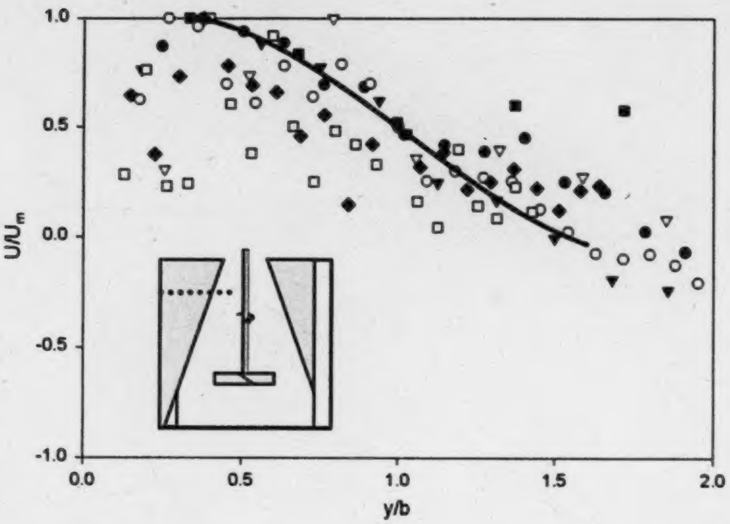

Figure A - 49: Velocity Profile at z/T=0.83 for a A310 C/D=0.5 D/T=0.33

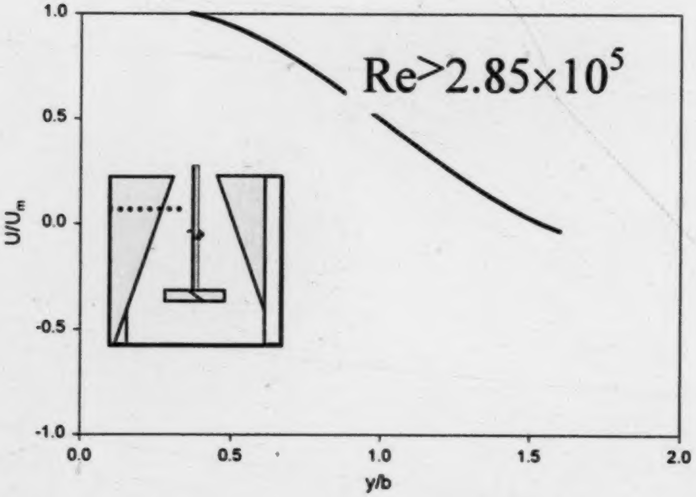

Figure A - 50: Fully Turbulent Profile at z/T=0.83 for a A310 C/D=0.5 D/T=0.33 (Profiles 1, 2, 3, 4, 5, 6 & 7 eliminated)

Profiles for a HE3 Impeller (D/T=0.25 C/D=0.5)

Legend for HE3, D/T=0.25 C/D=0.5

	Symbol	Re	Fluid
Profile 1	●	1.8×10^5	**Water**
Profile 2	○	1.0×10^5	**Water**
Profile 3	▼	6.0×10^4	**Bayol**
Profile 4	▽	3.6×10^4	**Bayol**
Profile 5	■	2.3×10^4	**T.G. and Water**
Profile 6	□	2.0×10^4	**Bayol**
Profile 7	◆	2.0×10^4	**Water**
Wall Jet Profile	—		

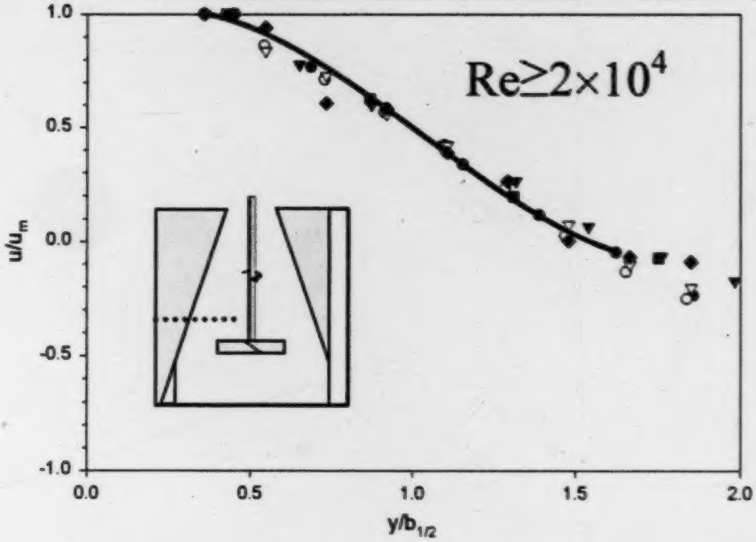

Figure A - 51: Fully Turbulent Profile at z/T=0.46 for a HE3 C/D=0.5 D/T=0.25

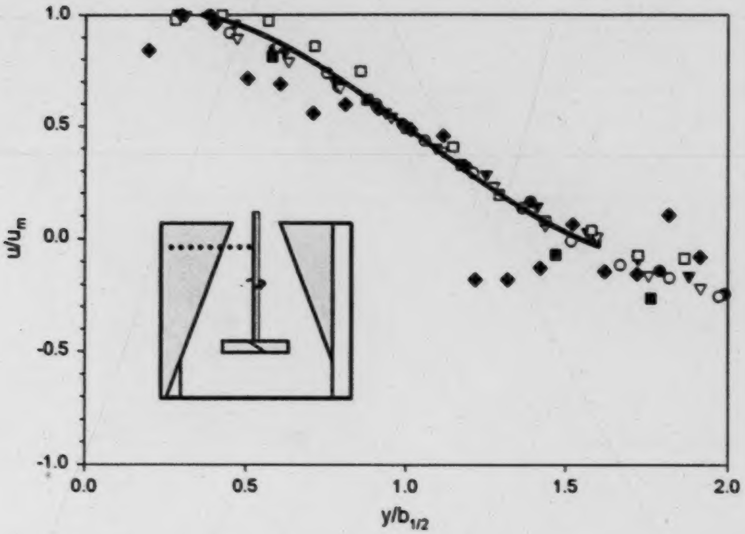

Figure A - 52: Velocity Profile at z/T=0.58 for a HE3 C/D=0.5 D/T=0.25

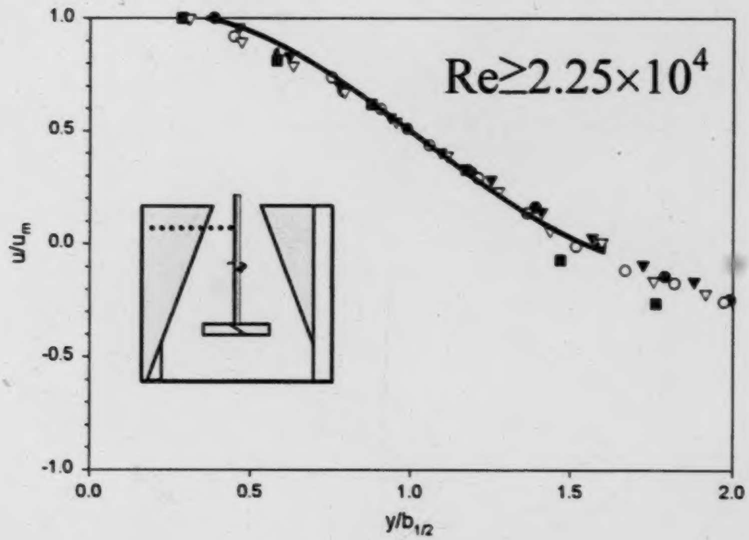

Figure A - 53: Fully Turbulent Profile at z/T=0.58 for a HE3 C/D=0.5 D/T=0.25
(Profiles 6 & 7 eliminated)

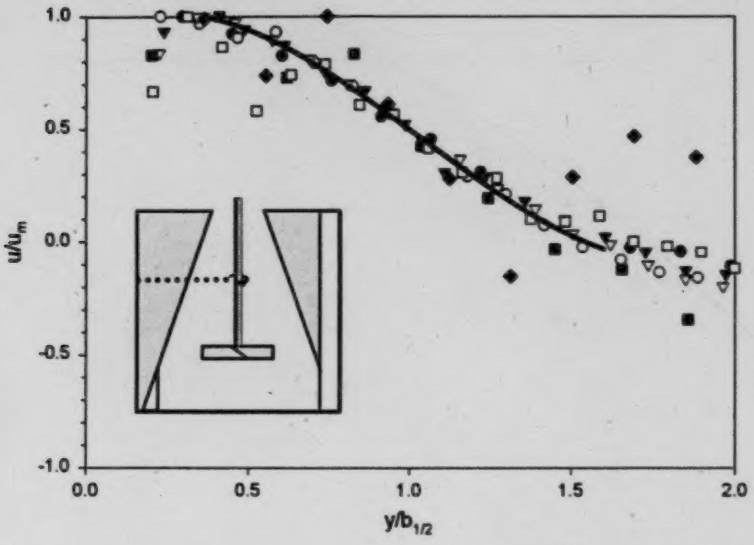

Figure A - 54: Velocity Profile at z/T=0.71 for a HE3 C/D=0.5 D/T=0.25

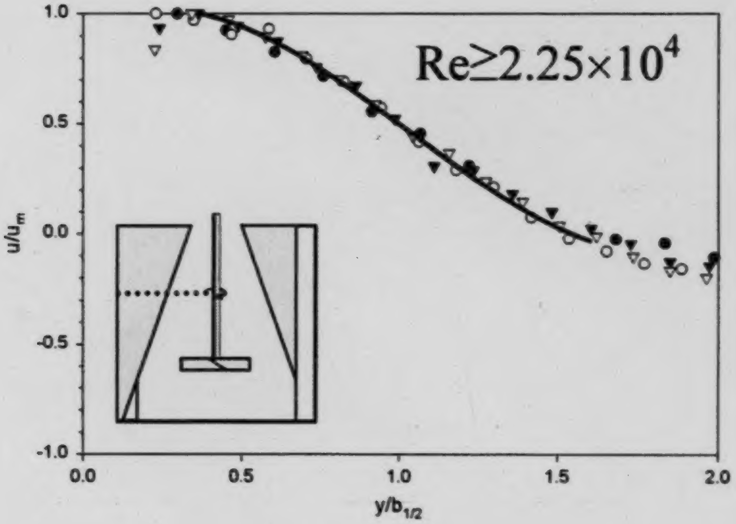

Figure A - 55: Fully Turbulent Profile at z/T=0.71 for a HE3 C/D=0.5 D/T=0.25 (Profiles 5, 6 & 7 eliminated)

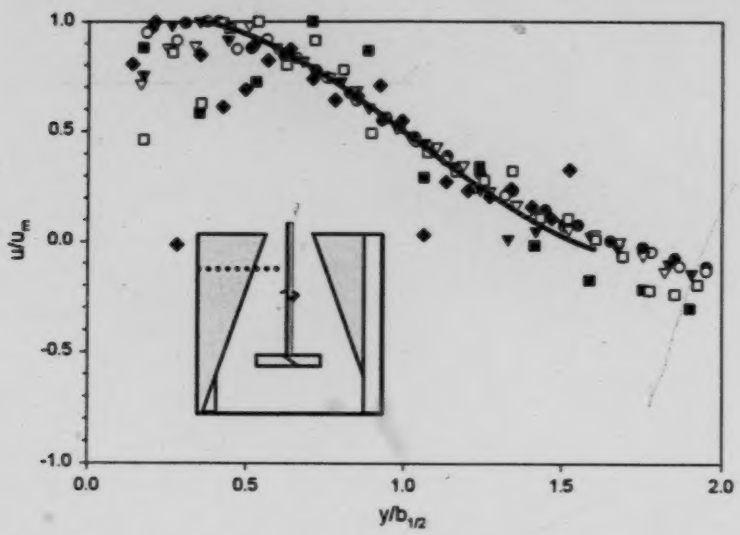

Figure A - 56: Velocity Profile at z/T=0.83 for a HE3 C/D=0.5 D/T=0.25

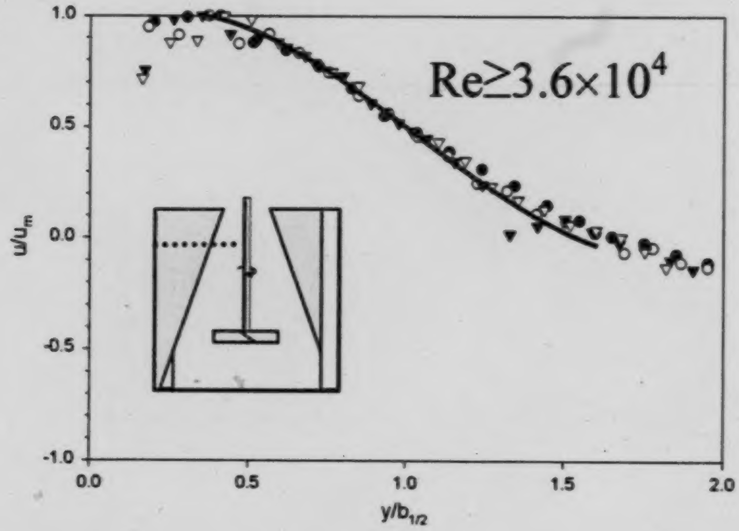

Figure A - 57: Fully Turbulent Profile at z/T=0.83 for a HE3 C/D=0.5 D/T=0.25 (Profiles 5, 6 & 7 eliminated)

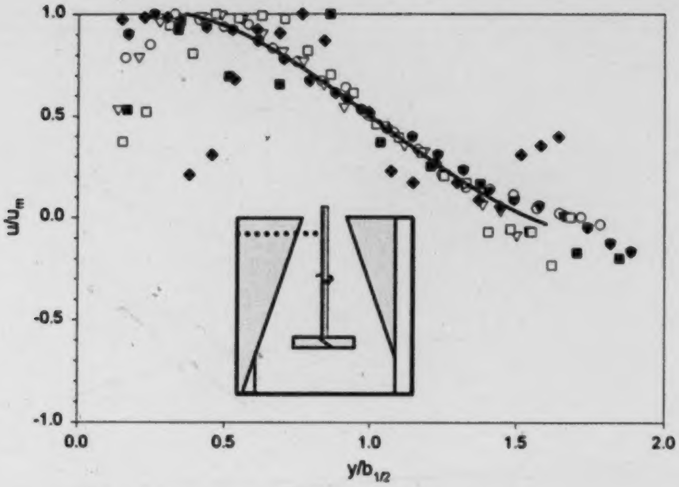

Figure A - 58: Velocity Profile at z/T=0.92 for a HE3 C/D=0.5 D/T=0.25

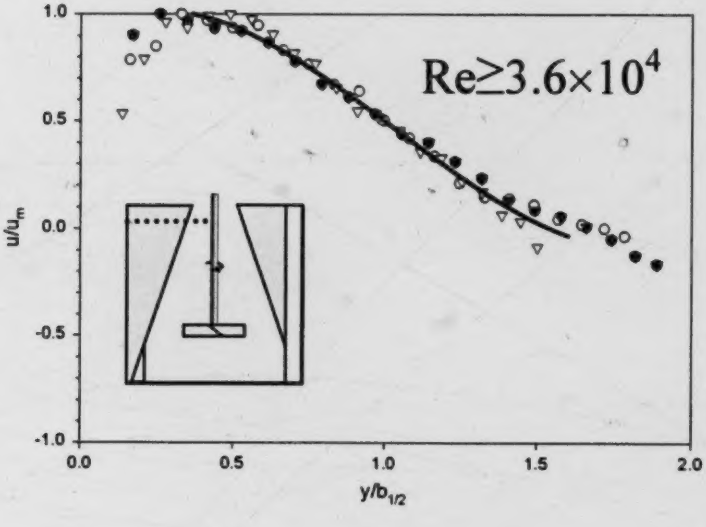

Figure A - 59: Fully Turbulent Profile at z/T=0.92 for a HE3 C/D=0.5 D/T=0.25 (Profiles 5, 6 & 7 eliminated)

Profiles for a HE3 Impeller
(D/T=0.25 C/D=1.33)

● Water Re_l=1.8E5 (Profile 1)
○ Water Re_l=1.0E5 (Profile 2)
▼ Bayol Re_l=6.0E4 (Profile 3)
▽ Bayol Re_l=3.6E4 (Profile 4)
■ TEG & Water Mix 2 Re_l=2.25E4 (Profile 5)
□ Bayol Re_l=2.0E4 (Profile 6)
◆ Water Re_l=2.0E4 (Profile 7)
— Wall Jet Profile

Legend for HE3, D/T=0.25 C/D=1.33

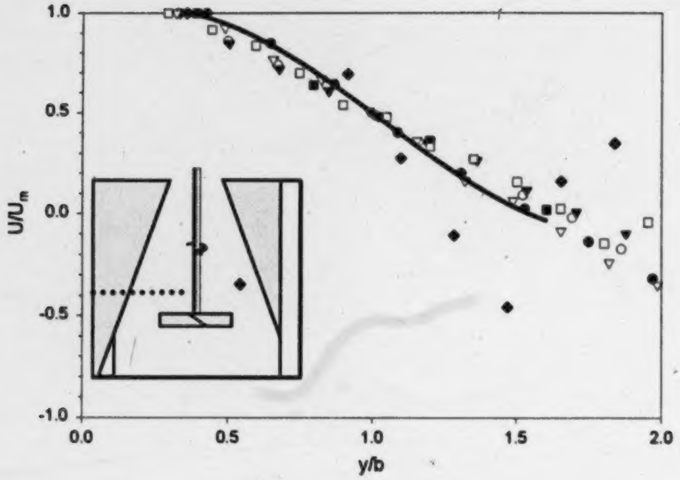

Figure A - 60: Velocity Profile at z/T=0.46 for a HE3 C/D=1.33 D/T=0.25

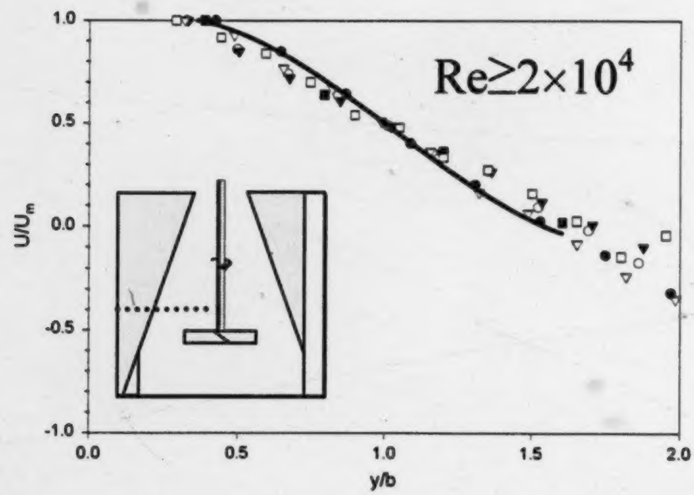

Figure A - 61: Fully Turbulent Profile at z/T=0.46 for a HE3 C/D=1.33 D/T=0.25 (Profile 7 eliminated)

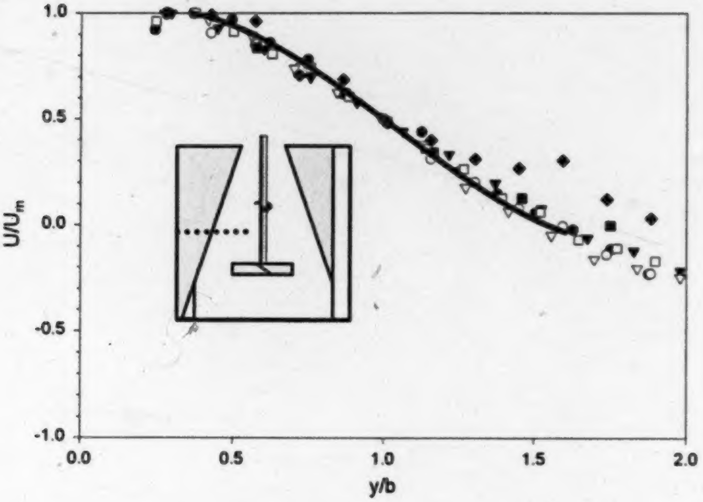

Figure A - 62: Velocity Profile at z/T=0.58 for a HE3 C/D=1.33 D/T=0.25

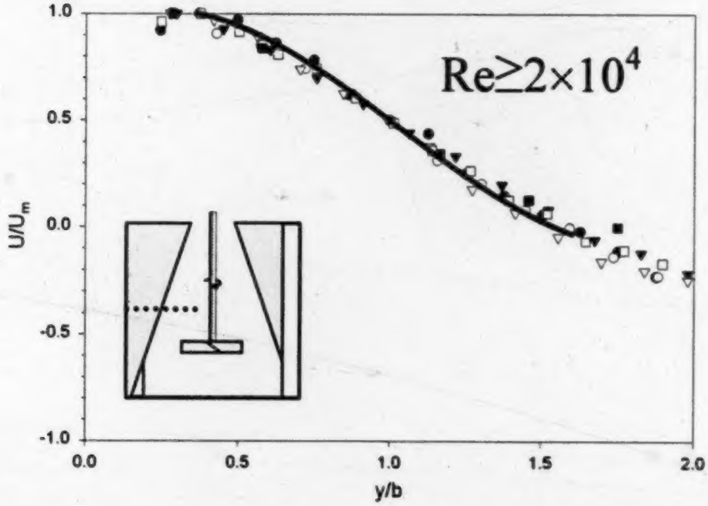

Figure A - 63: Fully Turbulent Profile at z/T=0.58 for a HE3 C/D=1.33 D/T=0.25 (Profile 7 eliminated)

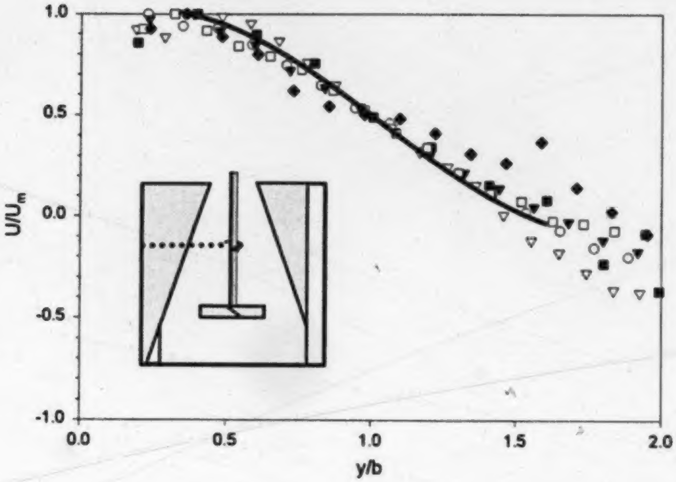

Figure A - 64: Velocity Profile at z/T=0.71 for a HE3 C/D=1.33 D/T=0.25

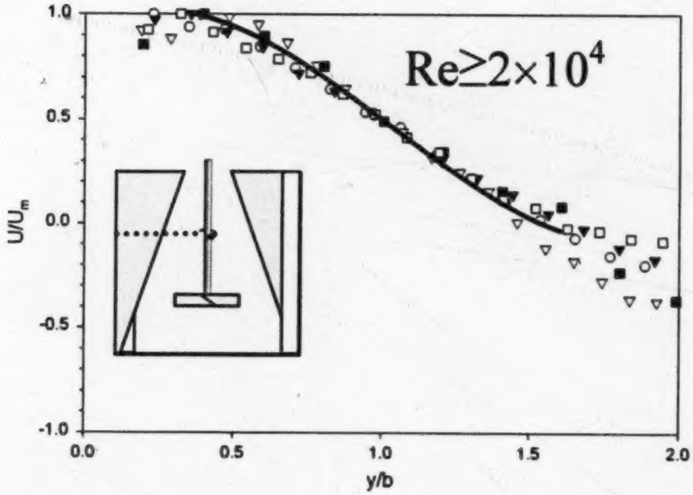

Figure A - 65: Fully Turbulent Profile at z/T=0.71 for a HE3 C/D=1.33 D/T=0.25 (Profile 7 eliminated)

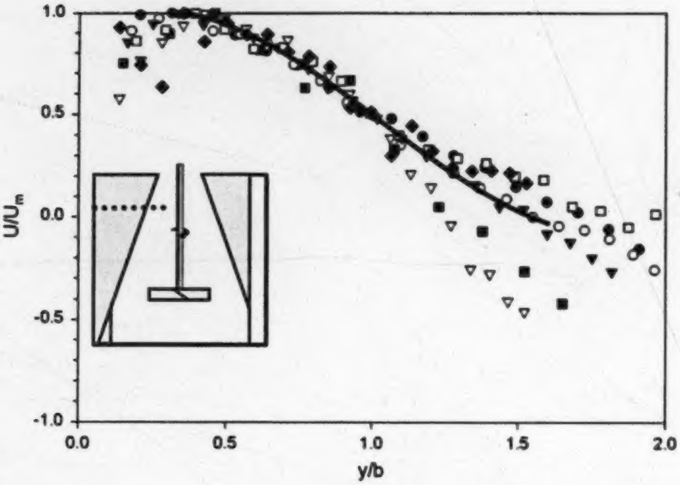

Figure A - 66: Velocity Profile at z/T=0.83 for a HE3 C/D=1.33 D/T=0.25

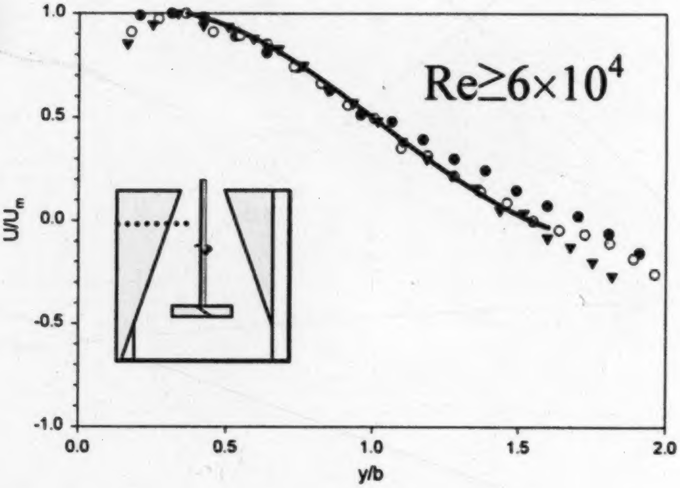

Figure A - 67: Fully Turbulent Profile at z/T=0.83 for a HE3 C/D=1.33 D/T=0.25
(Profiles 4, 5, 6, & 7 eliminated)

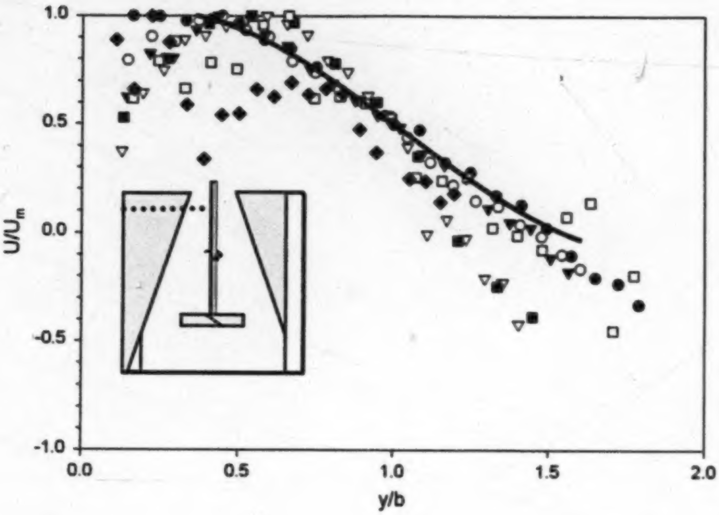

Figure A - 68: Velocity Profile at z/T=0.92 for a HE3 C/D=1.33 D/T=0.25

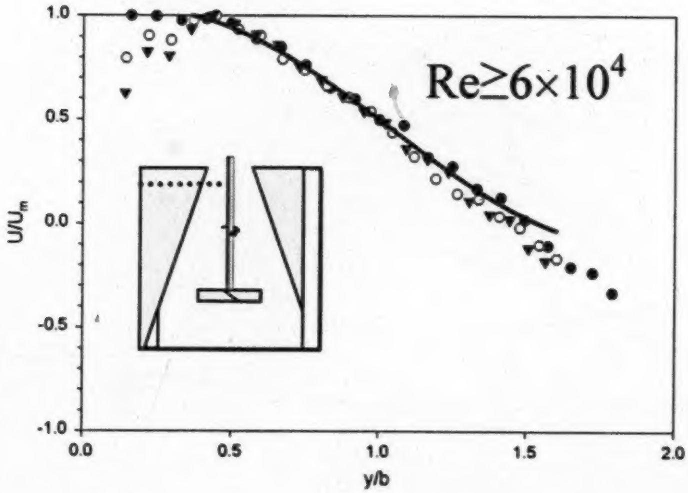

Figure A - 69: Fully Turbulent Profile at z/T=0.92 for a HE3 C/D=1.33 D/T=0.25 (Profiles 4, 5, 6, & 7 eliminated)